

Development of the Timing System for the Bunch-to-Bucket Transfer between the FAIR Accelerators

Dissertation
zur Erlangung des Doktorgrades
der Naturwissenschaften

vorgelegt beim Fachbereich Physik
der Goethe-Universität
in Frankfurt am Main

von
Jiaoni Bai
aus Taiyuan, Shanxi, China

Frankfurt am Main 2017
(D 30)

vom Fachbereich Physik der Goethe-Universität
als Dissertation angenommen.

Dekan:

Prof. Dr. Owe Philipsen

Gutachter:

Prof. Dr. Oliver Kester

Prof. Dr. Ulrich Ratzinger

Datum der Disputation:

I would like to dedicate this dissertation to my dear parents,
loving husband and good friends ...

Acknowledgement

First and foremost, I would like to thank my professor, Dr. Oliver Kester. It has been an honor to be his Ph.D. student. I appreciate all his contributions of time and ideas to make my Ph.D. successful. I am deeply influenced by his enthusiasm for his research and his selfless support for his students.

I wish to express my sincere gratitude to Dr. David Ondreka and Dr. Dietrich Beck for their supervision, valuable guidance and helpful suggestions throughout my Ph.D. study. I have been greatly lucky to have so good supervisors, who cared much about my work and who answered my doubts patiently. They are not only my scientific supervisors, but also my mentors. They encouraged and motivated me during tough time of my Ph.D. Hence, I kept a positive attitude and moving forward when I faced with challenges, difficulties and temporary setbacks.

I would like to acknowledge all colleagues in the timing group, CSCO department, GSI, Dr. Mathias Kreider, Stefan Rauch, Marcus Zweig, Alexander Hahn and former employee Dr. Wesley Terpstra, who provided me much technical support. I would like to extend my appreciation to department leader Dr. Ralph Bär, who gave much support for my Ph.D. topic. Thanks for their friendship and collaboration. I am especially grateful for the group member Cesar Prados, by whom I learned not only technical knowledge, but also how to work efficiently and how to become a good engineer. I would also like to thank Matthias Thieme, who provided me the devices for the test setup and Marko Stanislav Mandakovic for the discussion about the Machine Protection System. I would like to extend gratitude to Dr. Udo Krause and Peter Kainberger for the information about the GSI control system.

I am also thankful for the good cooperation with Thibault Ferrand, who studies at Technische Universität Darmstadt and works in PBRF department, GSI. Thanks for his valuable contribution of the development of the LLRF system for the B2B transfer system for FAIR. I would like to extend my sincerest thanks and appreciation to PBRF department leader Prof. Dr. Ing. Harald Klingbeil for his support. In addition, a special thanks is also extended to Dr. Dieter Lens and Stefan Schäfer for their technical support. Thanks for Dr. Bernhard Zipfel to give me support about BuTiS.

I wish to express my sincere gratitude to SBES department leader Dr. Markus Steck for his technical support of the ESR and the CRYRING, Dr. Udo Blell in PBHV department for the technical support of kicker and Dr. Michael Block in SHE-P department for the supply of two SRS function generators.

I would like to express my gratitude to GSI and also HGS-HIRE, who provided the scholarship which allowed me to undertake this research.

Lastly, I would like to thank my family for all their love and encouragement. They always encourage me to pursue and realize my dreams. Thank you.

Abstract

The Facility for Antiproton and Ion Research (FAIR) is a new international particle accelerator facility under construction at GSI Helmholtz center for Heavy Ion Research GmbH. It is aiming at providing high-energy beams of ions of all elements from hydrogen to uranium with high intensities, as well as beams of rare isotopes and beams of antiprotons. The FAIR accelerators will be supplied with ion beams by the GSI accelerator facility, which comprises the injectors for the FAIR accelerators. The injection chain consists of the linear accelerator UNILAC and the heavy ion synchrotron SIS18. In addition, the GSI accelerator facility comprises the experimental storage ring (ESR) and the CRYRING, which complement the planned accelerators of FAIR. The FAIR facility in its start version will consist of three circular accelerators, which add to the three rings at GSI. The driver accelerator of FAIR is the fast ramping, superconducting heavy ion synchrotron SIS100, that allows the acceleration of the most intense beams of stable elements. The primary beams are used to produce secondary beams, which are delivered to the collector ring (CR) via high energy separators. The CR will accumulate the secondary beams and improve their quality by stochastic cooling. The storage ring HESR will host a large fraction of the experiment platforms with a variety of different experiments. These circular accelerators of GSI and FAIR have different ratios in their circumference. For example, the circumference ratio between the SIS100 and the SIS18 is an integer and between the SIS18 and the ESR is close to an integer and between the CR and the HESR is far away from an integer. The ring accelerators are connected via a complicated system of beam transfer lines, targets for the secondary particle production and the high energy separators mentioned above. For FAIR, not only the primary beams are required to be transferred from one ring to another, but also the secondary beams. e.g. the antiproton or rare isotope beams produced by the pbar target, the Fragment Separator (FRS) or the Super FRS. An important topic for this system of accelerators is the precise transfer of beam between the different machines. Bunches of one ring must be transferred into buckets of another ring within an upper bound time constraint (e.g. 10 ms for most FAIR use cases) and with an acceptable bunch-to-bucket injection center mismatch (e.g. $\pm 1^\circ$ for most FAIR use cases). Hence, a flexible FAIR Bunch-to-Bucket (B2B) transfer system is required to realize the different complex bunch-to-bucket transfers between the FAIR rings in the future. In the focus of the system development **and of this thesis?** is the transfer from the SIS18 to the SIS100, which can be tested at GSI on the transfer from the SIS18 to the ESR and from the ESR to the CRYRING. The system is based on the existing technical basis at GSI, the low level radio frequency (LLRF) system and the FAIR control system. It coordinates with the Machine Protection System, which protects SIS100 and subsequent accelerators and experiments from damage caused by high intensity primary beams in case of malfunctioning. Besides, it indicates the

beam status and the actual beam injection time for the beam instrumentation and diagnostics.

In this thesis the basic idea, the basic procedure and the conceptual realization of the bunch-to-bucket transfer system are described in detail and the mathematical evaluation of the required timing parameters is presented. In order to trigger the extraction and injection kickers correctly, the FAIR B2B transfer system is composed of two synchronization processes, a coarse synchronization and a fine synchronization. The coarse synchronization gives a coarse time frame, within which bunches are transferred into buckets with a bunch-to-bucket center mismatch smaller than a well defined bound. This time frame is called the “synchronization window”. With the synchronization window, the extraction and injection kickers are triggered at the correct time in order to transfer bunches into correct empty buckets. The process of the kicker trigger at the correct time is the “fine synchronization”. The fine synchronization is achieved based on a bucket indication signal plus a fixed delay. The bucket indication signal is derived from the rf revolution frequency signal and always indicates the first bucket. A fixed delay is used to indicate the correct buckets to be filled.

The coarse synchronization is based on the phase difference between the two rf systems of two rings, which is obtained by the phase deviation measurement between the rf system and a campus-wide distributed synchronization reference signal at both rings. When the circumference ratio between two rings is an integer, the phase difference between the two rf systems is constant. In order to get the correct phase difference, the phase of either (or both) rf systems must be shifted by means of an rf frequency modulation. This is called “phase shift method”. After the rf frequency modulation, the phase difference between the two rf systems is correct and the synchronization window is infinitely long theoretically. When the circumference ratio between two rings is not an integer, the phase difference between the two rf systems varies periodically. The synchronization window brings a symmetric time frame with respect to the time, when the phase difference between two rf systems is closest to the required phase difference. This is called “frequency beating method”. The frequency beating method is also applicable when the circumference ratio between two rings is an integer. In this case, the rf frequency of either (or both) rf systems is detuned at the end of the acceleration ramp, so that two rf systems are beating. For the FAIR project, the frequency beating method is preferable, because it is applicable for all beam transfer scenarios. In addition, it reduces the synchronization time, because the rf frequency detune is executed during the rf acceleration ramp. For the phase shift method, the rf frequency modulation must be executed slowly enough at the rf flattop for beams to follow according to the calculated limits. **The phase shift method therefore needs much more time to be executed?** However, there are also some advantages of the phase shift method. The synchronization window is relatively long and the bunch-to-bucket injection center mismatch is approximately 0°. Besides, the duration of the rf frequency modulation is known in advance and the time point for the transfer is predictable. The phase of the rf system can jump to a desired value, when there is no bunch at the ring.

In this thesis, a systematic investigation has been done? from the beam dynamics, timing requirement of the transfer and kicker trigger perspectives. The timing perspective includes the accuracy of the start of the synchronization window, the characterization of the White Rabbit network for the B2B transfer, the flow chart

and the time constraints of the system. A test setup of the timing system required for the transfer using the frequency beating method **has been developed and tested?**, which proves that the firmware running on the soft CPU meets the functional requirement and the time constraints. Finally, all FAIR use cases with the frequency beating method have been discussed.

The dissertation plays a significant important role for the realization of the FAIR B2B transfer system of the released version and the further practical application of the system to all FAIR use cases.

Kurzfassung

Die *Facility for Antiproton and Ion Research* (FAIR) ist eine im Bau befindliche, internationale Teilchenbeschleunigeranlage, die unter der Leitung von der GSI Helmholtzzentrum für Schwerionenforschung GmbH errichtet wird. Sie hat zum Ziel, hochenergetische Ionenstrahlen zu erzeugen. FAIR wird in der Lage sein Strahlen höchster Intensität für Elemente vom leichten Wasserstoff bis zum schweren Uran zur Verfügung zu stellen und darüber hinaus in der Lage sein Antiprotonen und exotische Nuklide zu erzeugen. Die existierende Beschleunigeranlage der GSI wird der Injektor der FAIR-Beschleuniger sein und umfasst den Linerabeschleuniger UNILAC und das Schwerionen-Synchrotron SIS18. Des Weiteren umfasst die GSI Beschleunigeranlage zwei Speicherringe, den Experimentierspeichering (ESR) und den CRYRING. Der FAIR-Beschleunigerkomplex in seiner Startversion, besteht aus drei Ringbeschleunigern mit unterschiedlichen Funktionalitäten und Aufgaben. Der Primärstrahltreiber ist das supraleitende Schwerionen-Synchrotron SIS100, das die Beschleunigung von stabilen Elementen mit höchster Intensität erlaubt. Der Primärestrahl wird dazu genutzt Sekundärteichen zu produzieren, die dem *Collector Ring* (CR) über Hochenergieseparatoren zugeführt werden. Für die Präparation der Sekundärstrahlen und die Experimente dienen der CR und der *High Energy Storage Ring* (HESR). Der CR dient zur Sekundärstrahl-Akkumulation und verbessert die Stahlqualität durch *stochastic cooling*. Die Ringbeschleuniger der GSI und von FAIR haben sehr unterschiedliche Verhältnisse ihrer Umfänge. Zum Beispiel ist das Umfangsverhältnis zwischen dem SIS18 und dem SIS100 ganzzahlig, zwischen dem SIS18 und dem ESR annähernd ganzzahlig und zwischen dem CR und dem HESR ist es weit weg von einem ganzzahligem Verhältnis. Alle FAIR-Ringbeschleuniger sind über Strahltransportlinien, die Targets zur Produktion von Sekundärteilchen und den zugehörigen Hochenergieseparatoren verbunden. Für FAIR ist es nicht nur erforderlich Primärstrahlen vom einen zum anderen Ring zu transferieren, sondern auch Sekundärstrahlen, wie Antiprotonen oder exotische Nuklide die im Antiprotonen-Target, im Fragmentseparator oder im Superfragmentseparator erzeugt werden, wieder in Speicherringe einzufangen. Zudem muss ein *bunch* von einem Ring in das *bucket* eines anderen Rings, innerhalb einer bestimmten Zeit (z.B. unter 10 ms in fast allen FAIR-Anwendungsfällen) und mit einem akzeptablen *Bunch-to-Bucket*-Injektions-Mittenversatz (z.B. in weniger als $\pm 1^\circ$ in den meisten FAIR-Anwendungsfällen) transferiert werden. Daher ist ein flexibles *FAIR Bunch-to-Bucket (B2B) transfer system* erforderlich, um die verschiedenen und komplexen B2B-Transfers zwischen den zukünftigen FAIR-Ringen realisieren zu können. Im Fokus dieser Arbeit ist natürlich der Teilchentransfer vom SIS18 zum SIS100, welcher am Beispiel des Transfers zwischen SIS18 zum ESR und vom ESR zum CRYRING an der GSI getestet werden kann. Das System wird auf Basis der für FAIR vorgesehen, technischen Infrastruktur entwickelt. Dazu zählen das FAIR-Low-Level-Radio-Frequency (LLRF)-System

und das Kontrollsysteem für FAIR. Das *FAIR B2B transfer system* hat eine Schnittstelle zum FAIR-Maschinenschutzsystem (*machine protection system*), welches das SIS100 und die nachgeschalteten Beschleuniger und Experimente vor Schaden durch Fehlerfunktionen und dadurch bedingten Primärstrahlverlust bei hohen Intensitäten bewahrt. Außerdem wird der Status des Strahls und der Zeitpunkt der Strahlinjektion vom *FAIR B2B transfer system* an die Geräte der Strahldiagnose gemeldet.

der bunch das bucket ???

Diese Doktorarbeit stellt vor allem die Grundidee, das grundlegende Verfahren und die konzeptionelle Realisierung des *FAIR B2B transfer system* vor. Darüber hinaus werden die Anforderungen an das Timing analytisch ermittelt und vorgestellt. Für das *FAIR B2B transfer system* wurde ein zweistufiger Synchronisationsprozess erarbeitet, welcher den exakten Kickzeitpunkt bestimmt. In der ersten Stufe, der „Grobsynchronisation“ gibt ein Synchronisationsfenster ein Zeitintervall vor, indem der B2B-Injektions-Mittenversatz zwischen *bunch* und *bucket* innerhalb der ermittelten Toleranzgrenze bleibt. Innerhalb dieses Synchronisationsfensters müssen die Kicker zum richtigen Zeitpunkt ausgelöst werden, um einen *bunch* in den richtigen, leeren *bucket* der Zielmaschine zu schießen. Das übernimmt die sogenannte „Feinsynchronisation“. Die „Feinsynchronisation“ ist das *bucket indication signal*, welches über ein festes Delay verzögert wird. Das *bucket indication signal* wird von den Hochfrequenzsignalen (HF-Signal) der Umlauffrequenzen abgeleitet und kennzeichnet immer das erste *bucket*. Ein weiteres Delay wird dazu benutzt, um die folgenden, zu befüllenden *bucket* zu kennzeichnen.

Für die Grobsynchronisation wird die Phasendifferenz zwischen den HF-Signalen der Quell- und Zielmaschine gemessen. Die Phasendifferenz erhält man, indem man die Phasenabweichung der HF-Signalen beider Ringe gegen ein campusweit verteiltes *synchronization reference signal* vermisst. Wenn das Umfangsverhältnis beider Ringe ganzzahlig ist, bleibt die Phasendifferenz der beiden HF-Signale während des Transfers konstant. Um die richtige Phasendifferenz zu erreichen, muss die Phase eines (oder beider) HF-Systeme mithilfe einer Frequenzmodulation verschoben werden. Das nennen wir die *phase shift method*. Nach der exakten Ausrichtung der Phasen, bleibt die gewünschte Phasendifferenz konstant und ermöglicht, theoretisch ein unendlich langes Synchronisationsfenster. Wenn das Umfangsverhältnis beider Ringe nicht ganzzahlig ist, verändert sich die Phasendifferenz periodisch. Innerhalb einer Periode gibt es dann nur einen Zeitpunkt, zu dem die Zielphase erreicht wird. Davor und danach kommt es zu einem B2B-Injektions-Mittenversatz zwischen *bunch* und *bucket*. Das nennen wir die *frequency beating method*. Diese ist auch anwendbar, wenn das Umfangsverhältnis beider Ringe ganzzahlig ist. In diesem Fall wird die HF-Frequenz eines (oder beider) HF-Systeme am Ende der Beschleunigungsrampe leicht verstimmt, sodass sich eine Schwebungsfrequenz zwischen den HF-Systemen der Quell- und Zielmaschine ergibt. Für FAIR wird die *frequency beating method* präferiert, weil diese Methode für sämtliche Transferszenarien bei FAIR anwendbar ist. Außerdem kann mit dieser Methode Zeit gespart werden, weil die Frequenzverstimmung während der Beschleunigungsrampe durchgeführt wird. Zur Erinnerung: Bei der *phase shift method* muss die Frequenzmodulation auf *rf flattop* entsprechend der Ergebnisse dieser Arbeit langsam genug ausgeführt werden, damit der Strahl stabil bleibt. Das kostet viel Zeit. Dennoch gibt es auch Vorteile, die für die *phase shift method* sprechen. Das Synchronisationsfenster ist theoretisch unendlich lang und der B2B-Injektions-Mittenversatz ist nahezu „Null“. Außerdem ist

die Dauer der Frequenzmodulation vorab bekannt und der Transfer-Zeitpunkt ist exakt bestimmbar. Vorteilhaft ist auch, dass die gewünschte Phase des HF-Systems sprungartig eingestellt werden kann, wenn sich kein *bunch* im Ring befindet.

Im Rahmen dieser Doktorarbeit wird eine systematische Untersuchung der strahldynamischen Aspekte, der zeitlichen Anforderungen an den B2B-Transfer-Prozess und der Trigger-Szenarien für die Kicker-Auslösung durchgeführt. Die Timing-Betrachtungen berücksichtigen die erforderliche Genauigkeit für den Beginn des Synchronisationsfensters, die Charakterisierung des *White Rabbit* Netzwerks, das Flussdiagramm mit Timing-Bedingungen für das *FAIR B2B transfer system*. Ein Messaufbau zur Untersuchung des Timings vorgestellt, der dazu verwendet wird die Firmware, die auf einer *soft-CPU* ausgeführt wird, hinsichtlich der Einhaltung der Timing- und Funktionsanforderungen zu überprüfen. Im Rahmen der Untersuchungen wurden sämtliche FAIR-Anwendungsfälle, bei denen die *frequency beating method* verwendet wird, erörtert.

Diese Doktorarbeit spielt eine wichtige Rolle bei der Realisierung der veröffentlichten Version des *FAIR B2B transfer system* und der weiteren praktischen Anwendung des Systems für alle FAIR-Transferszenarien.

Contents

| | |
|---|-----------|
| Abstract | i |
| 1 Introduction | 1 |
| 1.1 Bunch-to-Bucket Transfer worldwide | 4 |
| 1.2 Objectives, Contribution and Structure of the Dissertation | 5 |
| 2 Theoretical Background | 8 |
| 2.1 Bunch and Bucket | 8 |
| 2.2 Phase Difference | 14 |
| 2.2.1 Circumference Ratio is an Integral | 16 |
| 2.2.2 Circumference Ratio is close to an Integer | 17 |
| 2.2.3 Circumference Ratio is far away from an Integer | 18 |
| 2.3 Phase Match of Two Rf Systems | 20 |
| 2.3.1 Phase Shift Method | 21 |
| 2.3.2 Frequency Beating Method | 24 |
| 2.4 Synchronization of Extraction and Injection Kicker Magnets | 26 |
| 3 Technical Basis for the FAIR B2B Transfer System | 30 |
| 3.1 FAIR Control System | 30 |
| 3.1.1 Bunch Phase Timing System | 30 |
| 3.1.2 General Machine Timing System | 31 |
| 3.1.3 Settings Management | 32 |
| 3.1.4 FESA | 32 |
| 3.2 Low-Level RF System | 32 |
| 3.2.1 Local Cavity Synchronization | 33 |
| 3.2.2 Longitudinal Feedback System | 34 |
| 3.3 Machine Protection System | 35 |
| 4 Concept of the FAIR B2B Transfer System | 36 |
| 4.1 Basic Idea | 36 |
| 4.1.1 Phase Alignment | 36 |
| 4.1.2 Trigger of Extraction and Injection Kickers | 38 |
| 4.1.2.1 Bucket Indication Signal | 39 |
| 4.1.2.2 Extraction and Injection Kicker Delay Compensation | 40 |
| 4.2 Basic Procedure | 41 |
| 4.3 Realization | 42 |
| 4.3.1 Phase Measurement and Corresponding Timestamp of Each Rf System | 45 |

CONTENTS

| | | |
|----------|--|-----------|
| 4.3.1.1 | Measurement of Actual Phase Values of Each Rf System | 45 |
| 4.3.1.2 | Phase Extrapolation of Each Rf System | 46 |
| 4.3.1.3 | Timestamp of the Extrapolated Phase | 47 |
| 4.3.2 | Exchange of Measured Data | 48 |
| 4.3.3 | Rf Synchronization | 49 |
| 4.3.3.1 | Rf Synchronization with the Phase Shift Method | 50 |
| 4.3.3.2 | Rf Synchronization with the Frequency Beating Method | 50 |
| 4.3.4 | Coarse Synchronization | 51 |
| 4.3.5 | Bucket Label | 53 |
| 4.3.5.1 | Bucket Label for the Normal Extraction and Injection | 54 |
| 4.3.5.2 | Maximum Bunch Spacing Label for the Emergency Extraction | 54 |
| 4.3.6 | Fine Synchronization of Extraction and Injection Kickers | 56 |
| 4.3.7 | B2B Transfer Status Check | 57 |
| 4.4 | Data Flow | 57 |
| 4.5 | Comparison between the FAIR B2B Transfer System and Current B2B Transfer | 61 |
| 5 | Realization and Systematic Investigation of the FAIR B2B Transfer System | 63 |
| 5.1 | Beam Dynamic Analysis of two Synchronization Methods for the B2B Transfer from SIS18 to SIS100 | 63 |
| 5.1.1 | Beam Dynamics of the Phase Shift Method for U^{28+} | 64 |
| 5.1.1.1 | Longitudinal Dynamic Analysis | 68 |
| 5.1.1.2 | Transverse Dynamics Analysis | 73 |
| 5.1.2 | Beam Dynamics of the Frequency Beating Method for U^{28+} | 73 |
| 5.1.2.1 | Longitudinal Dynamics Analysis | 73 |
| 5.1.3 | Beam Dynamics of the Phase Shift Method for H^+ | 73 |
| 5.1.3.1 | Longitudinal Dynamics Analysis | 74 |
| 5.1.3.2 | Transverse Dynamics Analysis | 74 |
| 5.1.4 | Beam Dynamics of the Frequency Beating Method for H^+ | 75 |
| 5.1.4.1 | Longitudinal Dynamics Analysis | 75 |
| 5.2 | GMT Systematic Investigation | 75 |
| 5.2.1 | Calculation of the Start of the Synchronization Window | 75 |
| 5.2.1.1 | Uncertainty of the Phase Alignment | 76 |
| 5.2.1.2 | Uncertainty of the Start of the Synchronization Window | 80 |
| 5.2.1.3 | Requirement of the Accuracy of the Start of the Synchronization Window | 81 |
| 5.2.2 | Characterization of the WR Network for the B2B Transfer | 82 |
| 5.2.2.1 | Traffic on the WR Network | 83 |
| 5.2.2.2 | Frame Loss of the WR Network for the B2B Transfer | 84 |
| 5.2.2.3 | WR Network Test Setup | 85 |
| 5.2.2.4 | Measurements | 88 |
| 5.2.2.5 | Measurements Result | 90 |
| 5.2.2.6 | Result Discussion | 90 |
| 5.2.2.7 | Conclusion of the Network Measurements | 91 |

CONTENTS

| | | |
|--|--|------------|
| 5.2.3 | Flowchart of the system for SCUs | 92 |
| 5.2.4 | Time Constraints | 96 |
| 5.3 | Kicker Systematic Investigation | 98 |
| 5.3.1 | Simultaneous Trigger for Extraction Kicker Magnets in a Common SIS18 Tank | 98 |
| 5.3.2 | A Fixed Trigger Delay between Extraction Kicker Magnets in the SIS18 1 st and 2 nd Tanks | 100 |
| 5.3.3 | Simultaneous Trigger for SIS100 Injection Kicker Magnets . . | 102 |
| 5.4 | A Test Setup for Timing Aspects | 104 |
| 5.4.1 | Test Setup | 104 |
| 5.4.2 | Comparison between the Test Setup and the Final Setup . . . | 106 |
| 5.4.3 | Procedure | 106 |
| 5.4.4 | Functional Test Result | 109 |
| 5.4.5 | Measurement Result Discussion | 110 |
| 6 | Application of the FAIR B2B Transfer System to FAIR Accelerators | 112 |
| 6.1 | Circumference Ratio is an Integer | 113 |
| 6.1.1 | U^{28+} B2B Transfer from SIS18 to SIS100 | 115 |
| 6.1.2 | H^+ B2B Transfer from SIS18 to SIS100 | 115 |
| 6.2 | Circumference Ratio is close to an Integer | 117 |
| 6.2.1 | $h=4$ B2B Transfer from SIS18 to ESR | 117 |
| 6.2.2 | $h=1$ B2B Transfer from SIS18 to ESR | 119 |
| 6.2.3 | B2B transfer from ESR to CRYRING | 119 |
| 6.3 | Circumference Ratio is far away from an Integer | 121 |
| 6.3.1 | H^+ B2B Transfer from SIS100 to CR | 122 |
| 6.3.2 | RIB B2B Transfer from SIS100 to CR | 123 |
| 6.3.3 | B2B Transfer from CR to HESR | 123 |
| 6.3.4 | RIB B2B Transfer from SIS18 to ESR via the FRS | 124 |
| 6.4 | Summary | 126 |
| Conclusion and Outlook | 130 | |
| Zusammenfassung | 134 | |
| Terminology | 139 | |
| Abbreviations | 143 | |
| Symbols | 147 | |
| A FAIR B2B Transfer Related Timing Frames | 153 | |
| B Timing Frames Transfer for the FAIR B2B Transfer System | 155 | |
| C Parameters of FAIR B2B Transfer Use Cases | 157 | |
| C.1 | Parameters of the B2B Transfer from SIS18 to SIS100 | 157 |
| C.2 | Parameters of the B2B Transfer from SIS18 to ESR | 158 |
| C.3 | Parameters of the B2B Transfer from SIS18 to ESR via the FRS . . | 159 |
| C.4 | Parameters of the B2B Transfer from ESR to CRYRING | 160 |

CONTENTS

| | |
|--|------------|
| C.5 Parameters of the B2B Transfer from CR to HESR | 161 |
| C.6 Parameters of the B2B Transfer from SIS100 to CR | 162 |
| D Parameters of the FAIR B2B Transfer System from Settings Management | 163 |
| E Parameters of FAIR Kicker Magnets | 165 |
| F Configuration for the Test Setup | 166 |
| F.1 Configuration of the B2B source SCU | 166 |
| F.2 Configuration of the B2B target SCU | 166 |
| F.3 Configuration of the Trigger SCU | 167 |
| F.4 Configuration of the packETH | 167 |
| Bibliography | 167 |
| List of Figures | 172 |
| List of Tables | 175 |
| Publications | 179 |

Chapter 1

Introduction

Beams of high energy particles are useful for both fundamental and applied research in the science, and also in many technical and industrial fields unrelated to fundamental research. It has been estimated that there are approximately 30000 accelerators worldwide. Only about 1% of them are research machines with energies above 1 GeV [1]. As we all know, particles are accelerated by electric fields. The radio frequency (rf) system of an accelerator is devoted to generate the electric field in rf cavities around the ring. Particles are accelerated when they pass through rf cavities in the right phase. Every rf cavity has a limited frequency range, so particles at rest can not be accelerated to several tens of GeV energy in one ring accelerator. Hence, the acceleration must be divided into several energy stages: The first energy stage is achieved usually by a linear accelerator followed by a small ring, which is called "booster" and the second stage by a large ring, which is usually called "main ring". The maximum energy of a beam is related to the 'magnetic rigidity' of the dipole magnets used in the accelerator, which is the multiplication of the magnetic field and the bending radius of a particle immersed in the magnetic field. At the time of the beam transfer, the magnetic rigidity of the booster must be equal to that of the main ring. Since the bending radius of the main ring is generally larger than that of the booster, the magnetic field in the main ring starts the further acceleration at a lower level. This allows a continuous increasing of the particle energy until the limits of the dipole magnets of the main ring are reached. The usage of the booster and the main ring works faster to reach the required beam energy, because the booster can be filled and accelerated, when the main ring accelerates particles. The faster acceleration has the advantage to reduce the interaction time between the accelerated particles and the residual-gas atoms in the vacuum chamber, achieving a better beam quality [2]. Furthermore, the particle beam transfer among different rings is also used for the production of high intensity beam, e.g. the beam is transferred to a storage ring for the beam accumulation and beam compression. Hence, the transfer of beam between rings is of great importance for high energy, high intensity and high quality beams.

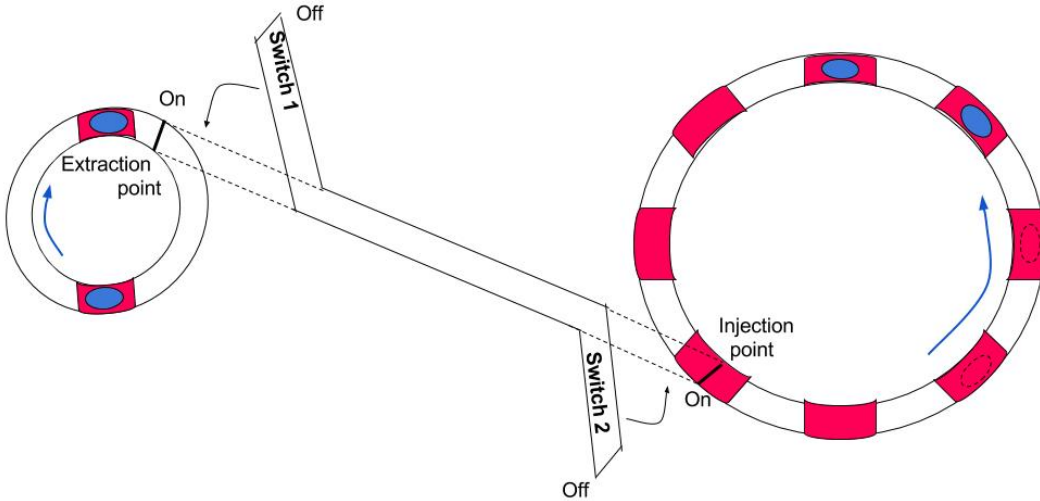


Figure 1.1: Illustration of a bunch-to-bucket transfer.

Red rectangles represent buckets and blue dots bunches.

The beam transfer is not arbitrary. A bunch of particles running in a ring should be transferred into the correct position of another ring. Fig. 1.1 illustrates the transfer of a bunch of particles between two rings. The example in Fig. 1.1 is with the circumference ratio between the right and left rings of four. Bunches of particles are transferred from the left ring to the right one. The blue ellipse represents a bunch of particles and the red rectangle represents the allowable area for particles to be injected. The red rectangles are equally spaced around the ring and determined by the rf frequency. The white space between two red rectangles is forbidden for particles. The allowable area (red rectangle) for particles is termed as a “bucket” and a bunch of particles (blue ellipse) as a “bunch”. The definition of a bunch and a bucket from the accelerator physics perspective, please see Chap. 2. There are two buckets at the left ring and every bucket keeps a bunch. There are eight buckets in the right ring and two of them are filled with bunches. The left ring is connected to a transfer beamline by a switch, which is called a “switch 1”. When the switch 1 is off, bunches circulate around the ring. When it is on, bunches will be guided from the ring to the transfer beamline at a specific position around the ring, which is called the “extraction point” (represented as a black short bar on the left ring). The transfer beamline is connected to the right ring by another switch, called a “switch 2”. When the switch 2 is on, bunches will be guided from the transfer beamline to the right ring at a specific position around the ring, which is called the “injection point” (represented as a black short bar on the right ring). Generally both switches are off. The bunch-to-bucket (B2B) transfer is defined as that bunches of the left ring are transferred to the correct buckets at the right ring. For the B2B transfer, bunches at the left ring and buckets at the right ring must have not only a constant but same velocity. Because the circumference of the right ring is four times longer than that of the left ring, bunches run four cycles of the left ring when buckets run one cycle of the right ring. The distance between two bunches of the left ring is equal to the distance between two continuous buckets of the right ring. Besides, the relative position between bunches and buckets must match. Bunches of the left ring are guided to the transfer beamline and transferred

CHAPTER 1. INTRODUCTION

to the right ring. They are guided exactly to two empty buckets of the right ring. Every time when a bunch of the left ring passes by the extraction point, a bucket of the right ring will pass by the injection point after a specific time delay, which equals to the time-of-flight of a bunch in the transfer beamline. What's more, the time for the beam guide in the transfer beamline is of great importance, determining which buckets to be filled. In Fig. 1.1, two empty buckets closely following the filled buckets of the right ring need to be filled (represented as the dotted ellipse). The switch 2 must be switched on when the first empty bucket following two filled buckets passes the injection point and the switch 1 must be switched on a specific time earlier, when a bunch passes by the extraction point.

The ring is called a “source ring“, from which the beam is extracted. The ring is called a “target ring“, into which the beam is injected. From the above illustration, several preconditions are compulsory for the B2B transfer. The first precondition is that bunches of the source ring and buckets of the target ring have a constant speed, namely the revolution frequencies of the two rf systems of the source and target rings must be constant and therewith the constant cavity rf frequencies, which are harmonics of the revolution frequencies. Beam feedback loops on the rf system are usually implemented in order keep the stability of the beam. The constant revolution frequency requires that the beam feedback loop must be switched off before the B2B transfer. The second precondition is that bunches and buckets are with a same speed, which requires that the revolution frequency ratio between two rings is equal to the reciprocal of the circumference ratio. When the circumference ratio between two rings is an integer, the phase difference between two revolution frequencies is constant. It means that bunches always pass the extraction position a constant time earlier/later before/after buckets pass the injection position. But the constant phase difference is not correct for the transfer. In order to get the correct phase difference, an azimuthal positioning of bunches in the source ring or buckets in the target ring must be adjusted. This is called “phase shift method“. After the phase shift, the phase difference of two revolution frequencies is correct and the correct phase difference stays for an infinite time theoretically. Because beam feedback loops are switched off, the beam is stable only for a short period of time. So the beam must be transferred as soon as possible. When the circumference ratio is not an integer, the phase difference between two revolution frequencies of particles orbiting in the rings varies periodically. Within one period, there must be one point in time when the phase difference between the two rf systems is correct. Before and after this time point, there exists the mismatch between bunches and buckets. The earlier and later than this time point within a period, the larger the mismatch. Waiting for the phase difference to match is called ”frequency beating method“. For both the phase shift and frequency beating methods, the transfer can only happen when the mismatch is smaller than a tolerable limit, introducing a time frame. The time frame is called the “synchronization window“, which achieves the “coarse synchronization“ between the machines.

Bunches are switched from one path to another path by kicker magnets (short: kicker). The extraction kicker kicks bunches out of the source ring to the transfer beamline and the injection kicker kicks them from the transfer beamline into buckets of the target ring. They are located at the extraction position and injection position in Fig. 1.1. When the phase difference between the two rf systems is correct, the extraction kicker could kick bunches out of the source ring at the exact time-of-flight

1.1. Bunch-to-Bucket Transfer worldwide

to the transfer beamline before empty buckets pass the injection kicker. With the synchronization window, the extraction and injection kickers must be fired at the correct time in order to transfer bunches into correct empty buckets. The process of the kicker firing at the correct time is termed as the “fine synchronization”.

1.1 Bunch-to-Bucket Transfer worldwide

Nowadays, there are several accelerator institutes in the world, who operate the B2B transfer among rings for specific purposes. CERN, the European Organization for Nuclear Research, is one of the world’s largest and most respected center for scientific research. The Large Hadron Collider (LHC) beam injection chain achieves the proton beam with the energy of 7 TeV. After accelerated by a linear accelerator, bunches are injected into buckets of the Proton Synchrotron Booster (PSB) and further into the Proton Synchrotron (PS), the Super Proton Synchrotron (SPS) and LHC [3]. For the LHC heavy ion beam injection chain with the achievement of the energy of 2.76 TeV/u, bunches are first of all injected into the Low Energy Ion Ring (LEIR) and the following transfer from PSB to LHC is same as the proton beam chain [3]. For the Japan Proton Accelerator Complex (J-PARC), bunches are transferred from the Rapid Cycle Synchrotron (RCS) to buckets of the Main Ring (MR) [4]. The Booster of Brookhaven National Laboratory (BNL) transfers bunches to buckets of the Alternating Gradient Synchrotron (AGS) and bunches of AGS are transferred further into the Relativistic Heavy Ion Collider (RHIC) [5]. Fermi National Accelerator Laboratory (Fermilab)’s accelerator complex provides high energy proton beams for a broad range of experiments. Proton beams are injected into the Recycler from the Fermi National Accelerator Laboratory (Fermilab) Booster. Then the proton beam enters the Main Injector from the Recycler. The beam is accelerated to the energy of 120 GeV. Some of the proton beam from the Booster will be used to produce a beam of special particles for the Muon Delivery Ring. The Muon Delivery Ring delivers the beam into a muon storage ring for further study [6]. Institute of Modern Physics of the Chinese Academy of Sciences (IMP) operates the Heavy Ion Research Facility in Lanzhou (HIRFL). Two existing cyclotrons, the Sector Focusing Cyclotron (SFC) and the Separated Sector Cyclotron (SSC), are used as an injector system for the Cooler Storage Ring main ring (CSRm) for the accumulation, cooling and acceleration. Then the beam is extracted from CSRm to produce radioactive ion beams or highly-charged heavy ions, which can be transferred to the Cooler Storage Ring experimental ring (CSRe) for many experiments [7].

FAIR, the Facility for Antiproton and Ion Research, is a new international accelerator facility under construction at GSI Helmholtz center for Heavy Ion Research GmbH (short: GSI)¹ [8, 9]. It is aiming at providing high-energy beams of ions from antiproton to uranium with high intensities. The new FAIR accelerator complex in its full version will consist of the SIS100², the SIS300³, the Collector Ring (CR) and the High Energy Storage Ring (HESR) [10, 11]. FAIR has so many rings, so the B2B transfer among FAIR ring accelerators is of great importance to

¹Planckstrasse 1, 64291 Darmstadt, www.gsi.de

²SIS18 stands for SchwerIonen Synchrotron (100 Tm magnetic rigidity).

³SIS300 stands for SchwerIonen Synchrotron (300 Tm magnetic rigidity).

1.2. Objectives, Contribution and Structure of the Dissertation

accelerate beams to higher energy with high intensity and achieve beams for various experiments. Based on the existing GSI UNILAC and SIS18 serving as injectors, high intensity ion beams over the whole range of stable isotopes will be accelerated in the new heavy ion machine SIS100/SIS300 to higher energy. The beam from the SIS100 will be transferred to the CR via the antiproton bar (pbar) target ⁴ or the Superconducting Fragment Separator (Super-FRS) ⁵. The CR has the purpose of stochastic cooling of both secondary rare isotope and antiproton beams and of measuring nuclear masses [12, 13]. The CR transfers the beam to the HESR for the accumulation. The HESR serves experiments with high energy antiproton and rare isotope beams [14]. The proton and heavy ion beams could also be transported from the SIS18 to the existing GSI Experimental Storage Ring (ESR) and further to the first FAIR-storage ring CRYRING@ESR (short: CRYRING) for the atomic and nuclear physics experiment [15, 16]. The proton and heavy ion beams could also be transferred from the SIS18 to the ESR via the Fragment Separator (FRS)⁶.

For many FAIR accelerator pairs, the circumference ratio between the large and small rings is an integer, e.g. the SIS100 and the SIS18, so the phase difference between two revolution frequencies of rings is constant. The frequency is in the MHz range. In this scenario, the phase shift method must be used for the match of the phase difference between the two rf systems. When the circumference ratio between FAIR accelerator pairs is not an integer, e.g. the SIS18 and the ESR ⁷, the phase difference between two revolution frequencies shifts automatically. The frequency of the phase difference variability is in the kHz range. The synchronization window for the FAIR B2B transfer is in the μ s range. The beams of ion species, from hydrogen to uranium as well as antiproton and rare isotope beams, should be transferred among all rings. And every transfer must be achieved within the upper bound 10 ms and the B2B injection mismatch in the range between -1° and $+1^\circ$. Both the phase shift and the frequency beating method should be applicable in the upcoming FAIR facility. The B2B transfer system is designed to work in a parallel operation, e.g. the transfer from the SIS18 to the SIS100 and the transfer from the ESR to the CRYRING can be performed at the same time. It is capable to transfer the beam between two rings via the pbar target, the FRS or the Super FRS. The B2B transfer system must coordinate with the SIS100 emergency dump for all unacceptable failure or situation.

1.2 Objectives, Contribution and Structure of the Dissertation

This dissertation contributes to the development of the FAIR B2B transfer system from the timing perspective. It concentrates on the introduction of the concept of the FAIR B2B transfer system and its application for FAIR accelerators. In addition,

⁴The antiproton bar is used to produce antiprotons in inelastic collisions of high energy protons with nucleons of a target nucleus.

⁵Super-FRS is used to produce rare isotopes of all elements up to uranium at relativistic energies and spatially separate them within a few hundred nanoseconds.

⁶An ion-optical device used to focus and separate products from the collision of relativistic ion beams with thin targets.

⁷ESR has an injection/extraction orbit, which is 15 cm longer than the design orbit. The orbit of ESR in this dissertation means the injection/extraction orbit.

1.2. Objectives, Contribution and Structure of the Dissertation

it explains the systematic investigation for the FAIR B2B transfer system in details.

The dissertation is structured as follows and as depicted in Fig. 1.2.

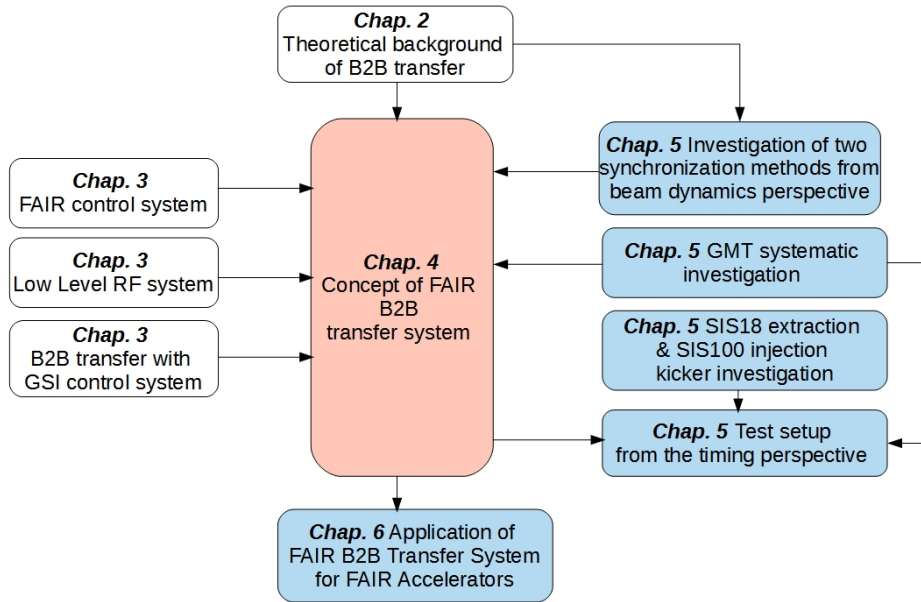


Figure 1.2: Structure of the dissertation.

Contributions are marked blue and red is team work, existing systems or theory are not colored.

In Chap.2, the theoretical background for the B2B transfer is reviewed. First of all, the energy, phase and voltage match between the source and target rings are introduced. Secondly, two rf synchronization methods are discussed from the perspective of beam dynamics for the phase alignment. At the end of this chapter, the synchronization of the extraction and injection kicker magnets are discussed.

Chap.3 is concerned with the existing FAIR technical basis for the development of the FAIR B2B transfer system. The B2B transfer system is realized based on the FAIR control system and low-level rf system, so these two systems are introduced.

In Chap.4, a brief overview on the basic idea of the B2B transfer system is presented. After that the basic procedure of the FAIR B2B transfer is introduced and the realization of each step of the procedure is explained. In addition, the FAIR B2B transfer system is explained from the data flow perspective. The comparison between the FAIR B2B transfer system and the current B2B transfer with the GSI control system is discussed before the chapter ends.

Chap.5 presents the systematic investigation for the B2B transfer system, mainly focusing on the timing aspect. The calculation of the synchronization window is explained and the transfer of the B2B messages via the white rabbit (WR) network is tested. In addition, for the B2B transfer from the SIS18 to the SIS100, two synchronization methods are analyzed from the perspective of the beam dynamics. The SIS18 extraction and the SIS100 injection kicker are systematically investigated. Finally, the test setup is presented and the result is analyzed.

The application of the FAIR B2B transfer system for FAIR accelerator pairs are outlined in Chap.6. The applications are classified into three categories according to the feature of the circumference ratio. Many FAIR use cases are with an inter-

1.2. Objectives, Contribution and Structure of the Dissertation

gral circumference ratio, e.g. the SIS18 and the SIS100, there is a constant phase difference between the two rf system. Although the phase shift can be used for the phase matching, the frequency beating method is preferred via the detune of one rf system. Because the phase shift must be executed slowly enough to guarantee the beam quality, which needs much longer time than the frequency beating method. The ratio of the circumference between many pair of machines in FAIR is close to an integer or far away from an integer, e.g. the SIS18 and the ESR, the SIS100 and the CR, the CR and the HESR. the phase matching is achieved by the frequency beating. For each category, the corresponding FAIR use cases are presented.

Chapter 2

Theoretical Background

In Chap. 1, the bunch and bucket are introduced with simplified definition. In this chapter, the bunch and bucket are first of all defined from the accelerator physics perspective in Sec. 2.1. Transferring bunches from a synchrotron into specific buckets of another synchrotron has several underlying basic principles. The energy of the beam is same before and after the B2B transfer, so the energy of the source synchrotron must match that of the target synchrotron. The amplitude of the accelerating voltage match of the two rf systems is needed to ensure that buckets capture bunches efficiently. Principally speaking, every synchrotron has its independent rf system. The phase difference between bunches and buckets must be precisely controlled before the transfer. The energy and voltage match will be done by machine physicists, which are out of the scope of this dissertation, so only the phase matching is explained in detail in Sec. 2.2. Two methods for the phase alignment between the two rf systems are discussed in Sec. 2.3. For the correct bucket injection, the bunch extraction must happen exactly the time-of-flight before the required bucket of the target synchrotron passes the injection kicker. The synchronization of extraction and injection kicker magnets are presented in Sec. 2.4.

2.1 Bunch and Bucket

For a ring accelerator, particles gain energy from electric field in longitudinal direction and are deflected by magnetic field to a particle orbit. An rf cavity operating at a resonance condition is used to provide a longitudinal accelerating voltage¹ u in the vacuum chamber.

$$u(t) = V_0 \sin(\phi_s + 2\pi f_{rf} t) \quad (2.1)$$

where V_0 is the amplitude of the rf voltage, ϕ_s is an initial phase, and f_{rf} is the frequency of the accelerating voltage. In order to accelerate particles with an accelerating voltage at the rf cavity, the cavity rf frequency must always be an integer multiple of the revolution frequency of particles.

$$f_{rf} = h f_{rev} \quad (2.2)$$

where the integer multiple h is called the “harmonic number”.

A particle who always sees the rf phase ϕ_s at the rf cavity with the revolution frequency f_{rev} and the momentum p is called a “synchronous particle”. For circular

¹Rf voltage with a single harmonic operation is considered in this dissertation.

2.1. Bunch and Bucket

accelerators, the revolution frequency is decided by the machine circumference and the particle velocity.

$$f_{rev} = \frac{\beta c}{2\pi R} \quad (2.3)$$

where R is the radius of the orbit $R = L/2\pi$, L is the orbit length. β is the relative velocity to the speed of light and c the speed of light. The differential of eq. 2.3 is

$$\frac{\Delta f_{rev}}{f_{rev}} = \frac{\Delta\beta}{\beta} - \frac{\Delta R}{R} \quad (2.4)$$

Because of the relation $\Delta f_{rf}/f_{rf} = \Delta f_{rev}/f_{rev}$, so eq. 2.4 can be written as

$$\frac{\Delta f_{rf}}{f_{rf}} = \frac{\Delta\beta}{\beta} - \frac{\Delta R}{R} \quad (2.5)$$

The momentum of the synchronous particle p is related to the particle energy and its velocity.

$$p = \gamma\beta m_0 c \quad (2.6)$$

where m_0 is the rest mass and $\gamma = (1 - \beta^2)^{-\frac{1}{2}}$. γ is the relativistic factor, which measures the total particle energy, $E = pc/\beta$, in units of the particle rest energy, $E_0 = m_0 c^2$.

The fractional change in β is related to the fractional change in p .

$$\frac{\Delta p}{p} = \gamma^2 \frac{\Delta\beta}{\beta} \quad (2.7)$$

Substituting $\Delta\beta/\beta$ into eq. 2.5, we get

$$\frac{\Delta f_{rf}}{f_{rf}} = \frac{1}{\gamma^2} \frac{\Delta p}{p} - \frac{\Delta R}{R} \quad (2.8)$$

For the constant magnetic field, a particle will have a different orbit, if it is slightly shifted in momentum. The “momentum compaction factor” α_p is defined as eq. 2.9. The FAIR complex is with $\alpha_p > 0$.

$$\frac{\Delta R}{R} = \alpha_p \frac{\Delta p}{p} \quad (2.9)$$

Substituting eq. 2.9 into eq. 2.8, we finally obtain the required relation between the frequency offset and the momentum error.

$$\frac{\Delta f_{rf}}{f_{rf}} = \left(\frac{1}{\gamma^2} - \alpha_p \right) \frac{\Delta p}{p} \quad (2.10)$$

The phase-slip factor η is defined as

$$\eta = \frac{1}{\gamma^2} - \alpha_p \quad (2.11)$$

which gives the relationship between the revolution frequency and the momentum for a given accelerator. When particles are at low energy ($\eta > 0$), they run faster and arrive earlier at the rf cavity. When they are at high energy close to the speed

2.1. Bunch and Bucket

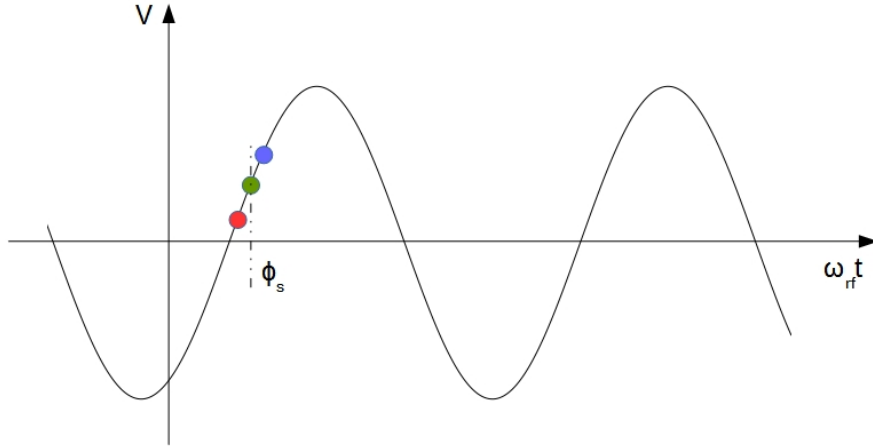


Figure 2.1: Longitudinal focusing of particles by an rf voltage ($\eta > 0$).

The red spot represents a particle with a higher energy, the blue spot a particle with a lower energy and the green dot the synchronous particle.

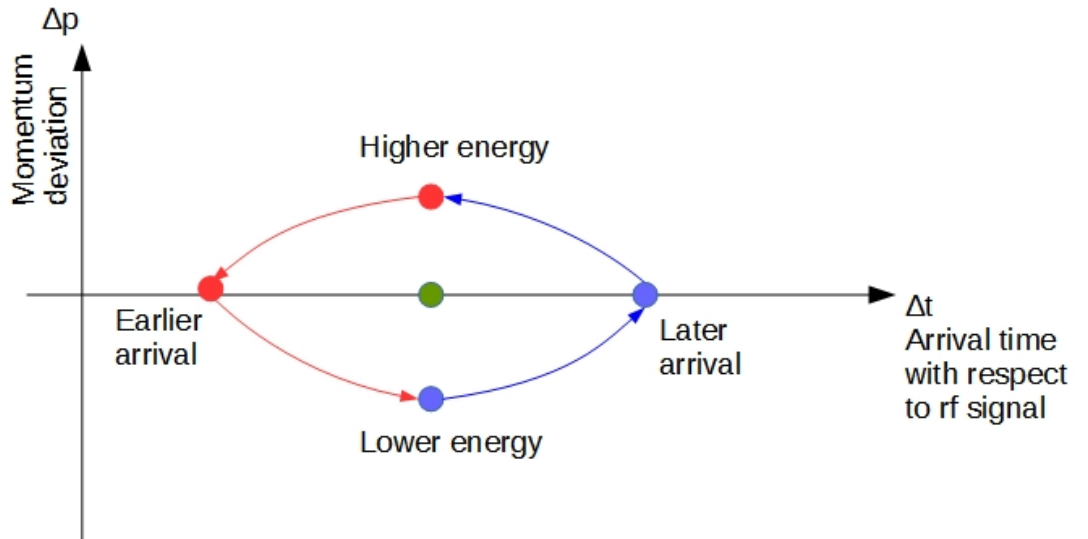


Figure 2.2: Longitudinal motion of asynchronous particles in the longitudinal phase space plane ($\eta > 0$).

The red spot represents a particle with a higher energy, the blue spot a particle with a lower energy and the green dot the synchronous particle. The red arrow shows the trend of a particle with a higher energy and the blue arrow the trend of a particle with a lower energy.

of light ($\eta < 0$), they cannot run faster, but rather obtain more mass and are pushed to a dispersive orbit, resulting a late arrival at the rf cavity [17].

A bunch of particles consists of particles with slightly different momentum as the synchronous particle, which are called “asynchronous particles”. When $\eta > 0$, the longitudinal focusing of particles is explained in Fig. 2.1.

2.1. Bunch and Bucket

The synchronous particle is indicated by the green spot in Fig. 2.1. It will gain the energy of $qV_0 \sin \phi_s$ per passage through an rf cavity, where q is the charge of a particle. When $\eta > 0$, a particle with a smaller energy (blue spot) than the synchronous particle will run slower and have a longer revolution period, arriving the same rf cavity later and seeing a higher accelerating voltage. This particle has a decreasing revolution period to the revolution period of the synchronous particle. During the decreasing process, the lack of energy is compensated step-by-step approaching to the energy of the synchronous particle. Oppositely for a particle with a higher energy. As it is faster than the synchronous particle and has a shorter revolution period, it will arrive at the rf cavity earlier, seeing a smaller accelerating voltage. This particle has an increasing revolution period to the revolution period of the synchronous particle. During the increasing process, the excess energy will be reduced step-by-step approaching to the synchronous particle. Asynchronous particles will oscillate longitudinally around the synchronous particle. This longitudinal motion is plotted in the longitudinal phase space plane, See Fig. 2.2.

All particles oscillate around the synchronous particle and stay together, forming a “bunch”. The “bunch gap” is the area without any particles. The area occupied by a bunch in the longitudinal phase space plane is called the “longitudinal emittance”. First of all, we consider the synchronous particle with the synchronous phase 0. In this scenario, particles with a small energy deviation follow an elliptical path inside the bunch. For a given rf system with a specific rf voltage and harmonic number, there exists a maximum energy deviation. For particles with energy deviations larger than the maximum energy deviation, they cannot be trapped around the synchronous particle. The trajectory of a particle with the maximum energy deviation in longitudinal phase space plane defines a region with a specific size and form. This region is called the “rf bucket” or “stationary rf bucket”, see Fig. 2.3. The maximum momentum deviation of the rf bucket is called the “bucket height”. These buckets will exist as soon as the rf voltage is switched on and the number of circulating buckets is determined by the harmonic number and the bucket area and height are proportional to the square root of the rf voltage [17]. The order of buckets to be filled is called the “bucket pattern”.

So far we give the definition of the bucket, when the synchronous particle sees no accelerating rf voltage. When the synchronous particle is accelerated, seeing the synchronous phase ϕ_s per passage through an rf cavity, it will gain the energy of $qV_0 \sin \phi_s$. Particles oscillate around the synchronous particle at ϕ_s with an elliptical orbit. The particle at $\pi - \phi_s$ traces a closed fish-shaped orbit, which defines a “running rf bucket”, see Fig. 2.4. Particles at bigger phase than $\pi - \phi_s$ cannot be captured by the bucket.

The “bucket size” is defined as the area of the longitudinal phase space plane enclosed by the bucket [17]. For a same rf voltage, the bucket size of a running bucket is always smaller than that of a stationary bucket. The ratio of the bucket size of a running bucket to that of a stationary bucket is called the “bucket area factor”, α_b . The bucket area factor can be calculated by [17].

$$\alpha_b(\phi_s) \approx \frac{1 - \sin \phi_s}{1 + \sin \phi_s} \quad (2.12)$$

The oscillation of asynchronous particles is called the “synchrotron motion”. The

2.1. Bunch and Bucket

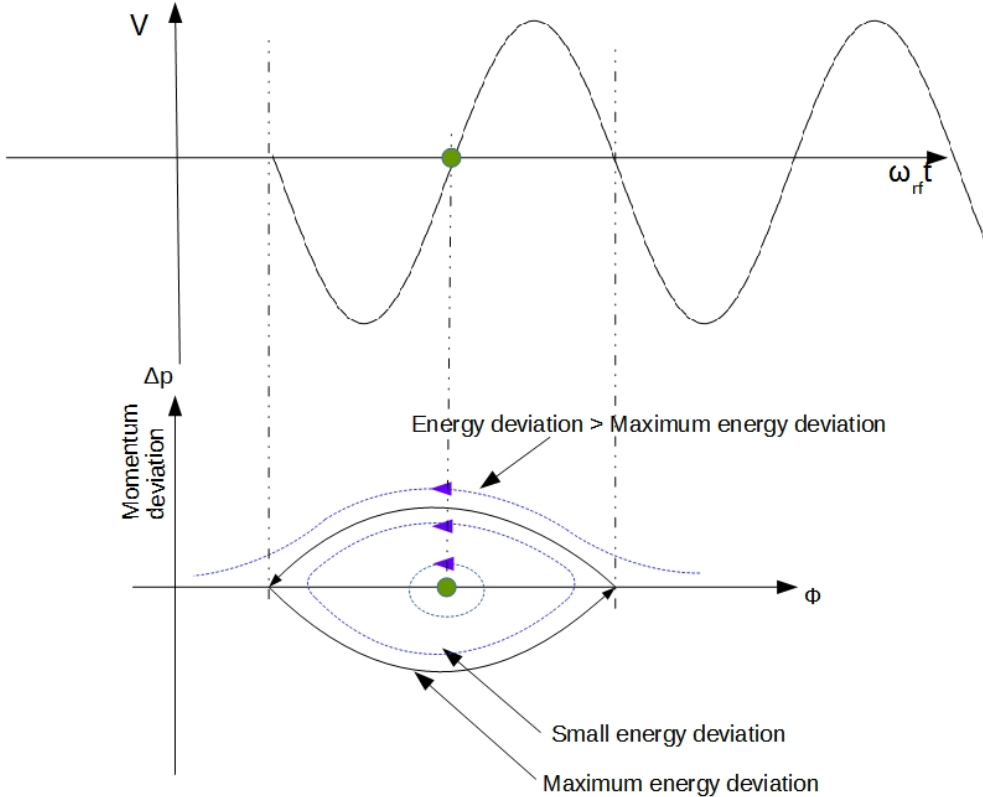


Figure 2.3: A stationary rf bucket.

The green dot represents the synchronous particle (top), the blue path orbits of asynchronous particles and the black path the boundary of a stationary rf bucket (bottom).

angular synchrotron frequency ² ω_s is [17]

$$\omega_s = 2\pi f_{rev} \sqrt{\frac{hqV_0|\eta \cos \phi_s|}{2\pi\beta^2 E_0}} \quad (2.13)$$

Bunches are always captured in buckets. A synchrotron can have same amount of bunches as buckets. It is also possible for a synchrotron to have less amount of bunches than buckets, e.g. only a part of buckets are filled by bunches. A train of bunches circulating along a synchrotron to be transferred to buckets is defined as a “batch”.

The energy of a beam is related to the ‘magnetic rigidity’, which is defined as the following:

$$B\rho = \frac{p}{q} \quad (2.14)$$

where B is magnetic field, and ρ is the bending radius of a particle immersed in a magnetic field B . The ratio of p to q describes the “stiffness” of a beam, it can be considered as a measure of how much angular deflection results when a particle travels through a given magnetic field [18]. The relation between the voltage of an rf cavity and the beam acceleration rate is

$$V_0 \sin \phi_s = 2\pi R\rho \dot{B} \quad (2.15)$$

²For the small-amplitude synchrotron motion.

2.1. Bunch and Bucket

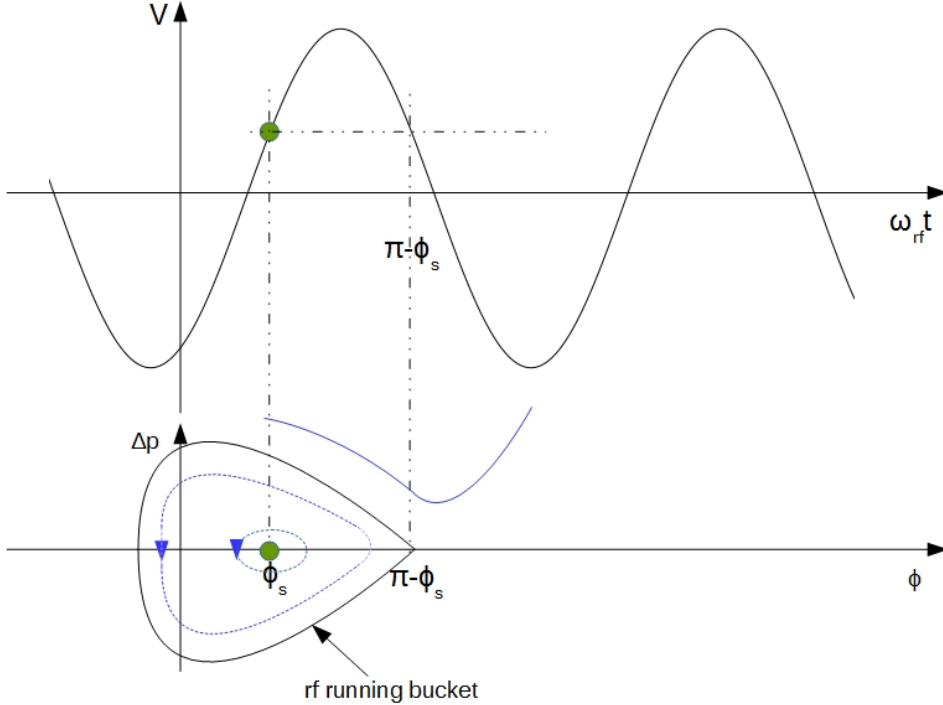


Figure 2.4: A running rf bucket.

The green dot represents the synchronous particle (top), the blue path orbits of asynchronous particles and the black path the boundary of a running rf bucket (bottom).

Bunches must be injected exactly in the center of buckets for the preservation of the longitudinal emittance, which requires the energy and phase matching between bunches and buckets. Besides, the shape of bunches to be transferred must match the shape of buckets to be injected in the longitudinal phase space plane. If the source and target synchrotrons have same cavity rf frequency, buckets of the source synchrotron must have same size and height as that of the target synchrotron. The voltage mismatch between bunches and buckets will cause an emittance blow-up. Fig. 2.5 illustrates a bunch-to-bucket injection with an energy, a phase or a voltage error.

The bunch coordinates in the longitudinal phase space plane of the source synchrotron, just before transfer, must be accurately controlled, according to the bucket to be filled [19]. The bunch is transferred from the source to the target synchrotron with the same energy. So the beam has the same momentum for both synchrotrons. According to eq. 2.14, the magnetic rigidity of two ring accelerators must be same.

$$(B\rho)^{src} = \frac{p}{q} = (B\rho)^{trg} \quad (2.16)$$

Where the superscript of the symbol denotes the synchrotron, *src* represents the source synchrotron and *trg* the target synchrotron.

Before the B2B transfer, the revolution frequency of two ring accelerators must meet the following relation based on eq. 2.3.

$$C^{src} f_{rev}^{src} = \beta c = C^{trg} f_{rev}^{trg} \quad (2.17)$$

2.2. Phase Difference

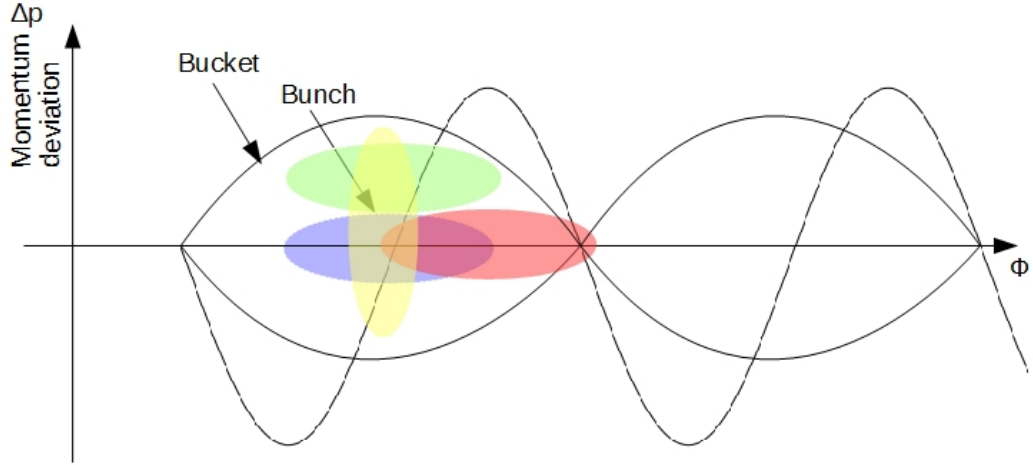


Figure 2.5: Bunch-to-Bucket injection with a phase, energy or voltage error.

The blue area represents an injection without any error, the red area an injection with a phase error, the green an injection with a energy error and the yellow an injection with a voltage error (e.g. the rf voltage in the target Synchrotron is too high).

where C^X represents the circumference of a specific synchrotron. A group of new symbols are necessary to be defined. The revolution frequency and cavity rf frequency are denoted by f_{rev}^X and f_{rf}^X , the cavity harmonic number by h_{rf}^X , the harmonic number of the revolution frequency by h_{rev}^X , which is defined as the first harmonic, namely $h_{rev}^X = 1$. The superscript X can be either *src* or *trg* denoting the source or target synchrotron.

Due to the relation between the revolution frequency and cavity rf frequency, eq. 2.2, the ratio between cavity rf frequencies of the two rf systems is

$$\frac{f_{rf}^{src}}{f_{rf}^{trg}} = \frac{h^{src}}{h^{trg}} \cdot \frac{f_{rev}^{src}}{f_{rev}^{trg}} = \frac{h^{src}}{h^{trg}} \cdot \frac{C^{trg}}{C^{src}} \quad (2.18)$$

The energy and voltage match will be done by machine physicists, which are out of the scope of this dissertation. The dissertation concentrates on the phase matching.

2.2 Phase Difference

The rf voltage of the two rf systems are $u_1(t)$ and $u_2(t)$.

$$u_1(t) = V_1 \sin(2\pi f_1 t + \phi_1) \quad (2.19)$$

$$u_2(t) = V_2 \sin(2\pi f_2 t + \phi_2) \quad (2.20)$$

where V_1 and V_2 are the amplitude, ϕ_1 and ϕ_2 the initial phases and f_1 and f_2 are the frequencies respectively.

The phase difference between u_1 and u_2 is

$$\Delta\phi = [2\pi(f_1 - f_2)t + \phi_1 - \phi_2] \mod 2\pi \quad (2.21)$$

The phase difference $\Delta\phi$ is constant when two frequencies are the same ($f_1 = f_2$). In order to change the phase difference for the phase matching between two rf

2.2. Phase Difference

voltages, the phase of either (or both) rf system can be shifted backward or forward by means of the rf frequency modulation. The frequency of one (or both) rf voltages is modulated away from the nominal value for a specified period of time and then modulated back. This is the so-called phase shift. Eq. 2.22 gives the relation between the required phase shift $\Delta\phi$ and the frequency modulation.

$$\Delta\phi = 2\pi \int_{t_0}^{t_0+T} \Delta f_{rf}(t) dt \quad (2.22)$$

The phase shift process starts at t_0 . The obtainable phase shift is determined by the frequency offset Δf_{rf} and the duration of the frequency modulation T .

When two frequencies are slightly different, the phase difference $\Delta\phi$ is a periodic function whose rate is the difference between two frequencies. This is the so-called frequency beating. The periodically variable rate is called the “beating frequency”, $\Delta f = |f_1 - f_2|$. The beating period is defined as a period of time for the periodical variation, namely $1/\Delta f$. Within one beating period, there exists a time point, which corresponds to a correct phase difference between the two rf systems, namely the phase alignment.

The phase alignment is realized based on two identical or two slightly different frequencies. These two frequencies are called “synchronization frequencies”, denoted as f_{syn}^X . Some FAIR use cases assume identical cavity rf frequencies or slightly different cavity rf frequencies. Therefore two cavity rf frequencies are chosen as the synchronization frequencies. There are quite some many FAIR use cases with big different cavity rf frequencies as well. In this scenario, two synchronization frequencies are an integer multiple of the same or slightly different derived rf frequencies, which are the fraction of the revolution frequencies. e.g. the fraction of the revolution frequency is f_{rev}^X/m and the synchronization frequency is $Y \cdot f_{rev}^X/m$, both m and Y are positive integers. The fraction of the revolution frequency and the integer multiple are determined by the circumference ratio and the harmonic number of two synchrotron. Because of the technical requirement (see Chap. 4), the synchronization frequencies cannot be higher than cavity rf frequencies, namely $Y/m \leq h_{rf}^X$. Besides, either m/Y or Y/m must be an integer for FAIR use cases, namely the revolution frequency is an integer multiple of the synchronization frequency or the synchronization frequency is an integer multiple of the revolution frequency, so the occurrence of positive zero-crossings of the synchronization frequencies and the positive zero-crossing of the revolution frequencies at the same time always indicates a specified bunch and bucket.

The calculation of the synchronization frequencies are explained for the different scenarios of the circumference ratio between two ring accelerators. For simplicity’s sake, the following analysis is from the perspective of the large and small synchrotrons instead of the source and target synchrotrons. The superscript X of C^X , f_{rev}^X , f_{rf}^X and h_{rf}^X will be either l or s denoting the large or small synchrotron. Δf represents the beating frequency, κ , m , n and Y are used to represent positive integers and λ a decimal number. The following analysis is based on the energy match between two ring accelerators.

2.2. Phase Difference

2.2.1 Circumference Ratio is an Integral

If the ratio of the circumference of the injection/extraction orbit of the large synchrotron to that of the small synchrotron is an integer, we have the following relation.

$$\frac{C^l}{C^s} = \kappa \quad (2.23)$$

From the circumference ratio, the revolution frequency ratio of two ring accelerators can be calculated.

$$\frac{f_{rev}^l}{f_{rev}^s} = \frac{1}{\kappa} \quad (2.24)$$

Based on eq. 2.24 and the harmonic number, the cavity rf frequency f_{rf}^X is calculated by eq. 2.25 and eq. 2.26

$$f_{rf}^s = h_{rf}^s \cdot f_{rev}^s = h_{rf}^s \cdot \kappa \cdot f_{rev}^l \quad (2.25)$$

$$f_{rf}^l = h_{rf}^l \cdot f_{rev}^l \quad (2.26)$$

Dividing eq. 2.26 by eq. 2.25, we get

$$\frac{f_{rf}^l}{f_{rf}^s} = \frac{h_{rf}^l}{h_{rf}^s \cdot \kappa} \quad (2.27)$$

In this scenario, the obvious choice of two same synchronization frequencies are f_{rf}^l/h_{rf}^l and $f_{rf}^s/(h_{rf}^s \kappa)$. The synchronization frequencies must be less than or equal to the cavity rf frequencies, otherwise they can not indicate the actual location of bunches and buckets. Generally, the rf frequency of $h=1$ is used as the revolution frequency and the phase/frequency modification is done for the revolution frequency due to the technical requirement, so the integer multiple of the revolution frequency is a preferable choice for the synchronization frequency. Hence, the best choice of two synchronization frequencies are

$$f_{syn}^l = \frac{f_{rf}^l}{h_{rf}^l/Y} = Y f_{rev}^l = h_{syn}^l f_{rev}^l \quad (2.28)$$

$$f_{syn}^s = \frac{f_{rf}^s}{h_{rf}^s \kappa / Y} = \frac{Y}{\kappa} f_{rev}^s = h_{syn}^s f_{rev}^s \quad (2.29)$$

where Y is defined as the Greatest Common Divisor (GCD) of h_{rf}^l and $h_{rf}^s \cdot \kappa$ and h_{syn}^X the harmonic number of the synchronization frequency.

In eq. 2.21, the phase difference between f_1 and f_2 equals to $\phi_1 - \phi_2$ when $f_1 = f_2$. The value of the initial phase is related to the choice of the rf frequency. e.g. when the phase of rf frequency f_1 is ϕ_1 , the phase of the rf frequency Nf_1 is $(N\phi_1 \bmod 2\pi)$. Hence, the phase difference must be defined with regard to the dedicated rf frequencies. The phase difference between two synchronization frequencies f_{syn}^l and f_{syn}^s is denoted as $\Delta\phi_{syn}$. ϕ_0^X denotes the initial phase of the synchronization frequency. The phase difference $\Delta\phi_{syn}$ calculated as

$$\Delta\phi_{syn} = (\phi_{syn}^l - \phi_{syn}^s) \bmod 2\pi \quad (2.30)$$

The cavity rf frequency of a synchrotron is h_{rf}^X/h_{syn}^X times as large as its synchronization frequency, so the phase difference between the cavity rf frequencies $\Delta\phi_{rf}$

2.2. Phase Difference

is also h_{rf}^X/h_{syn}^X times as large as the phase difference between two synchronization frequencies $\Delta\phi_{syn}$. $\Delta\phi_{rf}$ is the bunch-to-bucket injection center mismatch, so $\Delta\phi_{rf}$ is always with regard to the target synchrotron, namely $X = \text{trg}$.

$$\Delta\phi_{rf} = \frac{h_{rf}^{\text{trg}}}{h_{syn}^{\text{trg}}} \Delta\phi_{syn} \mod 2\pi \quad (2.31)$$

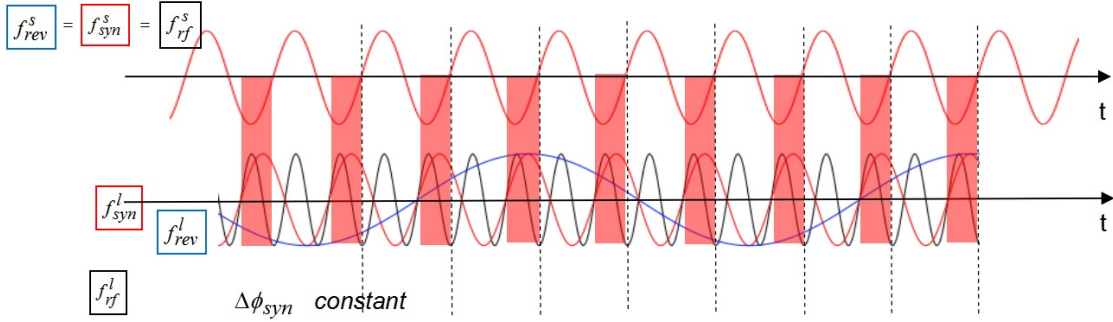


Figure 2.6: A constant phase difference between two synchronization frequencies f_{syn}^l and f_{syn}^s when $\kappa = 5$, $h_{rf}^s = 1$ and $h_{rf}^l = 10$.

Red planes represent the constant phase difference between two synchronization frequencies. The red sinusoidal waves in Fig. 2.6 are the individual synchronization frequencies. Black sinusoidal waves represent the individual cavity rf frequencies and the blue sinusoidal wave the revolution frequency. The red sinusoidal wave at the top time axis represents the synchronization frequency, the cavity rf frequency and the revolution frequency.

Fig. 2.6 illustrates two synchronization frequencies f_{syn}^l and f_{syn}^s , when $\kappa = 5$, $h_{rf}^s = 1$ and $h_{rf}^l = 10$. The GCD of h_{rf}^l and $h_{rf}^s \cdot \kappa$ is 5, namely $Y = 5$, $f_{rf}^l/f_{rf}^s = 2$, $f_{syn}^l = f_{rf}^l/2 = 5f_{rev}^s$, $f_{syn}^s = f_{rf}^s/1 = f_{rev}^s$ and $\Delta\phi_{rf} = 2\Delta\phi_{syn}$. The parameters are from the FAIR use case of the H^+ B2B transfer from the SIS18 to the SIS100, which will be explained in Sec. 6.1.2.

2.2.2 Circumference Ratio is close to an Integer

If the ratio of the circumference of the injection/extraction orbit of the large synchrotron to that of the small synchrotron is a decimal number close to an integer. Eq. 2.23 changes to

$$\frac{C^l}{C^s} = \kappa + \lambda \quad (2.32)$$

where κ is the integer part and λ is the decimal part of the decimal number and the absolute value of λ is smaller than 0.005 for FAIR use cases. The bound of λ is shown in Chap. 6. From the circumference ratio, the revolution frequency ratio of two ring accelerators can be calculated.

$$\frac{f_{rev}^l}{f_{rev}^s} = \frac{1}{\kappa + \lambda} \quad (2.33)$$

Based on eq. 2.33 and harmonic number, the f_{rf}^X are calculated by eq. 2.34 and eq. 2.35

$$f_{rf}^s = h_{rf}^s \cdot f_{rev}^s = h_{rf}^s \cdot (\kappa + \lambda) \cdot f_{rev}^s \quad (2.34)$$

2.2. Phase Difference

$$f_{rf}^l = h_{rf}^l \cdot f_{rev}^l \quad (2.35)$$

We get the relation between f_{rf}^s and f_{rf}^l by dividing eq. 2.35 by eq. 2.34.

$$\frac{f_{rf}^l}{f_{rf}^s} = \frac{h_{rf}^l}{h_{rf}^s \cdot (\kappa + \lambda)} = \frac{h_{rf}^l}{h_{rf}^s \cdot \kappa + h_{rf}^s \cdot \lambda} \quad (2.36)$$

In eq. 2.36, $h_{rf}^s \lambda$ is much smaller than $h_{rf}^s \kappa$, therefore $h_{rf}^s \lambda$ can be neglected for the calculation of the synchronization frequencies. Apart from the similar reasons mentioned in the scenario of the integral circumference ratio in Sec. 2.2.1, the synchronization frequencies with the integer multiple of f_{rf}^l/h_{rf}^l and $f_{rf}^s/(h_{rf}^s \kappa)$ achieve a more precise phase difference. Two best slightly different synchronization frequencies are

$$f_{syn}^l = \frac{f_{rf}^l}{h_{rf}^l/Y} = Y f_{rev}^l = h_{syn}^l f_{rev}^l \quad (2.37)$$

$$f_{syn}^s = \frac{f_{rf}^s}{h_{rf}^s \kappa / Y} = \frac{Y}{\kappa} f_{rev}^s = h_{syn}^s f_{rev}^s \quad (2.38)$$

Y is the GCD of h_{rf}^l and $h_{rf}^s \cdot \kappa$. Substituting two synchronization frequencies into eq. 2.21, we get the periodically variable phase difference between two synchronization frequencies $\Delta\phi_{syn}$.

$$\Delta\phi_{syn}(t) = [2\pi(f_{syn}^l - f_{syn}^s)t + \phi_{syn}^l - \phi_{syn}^s] \mod 2\pi \quad (2.39)$$

Substituting f_{rf}^l in eq. 2.36 into eq. 2.39, we get

$$\Delta\phi_{syn}(t) = [2\pi Y \frac{-\lambda f_{rf}^s}{(\kappa + \lambda) h_{rf}^s \kappa} t + \phi_{syn}^l - \phi_{syn}^s] \mod 2\pi \quad (2.40)$$

Eq. 2.40 shows that the phase difference is a periodic function. The beating frequency between two synchronization frequency is $\Delta f = |f_{syn}^l - f_{syn}^s|$. The beating frequency must not be too large in order to guarantee the precision, but also not too small to satisfy the time constraint for the phase matching. The phase difference between two cavity rf frequencies is

$$\Delta\phi_{rf} = \left(\frac{h_{rf}^{trg}}{h_{syn}^{trg}} \Delta\phi_{syn} \right) \mod 2\pi \quad (2.41)$$

Fig. 2.7 shows the periodically variable phase difference between two slightly different synchronization frequencies f_{syn}^l and f_{syn}^s when $\kappa = 2$, $\lambda = -0.003$, $h_{rf}^s = 2$ and $h_{rf}^l = 4$. The GCD of h_{rf}^l and $h_{rf}^s \cdot \kappa$ is 4, namely $Y = 4$. Hence, according to eq. 2.37 and eq. 2.38, two synchronization frequencies are $f_{syn}^l = f_{rf}^l = 4f_{rev}^l$, $f_{syn}^s = f_{rf}^s = 2f_{rev}^s$ and $\Delta\phi_{rf} = \Delta\phi_{syn}$. The parameters are from the FAIR use case of the h=4 B2B transfer from the SIS18 to the ESR, which will be explained in Sec. 6.2.1.

2.2.3 Circumference Ratio is far away from an Integer

When the circumference ratio of the large synchrotron to that of the small synchrotron is far away from an integer, the circumference ratio is a decimal number

2.2. Phase Difference

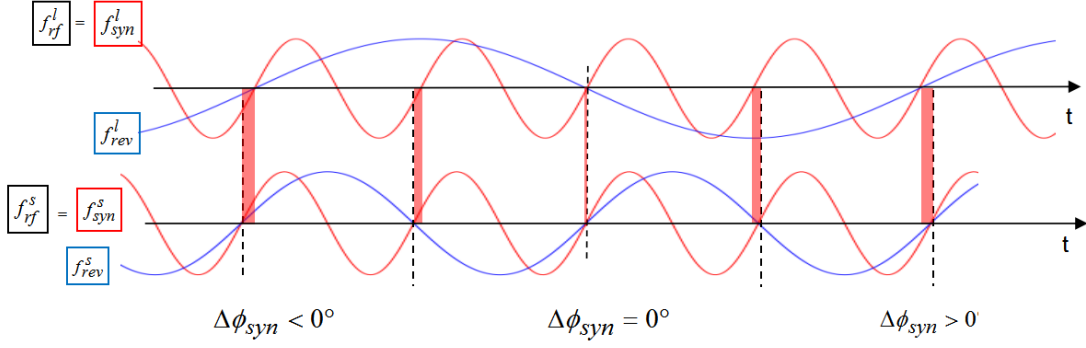


Figure 2.7: A periodically variable phase difference between two slightly different synchronization frequencies f_{syn}^l and f_{syn}^s when $\kappa = 2$, $\lambda = -0.003$, $h_{rf}^s = 2$ and $h_{rf}^l = 4$.

Red planes represent the periodical variable phase difference and red sinusoidal waves the synchronization frequencies and cavity rf frequencies and blue sinusoidal waves the revolution frequencies.

and eq. 2.23 can be expressed as a rational number plus a small remainder of the decimal number.

$$\frac{C^l}{C^s} = \frac{m}{n} + \lambda \quad (2.42)$$

where m/n represents a quotient of two integers, m is a numerator and n is a non-zero denominator. λ represents the remainder of the decimal part and the absolute value of λ is smaller than 0.05 for FAIR use cases.

Substituting κ by m/n into eq. 2.36, we get the relation between f_{rf}^s and f_{rf}^l .

$$\frac{f_{rf}^l}{f_{rf}^s} = \frac{h_{rf}^l \cdot n}{h_{rf}^s \cdot m + h_{rf}^s \cdot \lambda \cdot n} \quad (2.43)$$

In eq. 2.43, $h_{rf}^s \lambda n$ is much smaller than $h_{rf}^s m$. Similarly as the scenario of the close to an integral circumference ratio in Sec. 2.2.2, two slightly different synchronization frequencies are

$$f_{syn}^l = \frac{f_{rf}^l}{h_{rf}^l n / Y} = \frac{Y}{n} f_{rev}^l = h_{syn}^l f_{rev}^l \quad (2.44)$$

$$f_{syn}^s = \frac{f_{rf}^s}{h_{rf}^s m / Y} = \frac{Y}{m} f_{rev}^s = h_{syn}^s f_{rev}^s \quad (2.45)$$

Y is the GCD of $h_{rf}^l n$ and $h_{rf}^s m$. Substituting two synchronization frequencies into eq. 2.21, we get the periodical phase difference $\Delta\phi_{syn}$.

$$\Delta\phi_{syn}(t) = [2\pi(f_{syn}^l - f_{syn}^s)t + \phi_{syn}^l - \phi_{syn}^s] \mod 2\pi \quad (2.46)$$

Substituting f_{rf}^l in eq. 2.43 into eq. 2.46, we get

$$\Delta\phi_{syn}(t) = [2\pi Y \frac{-\lambda f_{rf}^s}{(m/n + \lambda) h_{rf}^s m} t + \phi_{syn}^l - \phi_{syn}^s] \mod 2\pi \quad (2.47)$$

2.3. Phase Match of Two Rf Systems

Eq. 2.47 shows that the phase difference is a periodic function. The beating frequency is $\Delta f = |f_{syn}^l - f_{syn}^s|$. It is possible to have various combination of m/n and λ . λ determines the beating frequency. The smaller, the more precise the phase matching between two synchronization frequencies. Y/n and Y/m determines two synchronization frequencies. For FAIR use cases, n/Y and m/Y are always integer. So the synchronization frequencies are the fraction of the revolution frequencies ($h=1$), which is called the “subharmonic”. Hence, we have to find a proper combination of m/n and λ . The phase difference between two cavity rf frequencies is

$$\Delta\phi_{rf} = \left(\frac{h_{rf}^{trg}}{h_{syn}^{trg}} \Delta\phi_{syn} \right) \bmod 2\pi \quad (2.48)$$

Fig. 2.8 shows the periodically variable phase difference between two slightly different synchronization frequencies f_{syn}^l and f_{syn}^s when $m = 26$, $n = 10$, $\lambda = -0.003$, $h_{rf}^s = 1$ and $h_{rf}^l = 1$. $f_{rf}^l/f_{rf}^s = 1 \cdot 10/(1 \cdot 26 - 1 \cdot 10 \cdot 0.003)$. The GCD of $h_{rf}^l n = 1 \cdot 10$ and $h_{rf}^s m = 1 \cdot 26$ is 2, namely $Y = 2$. Hence, according to eq. 2.44 and eq. 2.45, two synchronization frequencies are $f_{syn}^l = f_{rf}^l/5 = f_{rev}/5$, $f_{syn}^s = f_{rf}^s/13 = f_{rev}/13$ and $\Delta\phi_{rf} = 5\Delta\phi_{syn}$. The parameters are from the FAIR use case of the B2B transfer from the CR to the HESR, which will be explained in Sec. 6.3.3.

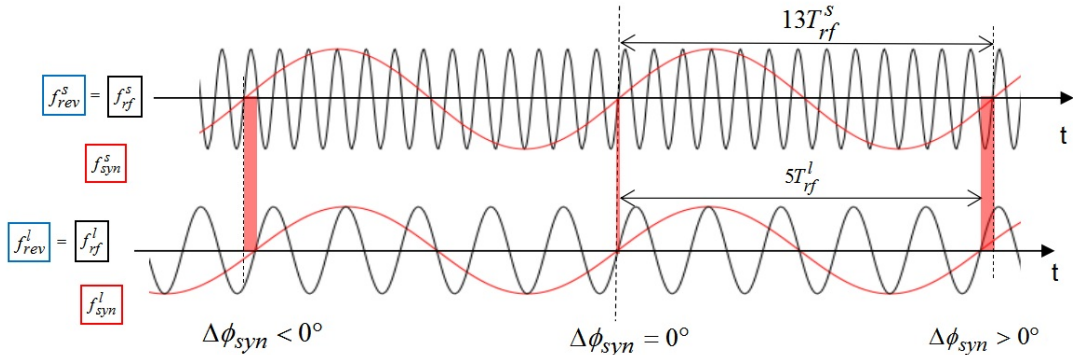


Figure 2.8: A periodically variable phase difference between two synchronization frequencies f_{syn}^l and f_{syn}^s when $m = 26$, $n = 10$, $\lambda = -0.003$, $h_{rf}^s = 1$ and $h_{rf}^l = 1$.

Red planes represent the periodical variable phase difference and red sinusoidal waves the synchronization frequencies. Black sinusoidal waves represent the cavity rf frequencies and the revolution frequencies.

2.3 Phase Match of Two Rf Systems

For the different scenarios mentioned in Sec. 2.2, two methods are available for the phase alignment of the two rf systems, the phase shift and the frequency beating methods. Both methods provide a time frame for the B2B transfer, within which bunches are transferred into buckets with the bunch-to-bucket injection center mismatch smaller than a given upper bound. This time frame is called the “synchronization window”. Both methods are based on the prerequisite that the phase difference between the two rf systems is predictable, so the LLRF feedback

2.3. Phase Match of Two Rf Systems

loops used for phase corrections must be switched off before the B2B transfer starts. e.g. beam phase feedback loop [20] and bunch-by-bunch longitudinal rf feedback loop [21].

2.3.1 Phase Shift Method

In order to change the constant phase difference between two synchronization frequencies, the phase of either (or both) rf system can be shifted backward or forward by means of the rf frequency modulation. The frequency of one (or both) rf system is modulated away from the nominal value for a specified period of time and then modulated back.

The phase shift process must be performed slowly enough for the preservation of the longitudinal emittance. After the phase shift, bunches of the source synchrotron are phase aligned with buckets of the target synchrotron. Theoretically the synchronization window is infinitely long. In fact, the beam feedback loops on the rf system are switched off before the B2B starts, so the beam is maybe only stable for a short period of time only, e.g. 10 ms. Hence, bunches must be transferred as soon as possible, introducing a synchronization window with a limited length.

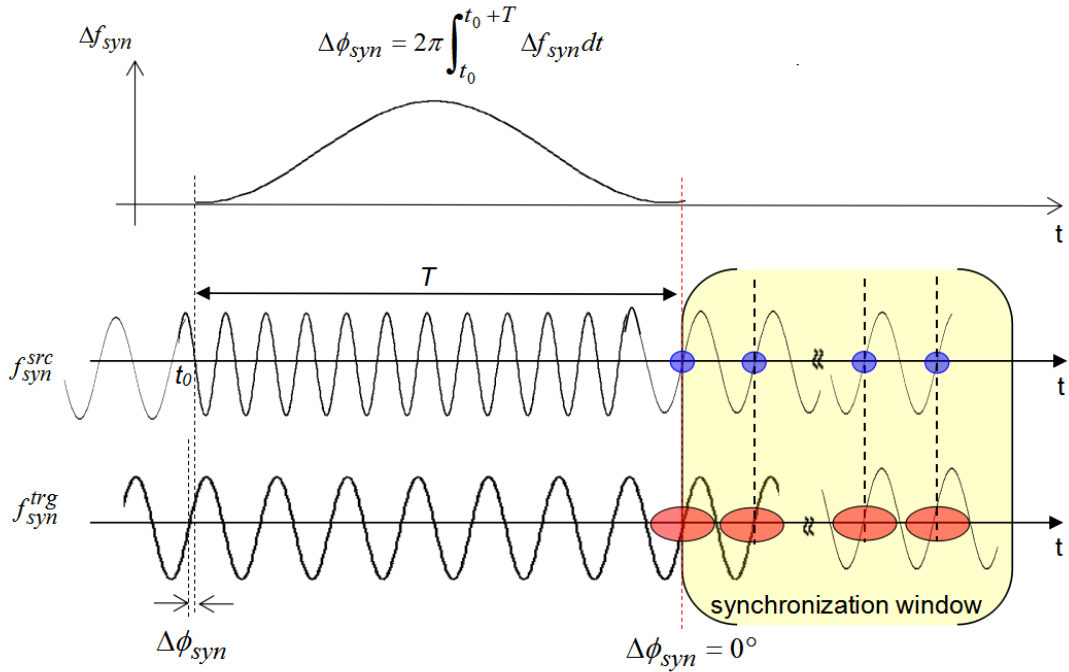


Figure 2.9: An example for the phase shift method with a sinusoidal rf frequency modulation.

Blue dots represent bunches of the source synchrotron and red dots buckets of the target synchrotron.

Fig. 2.9 illustrates an example for the phase shift method with a sinusoidal rf frequency modulation. The f_{syn}^l and f_{syn}^s are the synchronization frequencies respectively from the large and small synchrotrons. The time-of-flight between bunches and buckets is compensated here. The phase shift is done for the small synchrotron in this example. The red dashed line shows the end of the phase shift process

2.3. Phase Match of Two Rf Systems

$(\Delta\phi_{syn} = 0^\circ)$ and the beginning of the synchronization window, drawn in yellow. After the phase shift, bunches match with buckets. A sinusoidal frequency modulation Δf_{syn} with a fixed duration time T is used for the rf frequency modulation on f_{syn}^s .

$$\Delta f_{syn}(t) = A[1 - \cos \frac{2\pi}{T}(t - t_0)] \quad (2.49)$$

where A is the amplitude of the sinusoidal wave. Based on eq. 2.22, the area of the sinusoidal wave equals to $\Delta\phi_{syn}/2\pi$. We can calculate the amplitude A

$$A = \frac{\Delta\phi_{syn}}{2\pi} \cdot \frac{1}{T} \quad (2.50)$$

When the rf frequency modulation on the synchronization frequency f_{syn}^X is Δf_{syn} , the rf frequency modulation on the cavity rf frequency Δf_{rf} and the phase shift for the cavity rf frequency $\Delta\phi_{rf}$ are

$$\Delta f_{rf} = \frac{h_{rf}^X}{h_{syn}^X} \Delta f_{syn} \quad (2.51)$$

$$\Delta\phi_{rf} = (\frac{h_{rf}^{trg}}{h_{syn}^{trg}} \Delta\phi_{syn}) \mod 2\pi \quad (2.52)$$

A particular case of the B2B synchronization occurs, when the target synchrotron is empty, i.e. it did not capture any bunches yet, the phase jump can be done for the target synchrotron.

Now we analyze the rf frequency modulation of the phase shift from the beam dynamics perspective.

- Momentum shift and average radial excursion

An rf frequency modulation introduces a momentum shift.

$$\frac{\Delta p}{p} = \frac{1}{\frac{1}{\gamma^2} - \alpha_p} \cdot \frac{\Delta f_{rf}}{f_{rf}} \quad (2.53)$$

Substituting $\Delta R/R$ in eq. 2.9 into eq. 2.53, we get the radial excursion due to the rf frequency modulation.

$$\frac{\Delta R}{R} = \frac{1}{\frac{1}{\alpha_p \gamma^2} - 1} \cdot \frac{\Delta f_{rf}}{f_{rf}} \quad (2.54)$$

The rf frequency modulation causes a radial excursion. The maximum allowed radial excursion is a design parameter, which is given for a synchrotron lattice. Thus, a maximum frequency offset for the rf frequency modulation also exists.

- Shift of the synchronous phase

The rf frequency modulation is accompanied with a beam acceleration or deceleration, so the synchronous phase deviates from 0. Based on eq. 2.14, we can get the first derivative of the magnetic rigidity

$$\dot{B}\rho = \frac{1}{q} \frac{d\Delta p}{dt} = \frac{B\rho}{p} \frac{d\Delta p}{dt} \quad (2.55)$$

2.3. Phase Match of Two Rf Systems

Substituting $\dot{B}\rho$ in eq. 2.55 into eq. 2.15, we get the relation between the change in the synchronous phase and the momentum shift rate based on the prerequisite that $\Delta R/R$ and ϕ_s is very small. Because the synchronous phase before the phase shift is 0° , the synchronous phase change equals to the synchronous phase ϕ_s . The maximum radial excursion of FAIR synchrotrons $\Delta R/R$ is on the order of 10^{-4} and the synchronous phase is less than 10° .

$$V_0 \sin \phi_s \approx V_0 \phi_s = \frac{2\pi R B \rho}{p} \frac{d\Delta p}{dt} \quad (2.56)$$

It is clear from eq. 2.56 that when the rf frequency is modulated, ϕ_s is only determined by $\frac{d\Delta p}{dt}$, since the change of other parameters are very small and negligible. ϕ_s is proportional to the momentum shift rate $\frac{d\Delta p}{dt}$. In eq. 2.53, γ change very slowly as compared to Δp during the rf frequency modulation. So we can get the relation between $\frac{d\Delta p}{dt}$ and the rf frequency modulation rate $\frac{d\Delta f_{rf}}{dt}$ by the first derivative of eq. 2.53.

$$\frac{1}{p} \frac{d\Delta p}{dt} = \frac{1}{(1/\gamma^2 - \alpha_p) f_{rf}} \frac{d\Delta f_{rf}}{dt} \quad (2.57)$$

Substituting $\frac{d\Delta p}{dt}$ in eq. 2.57 into eq. 2.56, we get the relation between the change in the synchronous phase ϕ_s and the change rate of the rf frequency modulation.

$$V_0 \phi_s = \frac{2\pi R B \rho}{(1/\gamma^2 - \alpha_p) f_{rf}} \frac{d\Delta f_{rf}}{dt} \quad (2.58)$$

Hence, the synchronous phase change is proportional to $\frac{d\Delta f_{rf}}{dt}$.

- Bucket size

At the flattop, the bucket is a stationary bucket. During the frequency modulation process, the bucket becomes a running bucket with $\phi_s \neq 0^\circ$. When the synchronous phase is very small, we get the bucket area factor from eq. 2.12.

$$\alpha_b(\phi_s) \approx \frac{1 - \phi_s}{1 + \phi_s} \quad (2.59)$$

Substituting ϕ_s in eq. 2.58 into eq. 2.59, we get

$$\alpha_b(\phi_s) \approx \frac{(1/\gamma^2 - \alpha_p) f_{rf} V_0 - 2\pi R B \rho \frac{d\Delta f_{rf}}{dt}}{(1/\gamma^2 - \alpha_p) f_{rf} V_0 + 2\pi R B \rho \frac{d\Delta f_{rf}}{dt}} \quad (2.60)$$

Buckets must be big enough to capture bunches. Eq. 2.60 shows that the bucket area factor is in inverse proportion to $\frac{d\Delta f_{rf}}{dt}$. Hence, $\frac{d\Delta f_{rf}}{dt}$ must be small enough to guarantee the bucket size, namely the change of the rf frequency modulation must be slow enough.

- Adiabaticity

A process is called “adiabatic” when the rf frequency is changed slowly enough for the beam to follow. The condition that the rf frequency varies slowly can be expressed by

$$\varepsilon = \frac{1}{\omega_s^2} \left| \frac{d\omega_s}{dt} \right| \quad (2.61)$$

2.3. Phase Match of Two Rf Systems

where ε is the adiabaticity parameter. For the angular synchrotron frequency, eq. 2.13, all of the other variables change very slowly compared with ϕ_s . From eq. (2.61) and eq. (2.13), the adiabaticity can be written as follows [22]:

$$\varepsilon \approx \frac{1}{2\omega_s} |\dot{\phi}_s \phi_s| \quad (2.62)$$

Substituting ϕ_s and $\dot{\phi}_s$ in eq. 2.58 into eq. 2.62, we get

$$\varepsilon \approx \frac{1}{2\omega_s} \left[\frac{2\pi RB\rho}{(1/\gamma^2 - \alpha_p)f_{rf}V_0} \right]^2 \left| \frac{d\Delta f_{rf}}{dt} \frac{d^2\Delta f_{rf}}{dt^2} \right| \quad (2.63)$$

where ω_s is the angular synchrotron frequency with no frequency modulation. Form the adiabaticity eq. 2.63, $\frac{d\Delta f_{rf}}{dt}$ and $\frac{d^2\Delta f_{rf}}{dt^2}$ must exist and must be small enough to guarantee the adiabaticity. Namely, $\frac{d\Delta f_{rf}}{dt}$ must be continuous and the change of $\frac{d\Delta f_{rf}}{dt}$ must be slow enough.

- Tune shift

So far the rf frequency modulation is analyzed from the longitudinal beam dynamics perspective. Because of the momentum shift, the rf frequency modulation has an influence on the transverse beam dynamics as well. The beam particle's tune $Q_{x/y}$ is defined as the frequency of the horizontal/vertical oscillations and chromaticity $Q'_{x/y}$ is defined as their horizontal/vertical dependence on particle momentum [23]. The momentum spread $\Delta p/p \neq 0$ during the phase shift process causes horizontal/vertical tune shifts $\Delta Q_{x/y}$ [24].

$$\Delta Q_{x/y} = Q'_{x/y} \frac{\Delta p}{p} \quad (2.64)$$

The momentum shift of FAIR synchrotrons $\Delta p/p$ is in the 10^{-4} range and the chromaticity is on the order of 10. So the tune shift is relative small and has almost no influence on the transverse motion.

According to the beam dynamics analysis, there are several requirements for the rf frequency modulation:

- There exists a maximum rf frequency offset Δf_{rf_max} .
- $\frac{d\Delta f_{rf}}{dt}$ must be continuous and small enough.
- $\frac{d^2\Delta f_{rf}}{dt^2}$ must be small enough.

Application of these criterion to FAIR use cases, please see Chap. 5.

2.3.2 Frequency Beating Method

The frequency beating method uses two slightly different synchronization frequencies. When two synchronization frequencies are slightly different, two rf systems are beating automatically. When they are identical, either the rf system of the source or that of the target is detuned to achieve the beating. The frequency is detuned at constant energy by changing the frequency and magnetic field. This will be done by

2.3. Phase Match of Two Rf Systems

operators and is out of the scope of this dissertation. The frequency detuning for the synchronization frequency is denoted as Δf_{syn} and that for the cavity rf frequency is denoted as Δf_{rf} , $\Delta f_{rf} = \frac{h_{rf}^X}{h_{syn}^X} \Delta f_{syn}$. The synchronization window has a certain length, which is denoted as T_w . The synchronization window brings a symmetric time frame with respect to the time, when the phase difference between two synchronization frequencies is closest to the required phase difference, see yellow region in Fig. 2.10. The red dashed line shows the time of the closest to the required phase difference. The phase difference between two synchronization frequencies within the synchronization window is denoted as σ_{syn} and the bunch-to-bucket injection center mismatch within the synchronization window is denoted as σ_{rf} . There exists the following relation

$$\sigma_{rf} = \frac{h_{rf}^{trg}}{h_{syn}^{trg}} \sigma_{syn} \quad (2.65)$$

The bunch-to-bucket injection center mismatch is related to the length of the synchronization window, see eq. 2.66.

$$\sigma_{rf} = \pm \frac{1}{2} \cdot 2\pi |f_{syn}^{src} - f_{syn}^{trg}| \cdot T_w \cdot \frac{h_{rf}^{trg}}{h_{syn}^{trg}} \quad (2.66)$$

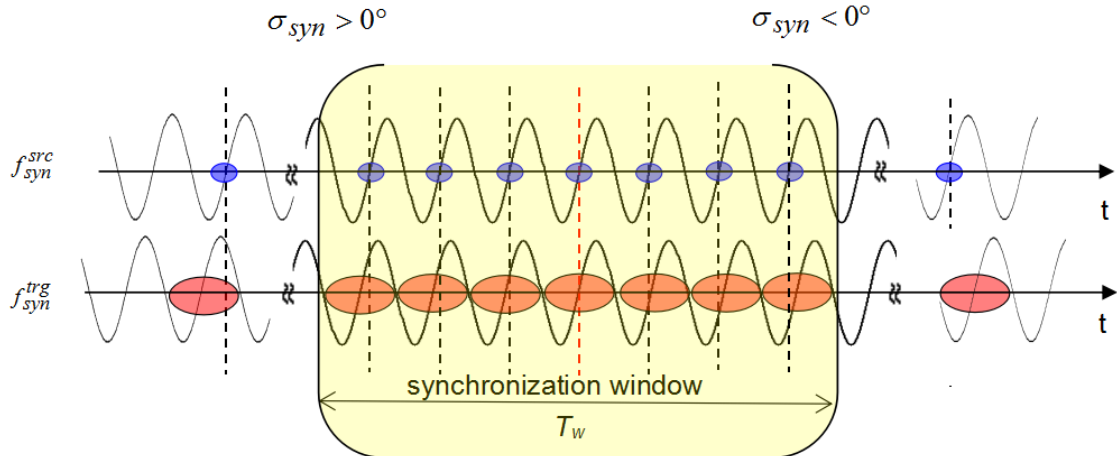


Figure 2.10: Illustration of the frequency beating method.

Blue dots represent bunches of the source synchrotron and red dots buckets of the target synchrotron.

In reality, all B2B transfer have a tolerable upper bound for the bunch-to-bucket center mismatch σ_{rf_max} (e.g. $\sigma_{rf_max} = \pm 1^\circ$ for FAIR use cases). The upper bound brings a maximum synchronization window T_{w_max} . The maximum synchronization window is

$$T_{w_max} = \frac{2|\sigma_{rf_max}| \cdot \frac{h_{syn}^{trg}}{h_{rf}^{trg}}}{2\pi} \cdot \frac{1}{|f_{syn}^{src} - f_{syn}^{trg}|} \quad (2.67)$$

The rf frequency is detuned at the end of the acceleration ramp. The rf frequency detuning is accompanied with the magnetic field and orbit change.

2.4. Synchronization of Extraction and Injection Kicker Magnets

- Radial excursion

Because the momentum should not be affected by the frequency detuning for the energy match, namely $\Delta p=0$, we can get the general relation between the radial excursion and the rf frequency change by substituting $\Delta p=0$ into eq. 2.8.

$$\frac{\Delta R}{R} = -\frac{\Delta f_{rf}}{f_{rf}} \quad (2.68)$$

$\frac{\Delta R}{R}$ constrained by the synchrotron lattice is used to check the acceptance.

2.4 Synchronization of Extraction and Injection Kicker Magnets

The proper bunch-to-bucket transfer requires not only that two rf systems are synchronized with each other, but also that the extraction and injection kicker magnets are synchronized with beam.

A kicker magnet (or kicker) is a dipole magnet, which is used to rapidly switch particles between two paths. An injection kicker merges one beam into a circulating beam in a synchrotron and an extraction kicker diverts a circulating beam to leave a synchrotron. Generally, the extraction or injection kicker is consisted of a certain number of kicker magnets instead of a single one. The B2B transfer needs a fast beam extraction and injection, which extracts and injects beam in a single-turn. Hence, a pulsed kicker magnet must be used with rapid rise time and fall time and the variable pulse flat-top [25]. Fig. 2.11 shows the schematic diagram of a kicker magnet. The energy storage module is charged with a high voltage power supply. It will be discharged via the transmission cable and the kicker magnet by using the pulse start switch. Before the increase of the magnetic field, there exist a preparation time for the kicker magnet. The magnet needs a certain period of time to increase from zero to a stable magnetic field, which is so-called a “kicker rise time” (short: rise time). The length of the “kicker flat-top” can be modified by switching on the stop switch in correlation with the pulse start switch. When the pulse stop switch is switched off, the magnet needs a certain period of time to reduce to zero magnetic field. This period is so-called a “kicker fall time” (short: fall time) [26]. For the proper B2B transfer, the extraction and injection kickers must be synchronized with the synchrotron rf signal. The start switch must be switched on the preparation time earlier before the tail of the circulating bunch passes the kicker, so that the transition of the kicker (the rise-up of the magnetic field) will be carried out during bunch gaps. The pulse stop switch must be switched off in time so that the transition of the kicker (the fall-down of the magnetic field) will not affect the head of the next coming bunch in the synchrotron. The kicker control electronic produces the ignition signal to switch on/off two switches. Generally a preparation time of FAIR kickers is within the 5–10 μ s range. Compared with the FAIR rf frequency in the MHz range, a preparation time is not negligible, which can cause an increase of the bunch-to-bucket injection center mismatch especially for the frequency beating method. The kicker control electronic must take the preparation time into consideration, igniting kickers in advance of the preparation time.

2.4. Synchronization of Extraction and Injection Kicker Magnets

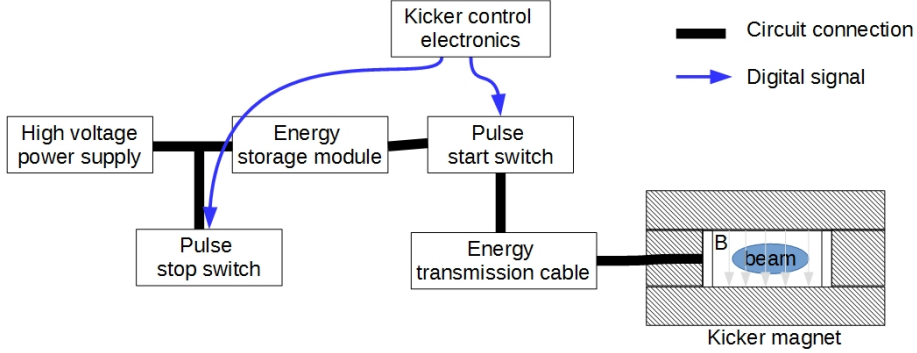


Figure 2.11: Schematic diagram of a kicker magnet.

Most commonly, an extraction kicker is used to eject all bunches. Fig. 2.12 illustrates the rise time, kicker flat-top and fall time of an extraction kicker. The tail of the circulating bunch passes the kicker at t_0 . The start switch is switched on the preparation time earlier than t_0 . The rise time starts at t_0 . The kicker flat-top of the magnetic field must be achieved before the head of the next circulating bunch passes the kicker at t_1 . So the rise time of the extraction kicker must be shorter than the bunch gap. The kicker flat-top has at least the length of bunches to be extracted. The stop switch is switched on earliest at t_2 , when all bunches are extracted. Then there is no more bunch left in the synchrotron, so there is no constraint for the fall time.

For multiple batches injection, see Fig. 2.13, the tail of the circulating bunch passes the kicker at t_0 . The start switch is switched on the preparation time earlier than t_0 . The rise time starts at t_0 . The kicker flat-top of the magnetic field must be achieved before bunches are injected at t_1 . So the rise time of the injection kicker must be shorter than the bunch gap. The length of the kicker flat-top is determined by the length of bunches to be injected. The stop switch is switched on as soon as the tail of the last injected bunch passes the kicker at t_2 . The magnetic field must be reduced to zero before the head of the circulating bunch passes the kicker at t_3 . So the fall time must be shorter than $t_3 - t_2$.

2.4. Synchronization of Extraction and Injection Kicker Magnets

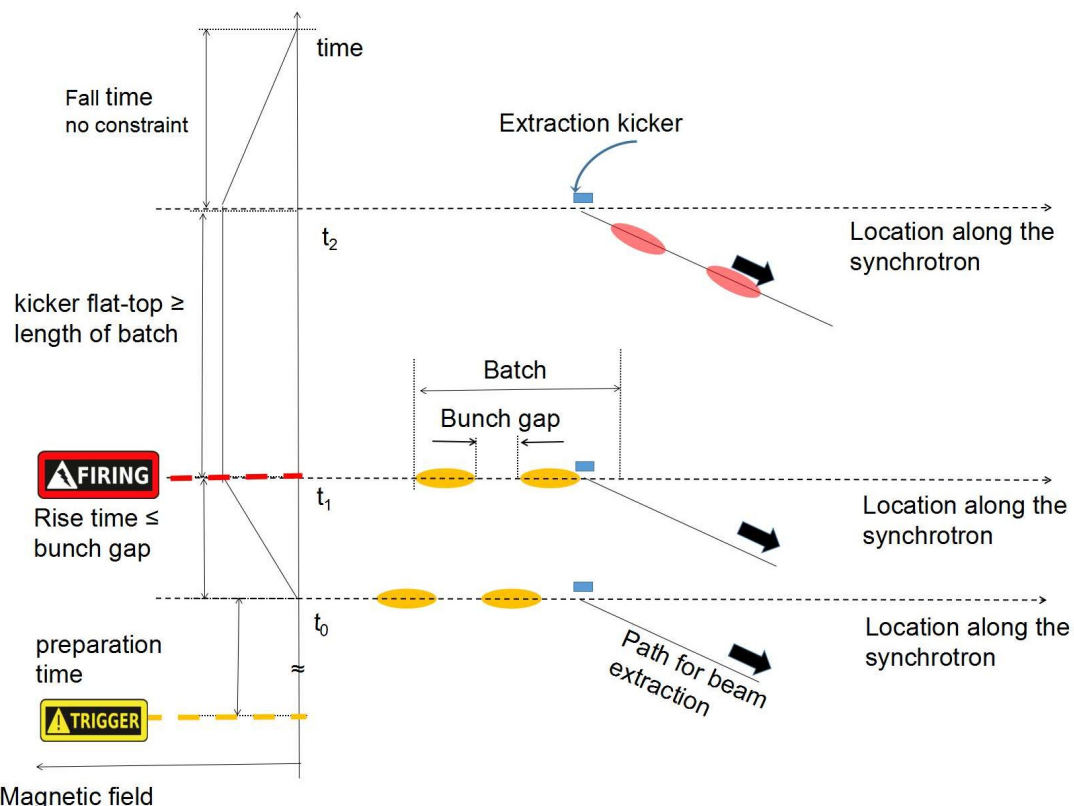


Figure 2.12: Rise time, kicker flat-top and fall time of an extraction kicker.

Yellow ellipses represent circulating bunches in the synchrotron, red ones extracted bunches. The warning sign indicates the kicker trigger and the flash sign indicates the kicker firing.

2.4. Synchronization of Extraction and Injection Kicker Magnets

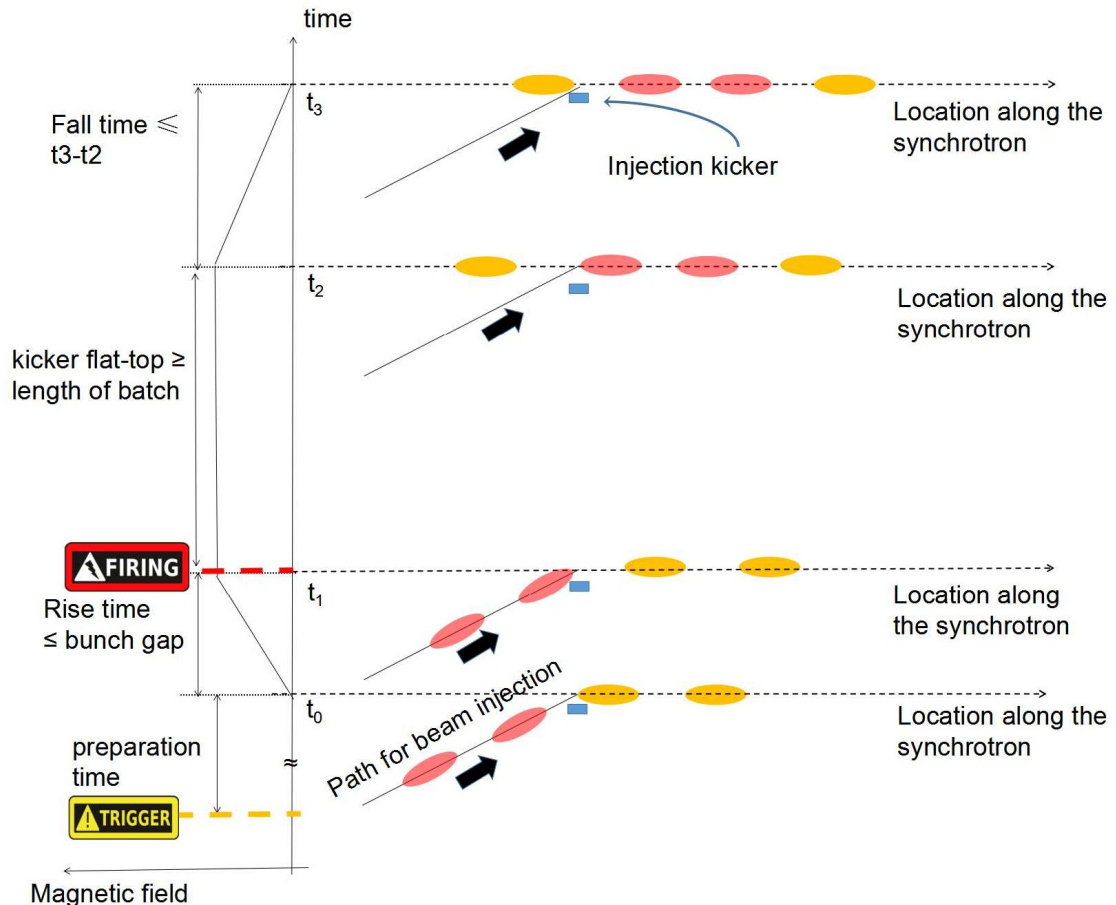


Figure 2.13: Rise time, kicker flat-top and fall time of an injection kicker for multiple batches injection.

Yellow ellipses represent circulating bunches in the synchrotron, red ones bunches to be injected.

Chapter 3

Technical Basis for the FAIR B2B Transfer System

For the FAIR accelerator complex, synchronization of the B2B transfer will be realized by the FAIR control system and the Low-Level RF (LLRF) system. For the synchronization of LLRF system, the General Machine Timing (GMT) system is complemented and linked to the Bunchphase Timing System (BuTiS). Machine Protection System (MPS) protects SIS100 and subsequent accelerators or experiments from damage. Hence, the B2B transfer system for FAIR coordinates with the MPS system.

3.1 FAIR Control System

The FAIR control system takes advantage of collaborations with CERN in using framework solutions like Front-End System Architecture (FESA) [27], LHC Software Architecture (LSA), White Rabbit (WR) [28]. It consists of the equipment layer, middle layer and application layer. The equipment layer consists of equipment interfaces, GMT and software representations of the equipment FESA. The middle layer provides service functionality both to the equipment layer and the application layer through the IP control system network. LSA is used for the Settings Management (SM). The application layer combines the applications for operators as GUI applications or command line tools. The application layer and the middle layer only request what the FAIR accelerator complex should do and transmit set values to the equipment layer. Before an accelerator cycle is started, the setting properties of FESA are pre-supplied by LSA from SM for all scheduled beams with specific settings accordingly. At run time, FESA real time software actions are triggered by timing message, the actual beam specific data is then selected based on information carried by the timing message and send to the equipment [28].

3.1.1 Bunch Phase Timing System

Bunch Phase Timing System (BuTiS) serves as a campus-wide clocks distribution system with sub nanosecond resolution and stability over distances of several hundred meters while maintaining 100 ps per km timing stability [29]. Two BuTiS reference clocks 100 kHz P0 pulse and 10 MHz S1 phase reference signal are generated centrally in the BuTiS center. A star-shaped optical fiber BuTiS distribution

3.1. FAIR Control System

system transfers these two reference clocks to the BuTiS local reference synthesizer all over the FAIR campus. The optical signal transmission delay between the BuTiS center and the different BuTiS local reference synthesizer is measured by a measurement setup in the BuTiS center. This measurement information is used to correct the phases of the signals generated in each BuTiS local reference synthesizer for the delay compensation. So at each BuTiS reference synthesizer, two delay compensated clock signals, 200 MHz C2 sine and 100 kHz T0 ident clocks, are generated from 100 kHz P0 and 10 MHz S1 reference clocks [29, 30]. The main task of BuTiS is the supply of the reference clock signals for phase measurement signal rf systems, see Sec. 3.2.

3.1.2 General Machine Timing System

The GMT system is contained in the equipment layer. It synchronizes all Front End Controllers (FEC) with nanosecond accuracy over the whole FAIR campus and distributes timing messages to all FECs and controls all FECs to execute real-time actions at a designated time [31]. The GMT system is a time based system. The GMT consists of the Timing Master (TM), the White Rabbit (WR) timing network and FECs. The timing master is a logical device, containing the data master (DM), the clock master (CM) and the management master (MM). The data master receives a schedule for the operation of the FAIR accelerator complex from the Settings Management and provides the real-time schedule by broadcasting timing messages to the WR timing network, which will be received and executed by the corresponding equipment connected to the FECs at the designated time. The clock master is a dedicated WR switch. It is the topmost switch layer of the WR timing network and provides the grandmaster clock and timestamps which are distributed to all other FECs in the timing network. The clock master derives its clock from BuTiS 200 MHz C2 and 100 kHz T0 clocks and timestamps distributed are phase locked to BuTiS clocks. The GMT system could generate BuTiS T0 and C2 with any FECs and FECs are capable to timestamp BuTiS T0 clocks and positive zero-crossings of BuTiS C2. All active components including FECs and WR switches are registered to the MM. The MM monitors and manages the active components of the GMT system [32, 33]. The Scalable Control Unit (SCU) [34] is a new generation of the standard FEC for the FAIR control system, which provides a compact and flexible solution for controlling all types of accelerator equipment.

A timing message is sent across the WR network, so it must be contained in the Ethernet frame. An Ethernet frame including one timing message has a length of 110 byte, which is called “timing frame” in this dissertation. For more details about the B2B transfer related timing frames, please see Appendix A. A Virtual LAN (VLAN)¹ is a group of FECs in the WR network that is logically segmented by function or application, without regard to the physical locations of the FECs. All FECs in the WR network are assigned to the DM VLAN, within which the DM forwards broadcast timing telegrams downwards to all FECs. For a specific VLAN, a broadcast frame is sent from one FEC to all other FECs within the VLAN and a unicast frame is sent from one FEC to another FEC.

¹https://en.wikipedia.org/wiki/Virtual_LAN

3.2. Low-Level RF System

3.1.3 Settings Management

The Settings Management (SM) is based on a physics model for accelerator optics, parameter space and overall relations between parameters and between accelerators. It supports off-line generation of accelerator settings, sending these settings to all involved devices, and programming the schedule for the GMT system [28]. The core component of SM is the LSA framework. A standardized LSA-API allows accessing data in a common way as basis for generic client applications for all accelerators. Using the LSA-API, applications can coherently modify settings [28]. E.g. the LSA generates timing constraints (e.g. ramp curve) as well as the equipment's data settings (e.g. the current) for all devices derived from physics parameters (e.g. beam energy). For FAIR, LSA is extended to model the overall schedule of all accelerators. Beams are described as “Beam Production Chains“ to allow a description from beam source to beam target for settings organization and data correlation.

3.1.4 FESA

The FESA² is a framework used to fully integrate the large amount of front-end equipment into the accelerator control system. FESA was developed by CERN and has already been implemented into the CERN control system. Now it is developed further in collaboration with GSI for the FAIR project. For the FAIR project the necessary interaction with the FECs is realized by FESA. For a specific type of equipment, a FESA implementation accesses to the control interface of the equipment. The FESA class models the equipment as device, so the FESA output is called device class. The FEC use FESA to implement generic and equipment specific functions in form of the device classes. FESA provides JAVA based graphical user interfaces (GUI) to design, deploy, instantiate and test the device classes. Interaction with the equipment is synchronized with the GMT system [27].

3.2 Low-Level RF System

The FAIR low-level rf (LLRF) system will be used in the existing synchrotrons SIS18 and ESR, as well as in the FAIR synchrotrons SIS100 and SIS300 and in CR and HESR. It supports fast ramp rates and large frequency span for the acceleration of a variety of ion species. It supports different rf manipulations, including operation at different harmonic numbers, barrier bucket generation, bunch compression and longitudinal feedback. [35].

Each rf supply room has a reference rf signal distribution system shown in Fig. 3.1. The reference rf signals in different supply rooms are synchronized by BuTiS. BuTiS 200MHz C2 and 100kHz T0 clock signals are generated by BuTiS receivers in different supply rooms in phase. In Fig. 3.1, a number of Group Direct Digital Synthesizer (DDS) units are located in each supply room, which are synchronized by BuTiS local reference. The Group DDS signals can be routed to the different cavity systems by a Switch Matrix. All cavities in a synchrotron could be providing with the same Group DDS signal. The cavities at different harmonic numbers could be realized by using Group DDS signals with different harmonic numbers

²<https://www-acc.gsi.de/wiki/FESA/WhatIsFESA>

3.2. Low-Level RF System

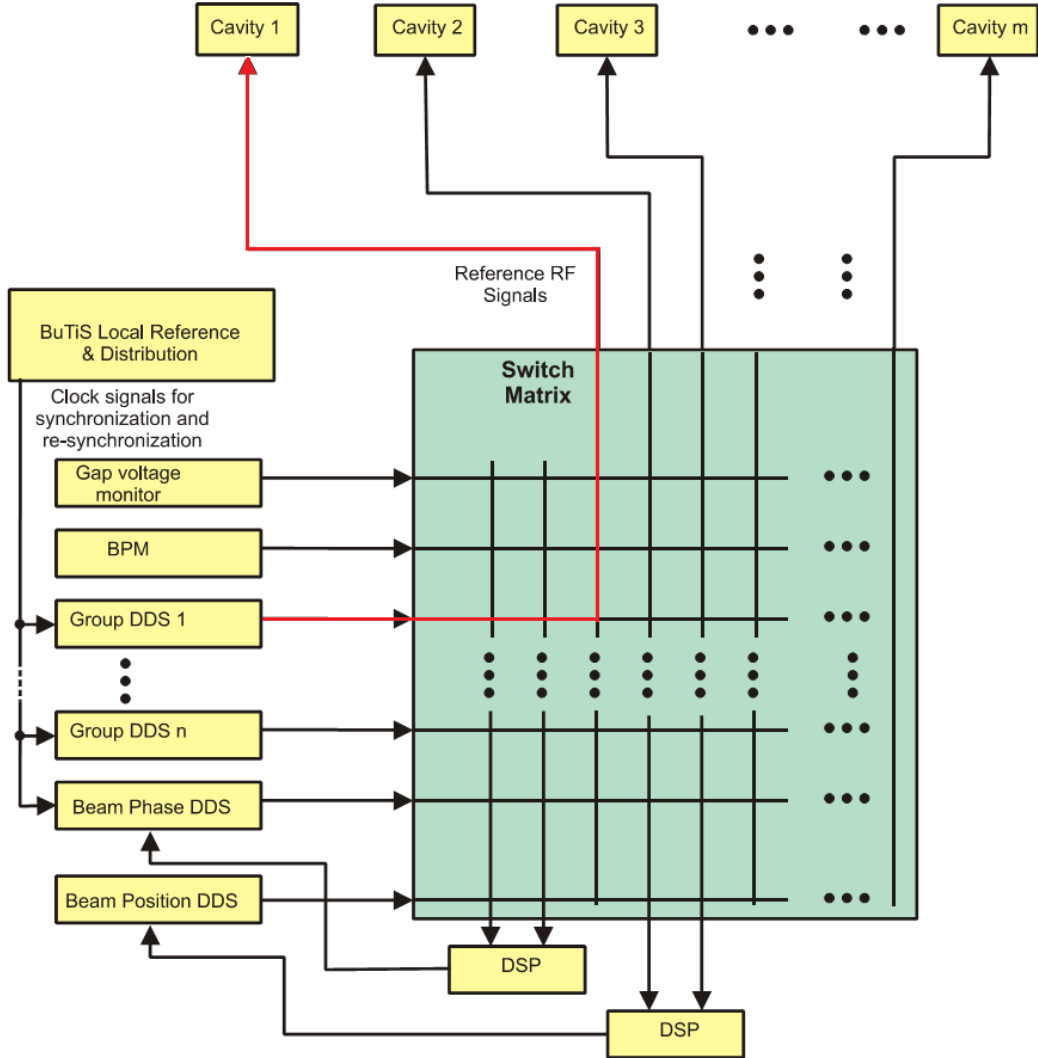


Figure 3.1: Reference rf signal distribution system

Adapted from “New Digital Low-Level RF System for heavy-ion Synchrotrons” by H. Klingbeil et al., 2011, *Physical Review Special Topics - Accelerators and Beams*, 14(10), 2011. ISSN 1098-4402. doi: 10.1103/PhysRevSTAB.14.102802. Adapted with permission.

and by adjusting the harmonic number at the Cavity DDS accordingly. The Group DDS concept allows to synchronize a variety of cavities in a very flexible way [35].

All the cavities of the SIS18 are driven from one supply room. The SIS100 cavities will be gathered in five acceleration sections, each of them is driven by a dedicated supply room.

3.2.1 Local Cavity Synchronization

All rf cavities are driven by one of reference rf signals, which are generated in each supply room . Fig. 3.2 shows the local cavity synchronization system, which synchronizes the local Cavity DDS unit to the reference rf signal with a specified phase offset. The cavity gets the rf signal from a local Cavity DDS unit, which receives rf frequency ramps from the Central Control System (CCS). A Digital Signal

3.2. Low-Level RF System

Processor (DSP)-System measures the phase difference between the reference rf signal and the gap voltage of the cavity. In the DSP system, a closed-loop control algorithm is implemented, which generates frequency corrections for the local Cavity DDS unit. This process is called local synchronization loop, which ensures that the phase of the gap voltage follows the phase of the reference rf signal [35]. The path from the Group DDS 1 to Cavity 1 marked with the red line in Fig. 3.1 is realized by the local cavity synchronization in Fig. 3.2. The virtual rf cavity is a virtual position around the ring, to which the reference rf signal corresponds.

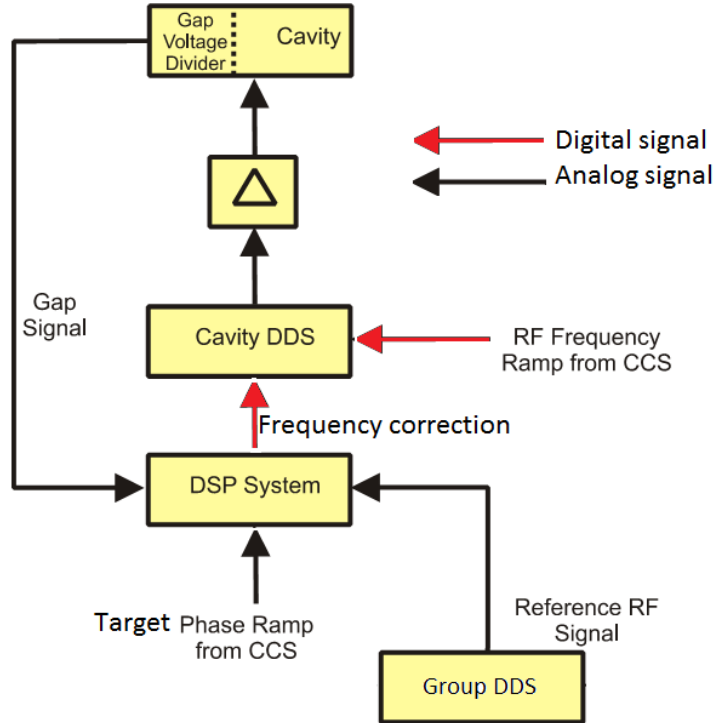


Figure 3.2: Local Cavity Synchronization

Adapted from “New Digital Low-Level RF System for heavy-ion Synchrotrons” by H. Klingbeil et al., 2011, *Physical Review Special Topics - Accelerators and Beams*, 14(10), 2011. ISSN 1098-4402. doi: 10.1103/PhysRevSTAB.14.102802. Adapted with permission.

3.2.2 Longitudinal Feedback System

In order to damp coherent longitudinal dipole oscillations, the beam phase control loop is used. The phase difference between the beam signal and the reference rf signal is fed back via an FIR filter. The beam signal is obtained by a fast current transformer or a beam position monitor. The filter output is converted in a phase-correction and forwarded to the Group DDS. The corrections are added to the phase of the frequency ramp in the Cavity DDS, which results in a change of the phase of the gap voltage and thus a feedback to the beam [36]. Unfortunately, the actual beam phase control loop in SIS18 is not able to damp incoherent longitudinal dipole oscillations. For SIS100, a bunch-by-bunch longitudinal feedback system will be

3.3. Machine Protection System

developed. The bunch-by-bunch longitudinal feedback system generates a correction voltage in dedicated feedback cavities for a specified bunch [21].

3.3 Machine Protection System

A MPS protects current accelerator and subsequent accelerators or experiments from damage or unacceptable failure, e.g. the beam position is out of tolerance, the rf cavity failure and so on. Thereby, the individual equipment is assumed self-protecting, which could triggers accelerator safety critical actions, such as an emergency beam dump ³, a shutdown of magnets or a beam injection inhibit. In case of relevant equipment failures or other inappropriate equipment states, a MPS signal is generated from this equipment [37]. The FAIR B2B transfer must coordinate with the SIS100 emergency dump signal and the beam injection inhibit signal from the MPS.

The SIS100 emergency dump signal indicates that the beam should be transferred to the emergency dump as soon as possible. If the beam injection inhibit signal is off, the B2B transfer extraction and injection kickers are allowed to be fired. If the beam injection inhibit signal is on, the injection and extraction kickers will be blocked for firing.

³A beam dump is a device designed to absorb the beam.

Chapter 4

Concept of the FAIR B2B Transfer System

In this Chapter, the basic idea of the FAIR B2B transfer system is presented in Sec. 4.1. The standard procedure of the system is defined and described in Sec. 4.2. Sec. 4.3 illustrates how the basic functionality of the system are realized. In Sec. 4.4, the data flow of the system is described. In Sec. 4.5 the FAIR B2B transfer system is compared with the current B2B transfer.

4.1 Basic Idea

The basic idea of the B2B transfer is simple. First of all, the two rf systems of the source and target accelerators must be correctly phase aligned. Secondly, the trigger for the extraction and injection kickers must be synchronized with the beam. In the end, the actual beam injection point must be indicated, which qualifies the beam instrumentation (BI) to measure the properties and the behavior of the beam directly after the injection.

4.1.1 Phase Alignment

The phase alignment is one of the most important prerequisites for the B2B transfer. It guarantees that extracted bunches will hit the dedicated empty buckets at the correct time. The phase alignment is based on the synchronization frequencies, see Sec. 2.2.

Before the basic steps for the achievement of the phase alignment are discussed, some basic concepts and their symbols are introduced, see Fig. 4.1.

- The bucket delay t_{bucket} , which specifies a certain bucket to be filled by delaying a certain number of the rf period compared to a marker.
- The Time-Of-Flight (TOF) between two ring accelerators t_{TOF} .
- The Time-Of-Flight between the virtual rf cavity and the extraction/injection kicker, t_{v_ext} and t_{v_inj} .
- The sum of the kicker preparation time, the rise time and the propagation delay of the kicker trigger signal in the cable of an extraction kicker and that of an injection kicker, t_{ext} and t_{inj} .

4.1. Basic Idea

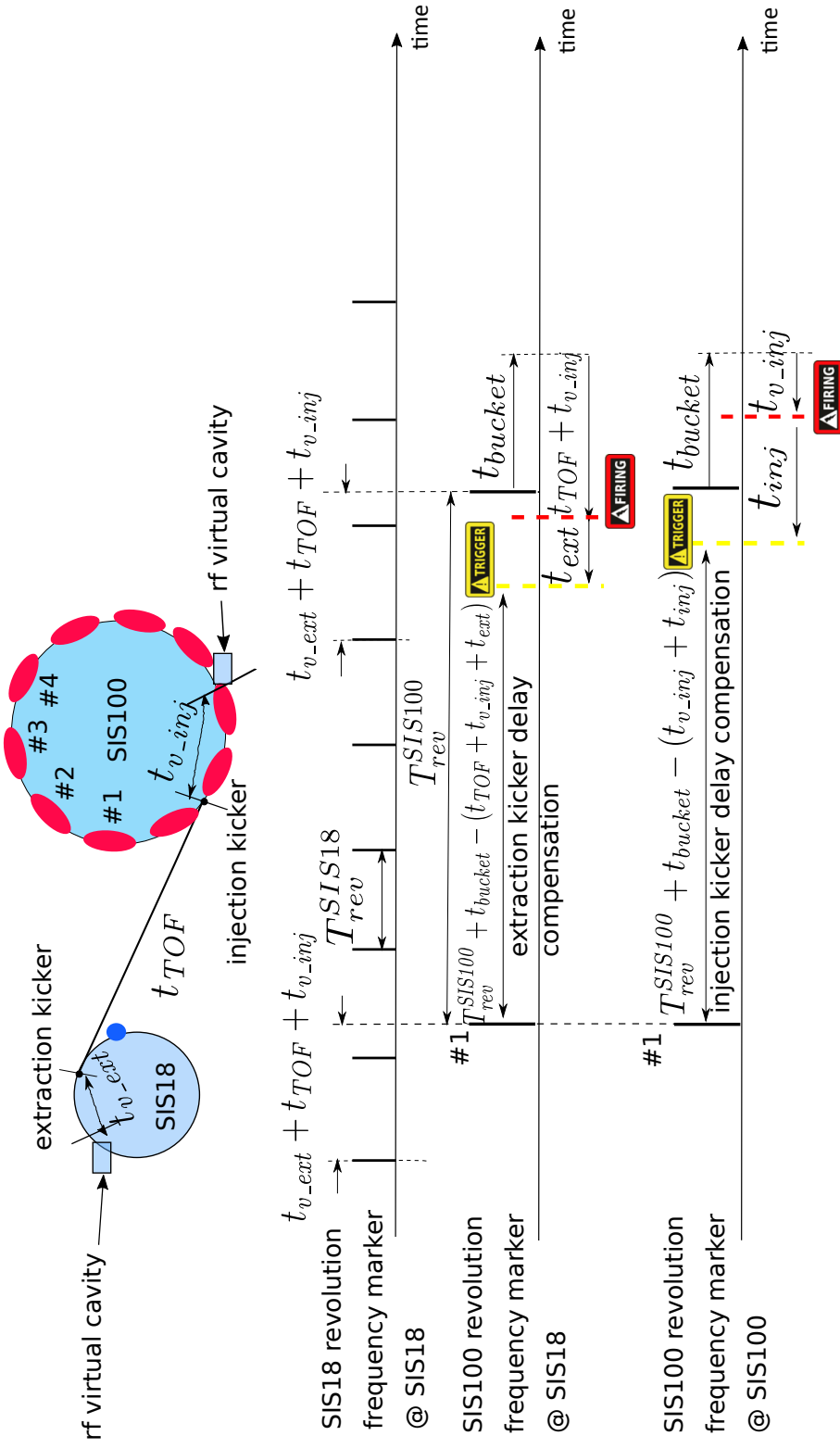


Figure 4.1: Illustration of the B2B transfer from the SIS18 to the SIS100.

The blue dot represents a bunch, red ones buckets.

4.1. Basic Idea

Fig. 4.1 illustrates the B2B transfer from the SIS18 to the SIS100. A super cycle is a sequence of cycles in a single machine within a beam pattern. The SIS18 U^{28+} super cycle consists of four SIS18 cycles. Each cycle produces two U^{28+} bunches. From the SIS18, four batches, each of two bunches, are injected into eight out of ten buckets of the SIS100. The SIS18 H^+ super cycle consists of four SIS18 cycles. Each cycle produces one H^+ bunch. From the SIS18, four batches, each of one bunch, are injected into four out of ten buckets of the SIS100 [38, 39]. The SIS18 and SIS100 revolution frequency markers (black bars on the first time axis and bars on the second/third time axis in Fig. 4.1) indicate the time when a bunch or the first bucket (#1) pass by the virtual rf cavity. The extraction and injection kicker trigger have a delay with respect to the first bars of the SIS100 revolution frequency marker at the SIS18 and at the SIS100. This delay is called the “extraction/injection kicker delay compensation”. The mentioned four instances of time are related to the second bars of the SIS100 revolution frequency marker. T_{rev}^X represents the revolution period of the accelerator X, e.g. the SIS18 revolution period is T_{rev}^{SIS18} . T_{rf}^X represents the period of the cavity rf frequency of the accelerator X, e.g. the SIS18 rf period of the cavity rf frequency is T_{rf}^{SIS18} . After the rf phase alignment, the time difference between the SIS18 and SIS100 synchronization frequency (denoted as t_{diff_sync}) for the U^{28+} and H^+ odd bucket injection is

$$t_{diff_sync} = (t_{v_ext} + t_{TOF} + t_{v_inj}) \bmod 1/f_{syn}^{trg} \quad (4.1)$$

For the H^+ even bucket injection t_{diff_sync} is

$$t_{diff_sync} = (t_{v_ext} + t_{TOF} + t_{v_inj} - T_{rf}^{SIS100}) \bmod 1/f_{syn}^{trg} \quad (4.2)$$

The phase alignment for the odd or even bucket injection is informed by the “extra phase shift” from the SM. For more details about the use cases of the B2B transfer from the SIS18 to the SIS100, please see Sec. 6.1.1 and Sec. 6.1.2. For more details about the parameters of the B2B transfer system from the SM, please see Appendix D.

For the phase alignment, the steps below must be carried out.

1. The measurement of the phase of the rf system and the corresponding timestamp in each accelerator.
2. The exchange of the measured phase and the timestamp.
3. The phase comparison between the two rf systems.
4. The adjustment of the phase on one (or both) rf system, when the phase shift method is used.
5. The calculation of the time duration for the required phase alignment of the two rf systems.

4.1.2 Trigger of Extraction and Injection Kickers

For the proper B2B transfer, not only the relative position of bunches and buckets, but also the firing of the extraction and injection kickers must be precisely controlled. The extraction kicker must kick the bunch exactly the time-of-flight earlier before

4.1. Basic Idea

a specific bucket passes the injection kicker and the transition of the magnetic field must be carried out during the bunch gap. For the calculation of the trigger time for the extraction and injection kickers, the following steps must be processed.

1. The kicker firing requires the bunch-to-bucket injection center phase mismatch within a upper bound, which defines a “coarse synchronization”.
2. The bucket label requires the kicker firing based on a bucket indication signal for the first bucket (e.g. the SIS100 revolution frequency markers in Fig. 4.1) plus a fixed delay (the extraction/injection kicker delay compensation), for more details please see Sec. 4.3.5. With the help of the bucket label, bunches are injected into correct buckets. This process is called the “fine synchronization”.

4.1.2.1 Bucket Indication Signal

The bucket indication signal of the phase shift method or the frequency beating method indicates the passing time of the first bucket of the target accelerator, when the first bucket is correct or periodical phase aligned with a bunch of the source accelerator for the bunch-to-bucket injection. For FAIR use cases, we have $f_{syn}^X = Y \cdot f_{rev}^X / m$ and either m/Y or Y/m must be an integer, see Sec. 2.2. Either the revolution period is the integer times of the period of the synchronization frequency or the period of the synchronization frequency is the integer times of the revolution period. The first bucket of the target accelerator is indicated by f_{rev}^{trg} . The correct or periodical phase alignment of the rf system of the target accelerator with the rf system of the source accelerator is indicated by f_{syn}^{trg} . Hence, the frequency of the bucket indication signal (denoted as “ f_{bucket} ”) depends on the relation between the revolution frequency and the synchronization frequency of the target accelerator. When the synchronization frequency of the target accelerator is greater than or equal to the revolution frequency of the target accelerator, namely the period of the synchronization frequency is equal to or less than the revolution period, the period of the synchronization frequency is not long enough to include all buckets. In this case, the frequency of the bucket indication signal equals to the revolution frequency of the target accelerator and the length of the synchronization window equals to one revolution period. On the contrary, the frequency of the bucket indication signal equals to the synchronization frequency of the target accelerator and the length of the synchronization window equals to the period of the synchronization frequency. The frequency of the bucket indication signal is expressed as

$$f_{bucket} = \begin{cases} f_{rev}^{trg} & f_{syn}^{trg} \geq f_{rev}^{trg} \\ f_{syn}^{trg} & f_{syn}^{trg} < f_{rev}^{trg} \end{cases} \quad (4.3)$$

The corresponding length of the synchronization window is expressed as

$$T_w = \frac{1}{f_{bucket}} \begin{cases} T_{rev}^{trg} & f_{syn}^{trg} \geq f_{rev}^{trg} \\ T_{syn}^{trg} & f_{syn}^{trg} < f_{rev}^{trg} \end{cases} \quad (4.4)$$

Fig. 4.2 shows one example when the frequency of the bucket indication signal equals to the revolution frequency of the target accelerator. Fig. 4.3 shows one example when the frequency of the bucket indication signal equals to the synchronization frequency of the target accelerator.

4.1. Basic Idea

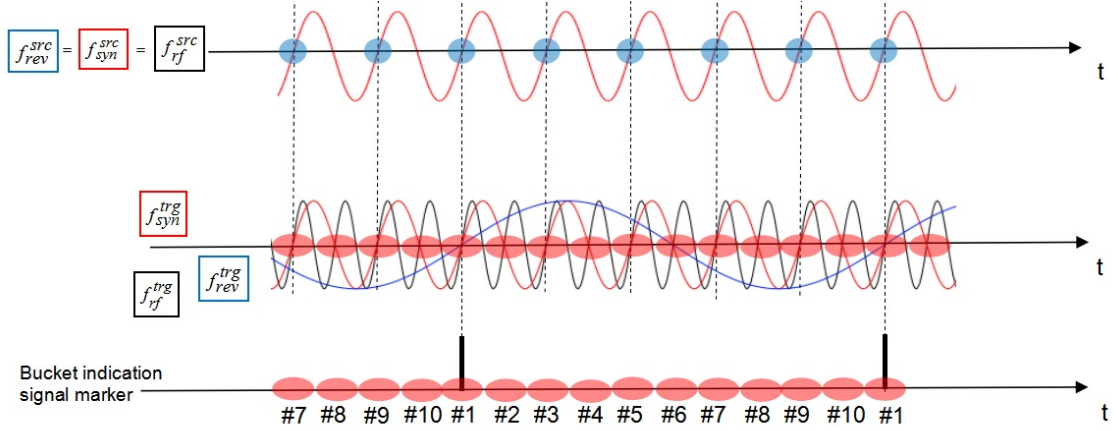


Figure 4.2: Frequency of the bucket indication signal equals to the revolution frequency of the target accelerator.

Red dots represent buckets of the target accelerator and blue ones represent bunches of the source accelerator. This example is the FAIR use case of the H^+ B2B transfer from the SIS18 to the SIS100. The correct phase alignment of the two rf systems is assumed with $\Delta\phi_{syn} = 0^\circ$ and only the buckets with the odd number (e.g. #1, #3) are to be filled in this example.

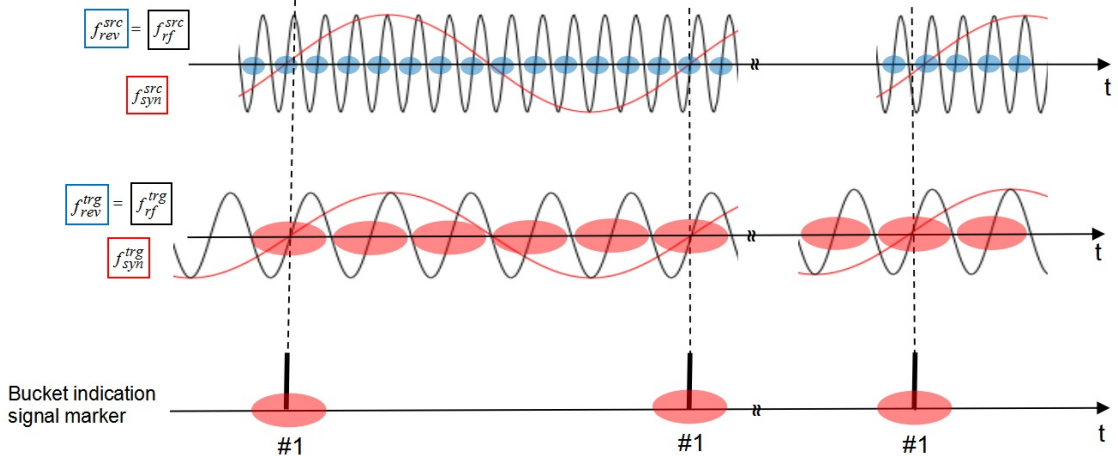


Figure 4.3: Frequency of the bucket indication signal equals to the synchronization frequency of the target accelerator.

Red dots represent buckets of the target accelerator and blue ones represent bunches of the source accelerator. This example is the FAIR use case of the B2B transfer from the CR to the HESR.

4.1.2.2 Extraction and Injection Kicker Delay Compensation

The calculation of the extraction and injection kicker delay compensation is explained in this section.

- Extraction kick

In order to inject into specific buckets, the extraction kicker delay compensa-

4.2. Basic Procedure

tion for the first bar of the SIS100 revolution frequency marker is $T_{rev}^{SIS100} + t_{bucket}$, see Fig. 4.1. For example, when two U^{28+} bunches of the SIS18 are to be injected into buckets #3 and #4 of the SIS100, $t_{bucket} = 1 \cdot T_{rev}^{SIS18}$. The extraction kicker must be fired $t_{v_inj} + t_{TOF} + t_{ext}$ earlier as the bucket passes the virtual rf cavity, so the extraction kicker delay compensation is $T_{rev}^{SIS100} + t_{bucket} - (t_{TOF} + t_{v_inj} + t_{ext})$.

- Injection kick

With the consideration of the bucket pattern, the injection kicker delay compensation for the first bar of the SIS100 revolution frequency marker is $T_{rev}^{SIS100} + t_{bucket}$, see Fig. 4.1. The injection kicker must be fired $t_{v_inj} + t_{inj}$ time earlier as the bucket passes the virtual rf cavity, so the injection kicker delay compensation is $T_{rev}^{SIS100} + t_{bucket} - (t_{v_inj} + t_{inj})$.

4.2 Basic Procedure

Fig. 4.4 illustrates the basic procedure of the B2B transfer with two different synchronization scenarios. The yellow region shows the synchronization window. The purple region shows the valid time for the emergency kicker.

The B2B transfer process basically needs to follow the six steps [40]:

1. The DM announces the B2B transfer and requests the switch off of the beam feedback loops on the rf system, when required.
2. Two accelerators measure the rf phase locally.
3. The source accelerator receives the measured rf phase from the target accelerator.
4. The source accelerator does the B2B related calculation.
 - The source accelerator calculates the synchronization window and sends it to the target accelerator and to the DM.

The source accelerator generally accomplishes the phase alignment in case of the phase shift method. A particular case is the empty target accelerator. The phase alignment can be achieved very fast and simple by the phase jump at the target accelerator. Although the synchronization window is theoretically infinite for the phase shift method, bunches should be transferred as soon as the phase shift is done, in order to guarantee the stability of the beam. For both synchronization methods, the synchronization window has a certain length.

- Besides, the bucket indication signal is reproduced at the source accelerator for the indication of the 1st bucket.
5. The trigger signals with the delay compensation are generated for the kickers.
 6. The kicker electronic fire the kickers. The extraction and injection kicker trigger and firing timestamp are sent to the source accelerator for the B2B status check. The actual beam injection timestamp and the B2B transfer status are send from the source accelerator to the DM and the DM sends them further to the BI.

4.3. Realization

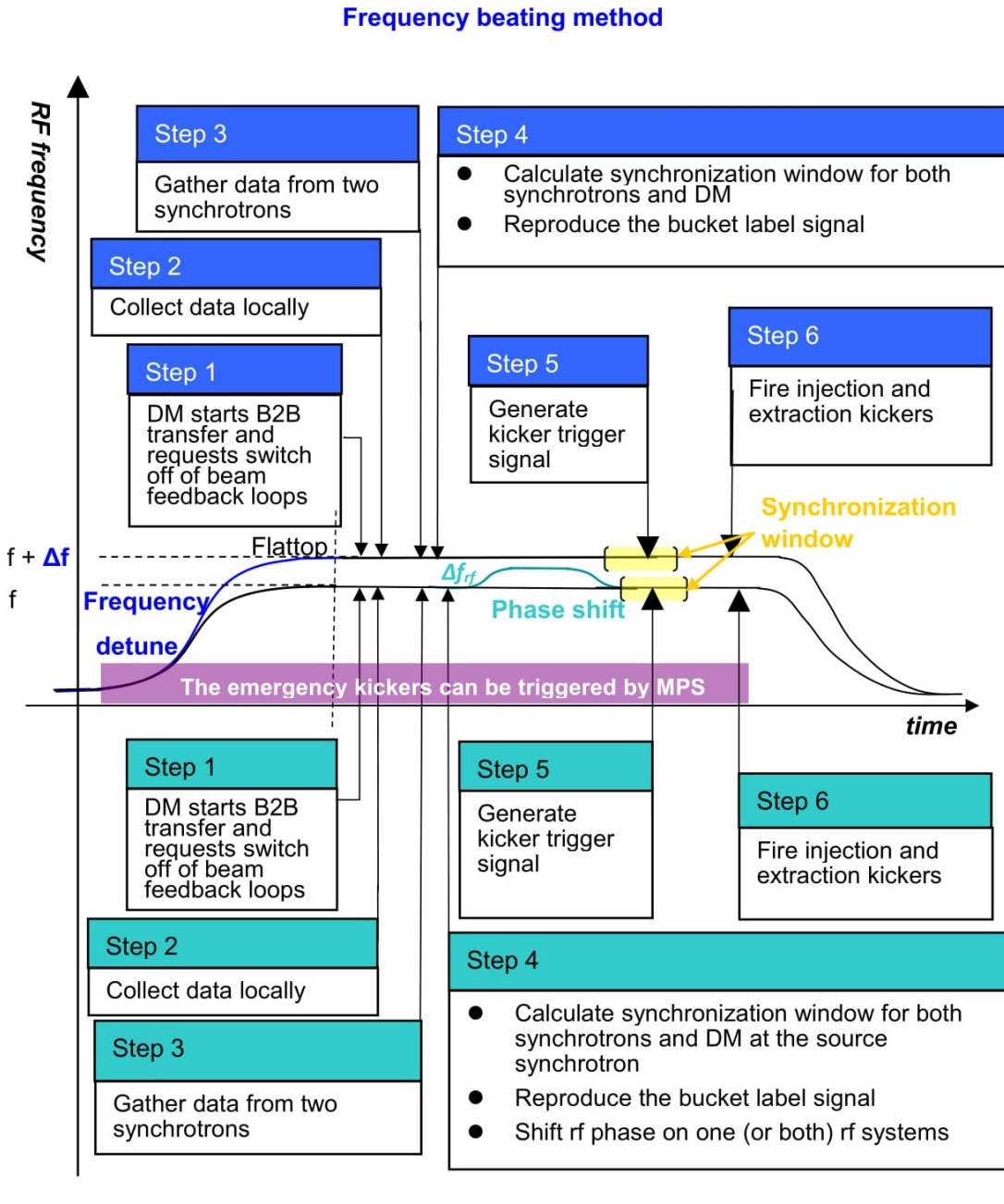


Figure 4.4: Procedure for the B2B transfer within one acceleration cycle.

Adapted from “F-TC-C-05, Concept of the FAIR Bunch To Bucket Transfer System“ by J. Bai and T. Ferrand, 2016, FAIR Technical Concept. Adapted with permission.

As illustrated here the procedure with the frequency beating method (blue, top) and that with the phase shift method (green, bottom).

4.3 Realization

This section describes the realization of the FAIR B2B transfer system based on the FAIR control system and LLRF system introduced in Chap. 3.

4.3. Realization

The phase alignment is based on the phase difference between two synchronization frequencies. Because it is not preferable to have a direct connection between two ring accelerators around such a big FAIR campus for a direct phase measurement based on the existing technical basis, a shared reference sinusoidal signal (which is called “synchronization reference signal” and denoted as f_{ref}) is used for the indirect phase difference measurement. The synchronization reference signal has a fixed frequency and is always in phase in different supply rooms. It is a sinusoidal wave, whose frequency is a multiple of BuTiS T0 100 kHz and whose positive zero-crossings are always aligned with the first positive zero-crossings of C2 clocks after T0 edges [41, 42]. The first positive zero-crossings of C2 clocks after T0 edges is called the “T0 incidents”. Thus, the synchronization reference signal is synchronous in different supply rooms by definition. The phase measurement of each rf system is based on the frequency beating between the synchronization frequency and the synchronization reference signal, achieved by measuring the phase deviation between these two frequencies (denoted by ϕ^X), see Fig. 4.5.

$$\phi^X(t) = [2\pi(f_{syn}^X - f_{ref})t + \phi_0^X] \bmod 2\pi - \pi \quad (4.5)$$

where ϕ_0^X is the initial value of the phase deviation between the synchronization frequency and the synchronization reference signal. $\phi^X(t)$ is within the range between $-\pi$ and π , which is determined by the phase deviation measurement, for more details, please see “Development of the LLRF system for a deterministic Bunch-to-Bucket transfer for FAIR” [43].

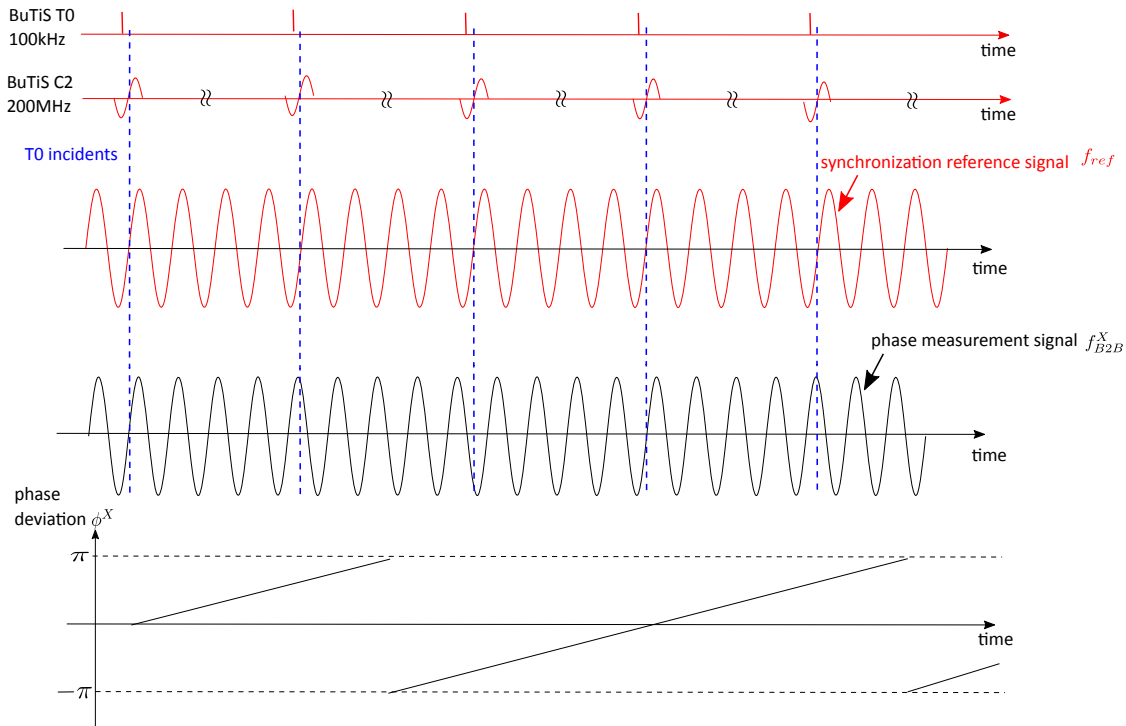


Figure 4.5: Phase deviation between the synchronization frequency and the synchronization reference signal.

The phase difference between two synchronization frequencies (denoted as $\Delta\phi_{syn}$) is calculated by the subtraction of the phase deviation of the source accelerator from

4.3. Realization

that of the target accelerator.

$$\Delta\phi_{syn}(t) = \phi^{trg}(t) - \phi^{src}(t) = [2\pi(f_{syn}^{trg} - f_{syn}^{src})t + (\phi_0^{trg} - \phi_0^{src})] \mod 2\pi \quad (4.6)$$

From eq. 4.6, we know that the phase difference between two synchronization frequencies is independent of the choice of the synchronization reference signal. For the phase shift method, $\Delta\phi_{syn}(t)$ is constant because of $f_{syn}^{trg} = f_{syn}^{src}$. For the frequency beating method, $\Delta\phi_{syn}(t)$ is a periodical variable, whose period is $1/(f_{syn}^{trg} - f_{syn}^{src})$.

For the reproduction of the bucket indication signal at the source accelerator, the phase deviation between the bucket indication signal and the synchronization reference signal (denoted by φ^{trg}) needs to be measured at the target accelerator.

$$\varphi^{trg}(t) = [2\pi(f_{bucket} - f_{ref})t + \varphi_0^{trg}] \mod 2\pi - \pi \quad (4.7)$$

where φ_0^{trg} is the initial value of the phase deviation between the bucket indication signal and the synchronization reference signal.

The actual phase of the bucket indication signal is irrelevant to the synchronization reference signal. Because the phase of the synchronization reference signal is 0° at T0 incidents, the extrapolated phase deviation at T0 incidents, denoted as $\varphi^{trg}(T0)$, is the actual phase of the bucket indication signal and will be used for the reproduction of the bucket indication signal at the source accelerator. For the target accelerator, the extrapolated phase deviation between the synchronization frequency and the synchronization reference signal at T0 incidents, denoted as $\phi^{trg}(T0)$, can be deduced from $\varphi^{trg}(T0)$, because the phase of the high harmonic frequency can be deduced from that of the low harmonic frequency.

$$\phi^{trg}(T0) = \begin{cases} \varphi^{trg}(T0) \mod 2\pi & f_{bucket} = f_{syn}^{trg} \\ \frac{h_{syn}^{trg}}{h_{rev}^{trg}} \varphi^{trg}(T0) \mod 2\pi & f_{bucket} = f_{rev}^{trg} \end{cases} \quad (4.8)$$

Hence, the measurement of the phase deviation between the bucket label signal and the synchronization reference signal at the target is enough for both the phase alignment and the reproduction of the bucket indication signal. It reduces the data transfer of the system and the transfer delay on the WR network. Besides, every phase deviation measurement and extrapolation process needs 500 μ s, so one phase deviation measurement is preferred due to the time constraints (see Chap. 5).

The frequency used for the phase deviation measurement is called “phase measurement signal” and denoted as f_{B2B}^X . For the target accelerator, the phase measurement signal is the bucket indication signal, namely

$$f_{B2B}^{trg} = f_{bucket} = \begin{cases} f_{syn}^{trg} & f_{bucket} = f_{syn}^{trg} \\ f_{rev}^{trg} & f_{bucket} = f_{rev}^{trg} \end{cases} \quad (4.9)$$

For the source accelerator, the frequency of the phase measurement signal is calculated as

$$f_{B2B}^{src} = \begin{cases} f_{syn}^{src} & f_{bucket} = f_{syn}^{trg} \\ \frac{h_{rev}^{trg}}{h_{syn}^{trg}} f_{syn}^{src} & f_{bucket} = f_{rev}^{trg} \end{cases} \quad (4.10)$$

For some cases, f_{B2B}^{src} is even smaller than the revolution frequency, e.g. $f_{B2B}^{CR} = f_{rev}^{CR}/13$ for the case of the B2B transfer from the CR to the HESR, for more details, please see Chap. 6.

4.3. Realization

The frequency of the synchronization reference signal f_{ref} is determined by f_{bucket} and calculated as

$$f_{ref} = \text{round}(f_{bucket}/100 \text{ kHz}) \cdot 100 \text{ kHz} \quad (4.11)$$

The function *round* rounds $f_{bucket}/100 \text{ kHz}$ up or down to an integer value, which is closest to $f_{bucket}/100 \text{ kHz}$. e.g. $f_{bucket} = f_{rev}^{SIS100} = 157.254 \text{ kHz}$, $f_{bucket}/100 \text{ kHz} = 1.57$, so $\text{round}(f_{bucket}/100 \text{ kHz}) = 2$ and $f_{ref} = 200 \text{ kHz}$. This is the FAIR use case of the U^{28+} B2B transfer from the SIS18 to the SIS100, for more details, please see Chap. 6. When $|f_{bucket}/100 \text{ kHz}| < 1$, $f_{ref} = 100 \text{ kHz}$. For the detailed realization of the synchronization reference signal, please see “Development of the LLRF system for a deterministic Bunch-to-Bucket transfer for FAIR” [43].

The measurement and extrapolation of the phase deviation is based on the frequency beating between the phase measurement signal and the synchronization reference signal, so the frequency difference between these two signals must not be too large. The extrapolation of the phase deviation requires at least two samples for every beating period and the sample time is $3.22 \mu\text{s}$ [43], so the maximum beating frequency is approximately 150 kHz .

4.3.1 Phase Measurement and Corresponding Timestamp of Each Rf System

The rf frequencies in the source and target accelerator need to be stable and constant during the B2B transfer process. The phase measurement of each rf system follows the principles as shown below.

1. The measurement of the actual phase values.
2. The extrapolated phase values into the future based on the measured phase values.
3. The timestamp for the extrapolated phase values.

4.3.1.1 Measurement of Actual Phase Values of Each Rf System

The phase measurement of each rf system is achieved by measuring the phase deviation between the phase measurement signal and the synchronization reference signal of a accelerator. The phase deviation (denoted by φ^X) has a linear relationship with time, whose range is from $-\pi$ to $+\pi$.

$$\varphi^X(t) = [(k^X t + \varphi_0^X) \bmod 2\pi] - \pi \quad (4.12)$$

where k^X is the slope of the phase deviation, namely $k^X = 2\pi(f_{B2B}^X - f_{ref})$ and φ_0^X the initial value of the phase deviation.

Fig. 4.6 shows the phase measurement of the rf system at a dedicated accelerator. The red sinusoidal wave represents the synchronization reference signal (e.g. 200 kHz) in a supply room and the black wave the phase measurement signal (e.g. 157.254 kHz) from the Group DDS. The phase deviation between the phase measurement signal and the synchronization reference signal is measured by the Phase Advance Measurement (PAM) module at the source accelerators and at the target

4.3. Realization

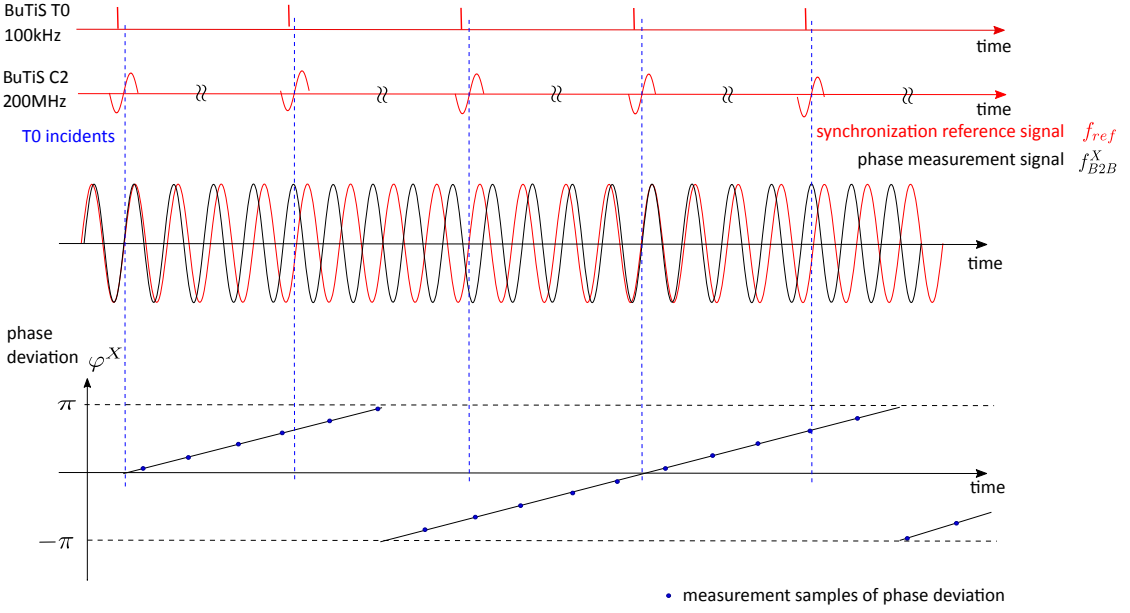


Figure 4.6: Realization of the phase deviation measurement at one accelerator

accelerator. The phase deviation measurement is performed synchronously to an internal clock, which is represented by the blue dots. The measured phase deviation can be expressed as

$$\varphi^X(nT_{sample_PAM}) = [(k^X \cdot nT_{sample_PAM} + \varphi_0^X) \bmod 2\pi] - \pi \quad (4.13)$$

where T_{sample_PAM} is the measurement sampling period of the phase deviation by the PAM module.

For more details about the implementation and realization of the PAM module, please see “Development of the LLRF system for a deterministic Bunch-to-Bucket transfer for FAIR“ [43].

4.3.1.2 Phase Extrapolation of Each Rf System

The phase deviation can be extrapolated due to the linear relationship between time and the phase deviation.

Based on a series of the measured samples of the phase deviation, the phase deviation at the T0 incidents (denoted by ψ^X and called the “extrapolated phase advance“) are extrapolated at the source and target accelerators by the Phase Advance Prediction (PAP) Module.

$$\psi^X(n) = \varphi^X(nT_{sample_PAP}) \quad (4.14)$$

where T_{sample_PAP} is the extrapolation sampling period of the phase extrapolation by the PAP module, $T_{sample_PAP} = 1/100\text{ kHz}$.

The extrapolated phase advance, ψ^{src} and ψ^{trg} at the source and target accelerator, is represented by red diamonds in Fig. 4.7. Because the phase advance is extrapolated at the T0 incidents and the synchronization reference signal is zero phase aligned with the T0 incidents, ψ^{src} and ψ^{trg} are the phase of the phase measurement signals at the virtual rf cavities of two ring accelerators at the T0 incidents

4.3. Realization

(represented as black dots in Fig. 4.7). For more details about the implementation and realization of the PAP module, please see “Development of the LLRF system for a deterministic Bunch-to-Bucket transfer for FAIR“ [43].

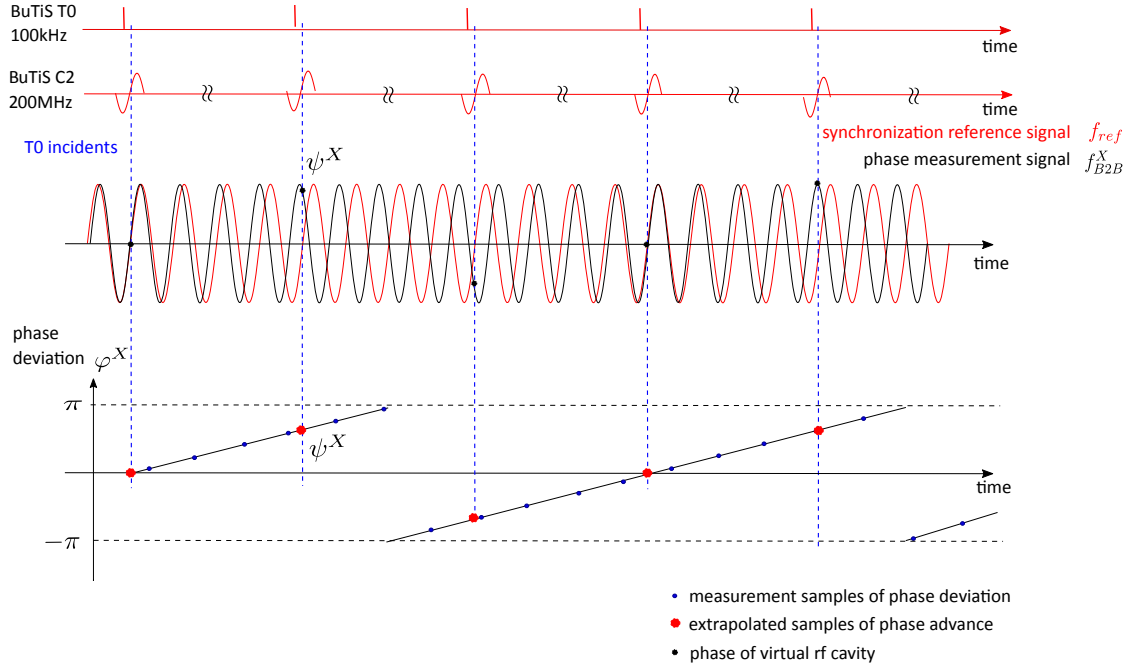


Figure 4.7: Realization of the phase advance extrapolation at one accelerator

4.3.1.3 Timestamp of the Extrapolated Phase

The extrapolated phase advance is synchronized with T0 incidents by the PAP module, but it is not synchronized with the absolute time. This is one of the tasks of the multi-purpose B2B source and target SCUs [31, 44], which are located in the source and target accelerators. The PAP module is a SCU slave¹, respectively integrated into the B2B source SCU and B2B target SCU. Both the B2B source and target SCUs could get the timestamp of the T0 incidents.

Fig. 4.8 illustrates the synchronization of the extrapolated phase to the timestamp. The DM broadcasts the timing frame of CMD_START_B2B to the WR network. This timing frame will be received by the B2B source SCU and the B2B target SCU. The B2B source and target SCUs start the B2B process at a designated time (represented as the pink dot in Fig. 4.8). The timestamp of the start is an integer multiple of 10 µs, the period of the T0 incident. They need maximum 1 µs to inform the PAP modules to start the phase advance extrapolation respectively. The PAP modules needs approximately 500 µs for the phase extrapolation and updates the extrapolated phase value every T0 incident. After 500 µs, the B2B source and target SCUs need another maximum 1 µs to receive the extrapolated phase ψ_0^X (represented as the red diamond in Fig. 4.8) from the PAP modules, as well as the slope of the phase deviation k^X . They also timestamp the T0 incidents t_ψ^X which corresponds to the extrapolated phase. The B2B source SCU obtains ψ_0^{src} , t_ψ^{src} and

¹[https://en.wikipedia.org/wiki/Master/slave_\(technology\)](https://en.wikipedia.org/wiki/Master/slave_(technology))

4.3. Realization

k^{src} at the source accelerator and the B2B target SCU obtains ψ_0^{trg} , t_ψ^{trg} and k^{trg} at the target accelerator. In fact, $t_\psi^{src} = t_\psi^{trg}$.

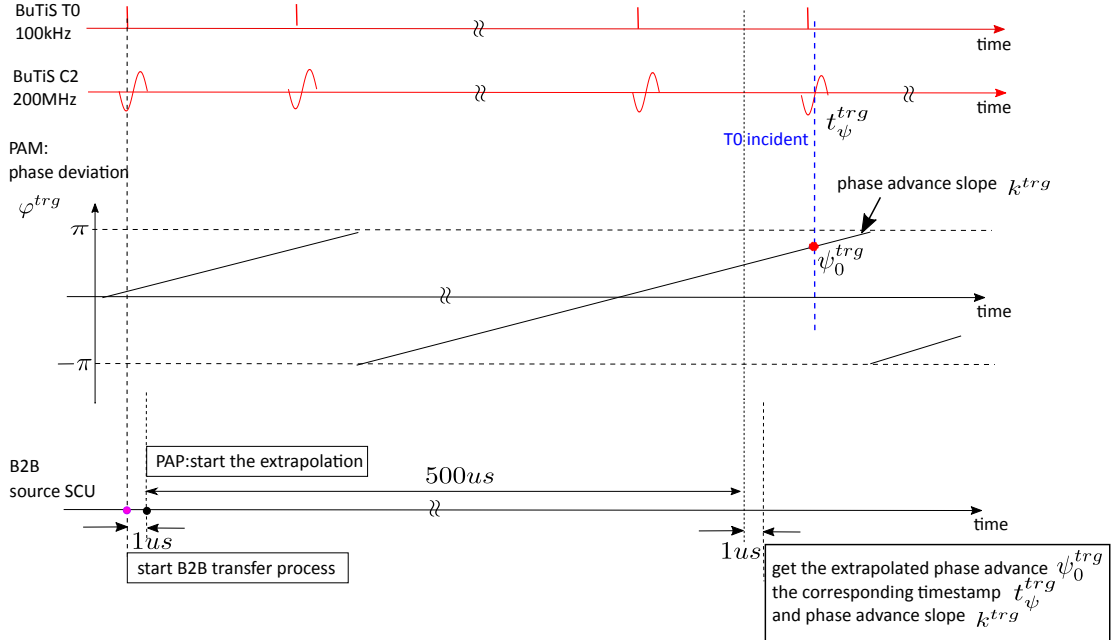


Figure 4.8: Synchronization of the extrapolated phase to the timestamp in one accelerator

Because the phase deviation of the phase measurement signal complies with the linear relation with time, the evolution of the phase deviation between the phase measurement signal and the synchronization reference signal can be calculated for any T0 incidents, (see eq. 4.15), which will be used for the phase correction of the bucket indication signal in sec. 4.3.5.

$$\varphi^X(t_\psi^X + nT_{sample_PAP}) = [(\psi_0^X + k^X \cdot nT_{sample_PAP}) \bmod 2\pi] - \pi \quad (4.15)$$

4.3.2 Exchange of Measured Data

For the B2B transfer, there is a “B2B transfer master“, which is responsible for the data collection of two ring accelerators, the data calculation, the data redistribution and the B2B transfer status check. The data of the source and target accelerator must be transferred to the B2B transfer master via the deterministic WR network in the format of the timing frame.

For the simplicity, the B2B source SCU works as the B2B transfer master, so the extrapolated phase ψ_0^{trg} , the corresponding timestamp t_ψ^{trg} and the phase deviation slope k^{trg} are transferred by the B2B target SCU to the B2B source SCU via the WR network. The transfer of the data is achieved by the timing frame TGM_PHASE_TIME. The B2B transfer involves a certain amount of timing frames. For more details about the B2B timing frames, please see Appendix A. The timing frames are not sent via the DM in order to reduce the traffic of the WR network and reduce the timing frame transfer delay on the WR network [45]. Therefore a specific VLAN, the B2B VLAN, is defined for the B2B timing frames. All SCUs

4.3. Realization

for the B2B transfer are assigned to the B2B VLAN. Fig. 4.9 illustrates an example of the transfer path of the B2B timing frames in the WR network. The frames are transferred along the path with orange color instead of the path with blue color. The tests which has been done in the framework of this thesis for the transfer delay of the B2B timing frames on the WR network is explained in Chap. 5.

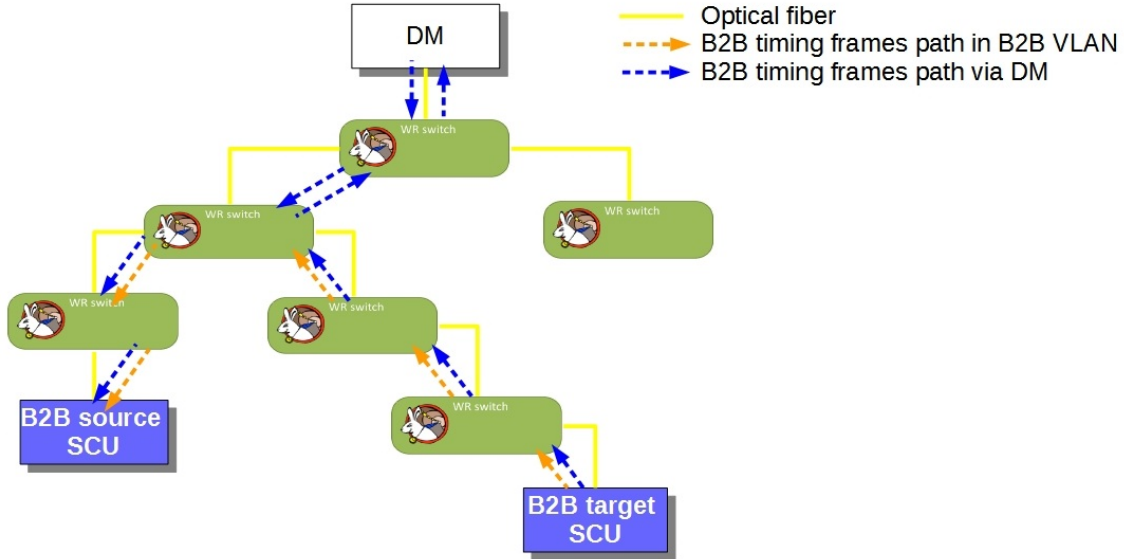


Figure 4.9: An example of the transfer path of the B2B timing frames in the WR network

4.3.3 Rf Synchronization

The FAIR B2B transfer system is available for both the phase shift and frequency beating methods, see Sec. 2.3. The rf synchronization of two ring accelerators is based on the phase difference between two synchronization frequencies of the two rf systems at time t_ψ^X , which is denoted as $\Delta\phi_{syn_0}$. $\Delta\phi_{syn_0}$ is calculated from the measurement of the phase difference between the phase measurement signals of the two rf systems.

$$\Delta\phi_{syn_0} = \begin{cases} (\psi_0^{trg} - \psi_0^{src}) \bmod 2\pi & f_{bucket} = f_{syn}^{trg} \\ \frac{h_{syn}^{trg}}{h_{rev}^{trg}}(\psi_0^{trg} - \psi_0^{src}) \bmod 2\pi & f_{bucket} = f_{rev}^{trg} \end{cases} \quad (4.16)$$

$\Delta\phi_{syn_0}$ is within the range between 0 and 2π . The SM provides the goal time difference between the synchronization frequencies of the two rf systems t_{diff_sync} , which considers the delay compensation for TOF, all propagation and the extra phase shift. The goal phase difference between two synchronization frequencies is denoted as $\Delta\phi_{goal}$ and calculated as

$$\Delta\phi_{goal} = t_{diff_sync} \cdot f_{syn}^{trg} \cdot 2\pi \quad (4.17)$$

The B2B source SCU calculates the required phase adjustment (denoted as $\Delta\phi_{adjust}$) for the synchronization frequency based on $\Delta\phi_{goal}$ and $\Delta\phi_{syn_0}$, see eq. 4.18. It is within the range between 0 and 2π .

$$\Delta\phi_{adjust} = (\Delta\phi_{syn_0} - \Delta\phi_{goal}) \bmod 2\pi \quad (4.18)$$

4.3. Realization

4.3.3.1 Rf Synchronization with the Phase Shift Method

For the rf synchronization, the maximum required phase shift of the synchronization frequency is 2π . In order to accomplish the phase alignment as fast as possible, the phase shift will be conducted backward or forward. Therefore a phase shift of up to $\pm\pi$ will be considered for the Group DDS with regard to the synchronization frequency f_{syn}^X . The rf frequency modulation achieves the phase shift of $\Delta\phi_{shift}$.

$$\Delta\phi_{shift} = \begin{cases} \Delta\phi_{adjust} & 0 < \Delta\phi_{adjust} \leq \pi \\ \Delta\phi_{adjust} - 2\pi & \pi < \Delta\phi_{adjust} \leq 2\pi \end{cases} \quad (4.19)$$

The required phase shift is implemented to the Group DDS with the revolution frequency, so the required phase shift on the revolution frequency (denoted as $\Delta\phi_{shift_imp}$) is

$$\Delta\phi_{shift_imp} = \frac{h_{rev}^{trg}}{h_{syn}^{trg}} \Delta\phi_{shift} \quad (4.20)$$

A normalized frequency modulation profile $f_{normalized}$ for π must be precalculated, which guarantees the adiabaticity. The actual frequency modulation profile f_{actual} is decided by $f_{normalized}$ and $\Delta\phi_{shift}$, see eq. 4.21.

$$f_{actual}(t) = \frac{\Delta\phi_{shift}}{\pi} f_{normalized}(t) \quad (4.21)$$

Fig. 4.10 shows an example of a normalized and several actual frequency modulation profiles and the corresponding phase shift profiles. A sinusoidal modulation is used as an example, which is best for the beam stability. For more details about the frequency modulation curves, please see Chap. 5. The magenta profile is the normalized profile $f_{normalized}$ with the phase shift of π . The blue one is $1/2f_{normalized}$ with the phase shift of $\pi/2$ and the green one is $1/3f_{normalized}$ with $\pi/3$.

The B2B source SCU sends the required phase shift to the PSM, which controls the phase shift of the phase measurement signal of Group DDS by means of either the frequency modulation (Fig. 4.10 (a)) or the phase modulation (Fig. 4.10 (b)). The required phase shift is distributed by the LLRF system to all the Group DDS of the accelerator. The Group DDS signals are routed to different cavity systems by a Switch Matrix to realize the phase shift of all cavities on the accelerator. For more details about the implementation and realization of the PSM module, please see “Development of the LLRF system for a deterministic Bunch-to-Bucket transfer for FAIR” [43].

A particular case of the B2B synchronization occurs, when the target accelerator is empty, i.e. it does not capture any bunch yet, the phase shift can be done for the target accelerator without adiabatical consideration (e.g. the phase jump is possible). In this case, the B2B source SCU sends the timing frame TGM_PHASE_JUMP to the B2B target SCU, which contains the required phase shift. After the B2B target SCU receives the timing frame, it sends the value to the PSM for the phase jump of the Group DDS with the synchronization frequency of the target accelerator.

4.3.3.2 Rf Synchronization with the Frequency Beating Method

With the frequency beating method, the phase difference varies at the rate of the synchronization frequency difference between the two rf systems. The frequency

4.3. Realization

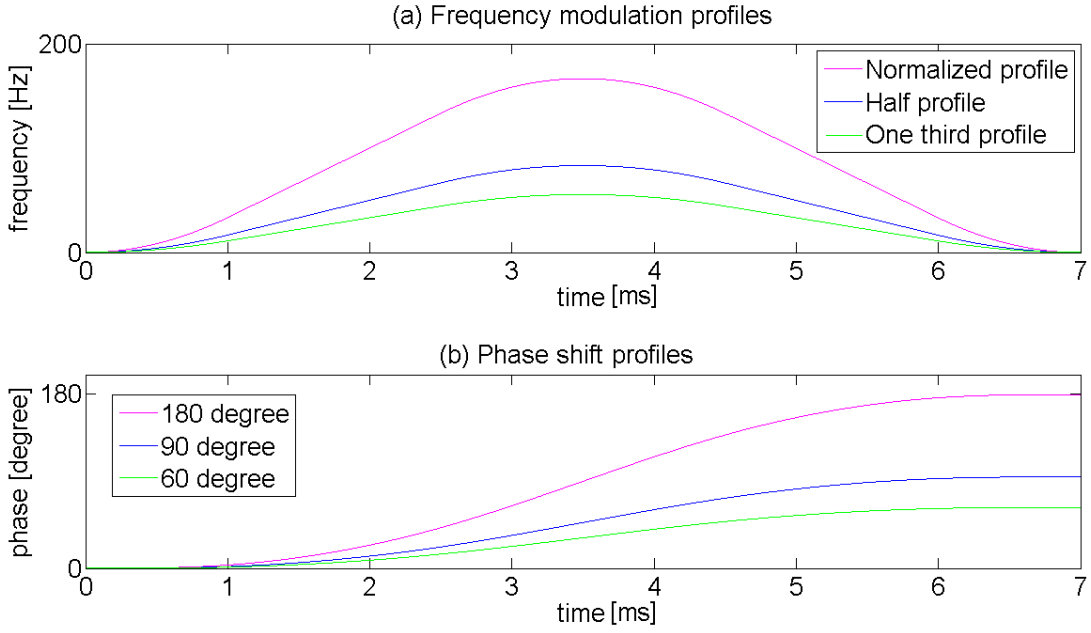


Figure 4.10: Normalized frequency and phase modulation profile and the actual profiles

beating method can achieve only positive phase adjustment, namely from 0 to 2π , so two rf systems are synchronized when the phase difference between two synchronization frequencies equals to $\Delta\phi_{adjust}$, namely

$$\Delta\phi_{syn} = \Delta\phi_{adjust} \quad (4.22)$$

The correct phase alignment is achieved by the proper waiting time T_{wait} .

$$T_{wait} = \frac{\Delta\phi_{adjust}}{2\pi} \cdot \frac{1}{|f_{syn}^{src} - f_{syn}^{trg}|} + n \cdot \frac{1}{|f_{syn}^{src} - f_{syn}^{trg}|} \quad (4.23)$$

The circumference ratio between many pair of machines in FAIR is not an integer, the synchronization frequencies of two ring accelerators begin beating automatically. For the pairs with an integral circumference ratio, the synchronization frequency of the source accelerator has to be detuned. The Group DDS produces the detuned phase measurement signal provided by the SM.

4.3.4 Coarse Synchronization

The coarse synchronization is achieved by the synchronization window with a certain length. Within this window, bunches are transferred into buckets with the center mismatch smaller than the upper bound. The length of the synchronization window T_w is one period of the bucket indication signal. For the phase shift method, the bunch-to-bucket injection center mismatch within the synchronization window is 0. For the frequency beating method, the maximum bunch-to-bucket injection center mismatch σ_{rf} within the synchronization window is calculated by eq. 4.24. For more details, please see Sec. 2.3.2.

$$\sigma_{rf} = \pm \frac{1}{2} \cdot 2\pi |f_{syn}^{src} - f_{syn}^{trg}| \cdot T_w \cdot \frac{h_{rf}^{trg}}{h_{syn}^{trg}} \quad (4.24)$$

4.3. Realization

The B2B source SCU obtains the delay compensation for the TOF, all propagation delays, the kicker preparation time and the bucket delay (denoted as t_{delay}) from the SM. It calculates the start of the synchronization window (denoted as t_w), taking the delay compensation into consideration.

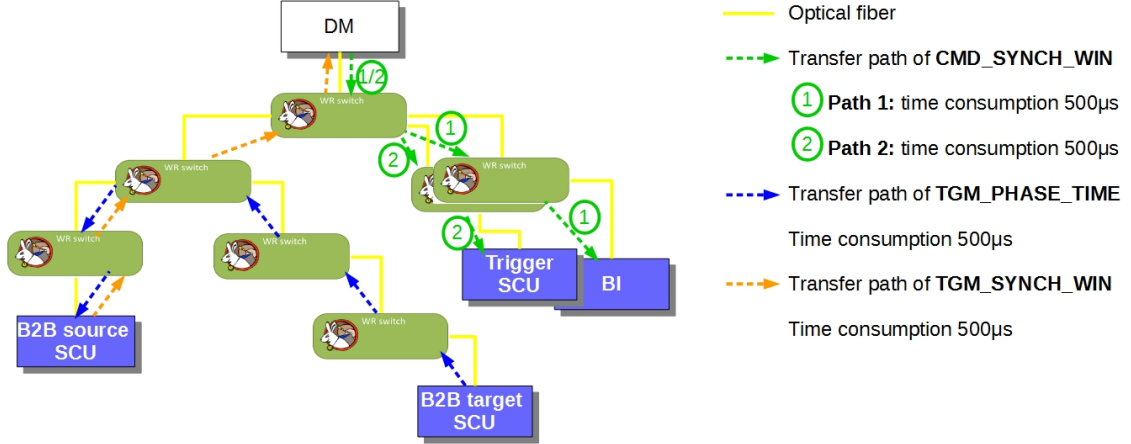


Figure 4.11: Transfer delay of the start of the synchronization window on the WR network.

Fig. 4.11 shows the transfer delay of the start of the synchronization window on the WR network. The timestamp of the start of the synchronization window t_w is first of all transferred from the B2B source SCU to the DM (the orange transfer path) by the timing frame TGM_SYNCH_WIN. Then t_w is repackaged by the DM into a new timing frame CMD_SYNCH_WIN and CMD_SYNCH_WIN is transferred from the DM to the source and target Trigger SCUs (the green transfer path with ②), as well as the BI (the green transfer path with ①) for the indication of the beam. The Trigger SCUs are used to produce the kicker trigger signals. The start of the synchronization window must be late enough to guarantee that the BI receives CMD_SYNCH_WIN and is activated before the start of the synchronization window. The start of the synchronization window must be at least 1.6 ms later than t_ψ^X . The time duration of 1.6 ms is the sum of the 500 μs upper bound transfer delay of TGM_PHASE_TIME (the blue transfer path), that of TGM_SYNCH_WIN (the orange transfer path), that of CMD_SYNCH_WIN (the green transfer path) on the WR network and 100 μs calculation time of the B2B source SCU. For more details of the time constraints, please see Chap. 5.

For the phase shift method, the rf frequency modulation has a fixed duration T . The start of the synchronization window for the phase shift method is calculated as

$$t_w = t_\psi^X + 500 \mu\text{s} + 100 \mu\text{s} + T - t_{delay} \quad (4.25)$$

where 500 μs is the upper bound transfer delay of TGM_PHASE_TIME on the WR network (the blue transfer path) and 100 μs the calculation time of the B2B source SCU. T must long enough to guarantee the activation of the BI timely, namely

$$500 \mu\text{s} + 100 \mu\text{s} + T - t_{delay} > 1.6 \text{ ms} \quad (4.26)$$

where T is generally longer than 5 ms, which is long enough to meet the time requirement of the BI.

4.3. Realization

The start of the synchronization window for the frequency beating method is calculated as

$$t_w = t_\psi^X + T_{wait} - \frac{T_w}{2} - t_{delay} \quad (4.27)$$

where the second term of T_{wait} , $n \cdot \frac{1}{|f_{syn}^{src} - f_{syn}^{trg}|}$, is used to guarantee the activation of the BI timely. n is calculated by the following relation.

$$\frac{\Delta\phi_{adjust}}{2\pi} \cdot \frac{1}{|f_{syn}^{src} - f_{syn}^{trg}|} + n \cdot \frac{1}{|f_{syn}^{src} - f_{syn}^{trg}|} - \frac{T_w}{2} - t_{delay} > 1.6 \text{ ms} \quad (4.28)$$

4.3.5 Bucket Label

The bucket label is realized based on the bucket indication signal plus a fixed delay for the indication of the correct buckets to be filled. The bucket indication signal indicates the first bucket.

The evolution of the phase deviation between the phase measurement signal and the synchronization reference signal of the target accelerator is calculated for any T0 incidents (same as eq. 4.15).

$$\varphi^{trg}(t_\psi^{trg} + nT_{sample_PAP}) = [(\psi_0^{trg} + k^{trg} \cdot nT_{sample_PAP}) \bmod 2\pi] - \pi \quad (4.29)$$

where ψ_0^{trg} is the phase advance extrapolated by the PAP module at t_ψ^{trg} of the target accelerator.

Therefore, the bucket indication signal can be corrected exactly in phase with the phase measurement signal of the target accelerator by $\varphi^{trg}(t_\psi^{trg} + nT_{sample_PAP})$ at the T0 incidents. The bucket indication signal is exactly a copy of the revolution frequency or the synchronization frequency of the target accelerator, so it is also called the "reproduced signal". The bucket indication signal can be reproduced campus-wide. A specific bucket is just a certain number of the cavity rf periods of the target accelerator delay based on the bucket indication signal.

The FAIR B2B transfer system needs the bucket indication not only at the rf flattop, but also during the whole acceleration cycle. The bucket indication at the rf flattop is used for the normal extraction and injection and the maximum bunch spacing indication during the whole acceleration cycle is used for the emergency dump. For the SIS100 emergency kick, the reproduced signal has always the same frequency and is always in phase with the SIS100 revolution signal, so it is called the "real-time reproduced signal". The bunch spacing label is realized based on the real-time reproduced signal for the first bucket plus a variable delay for the indication of the bunch spacing.

The bucket label is realized by the Trigger SCU, the Signal Reproduction (SR) module and the Phase Correction Module (PCM). The reproduced signal is produced by SR module. The Trigger SCU is responsible for the receipt of the phase correction value from the B2B source SCU and the transfer of this value to the PCM. The PCM module is used to correct the phase of the reproduced signal. The PCM module is a SCU slave in the Trigger SCU. The SR module produces the bucket indication signal marker in the format of the TTL signal, whose rising edges are aligned with the positive zero-crossings of the rf signal of the revolution frequency or the synchronization frequency. For more details about the implementation and realization of the PCM and the SR module, please see "Development of the LLRF system for a deterministic Bunch-to-Bucket transfer for FAIR" [43].

4.3. Realization

4.3.5.1 Bucket Label for the Normal Extraction and Injection

To determine the bucket label for the normal extraction and injection, three steps are necessary. Fig. 4.12 shows these three steps for the reproduction of the bucket label. Here the B2B transfer from the SIS18 to the SIS100 is taken as an example.

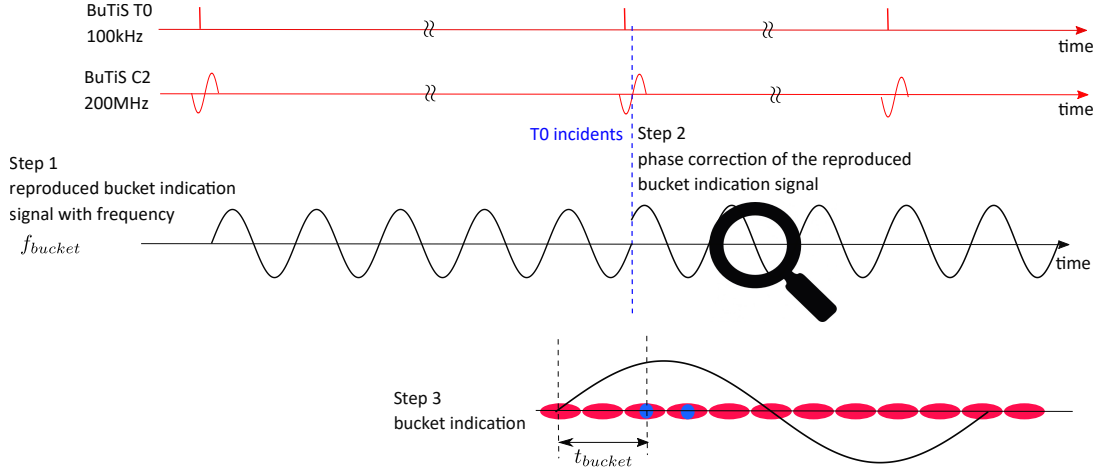


Figure 4.12: Realization of the bucket label for the normal extraction and injection.

- Step 1. Frequency correction

The SR module produces the "reproduced signal" with the frequency f_{bucket} . The positive zero-crossing of the reproduced signal always indicates the start of the 1st bucket.

- Step 2. Phase correction

The reproduced signal must do the phase correction at a specified T0 incident. The phase correction value and the phase correction timestamp are calculated by the B2B source SCU. The phase correction value is transferred by the timing frame TGM_PHASE_CORRECTION to the Trigger SCU. The timestamp of the phase correction is embodied in the execution time of TGM_PHASE_CORRECTION at the Trigger SCU, when the phase correction value is given by the Trigger SCU to the SR module via the PCM.

- Step 3. Bucket indication

The SM considers the bucket delay t_{bucket} within the kicker delay compensation, see Sec. 4.1.2. In Fig. 4.12, the reproduced signal is with the SIS100 revolution frequency and the 3rd and 4th buckets of ten buckets will be filled with $t_{bucket} = 1 \cdot T_{rev}^{SIS18}$.

4.3.5.2 Maximum Bunch Spacing Label for the Emergency Extraction

Only for the SIS100 emergency procedure, the maximum bunch spacing label is important during the whole acceleration cycle, because the emergency kicker can be triggered only at the maximum bunch spacing. There are two steps for the realization of the maximum bunch spacing label, see Fig. 4.13.

4.3. Realization

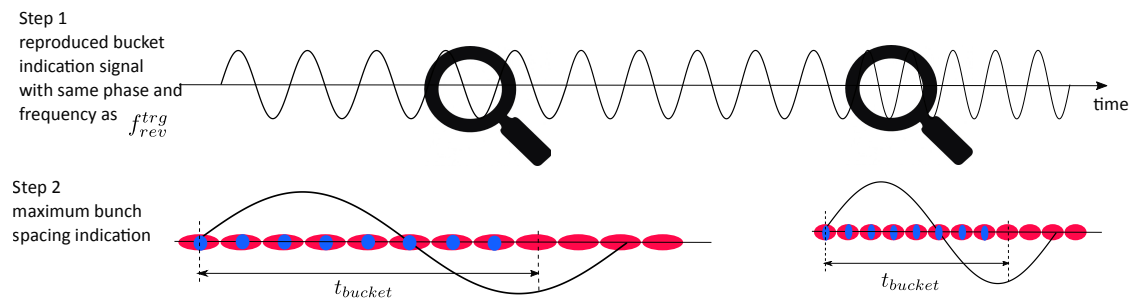


Figure 4.13: Realization of the maximum bunch spacing label for the emergency extraction.

- Step 1. Reproduced signal synchronized with the phase measurement signal of the revolution frequency

4.3. Realization

The real-time reproduced signal is directly distributed from the switch matrix, which synchronizes with the revolution frequency in frequency and phase.

- Step 2. Maximum bunch spacing indication

The SM considers the bunch train length t_{bucket} within the kicker delay compensation. In Fig. 4.13, the real-time reproduced signal is with the SIS100 revolution frequency and the eight of ten buckets (e.g. from the 1st to 8th buckets) will be injected by bunches. Hence, the maximum bunch spacing is composed of the empty 9th and 10th buckets and the bunch train length t_{bucket} equals to $4 \cdot T_{rev}^{SIS18}$.

4.3.6 Fine Synchronization of Extraction and Injection Kickers

After the synchronization of the rf systems between two ring accelerators, the TOF, all propagation and kicker preparation delays are compensated. Now, the extraction and injection kickers must be fired at the calculated trigger time within the bunch gap before the specific bunch or bucket passes the kickers.

This is the task of the Trigger Decision (TD) module in the Trigger SCU. The TD receives the synchronization window in the form of an enable signal. The fine synchronization will be accomplished by the marker of the reproduced signal plus the extraction or injection kicker delay compensation from the SM. This achieves the fine synchronization of the B2B transfer. The TD transmits the kicker pulse directly to the kicker electronic.

In case of fatal errors, the emergency kicker must kick the beam immediately into the emergency dump.

The kicker trigger is realized based on the first rising edge of the bucket indication signal marker within the synchronization window plus the kicker delay compensation. For the normal B2B extraction/injection, the synchronization window is received by the source and target Trigger SCUs from the WR network by CMD_SYNCH_WIN. The extraction kick delay compensation is $T_{rev}^{SIS100} + T_{rev}^{SIS18} - (t_{TOF} + t_{v_inj} + t_{ext})$ and the injection kicker delay compensation is $T_{rev}^{SIS100} + T_{rev}^{SIS18} - (t_{v_inj} + t_{inj})$ in the example in Fig. 4.1, when the bucket indication signal has the frequency of f_{rev}^{trg} .

For some FAIR use cases, not in case of the B2B transfer from the SIS18 to the SIS100, there is only one bucket in the target accelerator when $f_{bucket} = f_{syn}^{trg}$. In this case, the bucket delay is not taken into consideration. The extraction kick delay compensation is $T_{syn}^{trg} - (t_{TOF} + t_{v_inj} + t_{ext})$ and the injection kicker delay compensation is $T_{syn}^{trg} - (t_{v_inj} + t_{inj})$, see Fig. 4.14.

Both extraction and injection kick delay compensation values are preloaded from the SM to the Trigger SCU and the Trigger SCU gives these values to the TD module. When the beam injection inhibit signal from the MPS is on, the TD module will block the extraction/injection trigger.

For the SIS100 emergency kick, the extraction delay compensation is calculated by $T_{rev}^{SIS100} + t_{bucket} - (t_{v_emg} + t_{emg})$, where t_{v_emg} is the time delay between the virtual rf cavity and the emergency extraction position, t_{emg} the emergency kicker delay and t_{bucket} always indicates the bunch train length. The emergency extraction delay compensation values are preloaded from the SM to the Trigger SCU and the

4.4. Data Flow

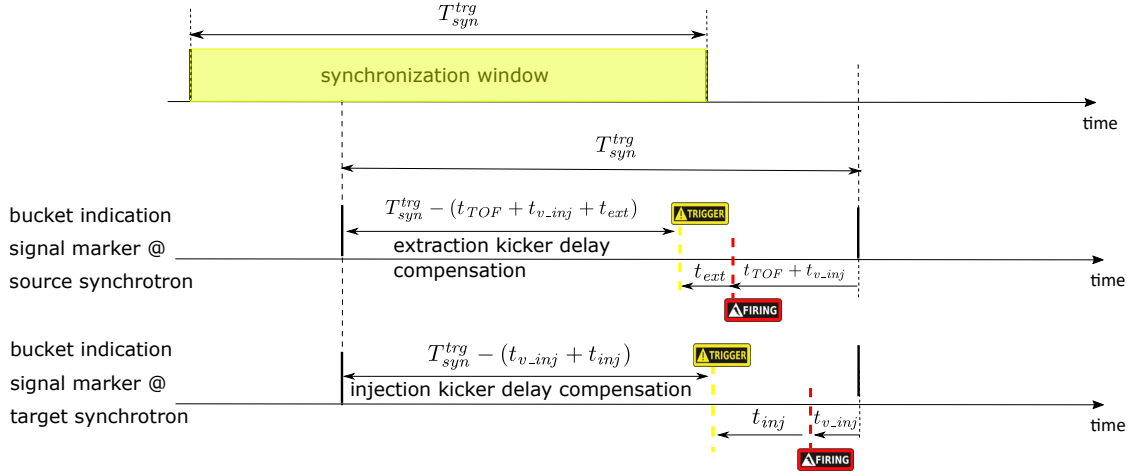


Figure 4.14: Illustration of the kicker delay compensation when the bucket indication signal has the frequency of f_{syn}^{trg} .

Trigger SCU gives these values to the TD module. The kicker delay compensation is applied to the real-time reproduced signal by TD module. Only when the emergency dump signal from MPS is valid, the emergency kicker will be triggered by the TD module.

4.3.7 B2B Transfer Status Check

The B2B transfer status must be known by the DM. The B2B source SCU, the B2B transfer master, is responsible for the status check. The B2B source SCU receives the trigger time of the extraction kicker and actual beam extraction time, TGM_KICKER_TRIGGER_TIME_S, from the source Trigger SCU via the WR network and also the trigger time of the injection kicker and actual beam injection time, TGM_KICKER_TRIGGER_TIME_T, from the target Trigger SCU via the WR network. The actual beam extraction time is the beginning of the kicker flat-top of the last extraction kicker magnet and the actual beam injection time is the beginning of the kicker flat-top of the first injection kicker magnet. The Trigger SCU is responsible for the collection of the kicker trigger time and the beam extraction/injection time. The B2B source SCU examines the status of the B2B transfer system and transfers the status and the actual beam injection time, TGM_B2B_STATUS, to the DM. If all components of the B2B transfer system have worked correctly, the B2B transfer process is successful. Otherwise it has failed.

The source and target Kicker SCUs individually get the timestamp of the beginning of the magnetic flattop of the last extraction kicker unit and the first injection kicker unit and transfer these information

4.4 Data Flow

In this section, the procedure for the B2B transfer is explained from the perspective of the data flow, which follows the basic six steps in Fig. 4.4. Fig. 4.15 shows the data flow in the source and target ring accelerators and between two ring accelerators. The rectangle with the different color represents the basic six steps. The left

4.4. Data Flow

part in each rectangle presents the data flow in the source accelerator and the right part the data flow in the target accelerator.

4.4. Data Flow

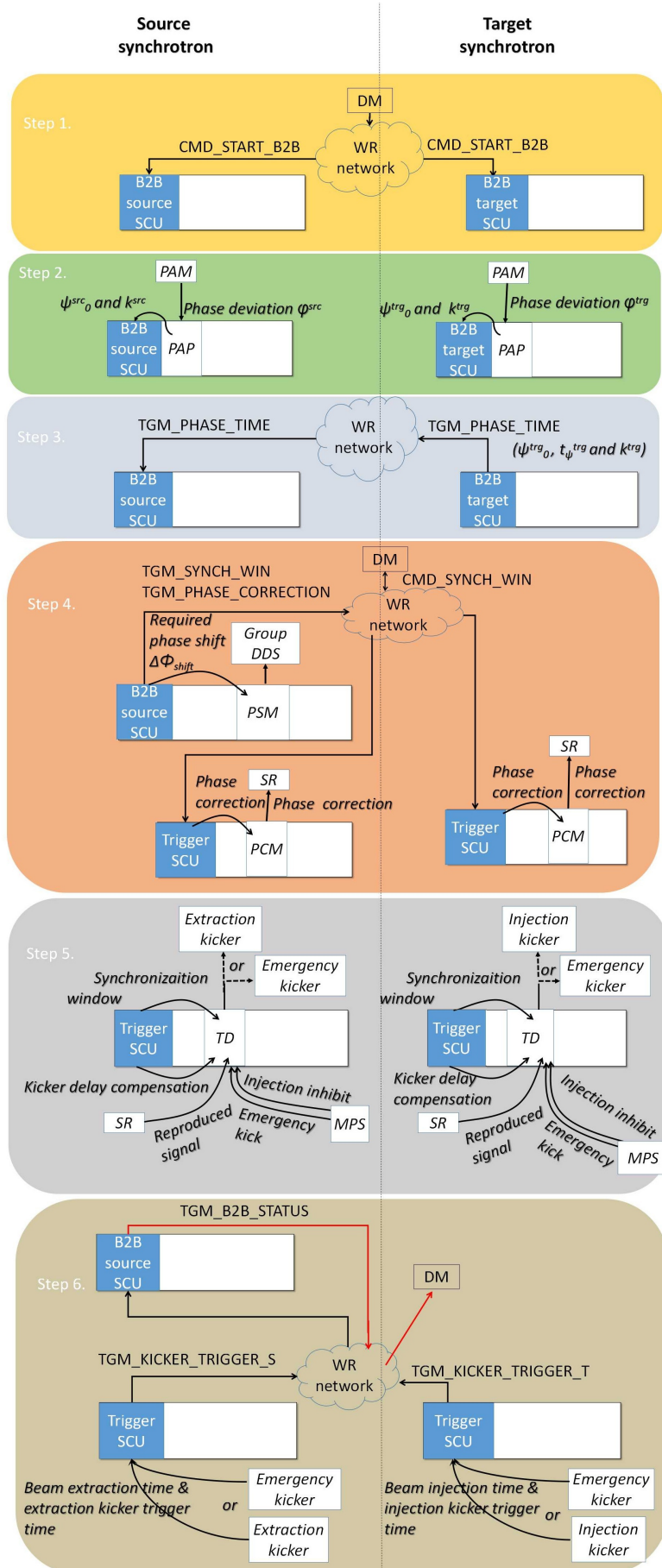


Figure 4.15: Data flow of the B2B transfer system

4.4. Data Flow

1. The DM sends the timing frame CMD_START_B2B to the B2B source and target SCUs for the start of the B2B transfer via the WR network. Besides, it requests the switch-off of the feedback loop.
2. After receiving CMD_START_B2B, the B2B source and target SCUs start the PAM module to measure the phase deviation φ^X with the help of the PAP module locally and the PAP module extrapolates the phase advance into the future. After a period of time, the B2B source and target SCUs read the extrapolated phase advance ψ_0^X and the slope of the phase deviation k^X from the PAP module locally, timestamping the ψ_0^X .
3. The B2B target SCU sends the extrapolated phase ψ_0^{trg} , the corresponding timestamp t_ψ^{trg} and the slope k^{trg} in the format of the timing frame TGM_PHASE_TIME to the B2B source SCU in the B2B VLAN.
4. When the B2B source SCU receives the timing frame TGM_PHASE_TIME, it calculates the synchronization window and transfers the timestamp of the start of the window to the DM in the format of the timing frame TGM_SYNCH_WIN. Then the DM transfers the start of the window to the Trigger SCUs at the source and target accelerators by CMD_SYNCH_WIN. The B2B source SCU calculates the phase correction value and transfers it to all Trigger SCUs via the WR network in the format of the timing frame TGM_PHASE_CORRECTION. Then the Trigger SCUs transfer the phase correction value to its PCM. The PCM starts the phase correction of the SR module.

Only for the phase shift method, the B2B source SCU calculates the required phase shift $\Delta\phi_{shift}$ and transfers it to the PSM. Then the PSM transfers the phase or frequency modulation profile to the Group DDS.

5. When the source and target Trigger SCUs receive the timing frame CMD_SYNCH_WIN, they produce the synchronization window pulse for the TD module. With the help of the reproduced signal from the SR module, the kicker delay compensation from the Trigger SCU and the indication signals (the emergency dump signal and the beam injection inhibit signal) from the MPS, the TD module produces the normal extraction/injection trigger signals or the emergency kick trigger for the kicker.
6. The extraction and injection kickers or emergency kicker are fired. After that, the source Trigger SCU gets the actual beam extraction time and the timestamp of the extraction trigger signal from the TD module and transfers them to the B2B source SCU in the format of the timing frame TGM_KICKER_TRIGGER_TIME_S. The target Trigger SCU gets the timestamp of actual beam injection time and the timestamp of the injection trigger signal from the TD module and transfers them to the B2B source SCU in the format of the timing frame TGM_KICKER_TRIGGER_TIME_T. Then the B2B source SCU checks the B2B transfer status and transfers the status together with the beam injection time to the DM in the format of the timing frame TGM_B2B_STAUS (represented as the red line in the rectangle of step 6 in Fig. 4.15).

4.5 Comparison between the FAIR B2B Transfer System and Current B2B Transfer

The existing GSI control system realizes the B2B transfer from the SIS18 to the ESR. It is an event based system, that event execution will start immediately at the event receipt. Events are directly sent from a “timing master”, who makes the schedule. Each accelerator has its own timing master, e.g. the ESR is equipped with the ESR-timing master and the SIS18 with the SIS-timing master [46, 47].

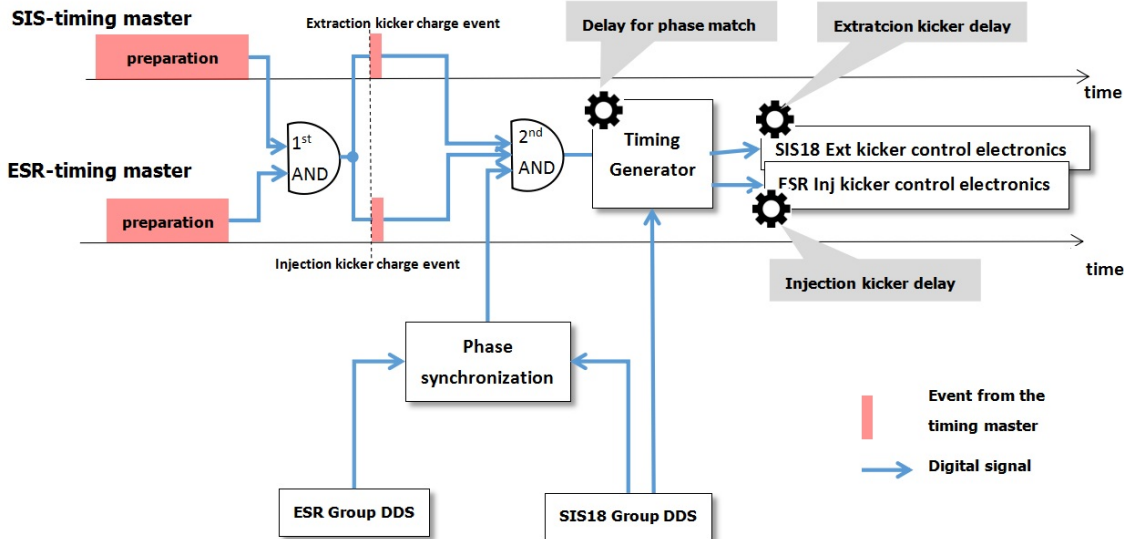


Figure 4.16: Current realization of the bunch-to-bucket transfer between the SIS18 and the ESR with the GSI control system.

Gear sign represents the configuration from operators.

Fig. 4.16 illustrates the current realization of the B2B transfer from the SIS18 to the ESR with the GSI control system. The SIS18 needs longer time for the preparation, e.g. the beam injection and the beam acceleration, before the extraction than that of the ESR before the injection, so the ESR is earlier fully prepared for the transfer. When the SIS18 is fully prepared with bunches to be transferred, the ready signal from the ESR-timing master and the SIS-timing master are forwarded into the first logic *AND* gate. When both the SIS18 and the ESR are prepared, namely the output of the first logic *AND* gate is high, the extraction kicker charge event is sent from the SIS-timing master and the injection kicker charge event from the ESR-timing master. The energy storage module of kicker will be charged by the high voltage power supply, see Chap. 2. When the energy storage module of two kickers are fully charged, the ready signal of the extraction and injection kickers from the ESR-timing master and the SIS-timing master are forwarded into the second logic *AND* gate, as well as the “phase synchronization signal” from the rf system. The phase synchronization signal indicates the alignment of the zero-crossing of the cavity rf frequencies from Group DDS of the SIS18 and the ESR, which is a “coarse synchronization”. The output of the second *AND* gate is an indication signal, starting the delay compensation of the time-of-flight, the bunch gap and all propagation delays on the SIS18 cavity rf signal for the correct

4.5. Comparison between the FAIR B2B Transfer System and Current B2B Transfer

phase matching between the SIS18 and ESR rf systems, denoted as “delay for phase matching” in Fig. 4.16. The delay compensation based on the SIS18 cavity rf signal is the process of a “fine synchronization”. The GSI control system realizes the B2B transfer from the SIS18 to the ESR with an acceptable bunch-to-bucket injection center mismatch.

The ESR uses the injection orbit instead of the design orbit, so the circumference ratio between the SIS18 and the ESR is close to an integer, $C^{SIS18}/C^{ESR} = 2 - 0.003$, the SIS18 has four bunches, $h^{SIS18} = 4$ and ESR has two buckets, $h^{ESR} = 2$, so $f_{rf}^{SIS18}/f_{rf}^{ESR} = 4/(4 - 0.006)$. The phase difference between rf systems of the SIS18 and the ESR varies at the speed of the beating frequency $\Delta f = |f_{rf}^{SIS18} - f_{rf}^{ESR}| = 1898$ Hz, see Appendix. C.2. The required phase adjustment $\Delta\phi_{adjust}$ happens T_{wait} after the indication signal, see eq. 4.30.

$$T_{wait} = \frac{\Delta\phi_{adjust}}{2\pi} \cdot \frac{1}{\Delta f} + n \frac{1}{\Delta f} \quad (4.30)$$

When the delay for the required phase difference is expired, trigger pulses are produced by the timing generator for both the SIS18 extraction and ESR injection kicker control electronics. Every kicker control electronics adds a separate delay to trigger pulses, denoted as “extraction kicker delay” and “injection kicker delay” in Fig. 4.16. The delay for the required phase matching, extraction kicker delay and injection kicker delay are configurable by operators. The precision of the ignition signal from the kicker control electronics is 1 ns.

The existing B2B transfer with the GSI control system only supports the B2B transfer with the frequency beating method. It does not support B2B transfer with the phase shift method. It gets the phase difference between the two rf systems of the SIS18 and the ESR via the direct phase comparison by the phase synchronization module. Parameters (e.g. the delay for the required phase matching, the extraction kicker delay and the injection kicker delay) must be properly configured and adjusted by operators. Besides, it does not support buckets filling by multiple batches, e.g. eight out of ten SIS100 buckets are filled by four SIS18 batches, each of them has two bunches.

Compared with the current B2B transfer with the GSI control system, the FAIR B2B transfer system has many advantages. It supports both the phase shift and frequency beating methods. The FAIR B2B transfer system is based on the GMT system, which is a time based system. All FECs of the GMT system are time synchronized with nano second accuracy, which achieves the bunch-to-bucket transfer with the acceptable bunch-to-bucket injection center mismatch. Besides, the FAIR B2B transfer system is more flexible. It supports several B2B transfers running at the same time, e.g. the B2B transfer from the SIS18 to the SIS100 and B2B transfer from the ESR to the CRYRING. It is capable to transfer different species beam from one machine cycle to another without the operator’s configuration. It is capable to transfer the beam between two ring accelerators via a FRS, pbar target or Super FRS. It can achieve various complex bucket pattern. In addition, the FAIR B2B transfer system coordinates with the MPS system, which protects accelerators from unacceptable failure or situation.

Chapter 5

Realization and Systematic Investigation of the FAIR B2B Transfer System

This chapter concentrates on the realization and systematic investigation of the B2B transfer system. In Sec. 5.1, both the phase shift and frequency beating synchronization methods are analyzed from the beam dynamic perspective. The characterization of the WR network is investigated for the B2B transfer, the calculation of the synchronization window, the flowcharts of the system and the corresponding timing constraints are presented in Sec. 5.2. The B2B transfer system for FAIR focuses first of all on the transfer from the SIS18 to the SIS100, so the different trigger scenarios of the SIS18 extraction and SIS100 injection kickers are systematically investigated in Sec. 5.3. Besides, the test setup from the timing aspect is introduced and the test result is analyzed in Sec. 5.4.

5.1 Beam Dynamic Analysis of two Synchronization Methods for the B2B Transfer from SIS18 to SIS100

This section analyzes the phase shift and frequency beating methods from the beam-dynamics perspective for the synchronization of the SIS18 with the SIS100. Because the most stringent requirement are from the lightest and heaviest ion species, the beam dynamics of the H^+ and U^{28+} beams are analyzed.

The dispersion function, a lattice parameter, defines the local sensitivity of the beam trajectory to a relative energy error [17]. For the rf frequency modulation of the phase shift method, the dispersion function is reflected in the relative momentum shift. The maximum tolerable relative momentum shift is decided by the semi-aperture $X_D(s)$ required for the beam and the dispersion function $D(s)$.

$$X_D(s) = D(s) \cdot \frac{\Delta p}{p} \Big|_{\frac{\Delta B}{B}=0} \quad (5.1)$$

The maximum tolerable relative momentum of the H^+ beam and that of the U^{28+} beam of the SIS18 are the same by coincidence, $\Delta p/p_{max} = \pm 0.008$, which is given by machine design.

5.1. Beam Dynamic Analysis of two Synchronization Methods for the B2B Transfer from SIS18 to SIS100

For the frequency beating method ($\Delta p/p = 0$), the dispersion function is reflected in the relative bending magnetic field shift instead of the relative momentum shift. The maximum tolerable relative bending magnetic field shift is decided by the semi-aperture required for the beam and the dispersion function.

$$X_D(s) = -D(s) \cdot \frac{\Delta B}{B} \Big|_{\frac{\Delta p}{p}=0} \quad (5.2)$$

The maximum tolerable relative bending magnetic field shift of the H^+ beam and that of the U^{28+} beam of the SIS18 are minus of their maximum tolerant relative momentum shift, namely $\Delta B/B_{max} = -\Delta p/p_{max} = \pm 0.008$. The constraint on the displacement of the orbit length $\Delta L/L_{max}$ is obtained by

$$\frac{\Delta L}{L} = \begin{cases} \alpha_p \cdot \frac{\Delta p}{p} & \text{Phase shift method} \\ -\alpha_p \cdot \frac{\Delta B}{B} & \text{Frequency beating method} \end{cases} \quad (5.3)$$

The reasonable bucket size of a running bucket is larger than 80% of that of a stationary bucket, namely $\alpha_b(\phi_s) \geq 80\%$. Due to the constraint of the bucket size, the synchronous phase must stay within the range between -6.4° and $+6.4^\circ$.

The acceptable range of the parameters accompanying with the frequency adjustment of the phase shift method for the SIS18 H^+ and U^{28+} beams are summarized in Tab. 5.1 and that accompanying with the frequency adjustment of the frequency beating method are summarized in Tab. 5.2. α_p equals to 0.01 for the H^+ beam and 0.03 for the U^{28+} beam [38].

Table 5.1: Acceptable range of the parameters accompanying with the frequency adjustment of the phase shift method for the SIS18 H^+ and U^{28+} beams

| $\Delta p/p_{max}$ | $\Delta L/L_{max}$ | $\alpha_b(\phi_s)_{min}$ | ϕ_s_{max} |
|--------------------|--|--------------------------|-----------------|
| ± 0.008 | $H^+ \pm 0.80 \cdot 10^{-4}$ $U^{28+} \pm 2.40 \cdot 10^{-4}$ | 80% | $\pm 6.4^\circ$ |

Table 5.2: Acceptable range of the parameters accompanying with the frequency adjustment of the frequency beating method for the SIS18 H^+ and U^{28+} beams

| $\Delta B/B_{max}$ | $\Delta L/L_{max}$ | $\alpha_b(\phi_s)_{min}$ | ϕ_s_{max} |
|--------------------|--|--------------------------|-----------------|
| ± 0.008 | $H^+ \pm 0.80 \cdot 10^{-4}$ $U^{28+} \pm 2.40 \cdot 10^{-4}$ | 80% | $\pm 6.4^\circ$ |

5.1.1 Beam Dynamics of the Phase Shift Method for U^{28+}

The obtained phase shift $\Delta\phi$ is determined by the rf frequency modulation Δf_{rf} and the duration of the frequency modulation T (same as eq. 2.22).

$$\Delta\phi = 2\pi \int_{t_0}^{t_0+T} \Delta f_{rf}(t) dt \quad (5.4)$$

5.1. Beam Dynamic Analysis of two Synchronization Methods for the B2B Transfer from SIS18 to SIS100

In order to make the rf frequency modulation effective, the beam feedback loops on the rf system are switched off before the B2B transfer starts. There are a list of criteria for the rf frequency modulation for the longitudinal emittance to be preserved (see Sec. 2.3.1).

- There exists a maximum rf frequency offset Δf_{rf_max} , which comes from the constraint of $\Delta p/p_{max}$ in Tab. 5.1. According to eq. 2.53, $|\Delta f_{rf}| \leq 8.137 \text{ kHz}$.
- $|\frac{d\Delta f_{rf}}{dt}|$ must be continuous and small enough. Buckets must be big enough to capture bunches. From eq. 2.60 we know that the bucket area factor is in inverse proportion to $\frac{d\Delta f_{rf}}{dt}$. Hence, $|\frac{d\Delta f_{rf}}{dt}|$ must be small enough to guarantee the bucket size. $|\frac{d\Delta f_{rf}}{dt}|$ must be smaller than 95 Hz/ms in order to guarantee the bucket area factor is larger than 80%. In addition, the synchronous phase must change continuously for the beam to follow. From eq. 2.58 we know that $\frac{d\Delta f_{rf}}{dt}$ is proportional to the change in the synchronous phase. Hence, $|\frac{d\Delta f_{rf}}{dt}|$ must be continuous.
- $|\frac{d^2\Delta f_{rf}}{dt^2}|$ must be small enough. From eq. 2.63 we know that the change rate of the synchronous phase must be slow enough for the beam to follow. If for instance the adiabaticity should be smaller than $1 \cdot 10^{-4}$, $|\frac{d^2\Delta f_{rf}}{dt^2}|$ must be smaller than 70 Hz/ms².

According to these criteria, some rf frequency modulations are obviously ruled out of consideration. e.g. a trapezoid modulation and a triangular modulation, whose first derivatives are not continuous. The following three examples of rf frequency modulation are analyzed, which comply with the above mentioned criteria. The case (1) is a sinusoidal modulation and the amplitude is determined by the sinusoidal period, the case (2) is a parabolic modulation, which consists of three parabolas and two lines between every two parabolas, and the case (3) is also a parabolic modulation, including three parabolas. All three cases give the same phase shift, $\Delta\phi = \pi$, which is proved by substituting each form of $\Delta f_{rf}(t)$ into eq. 5.4 and performing integration. The phase shift is assumed to be achieved within 7 ms, namely $T = 7 \text{ ms}$. Three rf frequency modulation cases are shown in Fig. 5.1.

5.1. Beam Dynamic Analysis of two Synchronization Methods for the B2B Transfer from SIS18 to SIS100

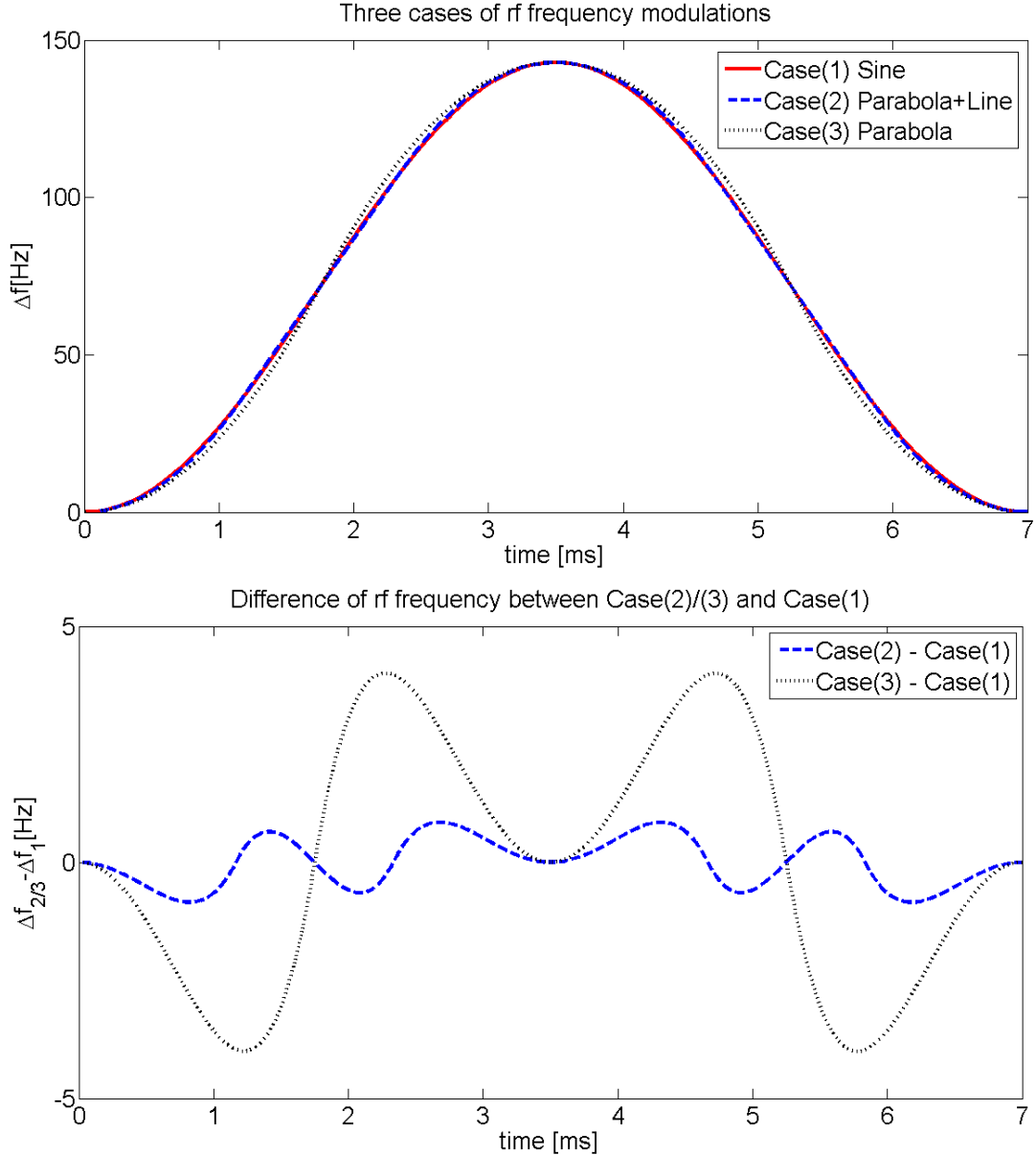


Figure 5.1: Examples of rf frequency modulation.

Case (1)

$$\Delta f_{rf}(t) = \frac{1}{2T} \left[1 - \cos\left(\frac{2\pi}{T}(t - t_0)\right) \right] \quad t_0 + 0 < t \leq t_0 + T \quad (5.5)$$

Case (2)

$$\Delta f_{rf}(t) = \begin{cases} \frac{9}{T^3}(t - t_0)^2 & t_0 + 0 < t \leq t_0 + \frac{T}{6} \\ \frac{1}{4T} + \frac{3}{T^2}(t - t_0 - \frac{T}{6}) & t_0 + \frac{T}{6} < t \leq t_0 + \frac{2T}{6} \\ \frac{1}{T} - \frac{9}{T^3}(t - t_0 - \frac{T}{2})^2 & t_0 + \frac{2T}{6} < t \leq t_0 + \frac{4T}{6} \\ \frac{3}{4T} - \frac{3}{T^2}(t - t_0 - \frac{4T}{6}) & t_0 + \frac{4T}{6} < t \leq t_0 + \frac{5T}{6} \\ \frac{9}{T^3}(t - t_0 - T)^2 & t_0 + \frac{5T}{6} < t \leq t_0 + T \end{cases} \quad (5.6)$$

5.1. Beam Dynamic Analysis of two Synchronization Methods for the B2B Transfer from SIS18 to SIS100

Case (3)

$$\Delta f_{rf}(t) = \begin{cases} \frac{8}{T^3}(t - t_0)^2 & t_0 + 0 < t \leq t_0 + \frac{T}{4} \\ \frac{1}{T} - \frac{8}{T^3}[(t - t_0) - \frac{T}{2}]^2 & t_0 + \frac{T}{4} < t \leq t_0 + \frac{3T}{4} \\ \frac{8}{T^3}[T - (t - t_0)]^2 & t_0 + \frac{4T}{4} < t \leq t_0 + T \end{cases} \quad (5.7)$$

Fig. 5.2 and Fig. 5.3 show the first and second derivative of three rf frequency modulations.

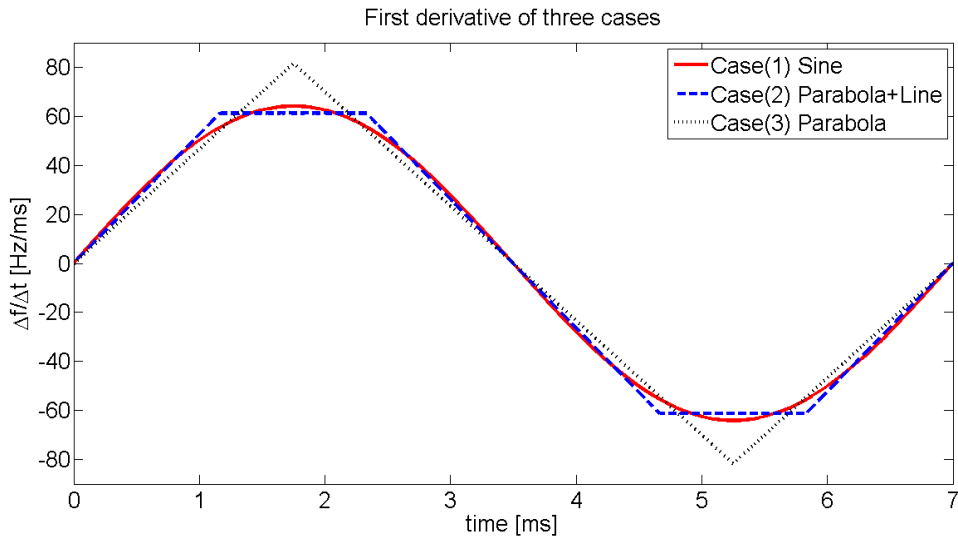


Figure 5.2: First derivative of three cases.

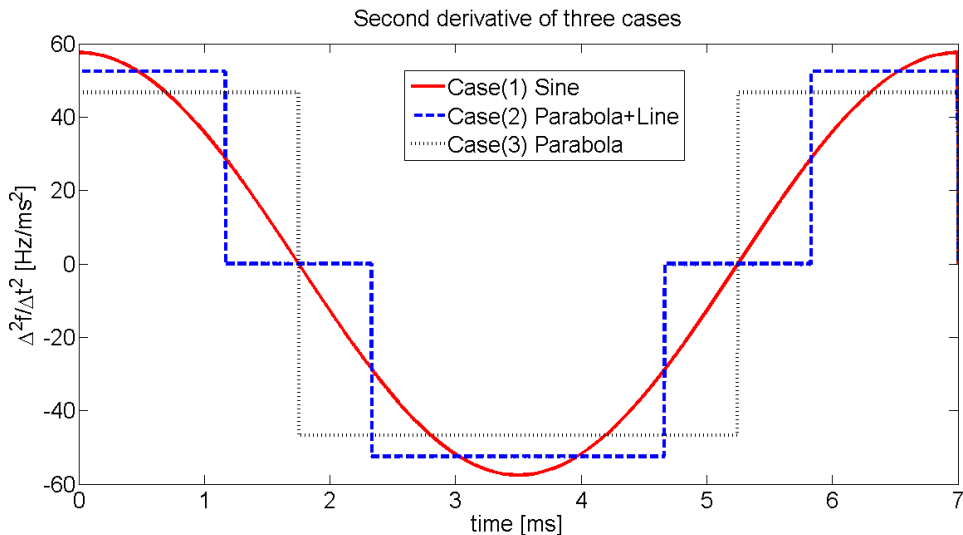


Figure 5.3: Second derivative of three cases.

Fig. 5.4 shows the corresponding phase shift modulation of three cases.

5.1. Beam Dynamic Analysis of two Synchronization Methods for the B2B Transfer from SIS18 to SIS100

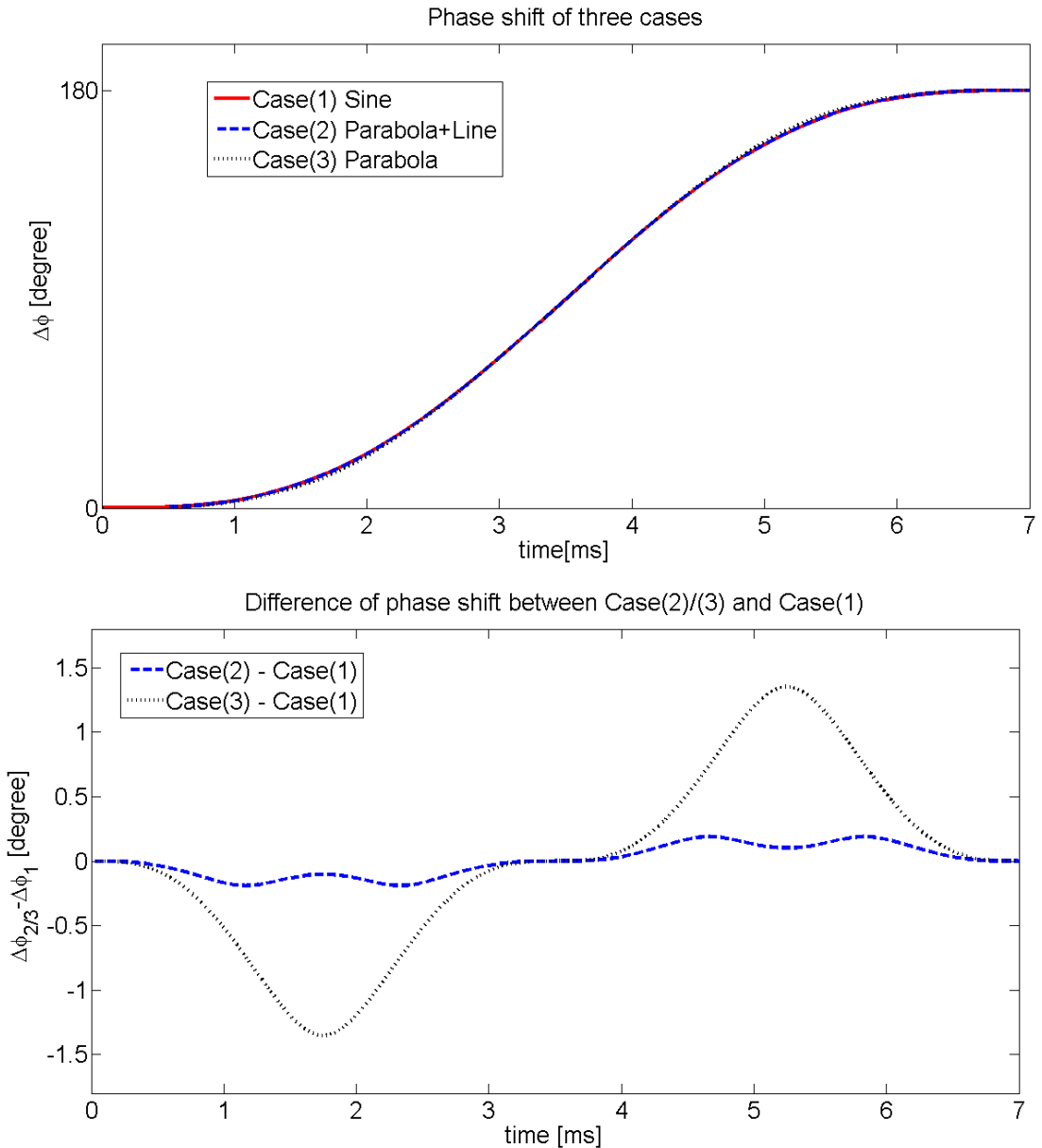


Figure 5.4: Phase shift modulation of three cases.

5.1.1.1 Longitudinal Dynamic Analysis

In this section, the average radial excursion, the relative momentum shift, the synchronous phase, the bucket size and the adiabaticity of three rf frequency modulations are analyzed.

- Orbit length displacement

The orbit length displacement is calculated for the three cases by eq. (2.54). Fig. 5.5 shows the calculation result.

5.1. Beam Dynamic Analysis of two Synchronization Methods for the B2B Transfer from SIS18 to SIS100

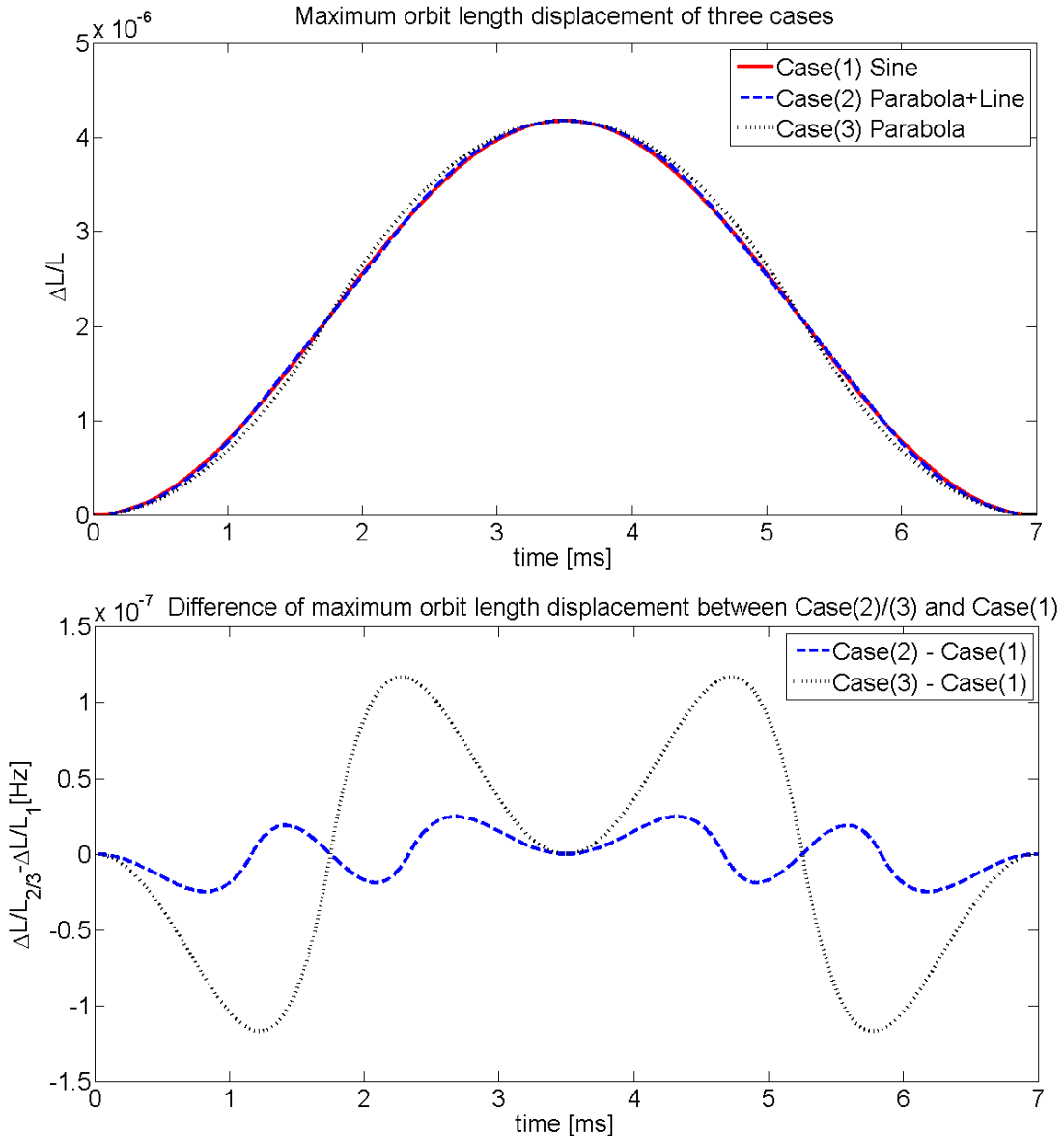


Figure 5.5: Maximum orbit length displacement of three cases.

Table 5.3: Maximum orbit length displacement of three cases

| | Case (1) | Case (2) | Case (3) |
|-----------------------------------|----------------------|----------------------|----------------------|
| Maximum orbit length displacement | $4.18 \cdot 10^{-6}$ | $4.18 \cdot 10^{-6}$ | $4.18 \cdot 10^{-6}$ |

As shown in Tab. 5.3 the maximum orbit length displacement is $4.18 \cdot 10^{-6}$ for all three cases, which is within the acceptable range in Tab. 5.1. Hence, all cases are applicable.

- Relative momentum shift

The relative momentum shift is calculated for three cases by eq. 2.53. Fig. 5.6 shows the calculation result.

5.1. Beam Dynamic Analysis of two Synchronization Methods for the B2B Transfer from SIS18 to SIS100

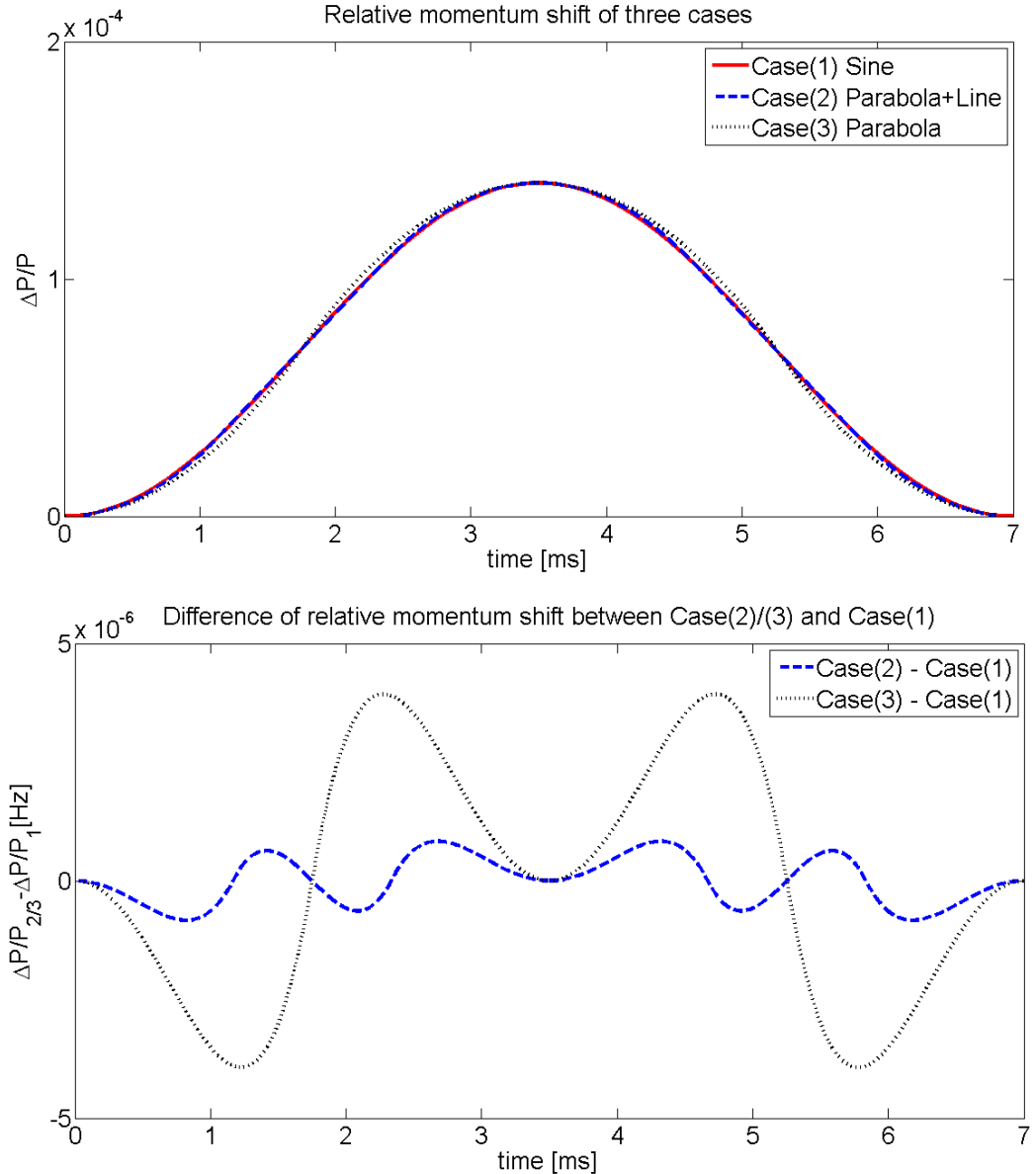


Figure 5.6: Relative momentum shift of three cases.

Table 5.4: Maximum relative momentum shift of three cases

| | Case (1) | Case (2) | Case (3) |
|---------------------------------|----------------------|----------------------|----------------------|
| Maximum relative momentum shift | $1.40 \cdot 10^{-4}$ | $1.40 \cdot 10^{-4}$ | $1.40 \cdot 10^{-4}$ |

As shown in Tab. 5.4 the maximum relative momentum shift is $1.40 \cdot 10^{-4}$ for all three cases, which is within the acceptable range in Tab. 5.1. Hence, all cases are applicable.

- Synchronous phase

The rf frequency modulations make the synchronous phase deviate from the nominal value 0. Fig. 5.7 shows the changes in the synchronous phase $\phi_s(t)$.

5.1. Beam Dynamic Analysis of two Synchronization Methods for the B2B Transfer from SIS18 to SIS100

It is calculated by substituting values into eq. 2.56. For three cases, the synchronous phase $\Delta\phi_s(t)$ during the modulations are continuous without any phase jumps and smaller than $\pm 6^\circ$. Hence, all cases are applicable.

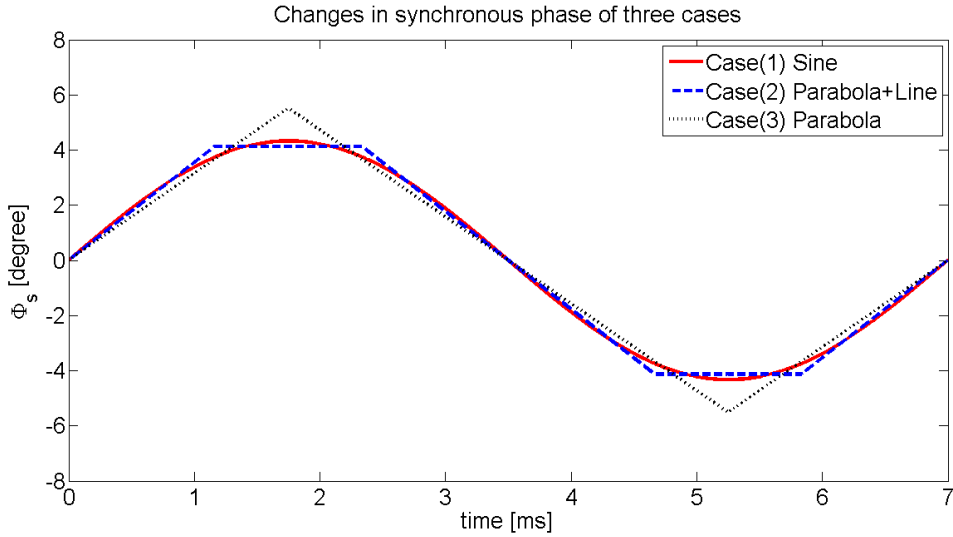


Figure 5.7: Changes in synchronous phase of three cases.

- Bucket size

The bucket area factor α_b varies during rf frequency modulations. Before the modulations, the synchronous phase $\phi_s=0$ and $\alpha_b(0^\circ) = 1$. By substituting the changes in synchronous phase into eq. 2.59, we get the ratio of bucket areas of a running bucket to the stationary bucket for three cases, see Fig. 5.8.

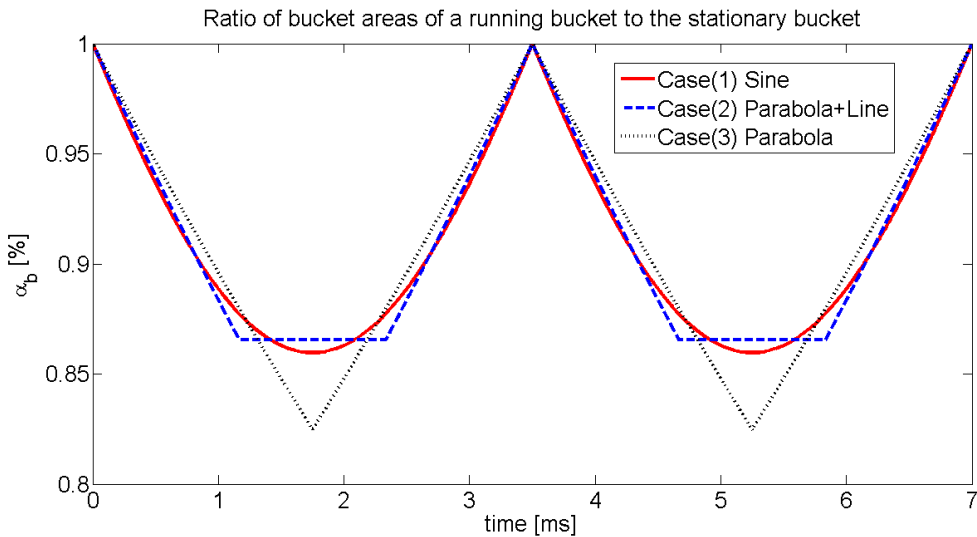


Figure 5.8: Ratio of bucket areas of a running bucket to the stationary bucket of three cases.

Tab. 5.5 shows the minimum bucket area factor for three cases. For case (1) and (2), the bucket area factor is larger than 86%, which is larger than that

5.1. Beam Dynamic Analysis of two Synchronization Methods for the B2B Transfer from SIS18 to SIS100

of the case (3). Hence, case (1) and (2) are preferred compared with the case (3).

Table 5.5: Minimum bucket area factor of three cases

| | Case (1) | Case (2) | Case (3) |
|----------------------------|----------|----------|----------|
| Minimum bucket area factor | 86.0% | 86.5% | 82.5% |

- Adiabaticity

By substituting the values of $\phi_s(t)$, $\dot{\phi}_s(t)$ and ω_s into eq. 2.63, we get the adiabaticity parameter ε for three cases, see Fig. 5.9.

Tab. 5.6 shows the maximum adiabaticity parameter for three cases. For case (1), the maximum of ε is 0.000030. For case (2), the maximum of ε occurs at $1/6T$, $2/6T$, $4/6T$ and $5/6T$, when the change rate of the synchronous phase $\dot{\phi}_s(t)$ has a maximum, shown in Fig. 5.7. For case (3), the maximum of ε occurs at $1/4T$ and $3/4T$, when the change rate of the synchronous phase $\dot{\phi}_s(t)$ has a maximum. For all three cases, the adiabaticity parameter has the order of magnitude 10^{-4} . The calculation of the criteria of the adiabaticity is beyond the scope of this dissertation.

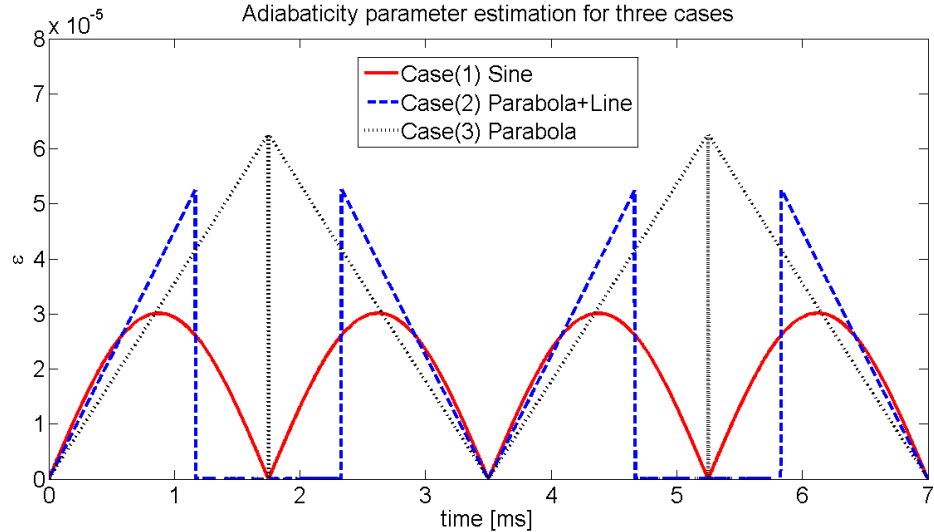


Figure 5.9: Adiabaticity parameter of three cases.

Table 5.6: Maximum adiabaticity of three cases

| | Case (1) | Case (2) | Case (3) |
|----------------------|----------------------|----------------------|----------------------|
| Maximum adiabaticity | $5.30 \cdot 10^{-5}$ | $5.90 \cdot 10^{-5}$ | $6.30 \cdot 10^{-5}$ |

5.1. Beam Dynamic Analysis of two Synchronization Methods for the B2B Transfer from SIS18 to SIS100

5.1.1.2 Transverse Dynamics Analysis

For the SIS18, the chromaticities Q'_x and Q'_y for the U^{28+} operation are -6.5 and -4.1 . Substituting the chromaticity and the maximum momentum shift (see. Tab. 5.4) into eq. 2.64, the chromatic tune shifts ΔQ_x and ΔQ_y during rf modulations for three cases can be calculated. Because case (1), case (2) and case (3) have the same maximum relative momentum shift, the chromatic tune shifts are same for the three rf frequency modulations.

$$\Delta Q_x = -6.5 \cdot 1.40 \cdot 10^{-4} = -9.10 \cdot 10^{-4} \quad (5.8)$$

$$\Delta Q_y = -4.1 \cdot 1.40 \cdot 10^{-4} = -5.74 \cdot 10^{-4} \quad (5.9)$$

The chromatic tune shift for three cases are negligibly small.

In a word, although all three cases meet the requirement of the parameters accompanying with the frequency adjustment, the case (1) of a sinusoidal modulation is the best one for the beam performance because of the smaller adiabaticity.

5.1.2 Beam Dynamics of the Frequency Beating Method for U^{28+}

In the case of the frequency beating method, we guarantee the extraction and injection energy always match, which means that the momentum of the synchronous particle is not affected by the frequency detuning. Hence, the frequency detuning has no influence on the chromaticity tune shift.

5.1.2.1 Longitudinal Dynamics Analysis

For the frequency beating method, the rf frequency detuning is done at the SIS18 rf flattop. The SIS18 U^{28+} acceptable displacement of the orbit length is $\pm 2.4 \cdot 10^{-4}$, see Tab. 5.2. Hence, the tolerable rf frequency change for U^{28+} at the extraction energy 200 MeV/u is calculated from eq. 2.68.

$$\frac{\Delta f_{rf}}{f_{rf}} = -\frac{\Delta L}{L} = \mp 2.4 \cdot 10^{-4} \quad (5.10)$$

where the maximum rf frequency detuning approximates to 377 Hz for the cavity rf frequency of 1.57 MHz of U^{28+} .

5.1.3 Beam Dynamics of the Phase Shift Method for H^+

For the frequency adjustment of the SIS18 for the U^{28+} beam, we know that the sinusoidal modulation is best for the beam stability. Now we will check whether the sinusoidal modulation is also applicable for the H^+ beam of the SIS18.

The criteria for the rf frequency modulation of the H^+ beam are

- The maximum rf frequency offset Δf_{rf_max} comes from the constraint of $\Delta p/p_{max}$ in Tab. 5.2. According to eq. 2.53, $|\Delta f_{rf}| \leq 283$ Hz.
- $|\frac{d\Delta f_{rf}}{dt}|$ must be continuous and smaller than 1.9 Hz/ms to guarantee the bucket area factor larger than 80%.

5.1. Beam Dynamic Analysis of two Synchronization Methods for the B2B Transfer from SIS18 to SIS100

- $|\frac{d^2\Delta f_{rf}}{dt^2}|$ must be smaller than 0.2 Hz/ms^2 to guarantee the adiabaticity smaller than 10^{-4} .

5.1.3.1 Longitudinal Dynamics Analysis

When the case (1), a sinusoidal modulation (same as the eq. 5.5) with $T = 7 \text{ ms}$, is used as the frequency modulation for the phase shift of π , we have the following parameters accompanying the modulation, see Tab. 5.7.

Case (1)

$$\Delta f_{rf}(t) = \frac{1}{2T} [1 - \cos(\frac{2\pi}{T}(t - t_0))] \quad t_0 + 0 < t \leq t_0 + T \quad (5.11)$$

Table 5.7: Parameters accompanying with a 7 ms sinusoidal modulation for the SIS18 H^+ beam

| Relative momentum shift | Maximum orbit length displacement | Bucket size | Synchronous phase | Adiabaticity |
|-------------------------|-----------------------------------|-------------|-------------------|--------------|
| $< 4.10 \cdot 10^{-3}$ | $< 4.09 \cdot 10^{-5}$ | $> 0\%$ | $\pm 90.0^\circ$ | < 2500 |

Compared with the acceptable range of the parameters in Tab. 5.1, the synchronous phase, the bucket size and the adiabaticity accompanying with the 7 ms sinusoidal modulation are far beyond the acceptable range. Hence, a sinusoidal modulation with longer period must be used to guarantee these requirement. A sinusoidal modulation with $T = 50 \text{ ms}$ is used as the frequency modulation for the phase shift of π , we have the following parameters accompanying the modulation, see Tab. 5.8. In this case, all parameters meet the requirement.

Table 5.8: Parameters accompanying with a 50 ms sinusoidal modulation for the SIS18 H^+ beam

| Relative momentum shift | Maximum orbit length displacement | Bucket size | Synchronous phase | Adiabaticity |
|-------------------------|-----------------------------------|-------------|-------------------|------------------------|
| $< 5.70 \cdot 10^{-4}$ | $< 5.70 \cdot 10^{-6}$ | $> 86\%$ | $\pm 4.2^\circ$ | $< 0.80 \cdot 10^{-4}$ |

For the frequency modulation of the SIS18 H^+ beam, a longer period sinusoidal modulation (e.g. 50 ms) must be used for the beam performance consideration.

5.1.3.2 Transverse Dynamics Analysis

For the SIS18, the chromaticity Q_x^c and Q_y^c of H^+ is -7.5 and -4.4 . Substituting the chromaticity and the maximum momentum shift (see. Tab. 5.8) into eq. 2.64.

5.2. GMT Systematic Investigation

The maximum chromatic tune shift ΔQ_x and ΔQ_y during the 50 ms sinusoidal modulation can be calculated.

$$\Delta Q_x = -7.5 \cdot 5.7 \cdot 10^{-4} = -4.28 \cdot 10^{-3} \quad (5.12)$$

$$\Delta Q_y = -4.4 \cdot 5.7 \cdot 10^{-4} = -2.51 \cdot 10^{-3} \quad (5.13)$$

The chromatic tune shift to the tune for three cases are negligibly small.

5.1.4 Beam Dynamics of the Frequency Beating Method for H^+

The frequency detuning has no influence on the chromaticity tune shift.

5.1.4.1 Longitudinal Dynamics Analysis

The SIS18 H^+ acceptable displacement of the orbit length is $\pm 0.80 \cdot 10^{-4}$, see Tab. 5.2. Hence, the tolerable rf frequency change for H^+ at the extraction energy 4 GeV/u is calculated from eq. 2.68.

$$\frac{\Delta f_{rf}}{f_{rf}} = -\frac{\Delta L}{L} = \mp 0.80 \cdot 10^{-4} \quad (5.14)$$

where the maximum rf frequency detuning approximates to 109 Hz for the cavity rf frequency of 1.36 MHz of the H^+ beam.

5.2 GMT Systematic Investigation

The B2B transfer system makes use of certain aspects of the GMT system to implement the data collection, merging and redistribution. The main task of the data merging is to calculate the start of the synchronization window, which is used for the selection of the bucket indication signal marker for the kicker trigger. The data collection and redistribution make use of the WR network, so the test and measurement of the WR network for the B2B transfer is important. In addition, the B2B transfer system has high timing requirement, therefore the flowcharts of the system and the corresponding time constraints are also presented in this section.

5.2.1 Calculation of the Start of the Synchronization Window

All calculations for the B2B transfer are based on the phase deviation measurement by the PAM module. With the help of the phase extrapolation by the PAP module and the timestamp for the extrapolated phase by the B2B source and target SCUs, the fine time point corresponding to the correct phase alignment between two synchronization frequencies is calculated, see Chap. 4. This fine time point is called the “best estimate time of alignment” and denoted by t_{align} . There are some unavoidable uncertainties [48] in the measurements. In this dissertation, the uncertainty analysis is based on the assumption that the rf frequency produced by DDS is exactly the same as the set value. There are three random measurement uncertainties, which need to be taken into consideration.

5.2. GMT Systematic Investigation

- The maximum error of the PAM module is 0.1° [49]. Therefore 0.1° is the uncertainty of a single phase measurement made by the PAM module. The phase extrapolation of the PAP module reduces the measurement uncertainty by averaging multiple measurement samples of the phase deviation. In this dissertation, 100 measurement samples are assumed to be used and the corresponding uncertainty of the extrapolated phase equals to $0.1^\circ/\sqrt{100} = 0.01^\circ$. The more measurement samples are used for the phase extrapolation, the smaller the uncertainty of the extrapolated phase will be. For more details, please see “Development of the LLRF system for a deterministic Bunch-to-Bucket transfer for FAIR“ [43].
- The maximum error of BuTiS clocks is 100 ps per kilometer [50]. Here we assume that the uncertainty of the BuTiS clocks is 100 ps. The phase is extrapolated at BuTiS T0 incidents. Hence, the uncertainty of the extrapolated phase caused by the BuTiS error is 100 ps.
- Because of the nanosecond deviation between the edges of a BuTiS clock and the re-synthesized clock on SCUs in the WR network, the uncertainty of the timestamp corresponding to the extrapolated phase is assumed to be 1 ns [51]. t_{align} is defined as the timestamp corresponding to the extrapolated phase ψ_0^X .

Because of the propagation of the uncertainties as mentioned above, the best estimate time of alignment lies within the time range between $t_{align} - \delta t_{align}$ and $t_{align} + \delta t_{align}$, where δt_{align} is the time uncertainty of the phase alignment. $[t_{align} - \delta t_{align}, t_{align} + \delta t_{align}]$ is called the “probable time range of alignment“. In order to achieve the highly precise bunch-to-bucket injection, the length of the probable time range of alignment must be much shorter than the length of the synchronization window. In Sec. 5.2.1.1, the calculation and examination of δt_{align} for the phase shift and frequency beating methods are explained. For the correct selection of the same rising edge of the bucket indication signal marker within the synchronization window at different SCUs, the start of the synchronization window must be properly calculated. In Sec. 5.2.1.2, the calculation of the start of the synchronization window is explained. In Sec. 5.2.1.3, the requirement of the accuracy of the start of the synchronization window is discussed.

5.2.1.1 Uncertainty of the Phase Alignment

In Chap. 4, we get the extrapolated phase ψ^X at the T0 incidents (see eq. 4.14)

$$\psi^X(t) = [(2\pi(f_{B2B}^X - f_{ref})t + \varphi_0^X) \bmod 2\pi] - \pi \quad (5.15)$$

where t corresponds to the T0 incidents. Because the phase of the synchronization reference signal at the T0 incidents is 0° , namely $2\pi \cdot f_{ref} \cdot t = 0$, eq. 5.15 can be deduced to

$$\psi^X(t) = [(2\pi \cdot f_{B2B}^X \cdot t + \varphi_0^X) \bmod 2\pi] - \pi \quad (5.16)$$

From eq. 5.16, we know that the uncertainty of the extrapolated phase is composed of two parts, the uncertainty of the phase measurement φ_0^X and the uncertainty of the BuTiS T0 incidents t . The uncertainty of the extrapolated phase

5.2. GMT Systematic Investigation

(denoted as $\delta\psi_0^X$) is calculated as

$$\delta\psi^X = \sqrt{\left(\frac{\partial\psi^X}{\partial\varphi_0^X}\delta\varphi_0^X\right)^2 + \left(\frac{\partial\psi^X}{\partial t}\delta t\right)^2} \quad (5.17)$$

The uncertainty of the extrapolated phase in the phase domain and that in the time domain are calculated as

$$\delta\psi_{\theta_phase}^X = \sqrt{(0.01^\circ)^2 + (100ps \cdot f_{B2B}^{trg} \cdot 2\pi)^2} \quad (5.18)$$

$$\delta\psi_{\theta_time}^X = \sqrt{\left(\frac{0.01^\circ}{2\pi} \cdot \frac{1}{f_{B2B}^{trg}}\right)^2 + (100ps)^2} \quad (5.19)$$

The phase difference $\Delta\phi_{syn_0}$ between two synchronization frequencies at t_ψ^X is calculated as (see eq. 4.16).

$$\Delta\phi_{syn_0} = \begin{cases} (\psi_0^{trg} - \psi_0^{src}) \bmod 2\pi, & f_{bucket} = f_{syn}^{trg} \\ \frac{h_{syn}^{trg}}{h_{rev}^{trg}}(\psi_0^{trg} - \psi_0^{src}) \bmod 2\pi, & f_{bucket} = f_{rev}^{trg} \end{cases} \quad (5.20)$$

Both the B2B source SCU and the B2B target SCU measure the timestamp t_ψ^X for the extrapolated phase and the uncertainty of the measured timestamp (denoted as δt_ψ^X) is 1 ns.

$$\delta t_\psi^X = 1 \text{ ns} \quad (5.21)$$

- Phase shift method

For the phase shift method, the duration of the rf frequency modulation is T , so the best estimate time of alignment is expressed by eq. 5.22 (derived from eq. 4.25)

$$t_{align} = t_\psi^X + 600 \text{ us} + T \quad (5.22)$$

The uncertainty of the rf frequency modulation is caused by the uncertainty of the phase extrapolation and the uncertainty of the timestamp. Hence, the phase alignment is calculated as

$$\begin{aligned} \delta t_{align} &= \sqrt{\left(\frac{\partial t_{align}}{\partial t_\psi^X}\delta t_\psi^X\right)^2 + \left(\frac{\partial t_{align}}{\partial\psi_0^{src}}\delta\psi_0^{src}\right)^2 + \left(\frac{\partial t_{align}}{\partial\psi_0^{trg}}\delta\psi_0^{trg}\right)^2} \\ &= \sqrt{(\delta t_\psi^X)^2 + 2 \cdot (\delta\psi_{\theta_time}^X)^2} \approx 1 \text{ ns} \end{aligned} \quad (5.23)$$

For all FAIR use cases, f_{B2B}^{trg} is in the 100 kHz range, so $\delta\psi_{\theta_time}^X$ is in the 300 ps range. The uncertainty of the phase alignment is approximately 1 ns, which is much smaller than T_w and is acceptable.

- Frequency beating method

The best estimate time of alignment is determined by the required phase difference $\Delta\phi_{adjust}$ and calculated by eq. 5.24 (derived from eq. 4.27).

$$t_{align} = t_\psi^X + \frac{\Delta\phi_{adjust}}{2\pi} \cdot \frac{1}{|f_{syn}^{src} - f_{syn}^{trg}|} + n \cdot \frac{1}{|f_{syn}^{src} - f_{syn}^{trg}|} \quad (5.24)$$

5.2. GMT Systematic Investigation

The uncertainty of the phase alignment is calculated as

$$\begin{aligned} \delta t_{align} &= \sqrt{\left(\frac{\partial t_{align}}{\partial t_\psi^X} \delta t_\psi^X\right)^2 + \left(\frac{\partial t_{align}}{\partial \psi_0^{src}} \delta \psi_0^{src}\right)^2 + \left(\frac{\partial t_{align}}{\partial \psi_0^{trg}} \delta \psi_0^{trg}\right)^2} \\ &= \left\{ (\delta t_\psi^X)^2 + \left(\frac{1}{2\pi} \frac{1}{|f_{syn}^{src} - f_{syn}^{trg}|} \frac{\partial \Delta\phi_{adjust}}{\partial \psi_0^{src}} \delta \psi_0^{src}\right)^2 \right. \\ &\quad \left. + \left(\frac{1}{2\pi} \frac{1}{|f_{syn}^{src} - f_{syn}^{trg}|} \frac{\partial \Delta\phi_{adjust}}{\partial \psi_0^{trg}} \delta \psi_0^{trg}\right)^2 \right\}^{1/2} \end{aligned} \quad (5.25)$$

The relation between $\Delta\phi_{adjust}$ and $\Delta\phi_{syn_0}$ is explained in Chap. 4, see eq. 4.18. Because $\Delta\phi_{adjust}$ and $\Delta\phi_{syn_0}$ have a linear relationship and the linear slope is 1, $\frac{\partial \Delta\phi_{adjust}}{\partial \psi_0^{trg}} = \frac{\partial \Delta\phi_{syn_0}}{\partial \psi_0^{trg}}$ and $\frac{\partial \Delta\phi_{adjust}}{\partial \psi_0^{src}} = \frac{\partial \Delta\phi_{syn_0}}{\partial \psi_0^{src}}$. Based on eq. 5.20, we get the partial derivative of $\Delta\phi_{adjust}$ with respect to ψ_0^{src} and ψ_0^{trg} .

$$|\frac{\partial \Delta\phi_{adjust}}{\partial \psi_0^{trg}}| = |\frac{\partial \Delta\phi_{adjust}}{\partial \psi_0^{src}}| = \begin{cases} 1, & f_{bucket} = f_{syn}^{trg} \\ \frac{h_{syn}^{trg}}{h_{rev}^{trg}}, & f_{bucket} = f_{rev}^{trg} \end{cases} \quad (5.26)$$

$\delta \psi_{0_phase}^{src} \approx \delta \psi_{0_phase}^{trg}$ and substituting eq. 5.26 into eq. 5.25, we get

$$\delta t_{align} = \begin{cases} \sqrt{(\delta t_\psi^X)^2 + 2\left(\frac{1}{2\pi} \frac{1}{|f_{syn}^{src} - f_{syn}^{trg}|} \delta \psi_{0_phase}^{src}\right)^2}, & f_{bucket} = f_{syn}^{trg} \\ \sqrt{(\delta t_\psi^X)^2 + 2\left(\frac{1}{2\pi} \frac{1}{|f_{syn}^{src} - f_{syn}^{trg}|} \frac{h_{syn}^{trg}}{h_{rev}^{trg}} \delta \psi_{0_phase}^{src}\right)^2}, & f_{bucket} = f_{rev}^{trg} \end{cases} \quad (5.27)$$

Tab. 5.9 shows the uncertainty of the phase alignment for all FAIR use cases. For more details about parameters, please see Chap. 6.

Table 5.9: Uncertainty of the phase alignment of all FAIR B2B use cases

| FAIR use cases | f_{B2B}^{trg} | $\delta\psi_{0_phase}^X$ | $ f_{syn}^{src} - f_{syn}^{trg} $ | δt_{align} | T_w | $\delta t_{align}/T_w$ |
|---|-----------------|---------------------------|-----------------------------------|--------------------|---------------|------------------------|
| U^{28+} B2B transfer from the SIS18 to the SIS100 | 157 kHz | 0.012° | 200 Hz | 2.36 μ s | 6.36 μ s | 0.37 |
| H^+ B2B transfer from the SIS18 to the SIS100 | 272 kHz | 0.014° | 200 Hz | 1.27 μ s | 3.68 μ s | 0.35 |
| $h=4$ B2B transfer from the SIS18 to the ESR | 686 kHz | 0.027° | 1899 Hz | 0.12 μ s | 1.46 μ s | 0.08 |
| $h=1$ B2B transfer from the SIS18 to the ESR | 988 kHz | 0.037° | 1368 Hz | 0.11 μ s | 1.02 μ s | 0.11 |
| B2B transfer from the ESR to the CRYRING | 685 kHz | 0.027° | 949 Hz | 0.12 μ s | 1.46 μ s | 0.08 |
| H^+ B2B transfer from the SIS100 to the CR via the pbar target | 55 kHz | 0.010° | 450 Hz | 0.09 μ s | 18.23 μ s | 0.005 |
| RIB B2B transfer from the SIS100 to the CR via the Super FRS | 102 kHz | 0.014° | 108 Hz | 0.51 μ s | 9.78 μ s | 0.05 |
| Antiproton B2B transfer from the CR to the HESR | 101 kHz | 0.013° | 136 Hz | 0.40 μ s | 9.86 μ s | 0.04 |
| B2B transfer from the SIS18 to the ESR via the FRS | 220 kHz | 0.018° | 4249 Hz | 0.02 μ s | 4.55 μ s | 0.004 |

5.2. GMT Systematic Investigation

In conclusion, the uncertainty of the extrapolated phase plays a leading role for δt_{align} of the frequency beating method. The uncertainty of the phase alignment for all FAIR use cases is smaller than the length of the synchronization window. However, there are several FAIR use cases, whose bunch-to-bucket injection center mismatch are significantly influenced by the uncertainty. They are the U^{28+} B2B transfer from the SIS18 to the SIS100, the H^+ B2B transfer from the SIS18 to the SIS100 and the $h=1$ B2B transfer from the SIS18 to the ESR, whose ratio between the uncertainty of the phase alignment and the length of the synchronization window is larger than 10%. Even though the bunch-to-bucket injection center mismatch of these cases is deteriorated, they still meet the mismatch requirement smaller than $\pm 1^\circ$. Hence, the uncertainty of the 0.01° phase extrapolation and the uncertainty of the 100 ps BuTiS and the uncertainty of the 1 ns timestamp are acceptable for the FAIR B2B transfer system.

In addition, the timestamp of the bucket indication signal markers (denoted as t_{marker}) can be calculated by the B2B source SCU as

$$t_{marker} = t_\psi^X + \frac{\pi - \psi_0^{trg}}{2\pi} \cdot \frac{1}{f_{bucket}} + n \cdot \frac{1}{f_{bucket}} \quad (5.28)$$

From the Tab. 5.9, we know the uncertainty of the extrapolated phase $\delta\psi_0^X$ for all FAIR use cases is smaller than 0.05° . f_{bucket} is in the 100 kHz range. Hence, the uncertainty of t_{marker} caused by the uncertainty of the extrapolated phase and the uncertainty of the timestamp is smaller than 2 ns. 2 ns is acceptable for the kicker trigger. Instead of the reproduction of the bucket indication signal, the B2B source SCU is able to calculate the timestamp corresponding to the 1st bucket indication signal marker within the synchronization window.

5.2.1.2 Uncertainty of the Start of the Synchronization Window

The start of the synchronization window is expressed as

$$t_w = t_\psi^X + \Delta t_w \quad (5.29)$$

with

$$\Delta t_w = \begin{cases} 600 \text{ }\mu\text{s} + T - t_{delay} & \text{Phase shift method} \\ \frac{\Delta\phi_{adjust}}{2\pi} \cdot \frac{1}{|f_{syn}^{src} - f_{syn}^{trg}|} + n \cdot \frac{1}{|f_{syn}^{src} - f_{syn}^{trg}|} - \frac{T_w}{2} - t_{delay} & \text{Frequency beating method} \end{cases} \quad (5.30)$$

For more details, please see Chap. 4.

The synchronization window is used to select the 1st bucket indication signal marker. In reality, the relative position between the start of the synchronization window and the 1st bucket indication signal marker is arbitrary. In order to guarantee the correct selection of the bucket indication signal marker at both the source and target accelerators, the start of the synchronization window will be rectified to half the period of the bucket indication signal before the selected marker. The rectified start is called the “best estimate time of the start of the synchronization window”, denoted as t_{w_rect} . The value used for the rectification is denoted as Δt_{w_rect} , see

5.2. GMT Systematic Investigation

Fig. 5.10. However, the actual start of the synchronization window is impossible to be exactly at t_{w_rect} because of the propagation of the uncertainty. The start of the synchronization window lies between $t_{w_rect} - \delta t_{w_rect}$ and $t_{align} + \delta t_{w_rect}$, where δt_{w_rect} is the uncertainty of the start of the synchronization window.

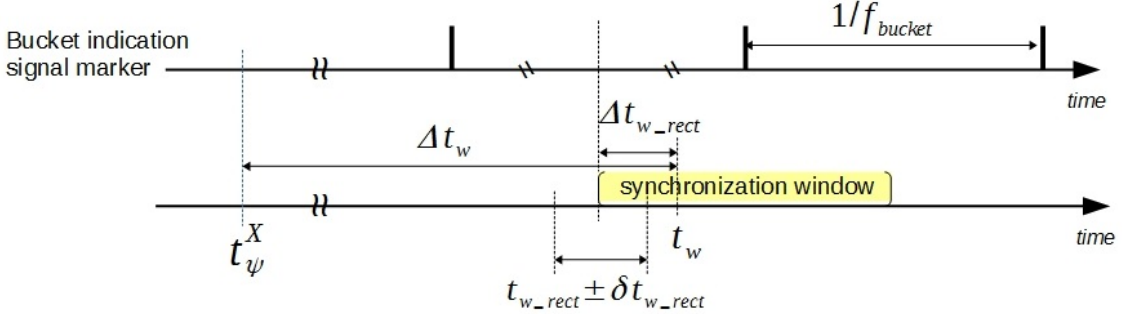


Figure 5.10: Illustration of the rectification for the start of the synchronization window.

The rectification for the start of the synchronization window is calculated by

$$\Delta t_{w_rect} = \frac{1}{2f_{B2B}^{trg}} - [(\Delta t_w - \frac{2\pi - \psi_0^{trg}}{2\pi} \frac{1}{f_{B2B}^{trg}}) \bmod \frac{1}{f_{B2B}^{trg}}] \quad (5.31)$$

The best estimate time of the start of the synchronization window is calculated by

$$t_{w_rect} = t_\psi^X + \Delta t_w + \Delta t_{w_rect} \quad (5.32)$$

The uncertainty of t_{w_rect} is caused by the uncertainty of the phase extrapolation and the uncertainty of the timestamp, calculated by

$$\begin{aligned} \delta t_{w_rect} &= \sqrt{\left(\frac{\partial t_{w_rect}}{\partial t_\psi^X} \delta t_\psi^X\right)^2 + \left(\frac{\partial t_{w_rect}}{\partial \psi_0^{src}} \delta \psi_0^{src}\right)^2 + \left(\frac{\partial t_{w_rect}}{\partial \psi_0^{trg}} \delta \psi_0^{trg}\right)^2} \\ &= \sqrt{(\delta t_\psi^X)^2 + \left(\frac{\partial \Delta t_w}{\partial \psi_0^{src}} + \frac{\partial \Delta t_{w_rect}}{\partial \psi_0^{src}}\right)^2 (\delta \psi_0^{src})^2 + \left(\frac{\partial \Delta t_w}{\partial \psi_0^{trg}} + \frac{\partial \Delta t_{w_rect}}{\partial \psi_0^{trg}}\right)^2 (\delta \psi_0^{trg})^2} \quad (5.33) \\ &= \sqrt{(\delta t_\psi^X)^2 + \left(\frac{1}{2\pi} \frac{1}{f_{B2B}^{trg}} \delta \psi_{0_phase}^X\right)^2} \end{aligned}$$

For FAIR use cases, f_{B2B}^{trg} is in the 100 kHz range and $\delta \psi_0^{trg}$ is less than 0.05° (see Tab. 5.9). Hence, δt_{w_rect} is smaller than 2 ns.

5.2.1.3 Requirement of the Accuracy of the Start of the Synchronization Window

The accuracy of the start of the synchronization window is the deviation between the theoretically calculated start time and the actual observed start time on SCUs. The FAIR B2B transfer system will be used for all FAIR use cases. Therefore, we have to find the most stringent accuracy requirement. The shortest synchronization window is 1.017 μs, which comes from h=1 B2B transfer from the SIS18 to the

5.2. GMT Systematic Investigation

ESR. We keep 5 ns before and after the bucket indication signal marker as the forbidden range, which takes account of the 2 ns uncertainty of the bucket indication signal. In Fig. 5.11, the green region represents the safety margin for the start of the synchronization window and the red region the forbidden range. So the requirement of the accuracy of the start of the synchronization window is

$$\text{Accuracy_requirement} = \frac{1.017 \text{ us} - 5 \text{ ns} \cdot 2}{2} \approx 500 \text{ ns} \quad (5.34)$$

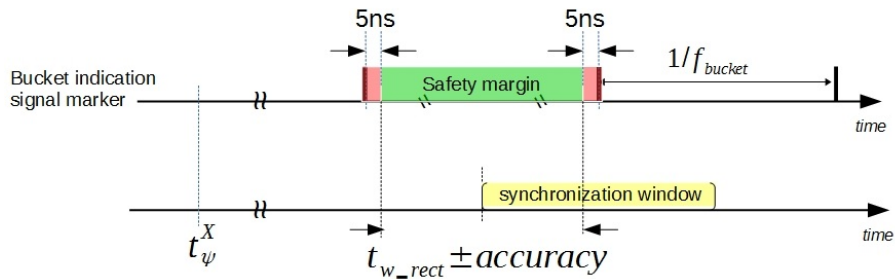


Figure 5.11: Illustration of the accuracy of the start of the synchronization window.

5.2.2 Characterization of the WR Network for the B2B Transfer

This section is part of the results of the characterization of the WR Network of the FAIR General Machine Timing System. The scenario and test definition is done by C. Prados as part of his PhD thesis [52]. I executed the test for the B2B scenario and discussed, evaluated and documented the results.

In the test, the Xena's Layer 2-3 test platform ¹ was used to characterize the properties of the WR network for the B2B transfer. The Xena's Layer 2-3 test platform was used to configure and generate Ethernet traffic at the data link layer and network layer and then to analyze how WR network in response. The test platform used the 4U XenaBay chassis which was equipped with an extensive range of copper and optical Gigabit Ethernet test modules. In the test, the test modules used 18 AXGE-1254 transceivers, 1.25 Gbps single fiber bidirectional small form-factor pluggable (SFP), to connect to ports of four WR switches via single mode fibers ². The chassis and test modules were controlled via Xena Manager-2G, a free Windows GUI client, which can be used to manage test equipment and execute test remotely. Fig. 5.12 shows an overview of the Xena's Layer 2-3 test platform for the WR network.

¹Xena's Layer 2-3 test platform
<http://xenanetworks.com/layer-2-3-test-platform/>

²A G.652.B type single mode fiber is used for the 1310 and 1550 nm wavelength region.

5.2. GMT Systematic Investigation

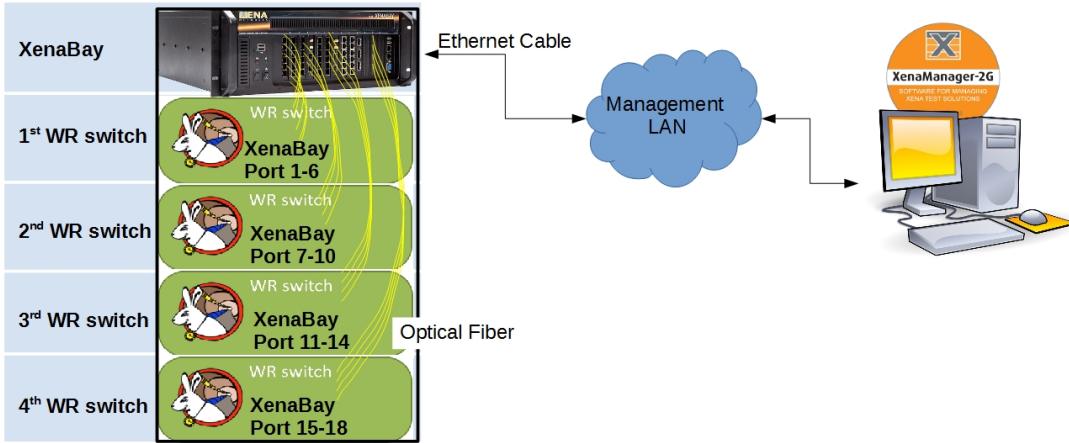


Figure 5.12: An overview of the Xena's Layer 2-3 test platform for the WR network.

The XenaBay sends traffic streams with a unique stream ID and receives the identical traffic streams for identifying the measurement. It can be used for the following measurements.

- Lost frame - the difference between the number of the sent frames and that of the received frames. In the following analysis, the frame loss rate (FLR) is used to assess the quality of network, which is defined as the ratio between the number of lost frames and the total number of sent frames.
- Misordered frame - the number of misordered frames arriving out of sending sequence.
- Frame transfer latency - the time interval between the time of XenaBay port receiving a frame and the time of another XenaBay port sending the same frame.

5.2.2.1 Traffic on the WR Network

For the measurement reported here, the following types of traffic are considered [53]. The bandwidth is defined in units of bits sent per second.

- DM Broadcast

The DM broadcasts timing frames, control messages, downwards to all FECs. The average bandwidth for the DM broadcast is 100 Mbit/s. The burst³ speed is 12 frames per 100 µs. The length of the DM Broadcast frame is 110 bytes.

- DM Unicast

The DM sends 10 Mbit/s unicast timing frames to some specified FECs at the burst speed of 3 frames per 300 µs. The length of the DM Unicast frame is 110 bytes.

³A group of consecutive frames with shorter inter frame gaps than frames arriving before or after the burst of frames.

5.2. GMT Systematic Investigation

- B2B Unicast

The B2B Unicast traffic are frames sent by the B2B source SCU and received only by the DM. The maximum cycle repetition frequency for FAIR is the SIS18 U^{28+} super cycle, which is 2.82 Hz [39]. The B2B source SCU sends 2 timing frames upwards to the DM within 10 ms for each cycle. The bandwidth is calculated as

$$\begin{aligned} \text{bandwidth} = & \text{cycle repetition frequency} \cdot \\ & \text{the number of frames per cycle} \cdot \text{frame length} \end{aligned} \quad (5.35)$$

Hence, the bandwidth of the B2B Unicast traffic can be calculated according to eq. 5.35 as $2.82 \cdot 2 \cdot 880 < 5 \text{ kbit/s}$. The burst speed is 2 frames per cycle, namely $1/2.82 \text{ Hz} = 350 \text{ ms}$.

- B2B Broadcast

The B2B Broadcast traffic are frames exchanged among B2B related SCUs. Maximum 10 B2B broadcast timing frames are sent within 10 ms for each cycle. Hence, the bandwidth of the B2B broadcast traffic can be calculated according to eq. 5.35 as $2.82 \cdot 10 \cdot 880 < 25 \text{ kbit/s}$. The burst speed is 10 frames per 350 ms.

- Management Traffic

The average bandwidth for the management traffic is 10 Mbit/s. It broadcasts packets with random Ethernet frame length from 64 bytes to 1518 bytes.

According to the importance of the network traffic, the prioritization of WR network traffic is implemented based on the VLAN technology. The DM Broadcast and Unicast traffic, the control messages, is the most importance traffic, which must be delivered deterministically and with very low loss. Hence, it is assigned to the VLAN 7 with the highest priority. Besides, the B2B Unicast traffic is also assigned to the VLAN 7, which realizes the communication between the B2B source SCU and the DM. In order to reduce the network traffic, the B2B Broadcast traffic is only broadcasted among the B2B related SCUs, therefore the B2B Broadcast traffic is assigned to the VLAN 6 with the secondary priority. Finally, the Management traffic is assigned to the VLAN 5 with the lowest priority [53].

5.2.2.2 Frame Loss of the WR Network for the B2B Transfer

Due to the transmission channel noise, interference, attenuation and other factors, the optical fiber connections cause unavoidable bit errors. When a frame with a bit error passes a WR switch, it will be dropped by the switch. The lost frame caused by bit errors is measured by the frame error rate (FER), which is defined as the ratio between the number of lost frames caused by bit errors and the number of sent frames. The FER varies with the number of fiber connections. The bit error rate (BER) is defined as the ratio between the number of bit errors and the total number of sent bits. The BER for fiber connections is calculated as [54]

$$BER = n \cdot 10^{-12} \quad (5.36)$$

5.2. GMT Systematic Investigation

where n is the number of the fiber connections used to establish the communication and the fiber's BER is specified by the manufacturer is 10^{-12} ⁴.

When no forward error correction mechanism is used. The relation between the FER and BER is

$$FER = (BER - m \cdot 10^{-12}) \cdot 880 = (n - m) \cdot 10^{-12} \cdot 880 \quad (5.37)$$

where 880 is the length of a B2B Broadcast or B2B Unicast frame and m represents the number of the fiber connections to the frame reception FECs and $n - m$ is the number of WR switch layers.

The duration for the occurrence of one lost frame caused by a bit error is calculated as

$$t = \frac{880}{FER} \cdot \frac{1}{bandwidth} \quad (5.38)$$

In actual application of the B2B transfer system, there is only one frame reception FEC for the B2B Unicast traffic, namely $m = 1$. For the B2B Broadcast traffic, there are total six ring accelerators (SIS18, SIS100, ESR, CR, HESR and CRYRING) and every ring needs three FECs for the data exchange, the B2B source/target SCU, the Trigger SCU and the Kicker SCU. Hence, there is one frame sending FEC and 17 frame reception FECs, namely $m = 17$. Fig. 5.13 shows the relation between the FER and the number of fiber connection for two traffics.

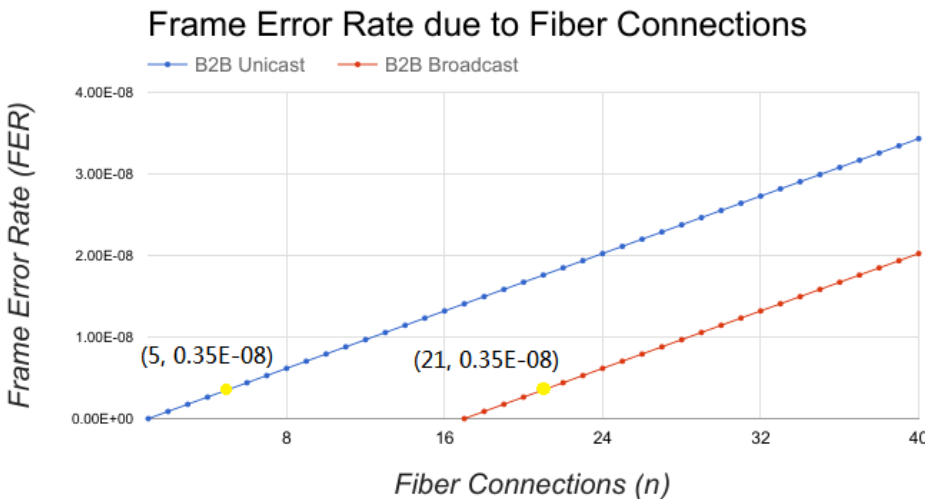


Figure 5.13: Relation between the FER and the fiber connections for B2B Unicast and Broadcast traffics.

5.2.2.3 WR Network Test Setup

In order to test the WR Network in the context of the B2B transfer, the following setup based on the Xena's Layer 2-3 test platform was developed in the framework of this thesis. Four WR switches were connected to the port 1 to 18 of the XenaBay chassis. Taking the network traffic requirements listed above into consideration, all ports of four WR switches were assigned to three VLANs, VLAN 5, VLAN 6 and VLAN 7. The DM Broadcast frames were sent by the XenaBay port 1 and received

⁴Datasheet of Draka optical fiber
<http://www.drakauc.com/ucfibre-optical-patchcords/>

5.2. GMT Systematic Investigation

by ports 2 - 6 through the 1st WR switch and received by ports 7 - 10 through the 1st and 2nd WR switches and received by ports 11 - 14 through the 1st, 2nd and 3rd WR switches and received by ports 15 - 18 ports through four WR switches. The DM Unicast frames were sent by the port 3 and received by the port 18 through four WR switches. The B2B Broadcast frames were sent by the port 16 and received by ports 15, 17 and 18 through the 4th WR switch and received by ports 11 - 14 through the 4th and 3rd WR switches and received by ports 7 - 10 through the 4th, 3rd and 2nd WR switches and received by ports 1 - 6 through four WR switches. The B2B Unicast frames were sent by the port 17 and received by the port 1 through four WR switches. The Management traffic were produced by 7 XenaBay ports and received by all ports, see Fig. 5.14. Tab. 5.10 shows the traffic characteristic produced by XenaBay ports in details.

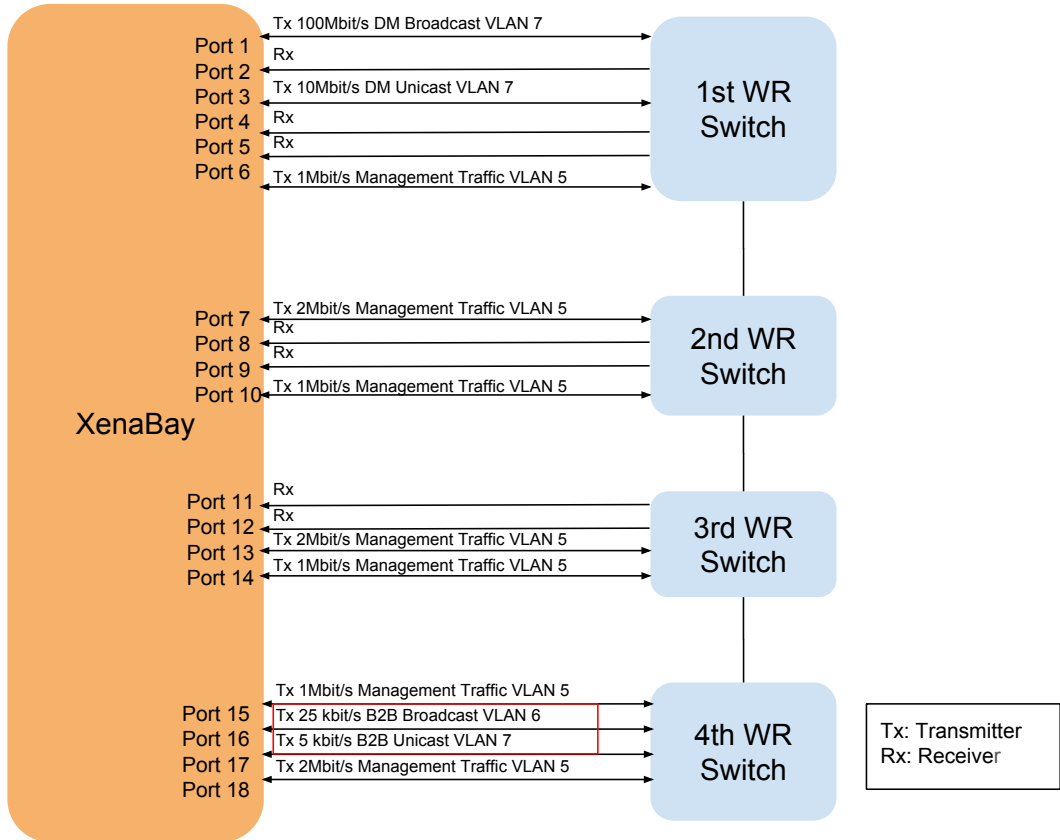


Figure 5.14: Connection between WR switches and the XenaBay of the test setup.

Adapted from “Testing the WR Network of the FAIR General Machine Timing System” by C. Prados and J. Bai, 2016, GSI Internal Document. Adapted with permission.

Firstly, the lost frame, misordered frame and the frame transfer latency on each frame transfer path of the WR network for the B2B Broadcast and B2B Unicast traffic were measured. Secondly, the FLR was calculated based on the number of lost frames and the total number of sent frames. Then the FLR and misordered frame measurement results were used to evaluate whether the WR switch with the latest hardware and firmware⁵ was qualified. A qualified WR switch should cause

⁵WR Hardware PCB: 3.30, FPGA:LX240T; WR Firmware: v4.2; compiled at Aug 28 2015 15:05:21

5.2. GMT Systematic Investigation

Table 5.10: Traffic produced by the XenaBay ports of the test setup

Adapted from “Testing the WR Network of the FAIR General Machine Timing System“ by C. Prados and J. Bai, 2016, GSI Internal Document. Adapted with permission.

| Switch | Xena Port | Traffic | Ethernet frame size | VLAN | Priority | Usage |
|-------------|-----------|------------|---------------------|------|----------|----------------------|
| WR switch 1 | Port 1 | 100 Mbit/s | 110 bytes | 7 | 7 | DM Broadcast |
| | Port 2 | | | | | |
| | Port 3 | 10 Mbit/s | 110 bytes | 7 | 7 | DM Unicast |
| | Port 4 | | | | | |
| | Port 5 | | | | | |
| | Port 6 | 1 Mbit/s | 64 - 1518 bytes | 5 | 5 | Management Broadcast |
| WR switch 2 | Port 7 | 2 Mbit/s | 64 - 1518 bytes | 5 | 5 | Management Broadcast |
| | Port 8 | | | | | |
| | Port 9 | | | | | |
| | Port 10 | 1 Mbit/s | 64 - 1518 bytes | 5 | 5 | Management Broadcast |
| WR switch 3 | Port 11 | | | | | |
| | Port 12 | | | | | |
| | Port 13 | 2 Mbit/s | 64 - 1518 bytes | 5 | 5 | Management Broadcast |
| | Port 14 | 1 Mbit/s | 64 - 1518 bytes | 5 | 5 | Management Broadcast |
| WR switch 4 | Port 15 | 1 Mbit/s | 64 - 1518 bytes | 5 | 5 | Management Broadcast |
| | Port 16 | 25 kbit/s | 110 bytes | 6 | 6 | B2B Broadcast |
| | Port 17 | 5 kbit/s | 110 bytes | 7 | 7 | B2B Unicast |
| | Port 18 | 2 Mbit/s | 64 - 1518 bytes | 5 | 5 | Management Broadcast |

null misordered frame and should have a FLR which is smaller than or equal to the calculated FER of the network. The FER is decided by the number of fiber connections n and the number of the frame reception FECs m , see eq. 5.37. In the test setup, the XenaBay ports are used as FECs. We have $m = 1$, $n = 5$ for the B2B Unicast traffic and $m = 17$, $n = 21$ for the B2B Broadcast traffic, so the corresponding FER for two traffic is same by coincidence, which equals to $0.35 \cdot 10^{-8}$. According to eq. 5.38, one frame is lost approximately every one and half years for the 5 kbit/s B2B Unicast traffic and one frame is lost approximately every four months for the 25 kbit/s B2B Unicast traffic of the test setup.

Together with the tolerable FER, the measurement result of the maximum frame transfer latency was used to identify the tolerable number of WR switch layers for the B2B related traffic, including the number of WR switch layers between the B2B related SCUs and the number of WR switch layers between the B2B related SCUs

5.2. GMT Systematic Investigation

and DM.

5.2.2.4 Measurements

The test setup was running for 45 days in order to investigate:

- Lost frame of the B2B Unicast traffic

The frame loss of the B2B Unicast traffic has been measured from the port 17 to the port 1 via four WR switches. The B2B Unicast traffic had no lost frame when approximate $2.2 \cdot 10^7$ frames were sent. Besides, there was no misordered frame. If frames get lost, the B2B source SCU will send an extra frame to the DM to indicate the error. The DM will arrange the corresponding schedule.

- Lost frame of the B2B Broadcast traffic

The number of lost frames of the B2B Broadcast traffic have been measured separately from the port 16 to other ports. There were two lost frames individually from the port 16 to the port 17 and 18 via the 4th WR switch when approximate $1.1 \cdot 10^8$ frames were sent by the port 16, so the 4th WR switch caused 4 lost frames. There were two lost frames individually from the port 16 to the port 11 and 12 via the 4th and 3rd WR switches, so the 3rd WR switch caused 4 lost frames. Hence, the FLR of the test was $7.12 \cdot 10^{-8}$. For the B2B Broadcast frames, there was no misordered frame. If frames get lost, the B2B source SCU will send an extra frame to the DM to indicate the error. The DM will arrange the corresponding schedule.

- Maximum frame transfer latency for the B2B Unicast frames

For the B2B Unicast frames, the maximum frame transfer latency of $23 \mu\text{s}$ from the port 17 to the port 1 through four WR switches has been measured, see Fig. 5.15.

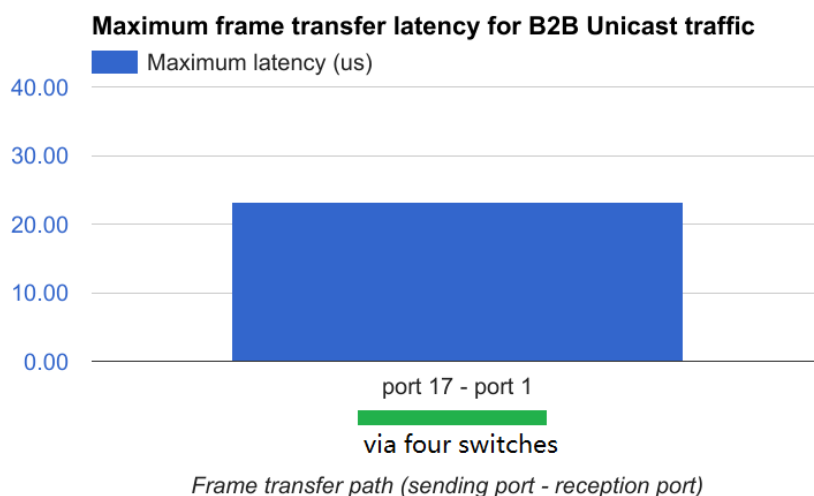


Figure 5.15: Maximum frame transfer latency for B2B Unicast frames.

- Maximum frame transfer latency of the B2B Broadcast frames

5.2. GMT Systematic Investigation

For the B2B Broadcast frames, the frame transfer latencies of the stream from the port 16 to ports 15, 17 and 18 via the 4th WR switch have been measured, namely the frame transfer latencies through one WR switch. The frame transfer latencies of the stream from the port 16 to ports 11 - 14 via the 4th and 3rd WR switches have been measured, namely the frame transfer latencies through two WR switches. The frame transfer latencies of the stream from the port 16 to ports 7 - 10 via 4th, 3rd and 2nd WR switches have been measured, namely the frame transfer latencies through three WR switches. The frame transfer latencies of the stream from the port 16 to ports 1 - 6 via four WR switches have been measured, namely the frame transfer latencies through four WR switches. Fig. 5.16 shows the measurement result.

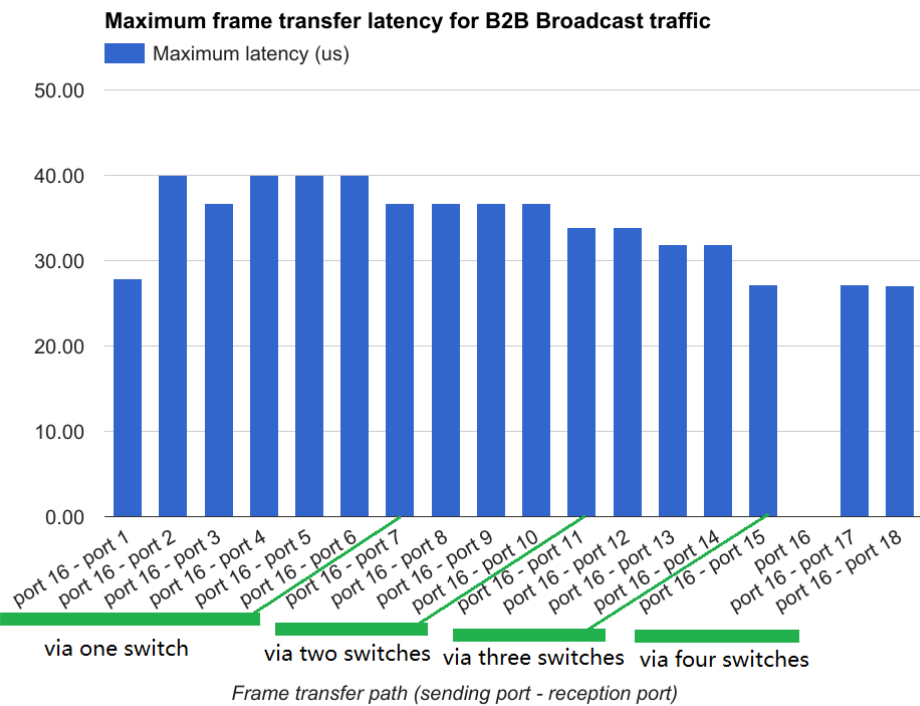


Figure 5.16: Maximum frame transfer latency for B2B Broadcast frames.

The more WR switches frames pass through, the longer frame transfer latency will be. The maximum frame transfer latency and the number of switches have a nonlinear relationship, because there is a very low possibility for one frame to pass through more than two switches with the maximum transfer latency for each switch. Tab. 5.11 lists the maximum frame transfer latency of the B2B Broadcast frames for different number of WR switch layers.

5.2. GMT Systematic Investigation

Table 5.11: The maximum frame transfer latency of the B2B Broadcast frames for different number of WR switch layers

| Number of WR switch layers | One WR switch | Two WR switches | Three WR switches | Four WR switches |
|--------------------------------|---------------|-----------------|-------------------|------------------|
| Maximum frame transfer latency | 28 μ s | 34 μ s | 37 μ s | 41 μ s |

From the test result, a maximum frame transfer latency of 28 μ s for every WR switch is used for the worst situation.

5.2.2.5 Measurements Result

According to the 45 days test, we get the following measurement result.

Table 5.12: The 45 days test result of the WR network for the B2B transfer

| | lost frame | FLR | misordered frame | maximum frame transfer latency |
|---------------|------------|------------------------------|------------------|--------------------------------|
| B2B Broadcast | 8/45_days | $7.1 \cdot 10^{-8}/45_days$ | 0/45_days | 28 μ s/switch |
| B2B Unicast | 0/45_days | 0/45_days | 0/45_days | 23 μ s/4_switches |

5.2.2.6 Result Discussion

According to the 45 days test result, the FLR of the B2B Broadcast traffic is $7.12 \cdot 10^{-8}$, which is larger than the FER of the fiber connection $0.35 \cdot 10^{-8}$, so the WR switch with the latest hardware and firmware doesn't meet the requirement. The firmware of the WR switch is still under development by CERN.

For the B2B transfer system, the upper bound latency of the frames on the WR network is 500 μ s. The latency measured in this test does not include the SCU sending and receiving time, which is around 100 μ s. According to the test result, the maximum B2B Broadcast frame transfer latency for each WR switch layer is 28 μ s and the maximum B2B Unicast frame transfer latency for four WR switch layers is 23 μ s. The latency of the WR network is decided by the number of WR switch layers and the length of the optical fiber. The propagation of light through the core of an optical fiber is roughly about 200 m/ μ s [55] and the longest distance in the FAIR campus is around 2 km, so the latency of a 2 km optical fiber is about 10 μ s. The number of WR switch layers plays a more important role in the latency.

From the perspective of the transfer latency, the tolerable number of WR switch layers between the B2B related SCUs is

$$\frac{500 \mu\text{s} - 10 \mu\text{s} - 100 \mu\text{s}}{28 \mu\text{s}/\text{switch}} > 13 \quad (5.39)$$

From the perspective of the latency, the tolerable number of WR switch layers

5.2. GMT Systematic Investigation

between the B2B related SCUs and DM is

$$\frac{500 \mu s - 10 \mu s - 100 \mu s}{23 \mu s / 4_switches} \cdot 4 > 67 \quad (5.40)$$

However, the more WR switch layers, the more fiber connections and the higher corresponding FER. When no forward error correction mechanism is used, the tolerable number of WR switch layers for the B2B related traffic depends on the tolerable FER and the transfer latency, see Tab. 5.13. The tolerable FER of the B2B transfer system is one lost frame per month. In this case, the tolerable number of WR switches layers is determined by the transfer latency, namely a maximum of 67 WR switches can be used between the B2B related SCUs and DM and a maximum of 13 WR switches can be used between the B2B related SCUs. If one lost frame is acceptable every two months, the tolerable number of WR switches layers is determined by the FER, namely a maximum of 38 and 8 WR switches can be used for the B2B Unicast and Broadcast traffic. If one lost frame is acceptable every 8 months, 9 and 2 WR switches can be used for two traffic. In this case, the forward error correction mechanisms need to be used, if more WR switches need to be used. e.g. the FER can be reduced to the order of magnitude 10^{-15} when specific forward error correction mechanisms are implemented in the WR network [54] and the number of WR switch layers is then determined by the transfer latency.

Table 5.13: The tolerable number of WR switch layers for the B2B related traffic

| | Requirement from FER | | Requirement from latency | |
|--|----------------------|---------------|--------------------------|---------------|
| one lost frame | B2B Unicast | B2B Broadcast | B2B Unicast | B2B Broadcast |
| per month | 76 | 15 | 67 | 13 |
| No forward error correction mechanism is implemented | | | | |
| every 2 months | 38 | 8 | 67 | 13 |
| every 4 months | 19 | 4 | 67 | 13 |
| every 8 months | 9 | 2 | 67 | 13 |
| every 18 months | 4 | 1 | 67 | 13 |
| Forward error correction mechanisms are implemented | | | | |
| every 8 months | 9 | 2 | 67 | 13 |
| every 18 months | 4 | 1 | 67 | 13 |

5.2.2.7 Conclusion of the Network Measurements

The tolerable number of WR switch layers depends not only on the upper bound transfer latency, but also the tolerable FER of the B2B transfer system. The tolerable FER of the B2B transfer system for FAIR has been determined to lose one frame every four month (a preliminary assumption).

If no forward error correction mechanism is used for the B2B network, the number of WR switch layers is mainly decided by the tolerable FER. In case of only one lost frame every four months, then a maximum of 19 WR switches can be used between the B2B related SCUs and DM and a maximum of 4 WR switches can be used between the B2B related SCUs.

5.2. GMT Systematic Investigation

If specific forward error correction mechanisms are implemented in the B2B network and the FER is 10^{-15} [54], the number of WR switch layers is mainly decided by the tolerable transfer latency. Hence, the tolerable number of WR switch layers is 67 between the B2B related SCUs and DM and the tolerable number of WR switch layers is 13 between the B2B related SCUs.

5.2.3 Flowchart of the system for SCUs

The B2B source, B2B target and Trigger SCUs control different flowcharts. In the following, the flowcharts of different SCUs are explained. An overview of the connections of the B2B related modules used for the data exchange is presented in Chap. 4, see Fig. 4.15.

- The flowchart for the B2B source SCU

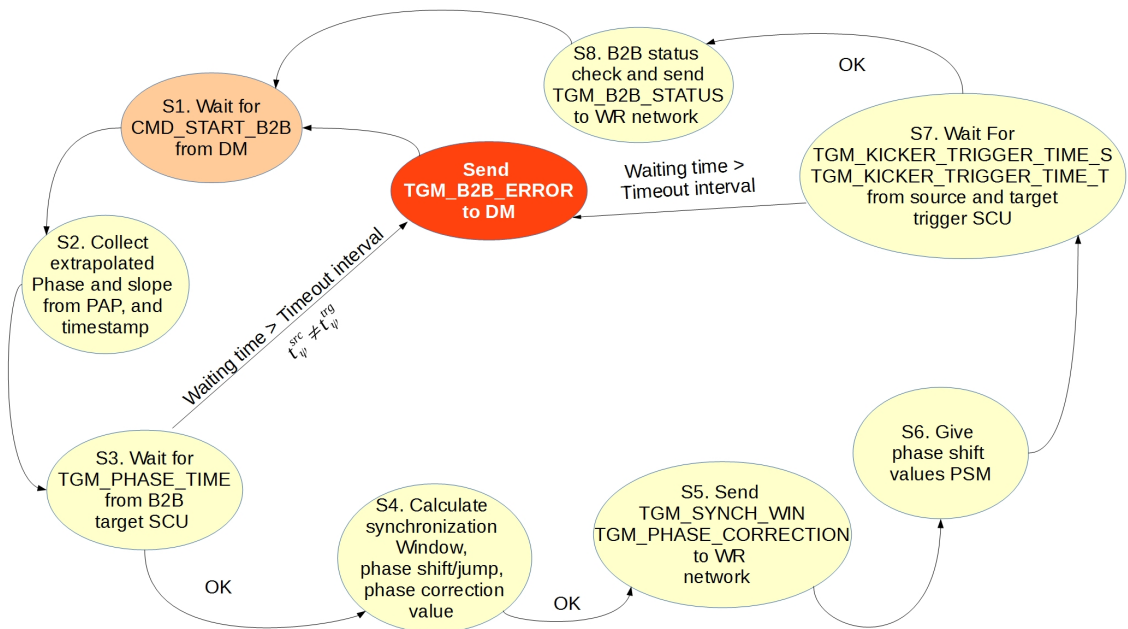


Figure 5.17: Flowchart of the B2B source SCU.

“Step“ is represented as “S“ in the figure.

Fig. 5.17 shows the flowchart of the B2B source SCU. The B2B source SCU, the B2B transfer master, is responsible for the data collection, data calculation, date redistribution and status check. The flowchart controls the following logical steps according to Fig. 5.17.

- Step 1. The program waits for the `CMD_START_B2B` timing frame.
- Step 2. When it receives the timing frame `CMD_START_B2B`, the program reads the extrapolated phase and the phase deviation slope from the PAP module, as well as the corresponding timestamp.
- Step 3. The program waits for the `TGM_PHASE_TIME` timing frame from the B2B target SCU, which contains the extrapolated phase, the corresponding timestamp and the slope of the phase deviation.

5.2. GMT Systematic Investigation

- Step 4. When the program receives the timing frame TGM_PHASE_TIME within a specified timeout interval, it checks whether the timestamp corresponding to the extrapolated phase of the target synchrotron equals to that of the source synchrotron. When they are equal, the program calculates the synchronization window, the phase shift/jump value and the phase correction value. When the program doesn't receive the timing frame TGM_PHASE_TIME within a specified timeout interval or two timestamp are not equal, it sends a timing frame TGM_B2B_ERROR to the WR network and goes back to the step 1, the TGM_B2B_ERROR indicates the error to the DM.
- Step 5. The program sends the timing frames TGM_SYNCH_WIN and TGM_PHASE_CORRECTION to the WR network. The TGM_SYNCH_WIN indicates the start of the synchronization window and the TGM_PHASE_CORRECTION is used for the Trigger SCUs for the reproduction of the bucket indication signal.
- Step 6. The program gives the phase shift value to corresponding module.
- Step 7. The program waits for the timing frame TGM_KICKER_TRIGGER_TIME_S from the source Trigger SCU and the timing frame TGM_KICKER_TRIGGER_TIME_T from the target Trigger SCU, which contains the extraction/injection kicker trigger and firing timestamp. When it does not receive the timing frames within a specified timeout interval, it sends a timing frame TGM_B2B_ERROR to the WR network and goes back to the step 1, which indicates the timeout error of the frame.
- Step 8. When the program receives the timing frames mentioned in the step 7 within a specified timeout interval, it checks the B2B transfer status and sends the TGM_B2B_STATUS to the WR network and goes to the step 1. The B2B transfer is successful, if all of the following checks are correct. Otherwise the B2B transfer is failure.
 - * Trigger time < firing time of the extraction kicker of the source ring
 - * Trigger time < firing time of the injection kicker of the target ring
- The flowchart for the B2B target SCU

5.2. GMT Systematic Investigation

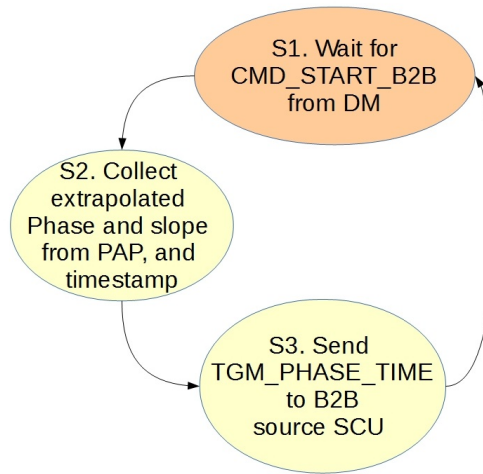


Figure 5.18: Flowchart of the B2B target SCU.

“Step“ is represented as “S“ in the figure.

Fig. 5.18 shows the flowchart of the B2B target SCU. The flowchart controls the following logical steps according to Fig. 5.18.

- Step 1. The program waits for the CMD_START_B2B timing frame.
- Step 2. When it receives the timing frame CMD_START_B2B, the program reads the extrapolated phase and the phase deviation slope from the PAP module, as well as the corresponding timestamp.
- Step 3. The program sends the TGM_PHASE_TIME timing frame to the B2B source SCU and goes back to the step 1.

- The flowchart for the Trigger SCU

5.2. GMT Systematic Investigation

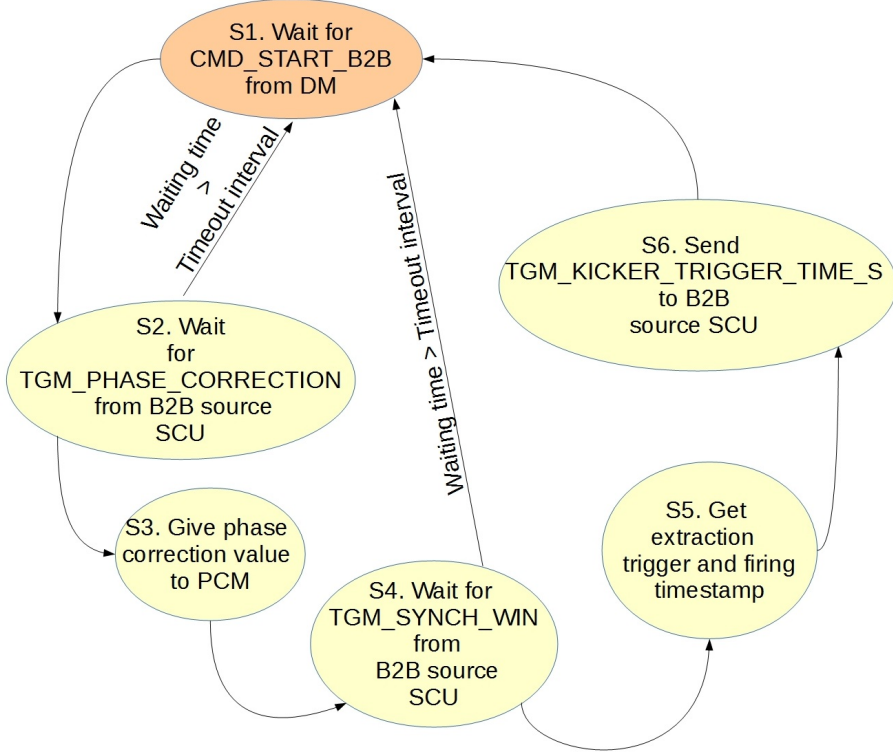


Figure 5.19: Flowchart of the B2B Trigger SCU.

“Step” is represented as “S” in the figure.

Fig. 5.19 shows the flowchart of the source Trigger SCU. For the target Trigger SCU, the logical steps are same only with the timing frame TGM_KICKER_TRIGGER_TIME_T. The flowchart controls the following logical steps according to Fig. 5.19.

- Step 1. The program waits for the CMD_START_B2B timing frame.
- Step 2. The program waits for the TGM_PHASE_CORRECTION timing frame. When it does not receive the timing frames within a specified timeout interval, it goes back to the step 1.
- Step 3. The program gives the phase correction value to the corresponding PCM.
- Step 4. The program waits for the timing frame CMD_SYNCH_WIN to indicate the synchronization window for the kicker trigger. When it does not receive the timing frames within a specified timeout interval, it goes back to the step 1.
- Step 5. After the beam extraction, the program collects the trigger and firing timestamp.
- Step 6. The program sends the TGM_KICKER_TRIGGER_TIME_S timing frame to the B2B source SCU and goes back to the step 1.

5.2.4 Time Constraints

For the FAIR B2B transfer system, the time constraints are very important and strict. Because beam feedback loops are switched off before the B2B transfer, the beam may be stable only for a short period of time. For most FAIR use cases, the upper bound B2B transfer time is 10 ms.

Fig. 5.20 shows the time constraint of the system. The CMD_START_B2B is executed at t_{B2B} . The PAP module needs 500 μ s for the phase extrapolation, so the B2B source and target SCUs collect the extrapolated phase and the slope from the PAP module at $t_{B2B} + 500 \mu\text{s}$. The upper bound latency of the timing frame TGM_PHASE_TIME transfer on the WR network from the B2B target SCU to the B2B source SCU is 500 μs , so the B2B source SCU receives the timing frame TGM_PHASE_TIME at around $t_{B2B} + 500 \mu\text{s} + 500 \mu\text{s} = t_{B2B} + 1 \text{ ms}$. After that, the B2B source SCU needs about 100 μs for the calculation, the sending of the timing frames TGM_SYNCH_WIN and TGM_PHASE_CORRECTION and the data transfer to the corresponding modules. The timing frames TGM_SYNCH_WIN and TGM_PHASE_CORRECTION are sent by the B2B source SCU at around $t_{B2B} + 1 \text{ ms} + 100 \mu\text{s} = t_{B2B} + 1.1 \text{ ms}$. The upper bound latency of the timing frame transfer on the WR network from the B2B source SCU to the Trigger SCUs is 500 μs , so the Trigger SCUs receive the TGM_PHASE_CORRECTION and CMD_SYNCH_WIN at around $t_{B2B} + 1.1 \text{ ms} + 500 \mu\text{s} = t_{B2B} + 1.6 \text{ ms}$. The start of the synchronization window must be later than $t_{B2B} + 1.1 \text{ ms} + 2 \cdot 500 \mu\text{s} = t_{B2B} + 2.1 \text{ ms}$. Two upper bound latency of the WR network are caused by the timing frame TGM_SYNCH_WIN transfer from the B2B source SCU back to the DM and by the timing frame CMD_SYNCH_WIN transfer further from the DM to the BI devices. After bunches are transferred into buckets, there is no hard real time requirement for the Trigger SCU to collect the trigger and firing timestamps and to send the timing frame TGM_KICKER_TRIGGER_TIME_S, so 1 ms is used for the source Trigger SCU to do this task and the source Trigger SCU sends the TGM_KICKER_TRIGGER_TIME_S at around $t_{B2B} + 10 \text{ ms} + 1 \text{ ms} = t_{B2B} + 11 \text{ ms}$. The same time constraints is also for the target Trigger SCU. The B2B source SCU receives the TGM_KICKER_TRIGGER_TIME_S and TGM_KICKER_TRIGGER_TIME_T from the WR network at around $t_{B2B} + 11 \text{ ms} + 500 \mu\text{s} = t_{B2B} + 11.5 \text{ ms}$. The B2B source SCU uses 100 μs to check the B2B transfer status and sends the TGM_B2B_STATUS at around $t_{B2B} + 11.5 \text{ ms} + 100 \mu\text{s} = t_{B2B} + 11.6 \text{ ms}$. The BI devices receives the timing frame TGM_B2B_STATUS at around $t_{B2B} + 11.6 \text{ ms} + 2 \cdot 500 \mu\text{s} = t_{B2B} + 12.6 \text{ ms}$. $2 \cdot 500 \mu\text{s}$ is two upper bound latency of the WR network, which is caused by the timing frame TGM_B2B_STATUS transfer from the B2B source SCU back to the DM and further from the DM to the BI devices.

5.2. GMT Systematic Investigation

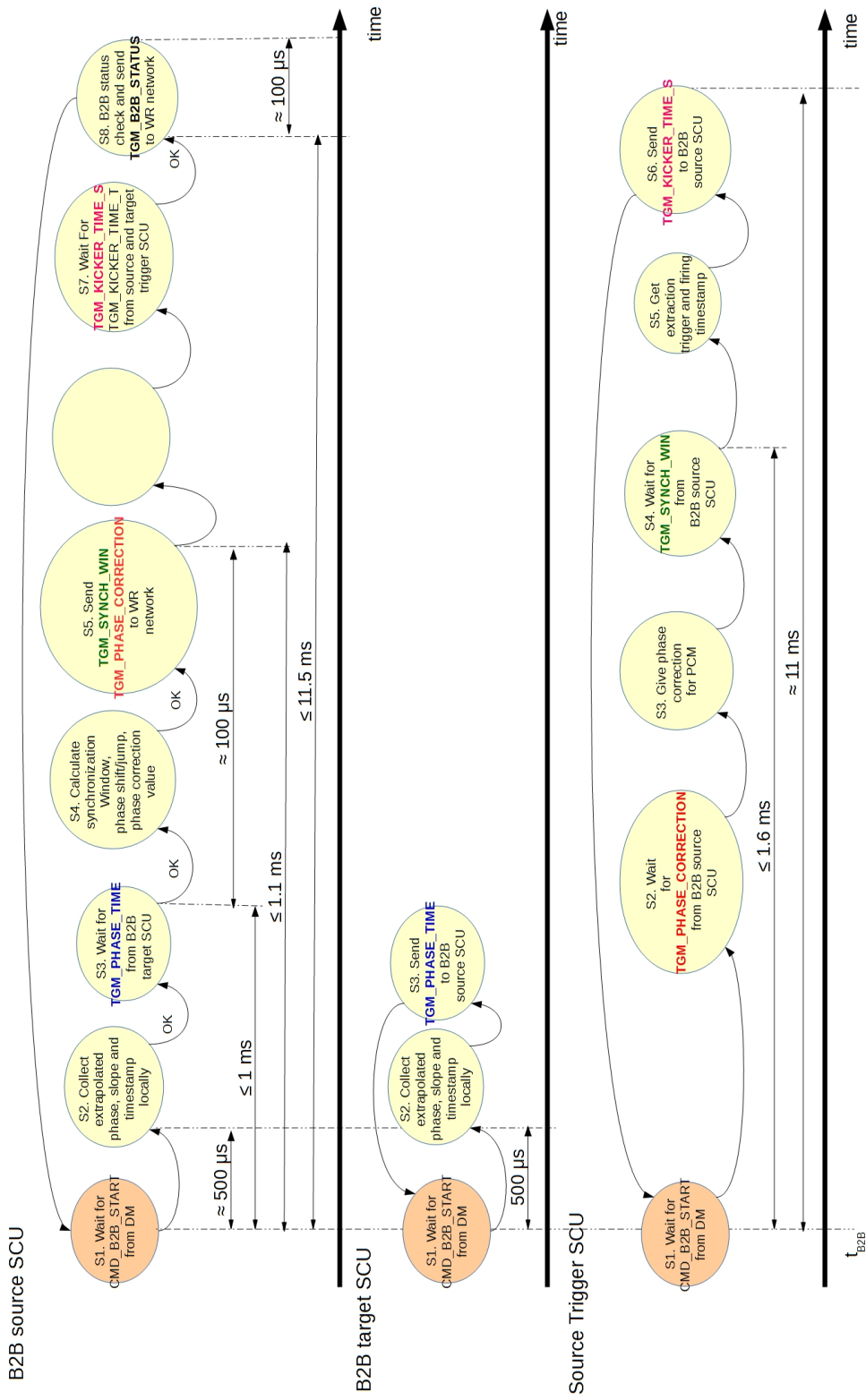


Figure 5.20: Time constraints of the B2B transfer system.

The sent and received timing frame pairs have the same color. (not drawn to accurate timescale)

5.3 Kicker Systematic Investigation

The SIS18 extraction kicker consists of nine kicker magnets. In the existing topology, five kicker magnets are evenly distributed in the 1st tank and the other four kicker magnets are evenly distributed in a 2nd tank. The investigation is based on the assumption that the kicker magnets in one tank are controlled by a common kicker control electronics, which receives a trigger signal from a common TD module. The nine kicker magnets can also be individually controlled by their own kicker control electronics and TD module. The kicker magnets in a common tank are triggered by trigger signals with a local delay compensation for the electronics, the length of the energy transmission cable for instance. Fig. 5.21 shows the schematic diagram of the controls and pulse electronics of the kicker magnets in the SIS18 2nd tank.

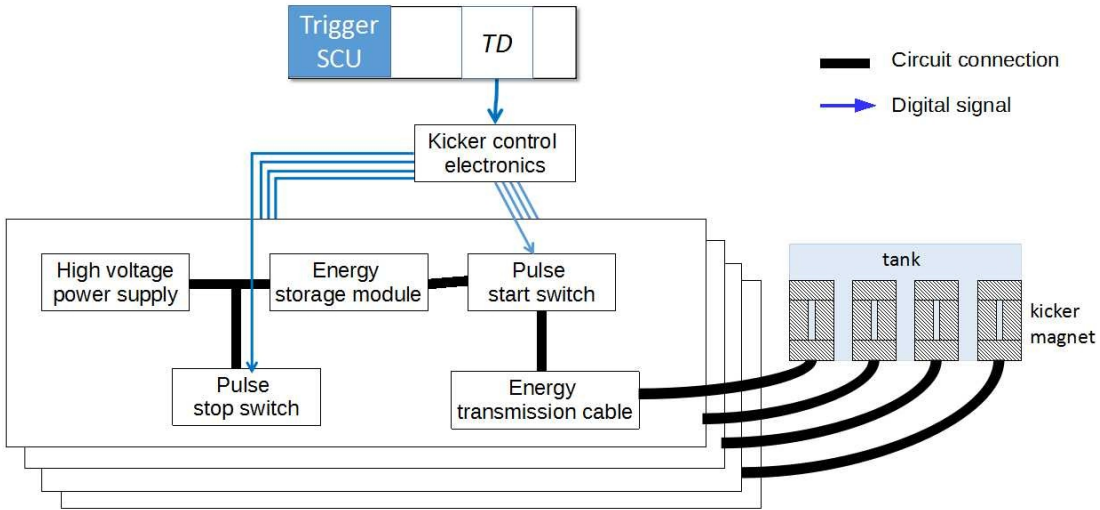


Figure 5.21: The schematic diagram of the controls and pulse electronics of the extraction kicker magnets in the SIS18 2nd tank.

The SIS100 injection kicker consists of six kicker magnets, which are evenly distributed in a common tank. For the B2B transfer, the kicker rise time, denoted by t_{rise} , must fit within the bunch gap, e.g. the bunch gap is 25% of the cavity rf period [26, 39]. The bunch gap is denoted by t_{gap} . All the analysis in this section dose not take the jitter of the kicker trigger signal into consideration (approximately 1 ns).

For ion beams over the whole range of stable isotopes, whether the extraction kicker magnets in a common SIS18 tank can be triggered simultaneously will be discussed. Besides, whether the kicker magnets in the SIS18 2nd tank can be simultaneously triggered a fixed delay after the simultaneous triggering of the kicker magnets in the SIS18 1st tank will also be discussed. For the SIS100 injection kicker, whether all kicker magnets can be triggered simultaneously will be investigated.

5.3.1 Simultaneous Trigger for Extraction Kicker Magnets in a Common SIS18 Tank

Two bunches from SIS18 will be transferred into two SIS100 rf buckets in each B2B transfer. The SIS18 extraction kicker must reach the kicker flat-top during the

5.3. Kicker Systematic Investigation

bunch gap. For the instantaneous trigger, all kicker magnets in a tank are triggered only if the tail of the circulating bunch passes the rightmost kicker magnet of the tank, see Fig. 5.22. The “kicker passing time“ is defined as the time needed for the tail of a bunch to pass from the leftmost magnet to the rightmost kicker magnet. The rise time of the kicker magnet t_{rise} is approximately 90 ns [56]. The width of each kicker magnet is 0.25 m and the distance between two kicker magnets is 0.09 m. The distance between the two tanks is 19.17 m [57]. $d_{tank1L-tank1R}$ represents the distance from the leftmost to the rightmost kicker magnet in the 1st tank, which equals to $1.61\text{ m} = 5 \cdot 0.25\text{ m} + 4 \cdot 0.09\text{ m}$. $d_{tank2L-tank2R}$ represents the distance from the leftmost to the rightmost kicker magnet in the 2nd tank, which equals to $1.27\text{ m} = 4 \cdot 0.25\text{ m} + 3 \cdot 0.09\text{ m}$. If the sum of the kicker passing time and rise time is shorter than the bunch gap, all kicker magnets can be triggered simultaneously.

$$\frac{d_{tankXL-tankXR}}{\beta c} + t_{rise} < t_{gap} \quad (5.41)$$

Three ion beams, H^+ , U^{28+} and U^{73+} , are used to check the instantaneous trigger of kicker magnets in a common tank, because these ion species have the most stringent requirements. Tab. 5.14 shows the kicker passing time, the rise time and the bunch gap for H^+ , U^{28+} and U^{73+} beams.

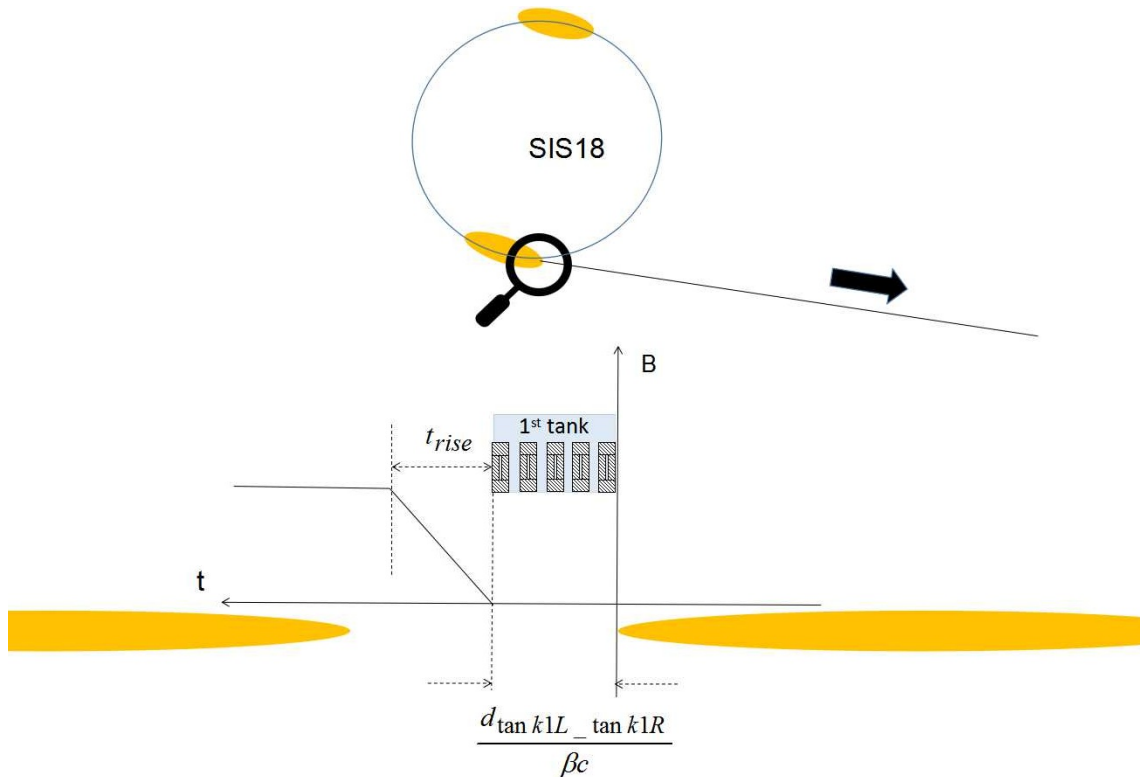


Figure 5.22: SIS18 extraction kicker.

Yellow ellipses represent circulating bunches in SIS18 and the head of the bunch is at the right side.

5.3. Kicker Systematic Investigation

Table 5.14: Calculated parameters related to the simultaneous trigger of the SIS18 extraction kicker magnets in a common tank

| Beam | β | $\frac{d_{tank1L-tank1R}}{\beta c}$ | $\frac{d_{tank2L-tank2R}}{\beta c}$ | t_{rise} | $\frac{d_{tank1L-tank1R}}{\beta c} + t_{rise}$ | $\frac{d_{tank2L-tank2R}}{\beta c} + t_{rise}$ | t_{gap} |
|-----------------------------------|---------|-------------------------------------|-------------------------------------|------------|--|--|-----------|
| $t_{gap} = 25\% / f_{rf}^{SIS18}$ | | | | | | | |
| H^+ | 0.982 | 5 ns | 4 ns | 90 ns | 95 ns | 94 ns | 184 ns |
| U^{28+} | 0.568 | 9 ns | 7 ns | 90 ns | 99 ns | 97 ns | 159 ns |
| U^{73+} | 0.872 | 6 ns | 5 ns | 90 ns | 96 ns | 95 ns | 104 ns |
| $t_{gap} = 20\% / f_{rf}^{SIS18}$ | | | | | | | |
| H^+ | 0.982 | 5 ns | 4 ns | 90 ns | 95 ns | 94 ns | 126 ns |
| U^{28+} | 0.568 | 9 ns | 7 ns | 90 ns | 99 ns | 97 ns | 157 ns |
| U^{73+} | 0.872 | 6 ns | 5 ns | 90 ns | 96 ns | 95 ns | 83 ns |

Tab. 5.14 shows that the sum of the kicker passing time and rise time of both tanks is always shorter than the bunch gap when the bunch gap is 25% of the cavity rf period. Hence, the kicker magnets in the SIS18 1st and 2nd tanks can be triggered simultaneously with the 25% bunch gap. When the bunch gap is 20% of the cavity rf period, the U^{73+} bunch gap is even shorter than the kicker rise time, the kicker magnets can neither be triggered simultaneously, nor one after another. Hence, the 20% bunch gap is not applicable for the SIS18 U^{73+} extraction.

5.3.2 A Fixed Trigger Delay between Extraction Kicker Magnets in the SIS18 1st and 2nd Tanks

Fig. 5.23 shows a possible triggering delay between kicker magnets in the two tanks. The bunch is firstly kicked by kicker magnets in the 1st tank and then kicked by the kicker magnets in the 2nd tanks to the transfer line. The yellow and red ellipse represents the position of the bunches, when the kicker magnets in the 1st and 2nd tank are triggered. The number in the ellipse is used to tell different bunches. The head of the bunch is at the right side. The bunch 2 is firstly kicked. The width of each kicker magnet is 0.22 m and the distance between two magnets is 0.23 m. $d_{tank1R-tank2L}$ denotes the distance between two tanks, which equals to 19.17 m. $d_{tank1L-tank2R}$ denotes the distance from the leftmost to the rightmost kicker magnets, which equals to 22.05 m = $d_{tank1R-tank2L} + 9 \cdot 0.25 \text{ m} + 7 \cdot 0.09 \text{ m}$. $d_{tank1R-tank2R}$ denotes the distance between the rightmost of the 1st tank to the rightmost of the 2nd tank, which equals to 20.44 m = $d_{tank1R-tank2L} + 4 \cdot 0.25 \text{ m} + 3 \cdot 0.09 \text{ m}$. The kicker magnets in the 1st tank are triggered simultaneously when the tail of the bunch 1 passes by the 1st tank completely. The kicker magnets in the 2nd tank are triggered simultaneously when the tail of the bunch 1 passes by the 2nd tank completely. The delay for the trigger two tanks in this scenario is $d_{tank1R-tank2R}/\beta c$.

5.3. Kicker Systematic Investigation

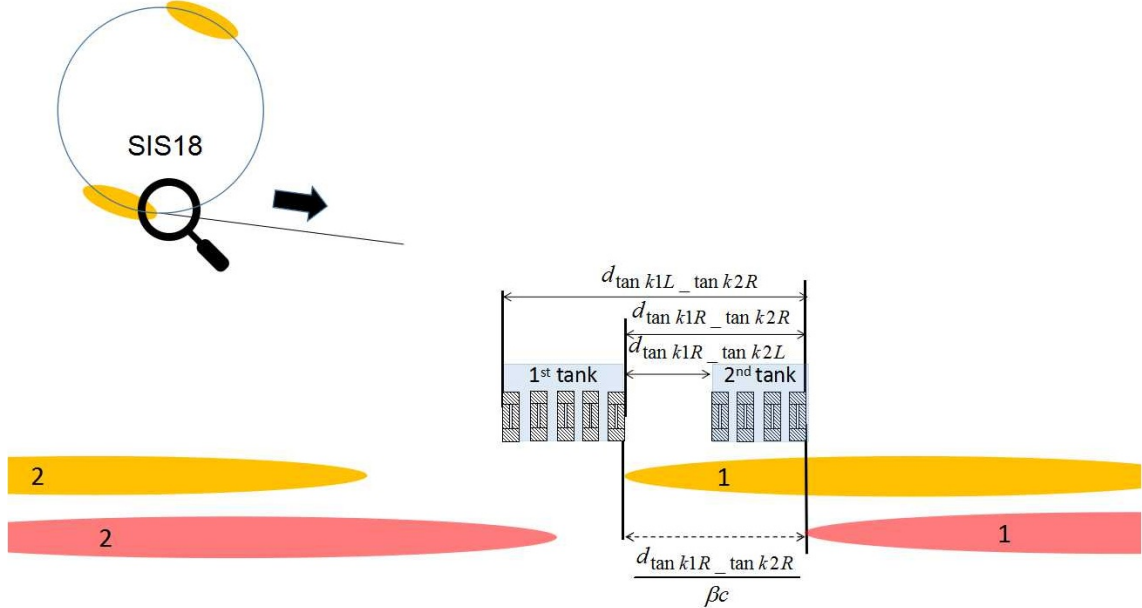


Figure 5.23: A possible triggering delay between extraction kicker magnets in the SIS18 two tanks.

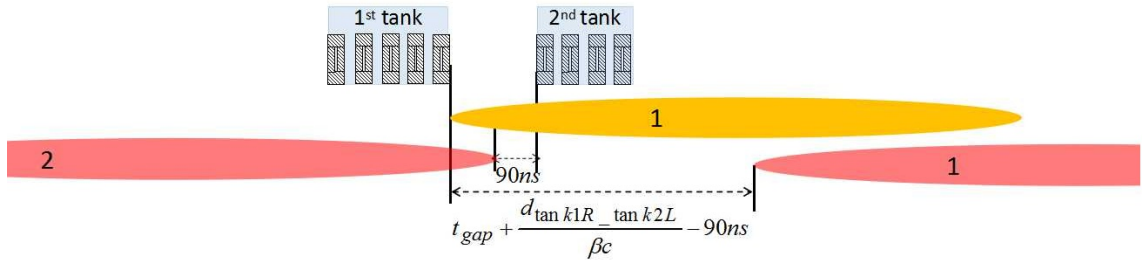


Figure 5.24: Maximum triggering delay between extraction kicker magnets in the SIS18 two tanks.

Fig. 5.24 shows the scenario of the maximum triggering delay between kicker magnets in the two tanks. The kicker magnets in the 1st tank are triggered simultaneously when the tail of the bunch 1 passes by the 1st tank completely. The kicker magnets in the 2nd tank are simultaneously triggered 90 ns before the head of the bunch 2 passes by it. The delay equals to $t_{gap} + \frac{d_{tan k1R - tan k2L}}{\beta c} - 90\text{ ns}$.

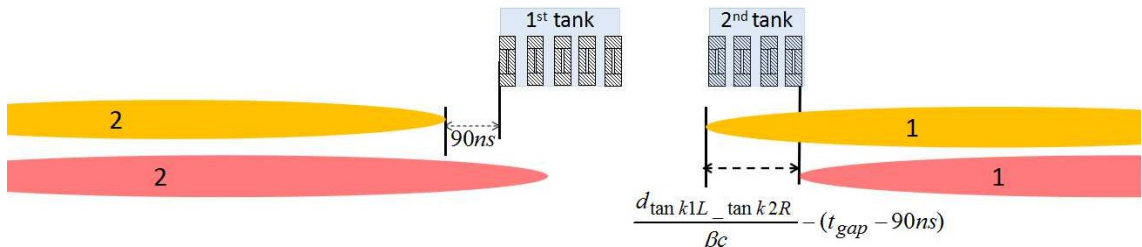


Figure 5.25: The minimum triggering delay between extraction kicker magnets in two SIS18 tanks.

5.3. Kicker Systematic Investigation

Fig. 5.25 shows the scenario of the minimum triggering delay. The kicker magnets in the 1st tank are simultaneously triggered 90 ns before the head of the bunch 2 passes by it. The kicker magnets in the 2nd tanks are simultaneously triggered when the bunch 1 passes by the 2nd tank. The delay is $d_{tank1L-tank2R}/\beta c - (t_{gap} - 90 \text{ ns})$.

Tab. 5.15 shows the maximum and minimum triggering delays for three ion beams.

Table 5.15: The triggering delay for the extraction kicker magnets in the two SIS18 tanks

| Beam | β | t_{gap} | minimum delay $\frac{d_{tank1L-tank2R}}{\beta c} - (t_{gap} - 90 \text{ ns})$ | maximum delay $t_{gap} + (\frac{d_{tank1R-tank2L}}{\beta c} - 90 \text{ ns})$ |
|-----------------------------------|---------|-----------|--|--|
| $t_{gap} = 25\% / f_{rf}^{SIS18}$ | | | | |
| H^+ | 0.982 | 184 ns | 0 ns | 163 ns |
| U^{28+} | 0.568 | 159 ns | 61 ns | 189 ns |
| U^{73+} | 0.872 | 104 ns | 70 ns | 92 ns |

According to the result, a constant triggering delay is available for the triggering of the extraction kicker magnets in the two SIS18 tanks for all ion beams when the bunch gap is 25% of the cavity rf period, e.g. 80 ns.

5.3.3 Simultaneous Trigger for SIS100 Injection Kicker Magnets

The SIS100 injection kicker must reach to the kicker flat-top during the bunch gap. For the instantaneous trigger, all kicker magnets are triggered only if the tail of the circulating bunch passes the rightmost kicker magnet, see Fig. 5.26. The rise time of the kicker magnet t_{rise} is 130 ns [56]. The distance from the leftmost to the rightmost kicker magnet $d_{tankL-tankR}$ is $3.79 \text{ m} = 6 \cdot 0.22 \text{ m} + 5 \cdot 0.23 \text{ m}$. If the sum of the kicker passing time and rise time is shorter than the bunch gap, all kicker magnets can be triggered simultaneously, see eq. 5.41. Tab. 5.16 shows the kicker passing time, the rise time and the bunch gap for H^+ , U^{28+} and U^{73+} beams.

5.3. Kicker Systematic Investigation

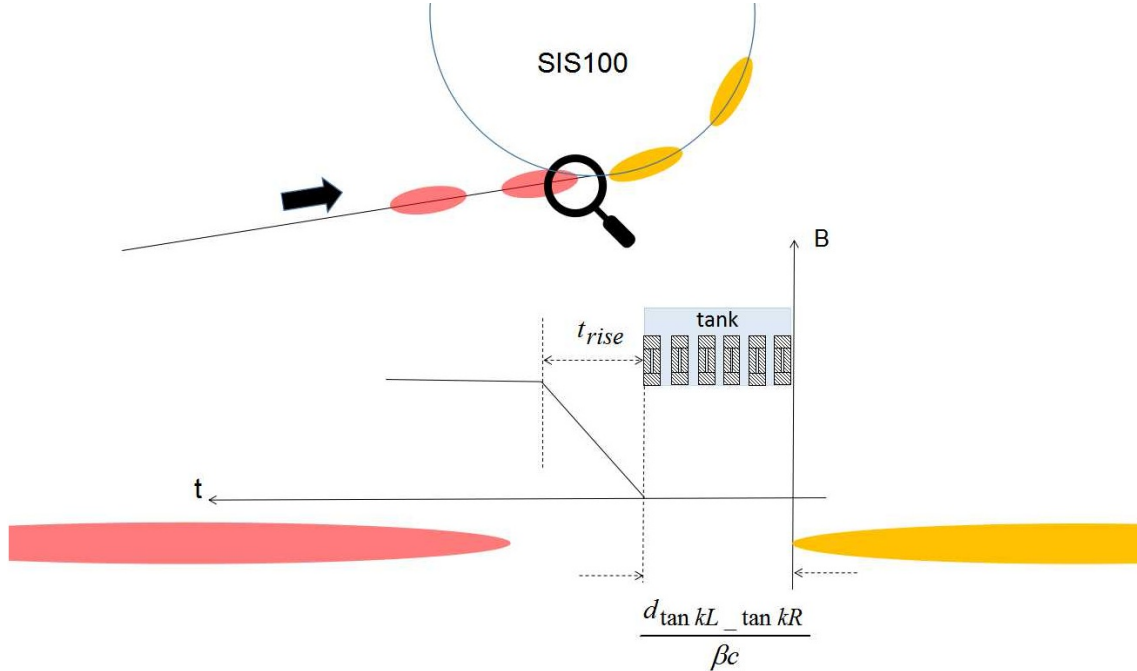


Figure 5.26: SIS100 injection kicker.

Yellow ellipses represent circulating bunches in SIS100 and red ones bunches to be injected. The head of the bunch is at the right side.

Table 5.16: Calculated parameters related to the simultaneous trigger of the SIS100 injection kicker magnets

| Beam | β | $\frac{d_{tan\ kL} - tan\ kR}{\beta c}$ | t_{rise} | $\frac{d_{tan\ kL} - tan\ kR}{\beta c} + t_{rise}$ | t_{gap} |
|------------------------------------|---------|---|------------|--|-----------|
| $t_{gap} = 25\% / f_{rf}^{SIS100}$ | | | | | |
| H^+ | 0.982 | 13 ns | 130 ns | 133 ns | 184 ns |
| U^{28+} | 0.568 | 22 ns | 130 ns | 152 ns | 159 ns |
| U^{73+} | 0.872 | 15 ns | 130 ns | 145 ns | 104 ns |
| $t_{gap} = 35\% / f_{rf}^{SIS100}$ | | | | | |
| H^+ | 0.982 | 13 ns | 130 ns | 133 ns | 258 ns |
| U^{28+} | 0.568 | 22 ns | 130 ns | 152 ns | 223 ns |
| U^{73+} | 0.872 | 15 ns | 130 ns | 145 ns | 146 ns |

Tab. 5.16 shows that the bunch gap of U^{73+} is even shorter than the kicker rise time, when the bunch gap is 25% of the cavity rf period. In this case, the kicker magnets can neither be triggered simultaneously, nor one after another. Hence, the 25% bunch gap is not applicable for the SIS100 U^{73+} injection. The SIS100 kicker magnets can be triggered simultaneously when bunches are longitudinally compressed, e.g. the bunch gap is 35% of the cavity rf period.

In conclusion, the U^{73+} beam has the most stringent requirement according to the above analysis. U^{73+} bunches have to be longitudinally compressed to approximately 65% of the cavity rf period for the application of the SIS18 extraction kickers

5.4. A Test Setup for Timing Aspects

with the 90 ns rise time and the application of SIS100 injection kickers with the 130 ns rise time. When the bunch gap is 35% of the cavity rf period, the extraction and injection kicker magnets in a common tank can be triggered simultaneously and the extraction kicker magnets in the SIS18 2nd tank can be triggered a fixed delay after the trigger of the kicker magnets in the SIS18 1st tank for ion beams over the whole range of stable isotopes.

5.4 A Test Setup for Timing Aspects

From a functional perspective, the test setup simulates that the B2B source SCU collects data from the B2B target SCU, the B2B source SCU calculates the start of the synchronization window and the B2B source SCU distributes the start of the synchronization window to the Trigger SCU. In addition, the test setup is used to check the firmware of the B2B related SCUs to verify that the firmware running on the soft CPU, LM32⁶, meets the time constraints of the B2B transfer system. In Sec. 5.4.1 the test setup will be introduced. The comparison between the test setup and the final setup will be presented in Sec. 5.4.2. The procedure and the flowchart of the firmware will be explained in Sec. 5.4.3. Sec. 5.4.4 shows the functional test result and the measurement of the firmware running time. The measurement result will be discussed in Sec. 5.4.5.

5.4.1 Test Setup

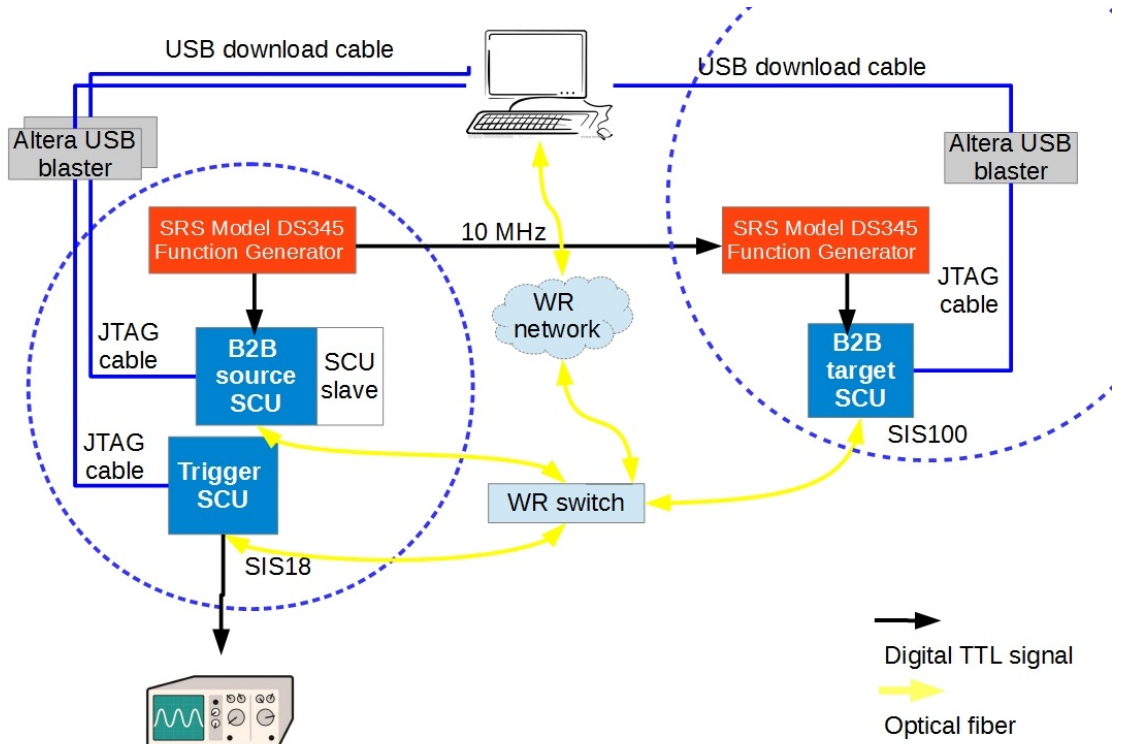


Figure 5.27: Schematic of the test setup.

⁶LatticeMico32 is a 32-bit microprocessor soft core from Lattice Semiconductor optimized for field-programmable gate arrays (FPGAs).

5.4. A Test Setup for Timing Aspects

Fig. 5.27 shows the schematic of the test setup. In this test setup, two SRS MODEL DS345 Synthesized Function Generators⁷ (short: DS345) were used to simulate the rf systems of the SIS18 and SIS100. The two DS345s needed to be synchronized to a common reference clock. For simplicity, the DS345 of the SIS100 used a 10 MHz clock from the DS345 of the SIS18 as an external reference clock. The B2B source SCU, the B2B target SCU and the Trigger SCU were connected to a WR switch via single mode fibers⁸, which connected to the WR network. There was a SCU slave in the B2B source SCU, which simulated the PAP and PCM modules. A personal computer (PC) was connected to the WR network, which was a Linux PC installed with the FEC tools⁹, the Altera's Quartus II software and the packETH software. The SCUs were connected to the PC via the Altera USB-Blaster Joint Test Action Group (JTAG) programmer. The PC was used to simulate the DM to produce the B2B start timing frame CMD_START_B2B. Besides, the PC monitored the status of the firmware in all SCUs and measured the running time of the firmware by the SignalTap II Logic Analyzer¹⁰ feature within the Quartus II software. An oscilloscope was connected to the Trigger SCU. Fig. 5.28 shows the front view of the test setup.

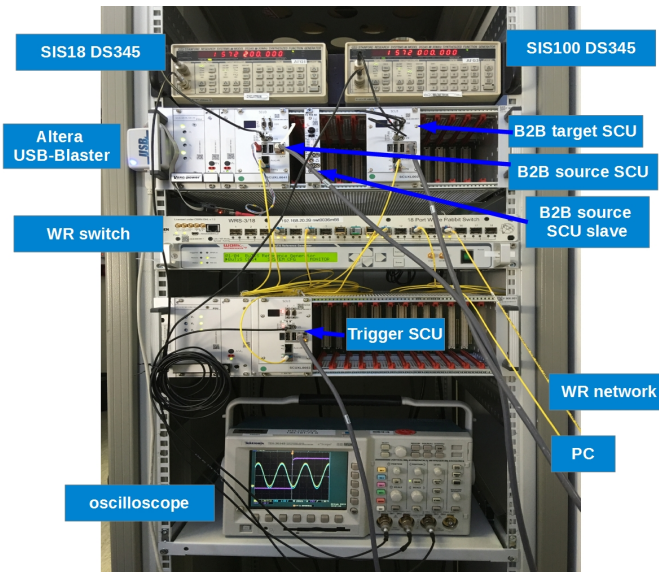


Figure 5.28: Front view of the test setup.

⁷The DS345 Synthesized Function Generator is a full-featured 30 MHz synthesized function generator that uses an innovative Direct Digital Synthesis architecture. It generates many standard waveforms with excellent frequency resolution ($1 \mu\text{Hz}$) and has versatile modulation capabilities including AM, FM, Burst, PM and frequency sweeps.

⁸A G.652.B type single mode fiber is used for the 1310 and 1550 nm wavelength region.

⁹FEC tools include the etherbone tools, the saftlib tools and the Linux drivers.

<https://www-acc.gsi.de/wiki/Timing/TimingSystemHowConfigureEnvironment>

¹⁰The SignalTap II Logic Analyzer is a system-level debugging tool that captures and displays signals in circuits designed for implementation in Altera's FPGAs.

5.4.2 Comparison between the Test Setup and the Final Setup

Fig. 5.29 shows the schematic of the final setup. Compared with the test setup, two DS345s will be replaced by the FAIR LLRF system. In addition, the B2B source/target SCU, the Trigger SCU and the Kicker SCU with their own slaves will be equipped at every ring. The SCU slaves will be connected to the LLRF system by the optical direct link¹¹. The SCUs on the source ring will be connected to one WR switch and the SCUs on the target ring will be connected to another WR switch, both WR switches will be connected to the WR network. The PC will be replaced by the DM. The maximum number of the WR switch layers among the B2B related SCUs and the DM must comply with the analysis result of the WR network for the B2B transfer in Sec. 5.2.2. For more details about the data communication among the B2B related SCUs and their slaves, please see Chap. 4.

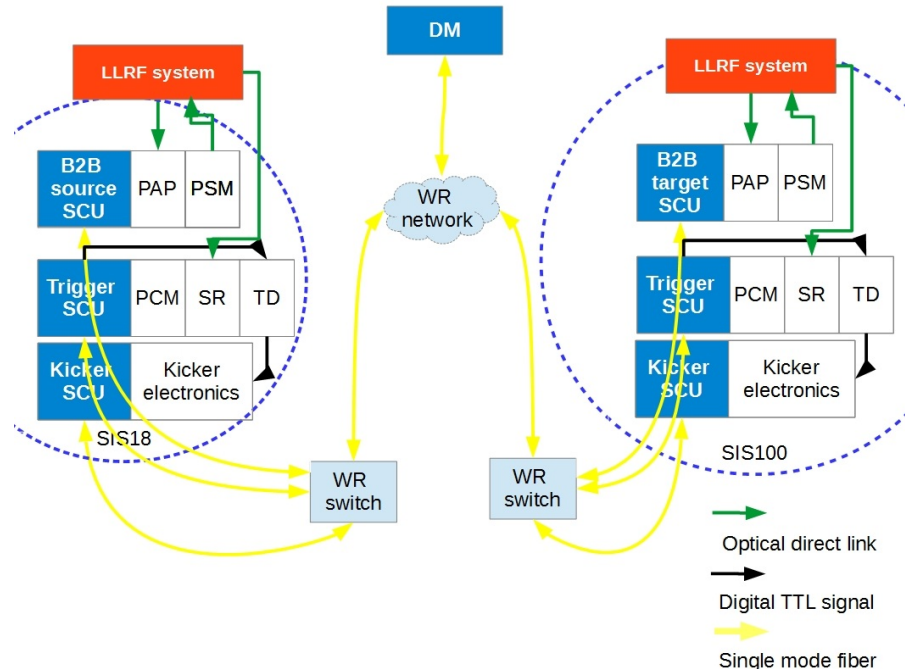


Figure 5.29: Schematic of the final setup.

5.4.3 Procedure

The test procedure which has been developed in the framework of this thesis is divided into several essential steps that include the different hardware systems described above.

1. Configure the B2B source SCU

- (a) Login the B2B source SCU.

¹¹The optical direct link is a multi-mode fiber with the bandwidth of 40 Mbit/s up to 100 m. It is used in the 650 nm wavelength region.

5.4. A Test Setup for Timing Aspects

(b) Use the saftlib library¹² function to configure the Event-Condition-Action (ECA) queue¹³ of the B2B source SCU to storage the B2B frames CMD_START_B2B and TGM_PHASE_TIME.

(c) Use the saftlib library function to configure one IO port as an input for the TTL signal of the SIS18 DS345.

(d) Load the B2B source SCU firmware to the LM32.

2. Configure the B2B target SCU

(a) Login the B2B target SCU.

(b) Use the saftlib library function to configure the ECA queue of the B2B target SCU to storage the B2B frame CMD_START_B2B.

(c) Use the saftlib library function to configure one IO port as an input for the TTL signal of the SIS100 DS345.

(d) Load the B2B target SCU firmware to the LM32.

3. Configure the Trigger SCU

(a) Login the Trigger SCU.

(b) Use the saftlib library function to configure one IO port as an output.

(c) Use the saftlib library function to configure ECA [58] to produce a TTL signal at the output port, when the frame TGM_SYNCH_WIN is executed.

(d) Load the Trigger SCU firmware to the LM32.

4. Use the packETH to generate the frame CMD_START_B2B.

More details of the configuration are shown in Appendix F. The flowchart of the firmware of the B2B source SCU and that of the B2B target SCU and that of the Trigger SCU are shown in Fig. 5.30, Fig. 5.31 and Fig. 5.32. The project is kept in the git repository¹⁴. The firmware of the test setup realizes partial function of the flowcharts described in Sec. 5.2.3.

¹²The saftlib library is simple application programming interface for timing.
<https://www-acc.gsi.de/wiki/Timing/TimingSystemDocumentsSaftlib>

¹³The ECA queue is used to storage filtered timing events, which are used for the SCU Soft CPU, LM32.

<https://www-acc.gsi.de/wiki/Timing/TimingSystemHowTriggerLM32FromEca>

¹⁴The B2B transfer system git repository
https://github.com/GSI-CS-C0/bel_projects/tree/lm32_B2B_merge

5.4. A Test Setup for Timing Aspects

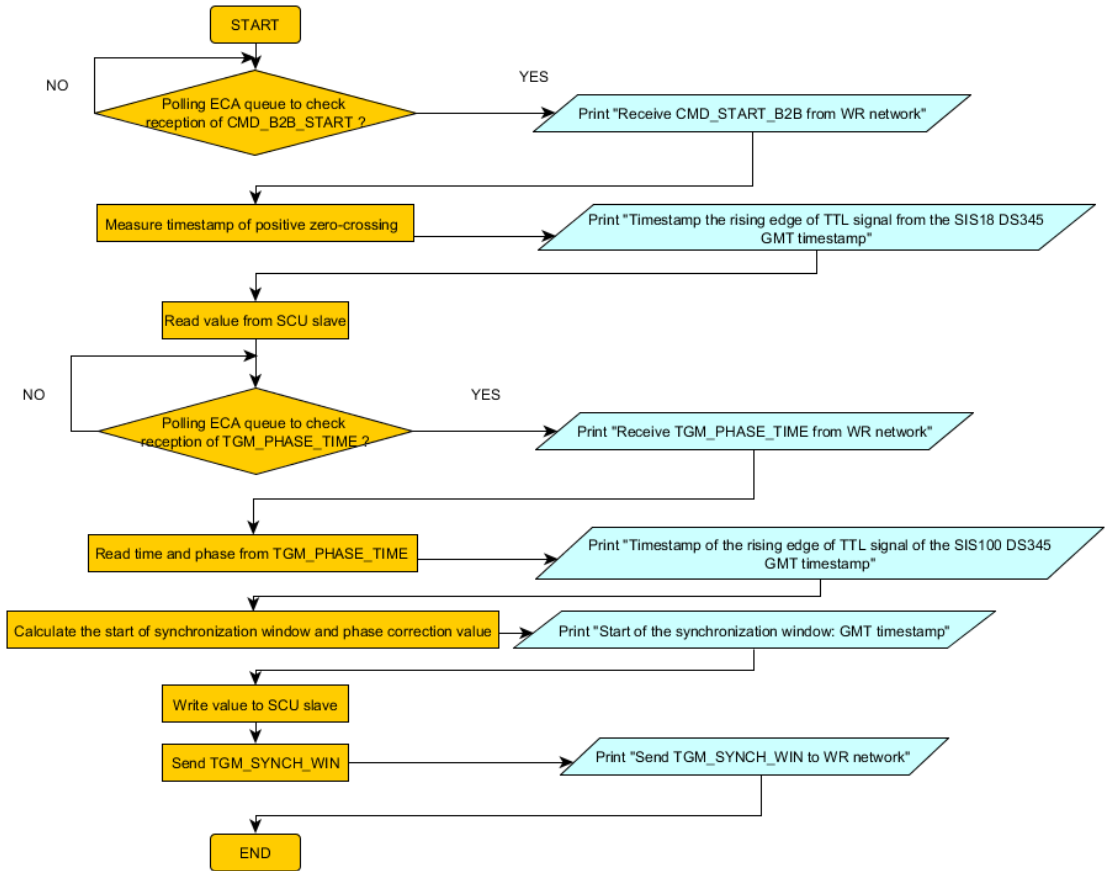


Figure 5.30: Flowchart of the firmware of the B2B source SCU for the test setup.

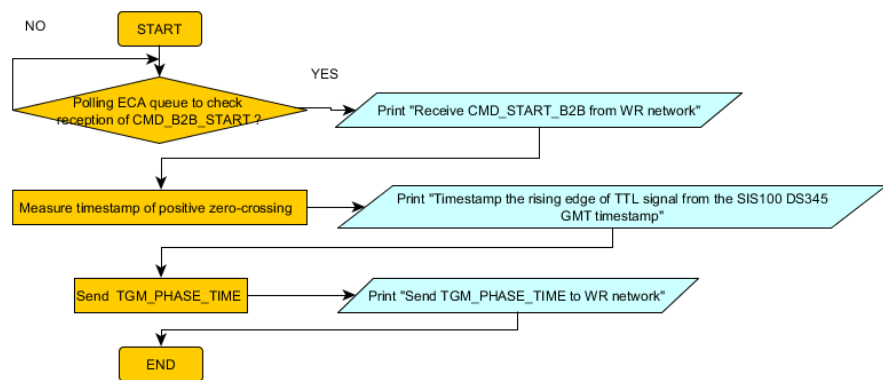


Figure 5.31: Flowchart of the firmware of the B2B target SCU for the test setup.

5.4. A Test Setup for Timing Aspects

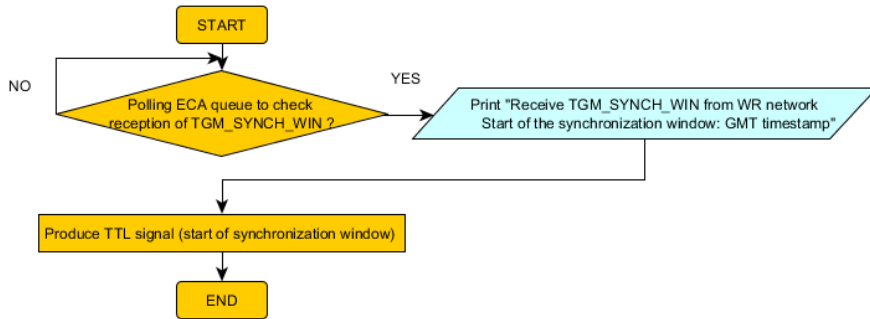


Figure 5.32: Flowchart of the firmware of the Trigger SCU for the test setup.

5.4.4 Functional Test Result

The test made use of the parameters from the FAIR use case of the U^{28+} B2B transfer from the SIS18 to the SIS100 and the frequency beating method. After the frequency detune, the SIS18 rf cavity frequency is 1.572 200 MHz and the SIS100 rf cavity frequency is 1.572 000 MHz. Hence, the SIS18 DS345 produced 1.572 200 MHz TTL signal for the B2B source SCU and the SIS100 DS345 produced 1.572 000 MHz TTL signal for the B2B target SCU. These two frequencies were given to the firmware of the B2B source SCU. The console of the PC showed the print information of the firmware on the B2B source, B2B target and Trigger SCUs. All print timestamps are in the format of Greenwich Mean Time (GMT).

```

1 U28+ B2B transfer from SIS18 to SIS100 => B2B source SCU
2 =====
3
4
5 Receive CMD\_START\_B2B from WR network
6 Timestamp the rising edge of TTL signal from the SIS18 DS345
7 GMT Thu, Jan 8, 1970, 21:07:27.445405856
8
9 Receive TGM_PHASE_TIME from WR network
10 Timestamp of the rising edge of TTL signal of the SIS100 DS345
11 GMT Thu, Jan 8, 1970, 21:07:27.445364560
12
13 Start of the synchronization window: GMT Thu, Jan 8, 1970,
14 21:07:27.450028674
15 Send TGM_SYNCH_WIN to WR network
  
```

```

1 U28+ B2B transfer from SIS18 to SIS100 => B2B target SCU
2 =====
3
4
5 Receive CMD\_START\_B2B from WR network
6 Timestamp the rising edge of TTL signal from the SIS100 DS345
7 GMT: Thu, Jan 8, 1970, 21:07:27.445364560
8
9 Send TGM_PHASE_TIME to WR network
  
```

5.4. A Test Setup for Timing Aspects

```

1 U28+ B2B transfer from SIS18 to SIS100 => Trigger SCU
2 =====
3
4
5 Receive TGM_SYNCH_WIN from WR network
6 Start of the synchronization window: GMT 1970-01-08 21:07:27.450028674

```

Besides, the TTL signal indicating the start of the synchronization window was observed on the oscilloscope. According to the test result, the test setup realized the functionality of the data collection, data calculation and data redistribution for the FAIR B2B transfer system.

During the test, the SignalTap II Logic Analyzer was used to measure the needed time for the tasks of the firmware. Tab. 5.17 shows the measured running time of different tasks of the B2B source SCU firmware. The LM32 is connected to other intellectual property cores by the System-on-Chip bus¹⁵. The test result was based on the precondition that the related System-on-Chip bus was not occupied by any other applications, when the firmware was running.

Table 5.17: The running time of the tasks of the B2B source SCU firmware

| Task | Average running time | Worst-case running time |
|--|----------------------|-------------------------|
| The LM32 uses polling to check the reception of the CMD_START_B2B after the ECA queue stores the CMD_START_B2B | 336 ns | 336 ns |
| The LM32 reads from/writes to the SCU slave | 450 ns | 450 ns |
| The LM32 uses polling to check the reception of the TGM_PHASE_TIME after the ECA queue stores the TGM_PHASE_TIME | 336 ns | 336 ns |
| The LM32 reads the phase and timestamp contained in the TGM_PHASE_TIME | 2.7 µs | 2.7 µs |
| The LM32 calculates the start of the synchronization window | 12.6 µs | 12.8 µs |
| The LM32 calculates the phase correction value | 2.0 µs | 2.2 µs |
| The LM32 sends the TGM_SYNCH_WIN to the WR network | 3.2 µs | 3.2 µs |

5.4.5 Measurement Result Discussion

The measurement result was used to evaluate whether the firmware running on the soft CPU, LM32, of the SCU meets the time constraint of the B2B transfer system or not.

¹⁵The system-on-Chip bus is intended to let the parts of an integrated circuit communicate with each other. e.g. the Wishbone bus is used for the FAIR standard FEC.

5.4. A Test Setup for Timing Aspects

After the ECA queue stores the frame CMD_START_B2B, the firmware of the B2B source SCU needs maximal 800 ns (336 ns+450 ns) to inform the PAP module to start the phase extrapolation. Compared with 500 μ s phase extrapolation duration, 800 ns is negligible. 500 μ s after the execution of the CMD_START_B2B, the firmware reads the extrapolated phase from the PAP module 800 ns after the BuTiS T0 incident, 800 ns is much shorter than 10 μ s (the BuTiS T0 period), which guarantees the correct extrapolated phases are read at both the B2B source and target SCUs.

After the ECA queue stores the frame TGM_PHASE_TIME, the firmware of the B2B source SCU needs maximal 3.1 μ s (336 ns+2.7 μ s) to get the phase and timestamp. The calculation time is maximal 15 μ s (12.8 μ s+2.2 μ s) and the sending time of the TGM_SYNCH_WIN is 3.2 μ s. The sum of these running time is approximately 22 μ s, which is negligible compared with 10 ms.

After the ECA queue stores the TGM_PHASE_CORRECTION, the Trigger SCU needs maximal 3.6 μ s (336 ns+2.7 μ s+450 ns) to transfer the phase correction value to the PCM. 3.6 μ s is shorter than 10 μ s, which guarantees the trigger of the phase correction at the correct BuTiS T0 incident.

In conclusion, the test setup proved the systematic functionality, the data collection, calculation and distribution. Besides, it proved that the firmware on LM32 meets the time constraints of the B2B transfer system, when the firmware is running and the related System-on-Chip bus is not occupied by any other applications.

Chapter 6

Application of the FAIR B2B Transfer System to FAIR Accelerators

For the FAIR B2B transfer system, both the phase shift and frequency beating methods are applicable. However, there is a constraint for many FAIR accelerator pairs to use the frequency beating method because of the non-integer ratio of the circumference between two ring accelerators. These pairs can also use the phase jump, a special phase shift without the adiabaticity consideration, on the target accelerator to realize the synchronization, when there is no beam in the target accelerator. When the ratio of the circumference between two ring accelerators is an integer, the phase shift method is preferred. In this chapter all FAIR use cases with the frequency beating method will be discussed in details. Based on the circumference ratio, there are three scenarios of the B2B transfer for FAIR.

- The circumference ratio between the large and small accelerators is an integer.
 - The B2B transfer from the SIS18 to the SIS100
- The circumference ratio between the large and small accelerators is close to an integer.
 - The B2B transfer from the SIS18 to the ESR¹
 - The B2B transfer from the ESR² to the CRYRING
- The circumference ratio between the large and small accelerators is far away from an integer.
 - The B2B transfer from the CR to the HESR

Besides, FAIR has many use cases of B2B transfers that the extraction and injection beam have different energy because of targets installed between two ring accelerators (e.g. the pbar target, the FRS and the Super FRS). Due to the energy loss at the target, the beam revolution frequency ratio between the small and large accelerators is used instead of the circumference ratio between the large and small accelerators.

¹Injection orbit

²Extraction orbit

6.1. Circumference Ratio is an Integer

The revolution frequency ratio takes the energy loss into consideration. For FAIR, there exists the following scenario.

- The revolution frequency ratio between the small and large accelerators is far away from an integer.
 - The B2B transfer from the SIS100 to the CR via the Super FRS
 - The B2B transfer from the SIS18 to the ESR via the FRS

Tab. 6.1 lists all FAIR use cases of the B2B transfer. m , n and κ are integers.

Table 6.1: List of the FAIR B2B transfer use cases

| Circumference ratio | C^l/C^s | f_{rev}^s/f_{rev}^l | Use cases of FAIR accelerators |
|---|------------------------|-----------------------|--|
| $C^l/C^s = \kappa$ an integer | 5 | | U^{28+} B2B transfer from the SIS18 to the SIS100 |
| | 5 | | H^+ B2B transfer from the SIS18 to the SIS100 |
| $C^l/C^s = \kappa + \lambda$ or $f_{rev}^s/f_{rev}^l = \kappa + \lambda$ close to an integer ($ \lambda \leq 0.005$) | 2 – 0.003 | | $h=4$ B2B transfer from the SIS18 to the ESR |
| | 2 – 0.003 | | $h=1$ B2B transfer from the SIS18 to the ESR |
| | 2 + 0.003 | | B2B transfer from the ESR to the CRYRING |
| $C^l/C^s = m/n + \lambda$ or f_{rev}^s/f_{rev}^l $= m/n + \lambda$ far away from an integer ($ \lambda \leq 0.05$) | not applicable | arbitrary | H^+ B2B transfer from the SIS100 to the CR via the pbar target |
| | not applicable | arbitrary | Rare isotope beams (RIB) B2B transfer from the SIS100 to the CR via the Super FRS |
| | $2\frac{3}{5} - 0.003$ | | B2B transfer from the CR to the HESR |
| | not applicable | arbitrary | RIB B2B transfer from the SIS18 to the ESR via the FRS |

6.1 Circumference Ratio is an Integer

When the circumference ratio of the large accelerator to that of the small accelerator is an integer, there exists the following relation between two cavity rf frequencies, see Chap. 2.

$$\frac{f_{rf}^l}{f_{rf}^s} = \frac{h_{rf}^l}{h_{rf}^s \cdot \kappa} \quad (6.1)$$

6.1. Circumference Ratio is an Integer

Two synchronization frequencies are

$$f_{syn}^l = \frac{f_{rf}^l}{h_{rf}^l/Y} = Y f_{rev}^l \quad (6.2)$$

$$f_{syn}^s = \frac{f_{rf}^s}{h_{rf}^s \kappa / Y} = \frac{Y}{\kappa} f_{rev}^s \quad (6.3)$$

Y is the GCD of h_{rf}^l and $h_{rf}^s \cdot \kappa$. For more details, please see Sec. 2.2.1.

For the frequency beating method, two slightly different frequencies are chosen based on f_{syn}^l and f_{syn}^s by detuning Δf_{syn} on the rf system of the source accelerator or of the target accelerator or of both accelerators. Generally the rf system of the source accelerator is preferred to be detuned, which is easy to be achieved during or after the acceleration ramp.

The frequency of the bucket indication signal depends on the relation between f_{syn}^{trg} and f_{rev}^{trg} , see Chap. 4. When the large accelerator is the target, there exists $f_{syn}^l = Y f_{rev}^l \geq f_{rev}^l$. The revolution period is Y times as long as the period of f_{syn}^l . The period of f_{syn}^l is not long enough to contain all buckets. So $f_{bucket} = f_{rev}^l$ and the length of the synchronization window $T_w = T_{rev}^l$ for this case. Tab. 6.2 shows the formulas for the frequency of the bucket indication signal f_{bucket} , the synchronization frequencies f_{syn}^X , the frequencies of two phase measurement signals f_{B2B}^X , the frequency of the synchronization reference signal f_{ref} , the length of the synchronization window T_w and the bunch and bucket injection center mismatch σ_{rf} when the large accelerator is the target. When the phase shift method is used, $\Delta f_{syn} = 0$.

Table 6.2: Parameters related to the B2B transfer when the circumference ratio is an integer and the large accelerator is the target

| | Large accelerator is target accelerator |
|---------------|--|
| f_{bucket} | f_{rev}^l |
| f_{syn}^X | $f_{syn}^s + \Delta f_{syn} = \frac{f_{rf}^s}{h_{rf}^s \kappa / Y} + \Delta f_{syn} = \frac{Y}{\kappa} f_{rev}^s + \Delta f_{syn}$ and $f_{syn}^l = \frac{f_{rf}^l}{h_{rf}^l / Y} = Y f_{rev}^l$ |
| f_{B2B}^X | $f_{B2B}^s = \frac{h_{rev}^l}{h_{syn}^s} \cdot (f_{syn}^s + \Delta f_{syn}) = \frac{1}{\kappa} (f_{rev}^s + \frac{\kappa}{Y} \Delta f_{syn})$ and $f_{B2B}^l = f_{rev}^l$ |
| f_{ref} | $round(f_{rev}^l / 100 \text{ kHz}) \cdot 100 \text{ kHz}$ |
| T_w | T_{rev}^l |
| σ_{rf} | $\pm \frac{1}{2} \cdot 2\pi f_{syn}^s - f_{syn}^l \cdot T_w \cdot \frac{h_{rf}^l}{h_{syn}^l}$ |

When the small accelerator is the target, the relation between $f_{syn}^s = \frac{Y}{\kappa} f_{rev}^s$ and f_{rev}^s is not fixed. If $f_{syn}^s \geq f_{rev}^s$, namely $\frac{Y}{\kappa} \geq 1$, the revolution period is $\frac{Y}{\kappa}$ times as long as the period of f_{syn}^s . Hence, $f_{bucket} = f_{rev}^s$ and $T_w = T_{rev}^s$ for this case. Oppositely, if $f_{syn}^s < f_{rev}^s$, namely $\frac{Y}{\kappa} < 1$, the period of f_{syn}^s is $\frac{\kappa}{Y}$ times as long as the revolution period. Hence, $f_{bucket} = f_{syn}^s$ and $T_w = T_{syn}^s$. Tab. 6.3 shows the formulas when the small accelerator is the target. When the phase shift method is used, $\Delta f_{syn} = 0$.

6.1. Circumference Ratio is an Integer

Table 6.3: Parameters related to the B2B transfer when the circumference ratio is an integer and the small accelerator is the target

| | Small accelerator is target accelerator | |
|---------------|--|--|
| Case | (1) $f_{syn}^s \geq f_{rev}^s (\frac{Y}{\kappa} \geq 1)$ | (2) $f_{syn}^s < f_{rev}^s (\frac{Y}{\kappa} < 1)$ |
| f_{bucket} | f_{rev}^s | f_{syn}^s |
| f_{syn}^X | $f_{syn}^s + \Delta f_{syn} = \frac{f_{rf}^s}{h_{rf}^s \kappa / Y} + \Delta f_{syn} = \frac{Y}{\kappa} f_{rev}^s + \Delta f_{syn}$ and $f_{syn}^l = \frac{f_{rf}^l}{h_{rf}^l / Y} = Y f_{rev}^l$ | |
| f_{B2B}^X | $f_{B2B}^l = \frac{h_{rev}^s}{h_{syn}^s} \cdot (f_{syn}^l + \Delta f_{syn}) = \kappa (f_{rev}^l + \frac{1}{Y} \Delta f_{syn})$ and $f_{B2B}^s = f_{rev}^s$ | $f_{B2B}^l = f_{syn}^l + \Delta f_{syn} = Y (f_{rev}^l + \frac{1}{Y} \Delta f_{syn})$ and $f_{B2B}^s = f_{syn}^s = \frac{Y}{\kappa} f_{rev}^s$ |
| f_{ref} | $round(f_{rev}^s / 100 \text{ kHz}) \cdot 100 \text{ kHz}$ | $round(f_{syn}^s / 100 \text{ kHz}) \cdot 100 \text{ kHz}$ |
| T_w | T_{rev}^s | T_{syn}^s |
| σ_{rf} | $\pm \frac{1}{2} \cdot 2\pi f_{syn}^s - f_{syn}^l \cdot T_w \cdot \frac{h_{rf}^s}{h_{syn}^s}$ | |

6.1.1 U^{28+} B2B Transfer from SIS18 to SIS100

The use case of the U^{28+} B2B transfer from the SIS18 to the SIS100 belongs to the scenario discussed above. Four batches of U^{28+} at 200 MeV/u are injected into continuous eight out of ten buckets of the SIS100. Each batch consists of two bunches [38, 39]. The large accelerator is the SIS100 and the small one the SIS18. $\kappa = 5$, $h_{rf}^{SIS100} = 10$ and $h_{rf}^{SIS18} = 2$. The GCD of $h_{rf}^{SIS100} = 10$ and $h_{rf}^{SIS18} \cdot \kappa = 2 \cdot 5 = 10$ is 10, namely $Y = 10$. Substituting these values into eq. 6.1, we get

$$\frac{f_{rf}^{SIS100}}{f_{rf}^{SIS18}} = \frac{h_{rf}^{SIS100}}{h_{rf}^{SIS18} \cdot \kappa} = \frac{10}{2 \cdot 5} = \frac{10}{10} \quad (6.4)$$

Because the SIS100 is the large accelerator and the target, substituting h_{rf}^X , κ , f_{rf}^X , f_{rev}^X and Y into formulas in Tab. 6.2, the parameters related to the U^{28+} B2B transfer from the SIS18 to the SIS100 is obtained, see Tab. 6.4. Here we assume that the SIS18 is detuned with 200 Hz for the synchronization frequency f_{syn}^{SIS18} .

The goal time difference between the SIS18 and SIS100 rf systems equals to $t_{v_ext} + t_{v_inj} + t_{TOF}$, provided by the SM. The SIS100 revolution frequency works for the bucket indication. When the 1st and 2nd buckets are to be filled, $t_{pattern} = 0$. When the 3rd and 4th buckets are to be filled, $t_{pattern} = T_{rev}^{SIS18}$. When the 5th and 6th buckets are to be filled, $t_{pattern} = 2 \cdot T_{rev}^{SIS18}$. When the 7th and 8th buckets are to be filled, $t_{pattern} = 3 \cdot T_{rev}^{SIS18}$. Detailed parameters of the U^{28+} B2B transfer from the SIS18 to the SIS100, please see Appendix C.1.

6.1.2 H^+ B2B Transfer from SIS18 to SIS100

Four batches of H^+ at 4 GeV/u are injected into continuous four out of ten buckets of the SIS100. Each batch consists of one bunch [38, 39]. The large accelerator is the SIS100 and the small one the SIS18. $\kappa = 5$, $h_{rf}^{SIS100} = 10$ and $h_{rf}^{SIS18} = 1$. The

³A Group DDS produces a given frequency with the mHz order of magnitude precision

6.1. Circumference Ratio is an Integer

Table 6.4: Parameters related to the U^{28+} B2B transfer from the SIS18 to the SIS100 with the frequency beating method

| | |
|---------------|--|
| | Large accelerator (SIS100) is target accelerator |
| f_{bucket} | $f_{rev}^{SIS100} = 157.254 \text{ kHz}^3$ |
| f_{syn}^X | $f_{syn}^{SIS18} = 2f_{rev}^{SIS18} = 1.572\,536 \text{ MHz} + 200 \text{ Hz}$ and $f_{syn}^{SIS100} = 10f_{rev}^{SIS100} = 1.572\,536 \text{ MHz}$ |
| f_{B2B}^X | $f_{B2B}^{SIS18} = \frac{1}{5}(f_{rev}^{SIS18} + \frac{1}{2}\Delta f_{syn}) = 157.254 \text{ kHz} + 20 \text{ Hz}$ and $f_{B2B}^{SIS100} = f_{rev}^{SIS100} = 157.254 \text{ kHz}$ |
| f_{ref} | 200 kHz |
| T_w | $T_{rev}^{SIS100} = 6.359 \mu\text{s}$ |
| σ_{rf} | $\pm 0.4^\circ$ |

GCD of $h_{rf}^{SIS100} = 10$ and $h_{rf}^{SIS18} \cdot \kappa = 1 \cdot 5$ is 5, namely $Y = 5$. Substituting these values into eq. 6.1, we get

$$\frac{f_{rf}^{SIS100}}{f_{rf}^{SIS18}} = \frac{h_{rf}^{SIS100}}{h_{rf}^{SIS18} \cdot \kappa} = \frac{10}{1 \cdot 5} = \frac{2}{1} \quad (6.5)$$

Because the SIS100 is the large accelerator and the target, substituting h_{rf}^X , κ , f_{rf}^X , f_{rev}^X and Y into formulas in Tab. 6.2, the parameters related to the H^+ B2B transfer from the SIS18 to the SIS100 is obtained, see Tab. 6.5. Here we assume that the SIS18 is detuned with 200 Hz for the synchronization frequency f_{syn}^{SIS18} .

Table 6.5: Parameters related to the H^+ B2B transfer from the SIS18 to the SIS100 with the frequency beating method

| | |
|---------------|---|
| | Large accelerator (SIS100) is target accelerator |
| f_{bucket} | $f_{rev}^{SIS100} = 271.872 \text{ kHz}$ |
| f_{syn}^X | $f_{syn}^{SIS18} = f_{rev}^{SIS18} = 1.359\,358 \text{ MHz} + 200 \text{ Hz}$ and $f_{syn}^{SIS100} = 5f_{rev}^{SIS100} = 1.359\,358 \text{ MHz}$ |
| f_{B2B}^X | $f_{B2B}^{SIS18} = \frac{1}{5}(f_{rev}^{SIS18} + \Delta f_{syn}) = 271.872 \text{ kHz} + 40 \text{ Hz}$ and $f_{B2B}^{SIS100} = f_{rev}^{SIS100} = 271.872 \text{ kHz}$ |
| f_{ref} | 300 kHz |
| T_w | $T_{rev}^{SIS100} = 3.678 \mu\text{s}$ |
| σ_{rf} | $\pm 0.4^\circ$ |

The SIS100 revolution frequency works for the bucket indication. In order to inject into the odd and even number buckets, there are two scenarios of the goal time difference between the SIS18 and SIS100 rf systems.

- Injection into odd number buckets

6.2. Circumference Ratio is close to an Integer

The goal time difference between the SIS18 and SIS100 rf systems equals to $t_{v_ext} + t_{v_inj} + t_{TOF}$. When the 1st bucket is to be filled, $t_{pattern}=0$. When the 3rd bucket is to be filled, $t_{pattern} = 1 \cdot T_{rev}^{SIS18}$.

- Injection into even number buckets

The goal time difference between the SIS18 and SIS100 rf systems equals to $t_{v_ext} + t_{v_inj} + t_{TOF} - T_{rf}^{SIS100}$. When the 2nd bucket is to be filled, $t_{pattern} = 0$. When the 4th bucket is to be filled, $t_{pattern} = 1 \cdot T_{rev}^{SIS18}$.

Detailed parameters of the H^+ B2B transfer from the SIS18 to the SIS100, please see Appendix C.1.

6.2 Circumference Ratio is close to an Integer

When the circumference ratio of the large accelerator to that of the small accelerator is very close to an integer, there exists the relation between two cavity rf frequencies, see Chap. 2.

$$\frac{f_{rf}^l}{f_{rf}^s} = \frac{h_{rf}^l}{h_{rf}^s \cdot (\kappa + \lambda)} = \frac{h_{rf}^l}{h_{rf}^s \cdot \kappa + h_{rf}^s \cdot \lambda} \quad (6.6)$$

Besides, it is also grouped to this scenario, that the revolution frequency ratio between the small and large accelerators is close to an integer when the beam passes a target (e.g. the FRS, the pbar target) between two ring accelerators. The ratio between two revolution frequencies can be expressed as

$$\frac{f_{rev}^s}{f_{rev}^l} = \kappa + \lambda \quad (6.7)$$

The relation between two cavity rf frequencies is same as eq. 6.6. Two synchronization frequencies are

$$f_{syn}^l = \frac{f_{rf}^l}{h_{rf}^l/Y} = Y f_{rev}^l \quad (6.8)$$

$$f_{syn}^s = \frac{f_{rf}^s}{h_{rf}^s \kappa / Y} = \frac{Y}{\kappa} f_{rev}^s \quad (6.9)$$

Y is the GCD of h_{rf}^l and $h_{rf}^s \cdot \kappa$.

Two synchronization frequencies are beating automatically. The choice of the frequency for the bucket indication signal and the calculation of the synchronization window are similar as that of the integral circumference ratio scenario, see Sec. 6.1. Tab. 6.6 shows the formulas related to the B2B transfer when the large accelerator is the target and Tab. 6.7 shows the formulas when the small accelerator is the target.

6.2.1 h=4 B2B Transfer from SIS18 to ESR

Continuous two of four bunches are injected into two buckets of the injection orbit of the ESR [59]. The beam is accumulated in the ESR. The large accelerator is the

6.2. Circumference Ratio is close to an Integer

Table 6.6: Parameters related to the B2B transfer when the circumference ratio is close to an integer and the large accelerator is the target

| | Large accelerator is target accelerator |
|---------------|---|
| f_{bucket} | f_{rev}^l |
| f_{syn}^X | $f_{syn}^s = \frac{f_{rf}^s}{(h_{rf}^s \cdot \kappa)/Y} = \frac{Y}{\kappa} f_{rev}^s$ and $f_{syn}^l = \frac{f_{rf}^l}{h_{rf}^l/Y} = Y f_{rev}^l$ |
| f_{B2B}^X | $f_{B2B}^s = \frac{h_{rev}^l}{h_{syn}^l} \cdot f_{syn}^s = \frac{1}{\kappa} f_{rev}^s$ and $f_{B2B}^l = f_{rev}^l$ |
| f_{ref} | $round(f_{rev}^l/100 \text{ kHz}) \cdot 100 \text{ kHz}$ |
| Δf | $ f_{syn}^s - f_{syn}^l $ |
| T_w | T_{rev}^l |
| σ_{rf} | $\pm \frac{1}{2} \cdot 2\pi f_{syn}^s - f_{syn}^l \cdot T_w \cdot \frac{h_{rf}^l}{h_{syn}^l}$ |

Table 6.7: Parameters related to the B2B transfer when the circumference ratio is close to an integer and the small accelerator is the target

| | Small accelerator is target accelerator | |
|---------------|---|--|
| Case | (1) $f_{syn}^s \geq f_{rev}^s (\frac{Y}{\kappa} \geq 1)$ | (2) $f_{syn}^s < f_{rev}^s (\frac{Y}{\kappa} < 1)$ |
| f_{bucket} | f_{rev}^s | f_{syn}^s |
| f_{syn}^X | $f_{syn}^s = \frac{f_{rf}^s}{(h_{rf}^s \cdot \kappa)/Y} = \frac{Y}{\kappa} f_{rev}^s$ and $f_{syn}^l = \frac{f_{rf}^l}{h_{rf}^l/Y} = Y f_{rev}^l$ | |
| f_{B2B}^X | $f_{B2B}^l = \frac{h_{rev}^s}{h_{syn}^s} \cdot f_{syn}^l = \kappa f_{rev}^l$ and $f_{B2B}^s = f_{rev}^s$ | $f_{B2B}^l = f_{syn}^l = Y f_{rev}^l$ and $f_{B2B}^s = f_{syn}^s = \frac{Y}{\kappa} f_{rev}^s$ |
| f_{ref} | $round(f_{rev}^s/100 \text{ kHz}) \cdot 100 \text{ kHz}$ | $round(f_{syn}^s/100 \text{ kHz}) \cdot 100 \text{ kHz}$ |
| Δf | $ f_{syn}^s - f_{syn}^l $ | |
| T_w | T_{rev}^s | T_{syn}^s |
| σ_{rf} | $\pm \frac{1}{2} \cdot 2\pi f_{syn}^s - f_{syn}^l \cdot T_w \cdot \frac{h_{rf}^s}{h_{syn}^s}$ | |

SIS18 and the small one is the ESR. $h_{rf}^{SIS18} = 4$ and $h_{rf}^{ESR} = 2$. The circumference ratio between the SIS18 and the ESR injection orbit is

$$\frac{C^l}{C^s} = \kappa + \lambda = 2 - 0.003 \quad (6.10)$$

The GCD of $h_{rf}^{SIS18} = 4$ and $h_{rf}^{ESR} \cdot \kappa = 2 \cdot 2 = 2$ is 4, namely $Y = 4$. Substituting h_{rf}^{SIS18} , h_{rf}^{ESR} , κ and λ into eq. 6.6, we get

$$\frac{f_{rf}^{SIS18}}{f_{rf}^{ESR}} = \frac{h_{rf}^{SIS18}}{h_{rf}^{ESR} \cdot (\kappa + \lambda)} = \frac{4}{2 \cdot (2 - 0.003)} \quad (6.11)$$

The ESR is the small accelerator and the target and there exists $Y/\kappa > 1$, so substituting h_{rf}^X , κ , λ , f_{rf}^X and Y into formulas of the case (1) in Tab. 6.7, the parameters related to the $h=4$ B2B transfer from the SIS18 to the ESR is obtained, see Tab. 6.8. Here we use the 30 MeV/u heavy ion B2B transfer as an example.

6.2. Circumference Ratio is close to an Integer

Table 6.8: Parameters related to the h=4 B2B transfer from the SIS18 to the ESR with the frequency beating method

| | Small accelerator (ESR) is target accelerator |
|---------------|---|
| f_{bucket} | $f_{rev}^{ESR} = 685.651 \text{ kHz}$ |
| f_{syn}^X | $f_{syn}^{SIS18} = 4f_{rev}^{SIS18} = 1.373\,201 \text{ MHz}$ and $f_{syn}^{ESR} = 2f_{rev}^{ESR} = 1.371\,302 \text{ MHz}$ |
| f_{B2B}^X | $f_{B2B}^{SIS18} = 2f_{rev}^{SIS18} = 686.601 \text{ kHz}$ and $f_{B2B}^{ESR} = f_{rev}^{ESR} = 685.651 \text{ kHz}$ |
| f_{ref} | 700 kHz |
| Δf | 1899 Hz |
| T_w | $T_{rev}^{ESR} = 1.456 \mu\text{s}$ |
| σ_{rf} | $\pm 0.5^\circ$ |

Detailed parameters of the $h = 4$ B2B transfer from the SIS18 to the ESR, please see Appendix C.2. The goal time difference between the SIS18 and ESR rf systems equals to $t_{v_ext} + t_{v_inj} + t_{TOF} - \frac{\theta}{2\pi} \frac{1}{f_{rf}^{ESR}}$, where θ depends on the accumulation method. E.g. $\theta = \pi$, when the unstable fixed point is used for the accumulation.

6.2.2 h=1 B2B Transfer from SIS18 to ESR

One bunch is injected into one bucket of the injection orbit of the ESR. The beam is accumulated in the ESR. The large accelerator is the SIS18 and the small one is the ESR. $h_{rf}^{SIS18} = 1$ and $h_{rf}^{ESR} = 1$. The circumference ratio between the SIS18 and the ESR is

$$\frac{C^l}{C^s} = \kappa + \lambda = 2 - 0.003 \quad (6.12)$$

The GCD of $h_{rf}^{SIS18} = 1$ and $h_{rf}^{ESR} \cdot \kappa = 1 \cdot 2 = 2$ is 1, namely $Y = 1$. Substituting h_{rf}^{SIS18} , h_{rf}^{ESR} , κ and λ into eq. 6.6, we get

$$\frac{f_{rf}^{SIS18}}{f_{rf}^{ESR}} = \frac{h_{rf}^l}{h_{rf}^s \cdot (\kappa + \lambda)} = \frac{1}{1 \cdot (2 - 0.003)} \quad (6.13)$$

The ESR is the target and there exists $Y/\kappa < 1$, so substituting h_{rf}^X , κ , λ , f_{rf}^X and Y into formulas of the case (2) in Tab. 6.7, the parameters related to the h=1 B2B transfer from the SIS18 to the ESR is obtained, see Tab. 6.9. Here we use the 400 MeV/u proton B2B transfer as an example.

Detailed parameters of the $h = 1$ B2B transfer from the SIS18 to the ESR, please see Appendix C.2. The goal time difference between the SIS18 and ESR rf systems equals to $t_{v_ext} + t_{v_inj} + t_{TOF} - \frac{\theta}{2\pi} \frac{1}{f_{rf}^{ESR}}$, where θ depends on the accumulation method.

6.2.3 B2B transfer from ESR to CRYRING

Only one bunch is injected into one bucket of the CRYRING [15, 60]. The large accelerator is the ESR and the small one is the CRYRING. $h_{rf}^{ESR} = 1$ and $h_{rf}^{CRYRING} = 1$. The circumference ratio between the ESR and the CRYRING is

$$\frac{C^l}{C^s} = \kappa + \lambda = 2 + 0.003 \quad (6.14)$$

6.2. Circumference Ratio is close to an Integer

Table 6.9: Parameters related to the h=1 B2B transfer from the SIS18 to the ESR with the frequency beating method

| | Small accelerator (ESR) is target accelerator |
|---------------|---|
| f_{bucket} | $f_{syn}^{ESR} = 988.388 \text{ kHz}$ |
| f_{syn}^X | $f_{syn}^{SIS18} = f_{rev}^{SIS18} = 989.756 \text{ kHz}$ and $f_{syn}^{ESR} = f_{rev}^{ESR}/2 = 988.388 \text{ kHz}$ |
| f_{B2B}^X | $f_{B2B}^{SIS18} = f_{rev}^{SIS18} = 989.756 \text{ kHz}$ and $f_{B2B}^{ESR} = f_{rev}^{ESR}/2 = 988.388 \text{ kHz}$ |
| f_{ref} | 1 MHz |
| Δf | 1368 Hz |
| T_w | $T_{syn}^{ESR} = 1.017 \mu\text{s}$ |
| σ_{rf} | $\pm 0.5^\circ$ |

The GCD of $h_{rf}^{ESR} = 1$ and $h_{rf}^{CRYRING} \cdot \kappa = 1 \cdot 2$ is 1, namely $Y = 1$. Substituting h_{rf}^{ESR} , $h_{rf}^{CRYRING}$, κ and λ into eq. 6.6, we get

$$\frac{f_{rf}^{ESR}}{f_{rf}^{CRYRING}} = \frac{h_{rf}^l}{h_{rf}^s \cdot (\kappa + \lambda)} = \frac{1}{1 \cdot (2 + 0.003)} \quad (6.15)$$

The CRYRING is the target and there exists $Y/\kappa < 1$, so substituting h_{rf}^X , κ , λ , f_{rf}^X and Y into formulas of the case (2) in Tab. 6.7, the parameters related to the B2B transfer from the ESR to the CRYRING is obtained, see Tab. 6.10. Here we use the 30 MeV/u proton B2B transfer as an example.

Table 6.10: Parameters related to the B2B transfer from the ESR to the CRYRING with the frequency beating method

| | Small accelerator (CRYRING) is target accelerator |
|---------------|---|
| f_{bucket} | $f_{syn}^{CRYRING} = 686.600 \text{ kHz}$ |
| f_{syn}^X | $f_{syn}^{ESR} = f_{rev}^{ESR} = 685.651 \text{ kHz}$ and $f_{syn}^{CRYRING} = f_{rev}^{CRYRING}/2 = 686.600 \text{ kHz}$ |
| f_{B2B}^X | $f_{B2B}^{ESR} = f_{rev}^{ESR} = 685.651 \text{ kHz}$ and $f_{B2B}^{CRYRING} = f_{rev}^{CRYRING}/2 = 686.600 \text{ kHz}$ |
| f_{ref} | 700 kHz |
| Δf | 949 Hz |
| T_w | $T_{syn}^{CRYRING} = 1.456 \mu\text{s}$ |
| σ_{rf} | $\pm 0.5^\circ$ |

The CRYRING synchronization frequency works for the bucket indication. The goal time difference between the ESR and CRYRING rf systems equals to $t_{v_ext} + t_{v_inj} + t_{TOF}$. Detailed parameters of the B2B transfer from the ESR to the CRYRING, please see Appendix C.4.

6.3 Circumference Ratio is far away from an Integer

When the circumference ratio of the large accelerator to that of the small accelerator is far away from an integer, there exists the relation between two cavity rf frequencies, see Chap. 2.

$$\frac{f_{rf}^l}{f_{rf}^s} = \frac{h_{rf}^l \cdot n}{h_{rf}^s \cdot m + h_{rf}^s \cdot \lambda \cdot n} \quad (6.16)$$

Besides, it is also grouped to this scenario, that the revolution frequency ratio between the small and large accelerators is far away from an integer when the beam passes a target between two ring accelerators. The revolution frequency ratio can be expressed as

$$\frac{f_{rev}^s}{f_{rev}^l} = \frac{m}{n} + \lambda \quad (6.17)$$

The relation between two cavity rf frequencies is same as eq. 6.16. Two synchronization frequencies are

$$f_{syn}^l = \frac{f_{rf}^l}{h_{rf}^l n / Y} = \frac{Y}{n} f_{rev}^l \quad (6.18)$$

$$f_{syn}^s = \frac{f_{rf}^s}{h_{rf}^s m / Y} = \frac{Y}{m} f_{rev}^s \quad (6.19)$$

Y is the GCD of $h_{rf}^l \cdot n$ and $h_{rf}^s \cdot m$.

Two synchronization frequencies are beating automatically. When the large accelerator is the target, the frequency of the bucket indication signal depends on the relation between f_{syn}^l and f_{rev}^l . When $f_{syn}^l \geq f_{rev}^l$, namely $\frac{Y}{n} \geq 1$, $f_{bucket} = f_{rev}^s$. When $f_{syn}^l < f_{rev}^l$, $f_{bucket} = f_{syn}^l$. Tab. 6.11 shows the formulas related to the B2B transfer when the large accelerator is the target.

Table 6.11: Parameters related to the B2B transfer when the circumference ratio is far away from an integer and the large accelerator is the target

| | Large accelerator is target accelerator | |
|---------------|---|---|
| Case | (1) $f_{syn}^l \geq f_{rev}^l$ ($\frac{Y}{n} \geq 1$) | (2) $f_{syn}^l < f_{rev}^l$ ($\frac{Y}{n} < 1$) |
| f_{bucket} | f_{rev}^l | f_{syn}^l |
| f_{syn}^X | $f_{syn}^s = \frac{f_{rf}^s}{(h_{rf}^s \cdot m) / Y} = \frac{Y}{m} f_{rev}^s$ and $f_{syn}^l = \frac{f_{rf}^l}{(h_{rf}^l \cdot n) / Y} = \frac{Y}{n} f_{rev}^l$ | |
| f_{B2B}^X | $f_{B2B}^s = \frac{h_{rev}^l}{h_{syn}^l} \cdot f_{syn}^s = \frac{n}{m} f_{rev}^s$ and $f_{B2B}^l = f_{rev}^l$ | $f_{B2B}^s = f_{syn}^s = \frac{Y}{m} f_{rev}^s$ and $f_{B2B}^l = f_{syn}^l = \frac{Y}{n} f_{rev}^l$ |
| f_{ref} | $round(f_{rev}^l / 100 \text{ kHz}) \cdot 100 \text{ kHz}$ | $round(f_{syn}^l / 100 \text{ kHz}) \cdot 100 \text{ kHz}$ |
| Δf | $ f_{syn}^l - f_{syn}^s $ | |
| T_w | T_{rev}^l | T_{syn}^l |
| σ_{rf} | $\pm \frac{1}{2} \cdot 2\pi f_{syn}^s - f_{syn}^l \cdot T_w \cdot \frac{h_{rf}^l}{h_{syn}^l}$ | |

6.3. Circumference Ratio is far away from an Integer

When the small accelerator is the target, the frequency of the bucket indication signal depends on the relation between f_{syn}^s and f_{rev}^s . When $f_{syn}^s \geq f_{rev}^s$, namely $\frac{Y}{m} \geq 1$, $f_{bucket} = f_{rev}^s$. When $f_{syn}^s < f_{rev}^s$, $f_{bucket} = f_{syn}^s$. Tab. 6.12 shows the formulas related to the B2B transfer when the small accelerator is the target.

Table 6.12: Parameters related to the B2B transfer when the circumference ratio is far away from an integer and the small accelerator is the target

| | Small accelerator is target accelerator | |
|---------------|---|---|
| Case | (1) $f_{syn}^s \geq f_{rev}^s$ ($\frac{Y}{m} \geq 1$) | (2) $f_{syn}^s < f_{rev}^s$ ($\frac{Y}{m} < 1$) |
| f_{bucket} | f_{rev}^s | f_{syn}^s |
| f_{syn}^X | $f_{syn}^s = \frac{f_{rf}^s}{(h_{rf}^s \cdot m)/Y} = \frac{Y}{m} f_{rev}^s$ and $f_{syn}^l = \frac{f_{rf}^l}{(h_{rf}^l \cdot n)/Y} = \frac{Y}{n} f_{rev}^l$ | |
| f_{B2B}^X | $f_{B2B}^s = f_{rev}^s$ and $f_{B2B}^l = \frac{h_{rev}^s}{h_{syn}^s} \cdot f_{syn}^l = \frac{m}{n} f_{rev}^l$ | $f_{B2B}^s = f_{syn}^s = \frac{Y}{m} f_{rev}^s$ and $f_{B2B}^l = f_{syn}^l = \frac{Y}{n} f_{rev}^l$ |
| f_{ref} | $round(f_{rev}^s / 100 \text{ kHz}) \cdot 100 \text{ kHz}$ | $round(f_{syn}^s / 100 \text{ kHz}) \cdot 100 \text{ kHz}$ |
| Δf | $ f_{syn}^s - f_{syn}^l $ | |
| T_w | T_{rev}^s | T_{syn}^s |
| σ_{rf} | $\pm \frac{1}{2} \cdot 2\pi f_{syn}^s - f_{syn}^l \cdot T_w \cdot \frac{h_{rf}^s}{h_{syn}^s}$ | |

6.3.1 H^+ B2B Transfer from SIS100 to CR

After the injection into the SIS100, four bunches are merged into one by the harmonic 5. This bunch is extracted from the SIS100 and goes to the pbar target, then antiprotons are produced and injected into one bucket of the CR [59]. The large accelerator is the SIS100 and the small one is the CR, $h_{rf}^{SIS100} = 5$ and $h_{rf}^{CR} = 1$. Here we take an example, that the proton energy before the pbar target is 28.8 GeV/u and the antiproton energy after the pbar target is 3 GeV/u. Substituting the extraction and injection revolution frequencies into eq. 6.17, we get

$$\frac{f_{rev}^{CR}}{f_{rev}^{SIS100}} = 4.8 - 0.041 = \frac{m}{n} + \lambda = \frac{24}{5} - 0.041 \quad (6.20)$$

The GCD of $h_{rf}^{SIS100} \cdot n = 5 \cdot 5 = 25$ and $h_{rf}^{CR} \cdot m = 1 \cdot 24 = 24$ is 1, namely $Y = 1$. Substituting h_{rf}^{SIS100} , h_{rf}^{CR} , m, n and λ into eq. 6.16, we get

$$\frac{f_{rf}^{SIS100}}{f_{rf}^{CR}} = \frac{h_{rf}^{SIS100} \cdot n}{h_{rf}^{CR} \cdot m + h_{rf}^{CR} \cdot \lambda \cdot n} = \frac{5 \cdot 5}{1 \cdot 24 - 1 \cdot 0.041 \cdot 5} \quad (6.21)$$

The CR is the small accelerator and the target and there exists $\frac{Y}{m} = 1/24 < 1$, so substituting h_{rf}^X , m, n, λ , f_{rf}^X and Y into formulas of the case (2) in Tab. 6.12, the parameters related to the H^+ B2B transfer from the SIS100 to the CR is obtained, see Tab. 6.13.

There exists an inevitable big bunch-to-bucket injection center mismatch with the frequency beating method. Other B2B injection mechanism should be used for

6.3. Circumference Ratio is far away from an Integer

Table 6.13: Parameters related to the H^+ B2B transfer from the SIS100 to the CR with the frequency beating method

| | |
|---------------|--|
| | Small accelerator (CR) is target accelerator |
| f_{bucket} | $f_{syn}^{CR} = 54.866 \text{ kHz}$ |
| f_{syn}^X | $f_{syn}^{SIS100} = f_{rev}^{SIS100}/5 = 55.340 \text{ kHz}$ and $f_{syn}^{CR} = f_{rev}^{CR}/24 = 54.866 \text{ kHz}$ |
| f_{B2B}^X | $f_{B2B}^{SIS100} = f_{rev}^{SIS100}/5 = 55.340 \text{ kHz}$ and $f_{B2B}^{CR} = f_{rev}^{CR}/24 = 54.866 \text{ kHz}$ |
| f_{ref} | 100 kHz |
| Δf | 526 Hz |
| T_w | $T_{syn}^{CR} = 18.226 \mu\text{s}$ |
| σ_{rf} | $\pm 41.5^\circ$ |

the transfer (e.g. the phase jump for the CR), which is beyond the scope of this dissertation. Detailed parameters of the H^+ B2B transfer from the SIS100 to the CR, please see Appendix C.6.

6.3.2 RIB B2B Transfer from SIS100 to CR

After the injection into the SIS100, eight bunches are merged into one by the harmonic 2. This bunch is extracted from the SIS100 and goes to the Super FRS, then the RIB is produced and injected into one bucket of the CR. The large accelerator is the SIS100 and the small one is the CR. $h_{rf}^{SIS100} = 2$ and $h_{rf}^{CR} = 1$. Here we take an example, that the energy of the heavy ion beam before the Super FRS is 1.5 GeV/u and the RIB energy after the Super FRS is 740 MeV/u. Substituting the extraction and injection revolution frequencies into eq. 6.17, we get

$$\frac{f_{rev}^{CR}}{f_{rev}^{SIS100}} = 4.4 - 0.0046 = \frac{m}{n} + \lambda = \frac{22}{5} - 0.0046 \quad (6.22)$$

Substituting h_{rf}^{SIS100} , h_{rf}^{CR} , m, n and λ into eq. 6.16, we get

$$\frac{f_{rf}^{SIS100}}{f_{rf}^{CR}} = \frac{h_{rf}^{SIS100} \cdot n}{h_{rf}^{CR} \cdot m + h_{rf}^{CR} \cdot \lambda \cdot n} = \frac{2 \cdot 5}{1 \cdot 22 - 1 \cdot 0.0046 \cdot 5} \quad (6.23)$$

The GCD of $h_{rf}^{SIS100} \cdot n = 2 \cdot 5 = 10$ and $h_{rf}^{CR} \cdot m = 1 \cdot 22 = 22$ is 2, namely $Y = 2$. the CR is the small accelerator and the target and there exists $\frac{Y}{m} = 1/11 < 1$, so substituting h_{rf}^X , m, n, λ , f_{rf}^X and Y into formulas of the case (2) in Tab. 6.12, the parameters related the RIB B2B transfer from the SIS100 to the CR is obtained, see Tab. 6.14.

Detailed parameters of RIB B2B transfer from the SIS100 to the CR, please see Appendix C.6.

6.3.3 B2B Transfer from CR to HESR

One bunch of the CR is injected into one bucket of the HESR. The beam is accumulated in the HESR [14]. The large accelerator is the HESR and the small one is

6.3. Circumference Ratio is far away from an Integer

Table 6.14: Parameters related to the RIB B2B transfer from the SIS100 to the CR with the frequency beating method

| | Small accelerator (CR) is target accelerator |
|---------------|---|
| f_{bucket} | $f_{syn}^{CR} = 102.218 \text{ kHz}$ |
| f_{syn}^X | $f_{syn}^{SIS100} = 2f_{rev}^{SIS100}/5 = 102.326 \text{ kHz}$ and $f_{syn}^{CR} = f_{rev}^{CR}/11 = 102.218 \text{ kHz}$ |
| f_{B2B}^X | $f_{B2B}^{SIS100} = 2f_{rev}^{SIS100}/5 = 102.326 \text{ kHz}$ and $f_{B2B}^{CR} = f_{rev}^{CR}/11 = 102.218 \text{ kHz}$ |
| f_{ref} | 100 kHz |
| Δf | 108 Hz |
| T_w | $T_{syn}^{CR} = 9.779 \mu\text{s}$ |
| σ_{rf} | $\pm 2.1^\circ$ |

the CR. $h_{rf}^{HESR} = 1$ and $h_{rf}^{CR} = 1$. The circumference ratio between the HESR and the CR is

$$\frac{C^{HESR}}{C^{CR}} = 2.6 - 0.003 = \frac{m}{n} + \lambda = \frac{13}{5} - 0.003 \quad (6.24)$$

The GCD of $h_{rf}^{HESR} \cdot n = 1 \cdot 5 = 5$ and $h_{rf}^{CR} \cdot m = 1 \cdot 13 = 13$ is 1, namely $Y = 1$. Substituting h_{rf}^{HESR} , h_{rf}^{CR} , m, n and λ into eq. 6.16, we get

$$\frac{f_{rf}^{HESR}}{f_{rf}^{CR}} = \frac{h_{rf}^{HESR} \cdot n}{h_{rf}^{CR} \cdot m + h_{rf}^{HESR} \cdot \lambda \cdot n} = \frac{1 \cdot 5}{1 \cdot 13 - 1 \cdot 0.003 \cdot 5} \quad (6.25)$$

The HESR is the large accelerator and the target and there exists $\frac{Y}{n} = 1/5 < 1$, so substituting h_{rf}^X , m, n, λ , f_{rf}^X and Y into formulas of the case (2) in Tab. 6.11, the parameters related to the B2B transfer from the CR to the HESR is obtained. Tab. 6.15 shows parameters of two operations, the antiproton and RIB B2B transfer.

The goal time difference between the two rf systems depends on the accumulation method. Detailed parameter about the B2B transfer from the CR to the HESR, please see Appendix C.5.

6.3.4 RIB B2B Transfer from SIS18 to ESR via the FRS

Only one bunch is extracted from the SIS18 and goes to the FRS, then a RIB is produced and injected into one bucket of the ESR. The large accelerator is the SIS18 and the small one is the ESR. $h_{rf}^{SIS18} = 1$ and $h_{rf}^{ESR} = 1$. Here we take an applied case as an example, that the energy of the heavy ion beam before the FRS is 550 MeV/u and the RIB energy after the FRS is 400 MeV/u. Substituting the extraction and injection revolution frequencies into eq. 6.17, we get

$$\frac{f_{rev}^{ESR}}{f_{rev}^{SIS18}} = 1.8 + 0.036 = \frac{m}{n} + \lambda = \frac{9}{5} + 0.036 \quad (6.26)$$

Substituting h_{rf}^{SIS18} , h_{rf}^{ESR} , m, n and λ into eq. 6.16, we get

$$\frac{f_{rf}^{SIS18}}{f_{rf}^{ESR}} = \frac{h_{rf}^{SIS18} \cdot n}{h_{rf}^{ESR} \cdot m + h_{rf}^{ESR} \cdot \lambda \cdot n} = \frac{1 \cdot 5}{1 \cdot 9 + 1 \cdot 0.036 \cdot 5} \quad (6.27)$$

6.3. Circumference Ratio is far away from an Integer

Table 6.15: Parameters related to the B2B transfer from the CR to the HESR with the frequency beating method

| | |
|---------------|--|
| | Larger accelerator (HESR) is target accelerator |
| | 3 GeV/u antiproton |
| f_{bucket} | $f_{syn}^{HESR} = 101.426 \text{ kHz}$ |
| f_{syn}^X | $f_{syn}^{CR} = f_{rev}^{CR}/13 = 101.290 \text{ kHz}$ and $f_{syn}^{HESR} = f_{rev}^{HESR}/5 = 101.426 \text{ kHz}$ |
| f_{B2B}^X | $f_{B2B}^{CR} = f_{rev}^{CR}/13 = 101.290 \text{ kHz}$ and $f_{B2B}^{HESR} = f_{rev}^{HESR}/5 = 101.426 \text{ kHz}$ |
| f_{ref} | 100 kHz |
| Δf | 136 Hz |
| T_w | $T_{syn}^{HESR} = 9.860 \mu\text{s}$ |
| σ_{rf} | $\pm 1.2^\circ$ |
| | 740 MeV/u RIB |
| f_{bucket} | $f_{syn}^{HESR} = 86.608 \text{ kHz}$ |
| f_{syn}^X | $f_{syn}^{CR} = f_{rev}^{CR}/13 = 86.493 \text{ kHz}$ and $f_{syn}^{HESR} = f_{rev}^{HESR}/5 = 86.608 \text{ kHz}$ |
| f_{B2B}^X | $f_{B2B}^{CR} = f_{rev}^{CR}/13 = 86.493 \text{ kHz}$ and $f_{B2B}^{HESR} = f_{rev}^{HESR}/5 = 86.608 \text{ kHz}$ |
| f_{ref} | 100 kHz |
| Δf | 113 Hz |
| T_w | $T_{syn}^{HESR} = 11.545 \mu\text{s}$ |
| σ_{rf} | $\pm 1.2^\circ$ |

The GCD of $h_{rf}^{SIS18} \cdot n = 1 \cdot 5 = 5$ and $h_{rf}^{ESR} \cdot m = 1 \cdot 9 = 9$ is 1, namely $Y = 1$. The ESR is the small accelerator and the target and there exists $\frac{Y}{m} = 1/9 < 1$, so substituting h_{rf}^X , m , n , λ , f_{rf}^X and Y into formulas into formulas of the case (2) in Tab. 6.12, the parameters related to the B2B transfer from the SIS18 to the ESR via the FRS is obtained, see Tab. 6.16.

Table 6.16: Parameters related to an applied case of the B2B transfer from the SIS18 to the ESR via the FRS with the frequency beating method

| | |
|---------------|---|
| | Small accelerator (ESR) is target accelerator |
| f_{bucket} | $f_{syn}^{ESR} = 219.642 \text{ kHz}$ |
| f_{syn}^X | $f_{syn}^{SIS18} = f_{rev}^{SIS18}/5 = 215.393 \text{ kHz}$ and $f_{syn}^{ESR} = f_{rev}^{ESR}/9 = 219.642 \text{ kHz}$ |
| f_{B2B}^X | $f_{B2B}^{SIS18} = f_{rev}^{SIS18}/5 = 215.393 \text{ kHz}$ and $f_{B2B}^{ESR} = f_{rev}^{ESR}/9 = 219.642 \text{ kHz}$ |
| f_{ref} | 200 kHz |
| Δf | 4249 Hz |
| T_w | $T_{syn}^{ESR} = 4.553 \mu\text{s}$ |
| σ_{rf} | $\pm 31.2^\circ$ |

There exists an inevitable big bunch-to-bucket injection center mismatch with the frequency beating method. Other B2B injection mechanism should be used for the transfer (e.g. the phase jump for the ESR or the barrier bucket injection), which is beyond the scope of this dissertation. More parameters about the B2B transfer from the SIS18 to the ESR via the FRS, please see Appendix C.3.

6.4 Summary

For all primary beam transfers of FAIR use cases, the B2B transfer system achieves the B2B transfer with the bunch-to-bucket injection center mismatch less than $\pm 1^\circ$. It doesn't work properly for the FAIR use cases that secondary beams are generated by the pbar target, the FRS or the Super FRS, because the energy ratio between the primary and secondary beams is arbitrary. For the RIB B2B transfer from the SIS100 to the CR via the Super FRS with the 1.5 Gev/u primary beam energy and the 740 Mev/u secondary beam energy, the bunch-to-bucket injection center mismatch is only $\pm 2.1^\circ$ by coincidence. For the antiproton B2B transfer from the SIS100 to the CR via the pbar target and the RIB B2B transfer form the SIS18 to the ESR via the FRS, the mismatch is as large as $\pm 40^\circ$. For these two cases, the FAIR B2B transfer system must work together with specific beam accumulation methods, e.g. the barrier bucket or the unstable point accumulation.

All the formulas are summarized. Tab. 6.17 summarizes the formulas related to the B2B transfer when the large accelerator is the target. Tab. 6.18 summarizes the formulas when the small accelerator is the target and the revolution period is longer than the period of the synchronization frequency of the target accelerator. Tab. 6.19 summarizes the formulas when the small accelerator is the target and the revolution period is shorter than the period of the synchronization frequency of the target accelerator.

6.4. Summary

Table 6.17: Summary of the formulas related to the B2B transfer when the large accelerator is the target

| Circumference ratio | Cavity rf frequency ratio f_{rf}^l / f_{rf}^s | Bucket indication signal f_{bucket} | Synchronization frequencies f_{syn}^X | phase measurement signal f_{B2B}^X |
|--|--|---|---|--|
| $C^l/C^s = \kappa$ Integer | $\frac{h_{rf}^l}{h_{rf}^s \cdot \kappa}$ | f_{rev}^l | $f_{syn}^s = \frac{Y}{\kappa} f_{rev}^s$ and $f_{syn}^l = Y f_{rev}^l$ | $f_{B2B}^s = \frac{1}{\kappa} (f_{rev}^s + \frac{\kappa}{Y} \Delta f_{syn})$ and $f_{B2B}^l = f_{rev}^l$ |
| $C^l/C^s = \kappa + \lambda$ or $f_{rev}^s / f_{rev}^l = \kappa + \lambda$ close to integer | $\frac{h_{rf}^l}{h_{rf}^s (\kappa + \lambda)}$ | f_{rev}^l | $\Delta f = \Delta f_{syn}$ $f_{syn}^l = Y f_{rev}^l$ and $f_{syn}^s = \frac{Y}{\kappa} f_{rev}^s$ | $f_{B2B}^s = \frac{1}{\kappa} f_{rev}^s$ and $f_{B2B}^l = f_{rev}^l$ |
| $C^l/C^s = m/n + \lambda$ $f_{rev}^s / f_{rev}^l = m/n + \lambda$ far away from integer | $\frac{h_{rf}^l}{h_{rf}^s n}$ | f_{rev}^l | $\Delta f = f_{syn}^l - f_{syn}^s $ $f_{syn}^l = \frac{Y}{n} f_{rev}^l$ and $f_{syn}^s = \frac{Y}{m} f_{rev}^s$ | $f_{B2B}^s = \frac{n}{m} f_{rev}^s$ and $f_{B2B}^l = f_{rev}^l$ |
| $C^l/C^s = m/n + \lambda$ $f_{rev}^s / f_{rev}^l = m/n + \lambda$ far away from integer | $\frac{h_{rf}^l}{h_{rf}^s (m/n + \lambda)}$ | f_{rev}^l if $Y/n < 1, f_{syn}^l$ if $Y/n > 1, f_{syn}^l$ | $\Delta f = f_{syn}^l - f_{syn}^s $ $f_{B2B}^s = \frac{Y}{m} f_{rev}^s$ and $f_{B2B}^l = \frac{Y}{n} f_{rev}^l$ | $f_{B2B}^s = \frac{n}{m} f_{rev}^s$ and $f_{B2B}^l = f_{rev}^l$ |

Note: $f_{ref} = round(f_{B2B}^{trg} / 100 \text{ kHz}) \cdot 100 \text{ kHz}$, $T_w = 1/f_{bucket}$ and $\sigma_{rf} = \pm \frac{1}{2} \cdot 2\pi |f_{syn}^s - f_{syn}^l| \cdot T_w \cdot \frac{h_{rf}^l}{h_{syn}^l}$

6.4. Summary

Table 6.18: Summary of the formulas related to the B2B transfer when the small accelerator is the target and the revolution period is longer than the period of the synchronization frequency of the target accelerator

| Circumference ratio | Cavity rf frequency ratio f_{rf}^l/f_{rf}^s | Bucket indication signal f_{bucket} | Synchronization frequencies f_{syn}^X | phase measurement signal f_{B2B}^X |
|--|--|--|--|---|
| $C^l/C^s = \kappa$ Integer | $\frac{h_{rf}^l}{h_{rf}^s \cdot \kappa}$ | $Y/\kappa \geq 1, f_{rev}^s$ | $f_{syn}^l = Y f_{rev}^l$ $f_{syn}^s = \frac{Y}{\kappa} f_{rev}^s$ | $f_{B2B}^l = \kappa (f_{rev}^l + \frac{1}{Y} \Delta f_{syn})$ and $f_{B2B}^s = f_{rev}^s$ |
| $C^l/C^s = \kappa + \lambda$ or $f_{rev}^s/f_{rev}^l = \kappa + \lambda$ close to integer | $\frac{h_{rf}^l}{h_{rf}^s \cdot (\kappa+\lambda)}$ | $Y/\kappa \geq 1, f_{rev}^s$ | $\Delta f = \Delta f_{syn}$ $f_{syn}^l = Y f_{rev}^l$ $f_{syn}^s = \frac{Y}{\kappa} f_{rev}^s$ | $f_{B2B}^l = \kappa f_{rev}^l$ and $f_{B2B}^s = f_{rev}^s$ |
| $C^l/C^s = m/n + \lambda$ or $f_{rev}^s/f_{rev}^l = m/n + \lambda$ far away from integer | $\frac{h_{rf}^l}{h_{rf}^s \cdot (m/n+\lambda)}$ | $Y/m \geq 1, f_{rev}^s$ | $\Delta f = f_{syn}^l - f_{syn}^s $ $f_{syn}^l = \frac{Y}{n} f_{rev}^l$ $f_{syn}^s = \frac{Y}{m} f_{rev}^s$ | $f_{B2B}^l = \frac{m}{n} f_{rev}^l$ and $f_{B2B}^s = f_{rev}^s$ |
| <i>Note:</i> $f_{ref} = round(f_{B2B}^{trg}/100 \text{ kHz}) \cdot 100 \text{ kHz}$, $T_w = 1/f_{bucket}$ and $\sigma_{rf} = \pm \frac{1}{2} \cdot 2\pi f_{syn}^s - f_{syn}^l \cdot T_w \cdot \frac{h_{rf}^s}{h_{syn}^s}$ | | | | |

Table 6.19: Summary of the formulas related to the B2B transfer when the small accelerator is the target and the revolution period is shorter than the period of the synchronization frequency of the target accelerator

| Circumference ratio | Cavity rf frequency ratio f_{rf}^l/f_{rf}^s | Bucket indication signal f_{bucket} | Synchronization frequencies f_{syn}^X | phase measurement signal f_{B2B}^X |
|---|--|--|--|--|
| $C^l/C^s = \kappa$ Integer | $\frac{h_{rf}^l}{h_{rf}^s \cdot \kappa}$ | $Y/\kappa < 1, f_{syn}^s$ | $f_{syn}^l = Y f_{rev}^l$ and $f_{syn}^s = \frac{Y}{\kappa} f_{rev}^s$ | $f_{B2B}^l = Y(f_{rev}^l + \frac{1}{Y} \Delta f_{syn})$ and $f_{B2B}^s = \frac{Y}{\kappa} f_{rev}^s$ |
| $C^l/C^s = \kappa + \lambda$ or $f_{rev}^s/f_{rev}^l = \kappa + \lambda$ close to integer | $\frac{h_{rf}^l}{h_{rf}^{s \cdot (\kappa+\lambda)}}$ | $Y/\kappa < 1, f_{syn}^s$ | $\Delta f = \Delta f_{syn}$ | $f_{syn}^l = Y f_{rev}^l$ and $f_{syn}^s = \frac{Y}{\kappa} f_{rev}^s$ |
| $C^l/C^s = m/n + \lambda$ or $f_{rev}^s/f_{rev}^l = m/n + \lambda$ far away from integer | $\frac{h_{rf}^l}{h_{rf}^{s \cdot (m/n+\lambda)}}$ $Y = \text{GCD}(h_{rf}^l, h_{rf}^s \kappa)$ | $Y/m < 1, f_{syn}^s$ $(h_{rf}^l n, h_{rf}^s m)$ | $\Delta f = f_{syn}^l - f_{syn}^s $ | $f_{syn}^l = \frac{Y}{n} f_{rev}^l$ and $f_{syn}^s = \frac{Y}{m} f_{rev}^s$ |
| <i>Note:</i> $f_{ref} = \text{round}(f_{B2B}^{trg}/100 \text{ kHz}) \cdot 100 \text{ kHz}$, $T_w = 1/f_{bucket}$ and $\sigma_{rf} = \pm \frac{1}{2} \cdot 2\pi f_{syn}^s - f_{syn}^l \cdot T_w \cdot \frac{h_{rf}^s}{h_{syn}^s}$ | | | | $f_{B2B}^l = \frac{Y}{n} f_{rev}^l$ and $f_{B2B}^s = \frac{Y}{m} f_{rev}^s$ |

Conclusion and Outlook

The FAIR project is aiming at providing high-energy beams of ions of all elements from hydrogen to uranium, antiprotons and rare isotopes with high intensities. The existing accelerator facility of GSI and the future FAIR facility employ a variety of circular accelerators like heavy ion synchrotrons (the SIS18 and the SIS100) and storage rings (the ESR, the CRYRING, the CR and the HESR) for the preparation of secondary beams and experiments. Bunches are required to be transferred into rf buckets among GSI and FAIR ring accelerators for different purposes. Without the proper transfer, the beam will be subject to various beam quality (emittance) deterioration and even to beam losses. Hence, the proper bunch-to-bucket transfer between two rings is of great importance for FAIR and is the topic, which has been investigated in this thesis. Although an implementation of the B2B transfer from the SIS18 to the ESR exists, this solution is not applicable for the new FAIR accelerator complex, because? it is realized based on the GSI control system, an event based system.? The FAIR control system is based on the sub-nanosecond synchronization White Rabbit network. Besides, the existing GSI control system? doesn't support the B2B transfer with the phase shift method and with the complex bucket pattern. It is not capable to transfer beams via targets. Hence, a new FAIR B2B transfer system is required, which relies on the FAIR technical basis, the FAIR timing and ?control system and the low level rf system.

The conceptual realization of the FAIR B2B transfer system was introduced in this thesis for the first time. It achieves the most FAIR B2B transfers with a tolerable bunch-to-bucket injection center mismatch (e.g. $\pm 1^\circ$) and within an upper bound time (e.g. 10 ms). It supports both the phase shift and frequency beating methods. It is flexible to support the beam transfer between two rings with different ratios in their circumference and several B2B transfers running at the same time, e.g. the B2B transfer from the SIS18 to the SIS100 and at the same time the B2B transfer from the ESR to the CRYRING. It is capable to transfer beam of different ion species from one machine cycle to another and? to transfer beams between two rings via the FRS, the pbar target and the Super FRS. It allows various complex bucket filling pattern. In addition, it coordinates with the MPS system, which protects the SIS100 and subsequent accelerators or experiments from beam induced damage.

A list of criteria for the preservation of beam qualities during the rf frequency modulation of the phase shift method was analyzed?. As an example? the beam reaction on three different? rf frequency modulation examples were analyzed for SIS18 beams. According to the beam dynamic analysis, there is a maximum value for the rf frequency modulation, which comes from the constraint of the momentum shift. The first derivative of the rf frequency modulation must be continuous and small enough to guarantee the size of the running bucket. The second derivative

Conclusion and Outlook

must be small enough to guarantee the change of the synchronous phase slow enough for the beam to follow, which is reflected by the parameter of the adiabaticity. In order to guarantee the bucket area factor larger than 80% and the adiabaticity smaller than 10^{-4} , for a SIS18 200 Mev/u U^{28+} beam, $|\Delta f_{rf}|$ must be smaller than 8.137 kHz and $|\frac{d\Delta f_{rf}}{dt}|$ must be continuous and smaller than 95 Hz/ms and $|\frac{d^2\Delta f_{rf}}{dt^2}|$ must be smaller than 70 Hz/ms². For the SIS18 4 Gev H^+ beam, $|\Delta f_{rf}|$ must be smaller than 283 Hz and $|\frac{d\Delta f_{rf}}{dt}|$ must be continuous and smaller than 1.9 Hz/ms and $|\frac{d^2\Delta f_{rf}}{dt^2}|$ must be smaller than 0.2 Hz/ms². In regard with these requirements, the sinusoidal and parabolic rf frequency modulation profiles with a certain duration were checked for the SIS18 U^{28+} beam. Both two modulation profiles meet the requirements and keep the beam stable. However, compared with the parabolic modulation, the sinusoidal modulation has the smaller adiabaticity. Hence, the sinusoidal modulation is preferable for the phase shift method. The sinusoidal rf frequency modulation for the SIS18 200 Mev/u U^{28+} needs 7 ms and the sinusoidal rf frequency modulation for the SIS18 4 Gev/u H^+ needs approximately 50 ms for the phase shift of π .

In addition to the analysis from the viewpoint of beam dynamics, two test setups were built. The first test setup was used to characterize the WR network for the B2B transfer. According to the test result, the tolerable number of WR switch layers for the B2B transfer depends not only on the upper bound transfer latency (e.g. 400 ms), but also the tolerable frame error rate of the B2B transfer system. If no forward error correction mechanism is used for the B2B transfer, the number of WR switch layers is mainly decided by the tolerable frame error rate. If for instance one lost frame is tolerable every two month, the maximum 38 WR switches can be used between the B2B related SCUs and DM and the maximum 8 WR switches can be used between the B2B related SCUs. If specific forward error correction mechanisms are used, the number of WR switch layers depends mainly on the tolerable transfer latency. In this case, the tolerable number of WR switches is 67 between the B2B related SCUs and DM and the tolerable number of WR switches is 13 between the B2B related SCUs. In the second test setup, the firmware of the FAIR B2B transfer system was evaluated, which was running on the soft CPU, LatticeMico32, of the SCUs. The running time of tasks of the firmware was measured. It has proven that the firmware running on the LatticeMico32 of the SCUs meets the requirement of the timing constraints, when the related System-on-Chip bus is not occupied by any other applications at the same time as the firmware is running.

Furthermore, the propagation of the measurement uncertainties (e.g. the 0.1° phase measurement uncertainty, the 100 ps BuTiS C2 clock uncertainty and the 1 ns timestamp measurement uncertainty) to the time of the phase alignment was checked for all FAIR use cases in this thesis. The bunch-to-bucket injection center mismatch is deteriorated by the time uncertainty of the phase alignment in various degrees. For some use cases the bunch-to-bucket injection center mismatch is seriously deteriorated. e.g. the mismatch is deteriorated by 37% for the U^{28+} B2B transfer from the SIS18 to the SIS100. However, the deteriorated mismatch still meet the requirement smaller than $\pm 1^\circ$. Hence, the measurement uncertainties are acceptable for the FAIR B2B transfer system. In addition, the requirement of the accuracy of the start of the synchronization window for all FAIR use cases was also checked in this thesis. The? most stringent requirement of the accuracy comes from the h=1 B2B transfer from the SIS18 to the ESR, which is approximately 500 ns.

Besides, the boundary conditions of the different? trigger scenarios of the SIS18 extraction and SIS100 injection kicker magnets were investigated. The nine SIS18 extraction kicker magnets are distributed into two tanks. The kicker magnets in each tank can be triggered simultaneously when the bunch gap is at least 25% of the cavity rf period. The four kicker magnets in the 2nd tank can be triggered a fixed delay to? the trigger of the five kicker magnets in the 1st tank for all ion beams, when the bunch gap is at least 25% of the cavity rf period. The six SIS100 injection kicker magnets are evenly distributed in one tank. They can be fired instantaneously for all ion beams, when the bunch gap is at least 35% of the cavity rf period.

Finally, the application of the FAIR B2B transfer system with the frequency beating method for all FAIR use cases was demonstrated. It has been shown that for all primary beam transfers of FAIR use cases, the B2B transfer with the bunch-to-bucket injection center mismatch less than $\pm 1^\circ$ and within the required B2B transfer time 10 ms can be achieved, because the circumference ratio between two rings is an integer or close to an integer. However, the system is also required for the FAIR use cases that the secondary beams are generated by the pbar target, the FRS or the Super FRS with an arbitrary energy ratio between the primary and secondary beams. For the rare isotope beam transfer from the SIS100 to the CR via the Super FRS with the 1.5 GeV/u primary beam energy and the 740 MeV/u secondary beam energy, the bunch-to-bucket injection center mismatch is only $\pm 2.1^\circ$ by coincidence. For the antiproton B2B transfer from the SIS100 to the CR via the pbar target and the rare isotope beam transfer from the SIS18 to the ESR via the FRS, the bunch-to-bucket injection center mismatch is as large as $\pm 40^\circ$, which is far beyond the upper bound injection center mismatch.

The dissertation at hand comprises the important investigations for the FAIR B2B transfer system from the beam dynamics, timing and kicker trigger perspectives. However, there are still some investigations which are required for the final system operation:

- The synchronization between the magnetic horn after the pbar target and the antiproton beam to the μ s order of magnitude.
- The synchronization between the bunch compressor of the SIS100 and the beam extraction.
- For several FAIR use cases of the secondary beam, the bunch-to-bucket injection center mismatch is larger than $\pm 40^\circ$. For these FAIR use cases, it is necessary to check whether the FAIR B2B transfer system can work together with specific beam accumulation methods, e.g. the barrier bucket or the unstable fixed point accumulation.

The FAIR B2B transfer system presented in the dissertation is applicable for all FAIR use cases. However, there is still potential for improvement. For the phase shift method, the rf frequency modulation must be slow enough (e.g. the 7 ms/50 ms sinusoidal modulation for the SIS18 U^{28+}/H^+ beam). In order to transfer bunches into buckets as soon as possible, the phase shift can be started during the acceleration ramp. At a certain time point during the acceleration, the phases difference between the two rf systems of the source and target rings is obtained with the help of the synchronization reference signal. There is a look-up table, which gives the phase difference at the rf flattop according to the phase difference obtained at the certain

Conclusion and Outlook

time point. Then, an rf frequency modulation is superposed on the initial frequency pattern of one (or both) rings. With this new frequency pattern, the phase difference will be the required phase difference when the cavity rf frequency of the source ring reaches the rf flattop.

Zusammenfassung

FAIR hat zum Ziel, hochenergetische Ionenstrahlung für die Elemente Wasserstoff bis Uran, Antiprotonen und exotische Nuklide mit höchsten Intensitäten zur erzeugen. Die existierende Beschleunigeranlage der GSI, wie auch die zukünftige FAIR-Anlage nutzen unterschiedliche Ringbeschleuniger wie beispielsweise Schwerionensynchrotrons (das SIS18 und das SIS100) und auch Speicherringe (den ESR, den CRYRING, den CR und den HESR) zur Präparation der Sekundärstrahlen und auch für die Experimente. Eine stabiler Transfer von *Bunchen* in *Buckets* zwischen allen GSI- und FAIR-Ringbeschleuniger, ist aus verschiedenen Gründen erforderlich. Bei einem nicht ordnungsgemäßen Strahltransfer besteht die Gefahr, dass es zu einer Degeneration der Strahlqualität (z.B. einer Emittanzerhöhung) bis hin zum Strahlverlust kommt. Ein stabiler *Bunch-to-Bucket-Transfer* zwischen zwei Ringen ist daher sehr wichtig für FAIR und ist das Thema, welches im Rahmen dieser Doktorarbeit untersucht wurde. Obwohl bereits zwischen dem SIS18 und dem ESR ein B2B-Transfer realisiert wurde, so ist diese Lösung aufgrund verschiedener Einschränkungen nicht nutzbar für FAIR. Es legt das alte GSI-Kontrollsysteem, ein eventbasiertes System zu Grunde, welches in Zukunft vollständig durch das neue FAIR-Kontrollsysteem ersetzt werden wird. Das FAIR-Kontrollsysteem basiert auf dem White-Rabbit-Netzwerk, dass eine Synchronisation im Sub-Nanosekundenbereich erlaubt. Des Weiteren unterstützt das alte System nicht die *phase shift method* und ermöglicht auch keine komplexen Bucket-Füllmuster. Zu einem Strahltransfer über Targets ist es ebenfalls nicht in der Lage. Die Entwicklung eines *FAIR B2B transfer systems*, basierend auf der für FAIR geplanten technischen Infrastruktur, dazu zählen das FAIR-Kontrollsysteem und das FAIR-LLRF-System ist daher unbedingt erforderlich.

Diese Doktorarbeit stellte erstmals die konzeptionelle Realisierung des *FAIR B2B transfer system* vor. In den meisten Fällen wird der B2B-Transfer mit einem B2B-Injektions-Mittenversatz von unter $\pm 1^\circ$ innerhalb der oberen Zeitgrenze von 10ms erreicht. Das *FAIR B2B transfer system* unterstützt die *phase shift method*, wie auch die *frequency beating method* und ist anpassungsfähig genug, um einen Transfer zwischen zwei Ringen mit beliebigem Verhältnis ihrer Umfänge zu ermöglichen. Es ist möglich, verschiedene B2B-Transfers zur gleichen Zeit auszuführen. Beispielsweise kann der B2B-Transfer vom SIS18 zum SIS100 zur gleichen Zeit stattfinden, wie der B2B-Transfer vom ESR zum CRYRING. Auch können verschiedene Ionenarten von einem Maschinenzyklus zum Anderen transferiert werden. Das *FAIR B2B transfer system* ist in der Lage, einen Transfer zwischen zwei Ringen auch über das Antiprotonen-Target, den Fragmentseparator oder den Superfragmentseparator durchzuführen. Es können verschiedene komplexe Bucket-Füllmuster berücksichtigt werden. Außerdem hat das *FAIR B2B transfer system* eine Schnittstelle zum FAIR-Maschinenschutzsystem, welches das SIS100 und die nachgeschalteten Beschleuniger und Experimente vor Schaden durch Primärstrahlen bei Fehlerfunktionen bewahrt.

Es wurde eine Liste von Kriterien vorgestellt, die für die HF-Frequenzmodulation bei der *phase shift method* die Erhaltung der Strahlqualität ermöglicht. Dazu wurde für den SIS18 Strahl das Strahlverhalten auf drei verschiedene HF-Frequenzmodulationsmuster hin analysiert. Entsprechend der strahldynamischen Analysen, wird der Maximalwert für die HF-Frequenzmodulation durch die Randbedingungen, die durch den *momentum shift* gegeben sind eingeschränkt. Die erste Ableitung der HF-Frequenzmodulation muss stetig und klein genug sein, um eine ausreichende Größe der umlaufenden *buckets* zu garantieren. Ein kleiner Wert der zweiten Ableitung garantiert, dass sich die synchrone Phase langsam genug ändert, damit der Strahl folgen kann. Das spiegelt sich auch im adiabatischen Parameter wieder. Um eine *bucket*-Fläche von größer 80% und einen adiabatischen Parameter von kleiner 10^{-4} für den SIS18 200 MeV/u U^{28+} Strahl garantieren zu können, muss $|\Delta f_{rf}|$ kleiner als 8.137 kHz sein und $|\frac{d\Delta f_{rf}}{dt}|$ muss stetig und kleiner als 95 Hz/ms sein. $|\frac{d^2\Delta f_{rf}}{dt^2}|$ muss kleiner als 70 Hz/ms² sein. Für den SIS18 4 GeV H^+ Strahl, muss $|\Delta f_{rf}|$ kleiner als 283 Hz sein und $|\frac{d\Delta f_{rf}}{dt}|$ muss stetig und kleiner als 1.9 Hz/ms sein. $|\frac{d^2\Delta f_{rf}}{dt^2}|$ muss kleiner als 0.2 Hz/ms² sein. Nach diesen Anforderungen wurden ein sinusförmiges und parabelförmiges HF-Frequenzmodulationsprofil mit einer bestimmten Zeitdauer für den SIS18 U^{28+} Strahl überprüft. Beide Modulationsprofile erfüllen die Anforderungen und halten den Strahl stabil. Dennoch ist der adiabatische Parameter bei der sinusförmigen Modulation kleiner als bei der parabelförmigen Modulation. Folglich sollte die sinusförmige Modulation bei der *phase shift method* präferiert werden. Die sinusförmige HF-Frequenzmodulation im SIS18 für 200 MeV/u bei U^{28+} benötigt 7 ms und die sinusförmige HF-Frequenzmodulation im SIS18 für 4 GeV bei H^+ benötigt circa 50 ms für eine Phasenverschiebung jeweils um π .

In Ergänzung zu den strahldynamischen Analysen, wurden zwei Messaufbauten errichtet. Der erste Messaufbau diente dazu, das WR-Netzwerk für den B2B-Transfer zu charakterisieren. Nach diesem Messergebnis, ist die zulässige Anzahl von WR-Switch-Layern für den B2B-Transfer nicht nur von der Obergrenze der Latenzzeit abhängig (z.B. 400 ms), sondern auch von der tolerierbaren Frame-Error-Rate (FER) des B2B-Transfer-Systems. Wenn keine Vorwärtsfehlerkorrektur für das B2B-Netzwerk verwendet wird, ist die Anzahl der zulässigen WR-Switches hauptsächlich durch die FER bestimmt. Unter der Annahme, dass der Verlust von einem Frame, innerhalb von zwei Monaten noch akzeptable ist, sind maximal 38 WR-Switches zulässig zwischen Data Master (DM) und den zugehörigen SCUs und maximal 8 WR-Switches direkt zwischen den SCUs, die dem B2B-Transfer-System zugeordneten sind. Wird eine Vorwärtsfehlerkorrektur für das B2B-Netzwerk verwendet, so ist die Anzahl der zulässigen WR-Switches durch die noch tolerierbare Latenzzeit bestimmt. In diesem Fall, sind dann 67 WR-Switches zwischen dem für das B2B-Transfer-System zugehörigen SCUs und DM erlaubt und 13 WR-Switches direkt zwischen den SCUs, die dem B2B-Transfer-System zugeordneten sind. Der zweite Messaufbau diente dazu, die Firmware die auf einer *Soft-CPU (LatticeMicro32)* in der SCU ausgeführt wird, für das *B2B transfer system* zu evaluieren. Gemessen wurden die Laufzeiten für die einzelnen Tasks in der Firmware. Es wurde nachgewiesen, dass die Firmware auf dem LatticeMicro32 in der SCU die Anforderungen an die Timing-Bedingungen erfüllt, wenn der zugehörige *System-on-Chip bus* nicht zur gleichen Zeit mit anderen Anwendung, die parallel zur B2B-Firmware ausgeführt werden belegt ist.

Des Weiteren wurden die Auswirkung der Fehlerfortpflanzung durch die Messunsicherheit (z.B. die Phasenmessgenauigkeit von $\pm 0.1^\circ$, der BuTiS C2-Clock-Sta-

bilität von die 100 ps und die Messgenauigkeit für den Zeitstempel von 1 ns) für die Zeit bis zum *phase alignment* in allen FAIR-Anwendungsfällen im Rahmen dieser Doktorarbeit überprüft. Der B2B Mittenversatz bei Injektion verschlechtert sich durch die Unsicherheiten bei der Bestimmung des Zeitpunkts des *phase alignment* auf unterschiedliche Art und Weise. In einigen Anwendungsfällen verschlechtert sich der B2B Mittenversatz bei Injektion sehr deutlich. Beispielsweise verschlechtert sich der Mittenversatz um 37% für den Transfer von U^{28+} vom SIS18 in den SIS100, was in allen FAIR-Anwendungsfällen den Worst-Case darstellt. Trotz dieser Verschlechterung wird die Anforderung von kleiner $\pm 1^\circ$ eingehalten. Daher ist die Messunsicherheit noch akzeptabel für das *FAIR B2B transfer system*. Zusätzlich wurden im Rahmen dieser Doktorarbeit auch die Genauigkeitsanforderungen an den Start des Synchronisationsfensters für alle FAIR-Anwendungsfälle überprüft. Der h=1 B2B-Transfer vom SIS18 zum ESR stellt mit ca. 500 ns die strengsten Genauigkeitsanforderungen an den Beginn des Synchronisationsfesters.

Außerdem wurden verschiedene Trigger-Szenarien für die SIS18 Extraktions- und die SIS100 Injektions-Kicker-Magnete untersucht. Die neun Extraktions-Kicker-Magnete des SIS18, sind auf zwei Tanks aufgeteilt. Die Kicker-Magnete jedes Tanks können gleichzeitig gezündet werden, wenn die Bunchlücke mindestens 25% der Kavitäten-HF-Periode beträgt. Die vier Kicker-Magnete in dem zweiten Tank, können über eine feste Verzögerungszeit nach dem Auslösen der fünf Kicker-Magnete im ersten Tank für alle Ionensorten ausgelöst werden, wenn die Bunchlücke mindestens 25% der Kavitäten-HF-Periode beträgt. Die sechs SIS100 Injektions-Kicker-Magnete sind gleichmäßig in einem Tank verteilt. Sie können für alle Ionensorten ausgelöst werden, wenn die Bunchlücke mindestens 35% der Kavitäten-HF-Periode beträgt.

Zum Abschluß wurde das *FAIR B2B transfer system* unter Anwendung der *frequency beating method* für alle FAIR-Anwendungsfälle veranschaulicht. Es wurde gezeigt, dass für alle Primärstrahl-Transfers in den FAIR-Anwendungsfällen, bei Injektion einen B2B Mittenversatz von besser $\pm 1^\circ$ innerhalb der erforderlichen Transferzeit von 10 ms erreicht wird, weil das Zahlenverhältnis der Umfänge der beiden Ringe ganzzahlig oder nahezu ganzzahlig ist. Entwicklungsbedarf besteht noch beim Ionentransfer von Sekundärstrahlen, wie sie vom Antiprotonen-Target, dem Fragmentseparator oder dem Superfragmentseparator erzeugt werden. Hier besteht das Problem, dass das Verhältnis der Energien zwischen Primär- und Sekundärstrahl sich stark unterscheiden. Für den Transfer von exotischen Nukliden vom SIS100 zum CR über den Superfragmentseparator mit 1.5 GeV/u Primärstrahlenergie und 740 MeV/u Sekundärstrahlenergie, beträgt der B2B Injektions-Mittenversatz zwar zufällig nur $\pm 2.1^\circ$, für den Antiprotonen B2B-Transfer vom SIS100 zum CR über das Antiprotonen-Target und den Strahltransfer von exotischen Nukliden vom SIS18 zum ESR über den Fragmentseparator, ist der B2B Mittenversatz aber schon größer als $\pm 40^\circ$ und damit weit außerhalb der Spezifikation.

Die vorliegende Doktorarbeit stellt die wesentlichen Untersuchungsergebnisse für das *FAIR B2B transfer system*, aus Sicht der Strahldynamik, Timing-Anforderung und Kicker-Auslösung vor. Dennoch sind weitere Untersuchungsaufgaben erforderlich, die für den finalen Anlagenbetrieb notwendig sind. Dazu zählen:

- Die Synchronisation im Mikrosekundenbereich des Antiprotonenstrahls mit dem magnetischen Horn nach dem Antiprotonen-Target.

- Die Synchronisation zwischen dem SIS100 Bunchkompressor und der Strahlextraktion.
- In einige FAIR-Anwendungsfällen ist für den Transfer des Sekundärstrahls der B2B Injektions-Mittenversatz größer als $\pm 40^\circ$. Für diese Anwendungsfälle muss überprüft werden, ob der B2B-Transfer unter Zuhilfenahme von speziellen Strahlakkumulations-Methoden wie Beispielsweise die *barrier bucket method* oder die *unstable point accumulation method* gelingt.

Das *FAIR B2B transfer system* das in dieser Doktorarbeit vorgestellt wird, ist anwendbar für alle FAIR-Anwendungsfälle. Dennoch gibt es Verbesserungspotential. Für die *phase shift method* muss die HF-Frequenzmodulation sehr langsam erfolgen, damit der Strahl der Frequenzänderung folgen kann (z.B. 7 ms/50 ms bei sinusförmiger Modulation für den SIS18 U^{28+}/H^+ Strahl). Um *Bunche* sobald wie möglich in *Buckets* transferieren zu können, kann mit der Phasenverschiebung bereits auf der Beschleunigungsrampe begonnen werden. Zu einem definierten Zeitpunkt während des Beschleunigungsprozesses wird die Phasendifferenz zwischen den beiden HF-Systemen der Quell- und Zielmaschine unter Zuhilfenahme eines *synchronisation reference signal* ermittelt. Die Phasendifferenz auf dem *rf flattop* wird über eine Look-Up-Table aus den Phasendifferenzen, die zu definierten Zeitpunkten auf der Rampe gewonnen wurden ermittelt. Daraus lässt sich die benötigte HF-Frequenzmodulation berechnen. Diese wird der ursprünglichen Frequenzrampe augenblicklich überlagert. Mit der so entstandenen Frequenzrampe, wird die gewünschte Phasendifferenz dann automatisch erzielt, wenn die HF-Frequenz der Quellmaschine das *rf flattop* erreicht.

Glossaries, Abbreviations and Symbols

Terminology

| | |
|---------------------------------|---|
| accuracy | Deviation between the theoretically calculated start time of the synchronization window and the actual observed start time |
| B2B transfer master | Responsible for the data collection of two ring accelerators, the data calculation, the data redistribution and the B2B transfer status check |
| B2B target SCU | Collects the predicted phase of the target synchrotron and transfers it to the source synchrotron |
| B2B source SCU | Works as the B2B transfer master |
| batch | A train of bunches circulating along a synchrotron to be transferred to buckets |
| best estimate time of alignment | Fine time for the alignment of two RF Reference Signals |
| bucket indication signal | Time indication of a dedicated bucket passing on the virtual rf cavity of the target synchrotron, when it is correct phase aligned with the rf system of the source synchrotron for the bunch-to-bucket injection |
| bucket pattern | Rules for the buckets to be filled |
| bucket area factor | Ratio of bucket size of a running bucket to a stationary bucket |
| bucket size | Area in longitudinal phase space plane enclosed by the bucket |
| bucket height | Maximum momentum deviation of the rf bucket |

Terminology

| | |
|------------------------|--|
| bunch | Collection of particles captured within one rf bucket |
| bunch gap | Area without any bunches in a batch |
| Cavity DDS | Cavity DDS provides rf signal for cavities |
| circumference ratio | Ratio of the circumference for synchrotrons of different size |
| coarse synchronization | Bunches are transferred into buckets with the bunch-to-bucket center mismatch smaller than the upper bound |
| extraction kicker | Diverts a circulating beam to leave a synchrotron |
| fine synchronization | Bunches are transferred into correct buckets |
| frame transfer latency | The time interval between the frame reception and sending |
| Group DDS | DDS module that generates an phase measurement signal for a group of cavities |
| harmonic number | Integer ratio between the rf frequency and the revolution frequency |
| injection kicker | Merges one beam into a circulating beam in a synchrotron |
| kicker fall time | A period of time of kicker magnet to reduce to zero magnetic field |
| kicker flat-top | A period of time of kicker magnet with a stable magnetic field |
| kicker rise time | A period of time for kicker magnet to reach a stable magnetic field |
| longitudinal emittance | Area occupied by a bunch in the longitudinal phase space plane |
| lost frame | The difference between the sent packets and the received packets |

Terminology

| | |
|----------------------------------|---|
| machine cycle | One complete operation cycle of a machine, i.e. injection, ramp up, flattop, ejection and ramp down |
| measurement uncertainty | A non-negative parameter characterizing the dispersion of the values attributed to a measured quantity |
| misordered frame | The number of misordered packets arriving out of sending sequence |
| phase measurement signal | Harmonic or subharmonic signal generated by the Group DDS and transmitted to the individual rf station as a reference signal |
| probable time range of alignment | Range within which the fine alignment lies because of the propagation of the uncertainty |
| revolution frequency ratio | Ratio of the revolution frequencies for synchrotrons of different size |
| running rf bucket | Rf system provides a region in the longitudinal phase space, within which all particles oscillate around the synchronous particle and stay together with energy gain/loss per turn |
| stationary rf bucket | Rf system provides a region in the longitudinal phase space, within which all particles oscillate around the synchronous particle and stay together without energy gain/loss per turn (short: bucket) |
| synchronization reference signal | Shared synchronous reference signal at each supply room (same frequency and in phase) |
| synchronization frequencies | An integer multiple of the derived rf frequency, which is a fraction of the revolution frequency. It is used for the phase alignment of the two rf systems |
| synchronous particle | A particle who always sees a constant rf phase at the rf cavity |
| synchrotron motion | Oscillation of asynchronous particles around the synchronous particle |
| T0 incidents | First positive zero-crossings of BuTiS C2 clocks after every BuTiS T0 edge |

Terminology

| | |
|-------------------|--|
| timing frame | A specific Ethernet frame with 110 byte frame length, which contains one timing message |
| Trigger SCU | Production of the trigger signal for kicker electronics |
| tune | Number of particle trajectory oscillations during one revolution in the ring (transverse and longitudinal) |
| virtual rf cavity | A virtual position around the ring, to which the phase measurement signal corresponds |

Abbreviations

| | |
|------|---|
| AGS | Alternating Gradient Synchrotron at BNL |
| API | Application Programming Interface |
| B2B | Bunch-to-bucket |
| BER | Bit Error Rate |
| BI | Beam Instrumentation |
| BNL | Brookhaven National Laboratory |
| CCS | Central Control System |
| CERN | Conseil Européen pour la Recherche Nucléaire |
| CM | Clock Master |
| CR | Collector Ring at GSI |
| CSCO | Common Systems Control Systems |
| CSRe | Cooler Storage Ring experimental ring at IMP |
| CSRm | Cooler Storage Ring main ring at IMP |
| DDS | Direct Digital Synthesizer |
| DM | Data Master |
| DSP | Digital Signal Processor |
| ESR | Experimental Storage Ring at GSI |
| FAIR | Facility for Antiproton and Ion Research at GSI |
| FEC | Front End Controller |

Abbreviations

| | |
|----------|---|
| FER | Frame Error Rate |
| Fermilab | Fermi National Accelerator Laboratory |
| FESA | Front-End software Architecture |
| FLR | Frame Loss Rate |
| FPGA | Field Programmable Gate Array |
| FRS | Fragment Separator |
| GCD | Greatest Common Divisor |
| GMT | General Machine Timing |
| GSI | GSI Helmholtzzentrum für Schwerionenforschung |
| GUI | Graphical User Interface |
| HESR | High Energy Storage Ring at GSI |
| HIRFL | Heavy Ion Research Facility at IMP |
| IMP | Institute of Modern Physics |
| J-PARC | Japan Proton Accelerator Complex |
| LEIR | Low Energy Ion Ring at CERN |
| LHC | Large Hadron Collider at CERN |
| LLRF | Low-level RF |
| LSA | LHC Software Architecture |
| MM | Management Master |
| MPS | Machine Protection System |
| MR | Main Ring at J-PARC |
| PAM | Phase Advance Measurement module |
| PAP | Phase Advance Prediction module |
| pbar | antiproton bar |

Abbreviations

| | |
|--------|---|
| PBHV | Primary Beam High Voltage |
| PBRF | Primary Beam Radio Frequency |
| PC | Personal Computer |
| PCM | Phase Correction Module |
| PS | Proton Synchrotron at CERN |
| PSB | Proton Synchrotron Booster at CERN |
| PSM | Phase Shift Module |
| RCS | Rapid Cycle Synchrotron at J-PARC |
| RHIC | Relativistic Heavy Ion Collide at BNL |
| RIB | Rare Isotope Beams |
| SBES | Experimentierspeicherring ESR |
| SCU | Scalable Control Unit |
| SFC | Sector Focusing Cyclotron at IMP |
| SHE-P | SHE-Physik |
| SIS100 | SchwerIonen Synchrotron (100 Tm magnetic rigidity) at GSI |
| SIS18 | SchwerIonen Synchrotron (18 Tm magnetic rigidity) at GSI |
| SIS300 | SchwerIonen Synchrotron (300 Tm magnetic rigidity) at GSI |
| SM | Settings Management |
| SPS | Super Proton Synchrotron at CERN |
| SR | Signal Reproduction module |
| SSC | Separated Sector Cyclotron at IMP |
| TM | Timing Master |

Abbreviations

| | |
|--------|-------------------------------------|
| TOF | Time-Of-Flight |
| UNILAC | Universal Linear Accelerator at GSI |
| VLAN | Virtual LAN |
| WR | White Rabbit |

Symbols

| | |
|------------|--|
| p | Particle momentum |
| R | Average orbit radius |
| L | Orbit length |
| β | Relative speed to the speed of light |
| c | Speed of the light |
| γ | Relativistic factor, which measures the total particle energy, E , in units of the particle rest energy, E_0 |
| E | Total particle energy |
| E_0 | Particle rest energy |
| α_p | Momentum compaction factor |
| η | Phase-slip factor |
| q | Charge of a particle |
| α_b | Bucket area factor |
| ω_s | Angular synchrotron frequency |
| B | Magnetic field |
| ρ | Bending radius of a particle immersed in a magnetic field B |
| h_{rf}^X | Cavity harmonic number of a specified synchrotron |

Symbols

| | |
|------------------|--|
| h_{rev}^X | Harmonic number of the revolution frequency of a specific synchrotron, which is defined as the first harmonic |
| f_{syn}^X | Synchronization frequency |
| h_{syn}^X | Harmonic number of the synchronization frequency of a specific synchrotron |
| ε | Adiabaticity parameter |
| $Q_{x/y}$ | Horizontal/vertical tune |
| $Q'_{x/y}$ | Horizontal/vertical chromaticity |
| $\Delta Q_{x/y}$ | Horizontal/vertical tune shift |
| T_w | Length of the synchronization window |
| t_{bucket} | Bucket delay for a specific bucket pattern |
| t_{TOF} | Time-of-Flight between two ring accelerators |
| t_{v_ext} | Time corresponding to the distance between the virtual rf cavity and the extraction position of the source synchrotron |
| t_{v_inj} | Time corresponding to the distance between the virtual rf cavity and the injection position of the target synchrotron |
| t_{ext} | Extraction kicker delay |
| t_{inj} | Injection kicker delay |
| t_{diff_sync} | Goal time difference between the synchronization frequencies of two ring accelerators in the format of time |
| ϕ^X | Measured phase deviation between the synchronization frequency and the synchronization reference signal of the synchrotron X |
| φ^X | Measured phase deviation between the phase measurement signal and the synchronization reference signal of the synchrotron X |

Symbols

| | |
|--------------------|---|
| φ_0^X | Initial value of the phase deviation between the phase measurement signal and the synchronization reference signal of the synchrotron X |
| T_{sample_PAM} | Measurement sampling period of the phase deviation measurement by the PAM module |
| ψ^X | Extrapolated phase advance between the phase measurement signal and the synchronization reference signal of the synchrotron X |
| T_{sample_PAP} | Extrapolation sampling period of the phase extrapolation by the PAP module |
| ψ_0^X | Phase advance extrapolated by the PAP module at t_ψ^X of the X synchrotron. |
| t_ψ^X | Timestamp corresponding to the extrapolated phase advance ψ^X |
| $f_{normalized}$ | Normalized rf frequency modulation profile, preloaded from SM |
| f_{actual} | Actual rf frequency modulation profile, calculated by PSM |
| t_{delay} | Delay compensation for the TOF, all propagation delays, the kicker preparation time and the bucket delay |
| t_w | Start of the synchronization window, calculated by B2B source SCU |
| t_{v_emg} | Time corresponding to the distance between the virtual rf cavity and the emergency extraction position of SIS100 |
| t_{emg} | Extraction kicker delay of SIS100 for the emergency kick |
| t_{align} | Best estimate of alignment of zero crossing points of phase measurement signals of source and target synchrotrons |
| δt_{align} | Uncertainty of the best estimate of alignment of zero crossing points of phase measurement signals of source and target synchrotrons |

Symbols

| | |
|----------------------|---|
| $\delta\psi_0^X$ | Uncertainty of the extrapolated phase of the synchrotron X in the phase domain |
| δt_ψ^X | Uncertainty of the measured timestamp |
| t_{w_rect} | Rectified start of the synchronization window, calculated by B2B source SCU |
| δt_{w_rect} | Uncertainty of the start of the synchronization window, calculated by B2B source SCU |
| t_{B2B} | Start time of the B2B transfer |
| t_{rise} | Kicker rise time. |
| t_{gap} | Bunch gap |
| $d_{tank1L-tank1R}$ | Distance between the leftmost and the rightmost kicker magnets in the 1 st SIS18 tank |
| $d_{tank2L-tank2R}$ | Distance between the leftmost and the rightmost kicker magnets in the 2 nd SIS18 tank |
| $d_{tank1R-tank2L}$ | Distance between two tanks of the SIS18 extraction kicker |
| $d_{tank1L-tank2R}$ | Distance from the leftmost to the rightmost of the SIS18 extraction/SIS100 injection kicker |
| $d_{tank1R-tank2R}$ | Distance between the rightmost of the 1 st tank and the rightmost of the 2 nd tank of the SIS18 extraction kicker |
| $d_{tankL-tankR}$ | Distance between the leftmost and the rightmost kicker magnets in the SIS100 tank |
| ϕ_s | Synchronous phase |
| f_{rf} | Rf frequency |
| h | Harmonic number |
| f_{rev} | Revolution frequency |
| f_{ref} | Frequency of the synchronization reference signal |

Symbols

| | |
|--------------------|--|
| f_{B2B}^X | Frequency of the specified phase measurement signal for the phase advance measurement |
| u | Longitudinal accelerating voltage at rf cavity |
| V_0 | Amplitude of the rf voltage |
| m_0 | Rest mass |
| C^X | Circumference of the extraction/injection orbit of a specific synchrotron |
| f_{rev}^X | or $f_{h=1}^X$. Revolution frequency of a specific synchrotron |
| f_{rf}^X | or $f_{h=cavity_harmonic}^X$. Cavity rf frequency of a specific synchrotron |
| T | Duration of rf frequency modulation for the phase shift method |
| Y | Greatest common divisor |
| ϕ_0^X | Initial phase deviation between the synchronization frequency and synchronization reference signal of the synchrotron X |
| $\Delta\phi_{rf}$ | Phase difference between two cavity rf frequencies of two ring accelerators |
| $\Delta\phi_{syn}$ | Phase difference between two synchronization frequencies of two ring accelerators |
| Δf_{syn} | Rf frequency modulation on the synchronization frequency for the phase shift method, rf frequency detuning on the synchronization frequency for the frequency beating method |
| Δf_{rf} | Rf frequency modulation on the cavity rf frequency for the phase shift method, rf frequency detuning on the cavity rf frequency for the frequency beating method |
| σ_{syn} | Phase mismatch between two synchronization frequencies within the synchronization window |

Symbols

| | |
|---------------------------|---|
| σ_{rf} | Phase mismatch between two cavity rf frequencies within the synchronization window |
| T_{rev}^X | Period of the revolution period of machine X |
| T_{rf}^X | Period of the cavity rf frequency of machine X |
| f_{bucket} | Rf frequency of the bucket indication signal |
| k^X | Slope of the phase deviation between the synchronization reference signal and a dedicated phase measurement signal of the synchrotron X |
| $\Delta\phi_{syn_0}$ | Phase difference between two synchronization frequencies of two ring accelerators at time t_ψ^X |
| $\Delta\phi_{goal}$ | Goal phase difference between the synchronization frequencies of two ring accelerators |
| $\Delta\phi_{adjust}$ | Required phase adjustment for the phase alignment on the synchronization frequency |
| $\Delta\phi_{shift}$ | Required phase shift for the Group DDS with the synchronization frequency |
| $\Delta\phi_{shift_imp}$ | Implemented phase shift for the Group DDS with the revolution frequency |
| T_{wait} | Waiting time for the phase matching of the frequency beating method |

Appendix A

FAIR B2B Transfer Related Timing Frames

APPENDIX A. FAIR B2B TRANSFER RELATED TIMING FRAMES

Table A.1: B2B timing frames

| No | Frame Name | Event ID | Priority | Source | Destination |
|----|--|----------|----------|--------------------|--|
| 1 | CMD_START_B2B | | 7 | DM | B2B source and target SCUs |
| 2 | TGM_PHASE_TIME | | 6 | B2B target SCU | B2B source SCU |
| 3 | TGM_SYNCH_WIN | | 6 | B2B source SCU | DM |
| 4 | CMD_SYNCH_WIN | | 7 | DM | BI, source and target Trigger SCUs |
| 5 | TGM_PHASE_JUMP | | 6 | B2B source SCU | B2B target SCU |
| 6 | TGM_PHASE_CORRECTION | | 6 | B2B source SCU | source Trigger SCU |
| 7 | TGM_KICKER_TRIGGER_TIME_S | | 6 | source Trigger SCU | B2B source SCU |
| 8 | TGM_KICKER_TRIGGER_TIME_T | | 6 | target Trigger SCU | B2B source SCU |
| 9 | TGM_B2B_STATUS | | 6 | B2B source SCU | DM |
| 10 | CMD_B2B_STATUS | | 7 | DM | BI |
| 11 | TGM_B2B_ERROR | | 7 | B2B source SCU | DM |
| No | Content | | | | Description |
| 1 | 64 bits timestamp(event execution) | | | | Begin of the B2B transfer process |
| 2 | 16 bits phase advance and 64 bits slop (param) | | | | Transfer of the phase advance and the slop |
| 3 | 64 bits timestamp (param) | | | | Transfer the start of the synchronization window |
| 4 | 64 bits timestamp (event execution) | | | | Indication the start of the synchronization window |
| 5 | 16 bits the expected jumped phase (param) | | | | Indication the jumped phase for the empty target machine |
| 6 | 16 bits phase correction (param) | | | | Target revolution frequency reproduction |
| 7 | 2 × 64 bits timestamp (param) | | | | Timestamps of trigger and firing of extraction kicker |
| 8 | 2 × 64 bits timestamp (param) | | | | Timestamps of trigger and firing of injection kicker |
| 9 | 64 bits timestamp + 1 bit (param) | | | | The actual beam extraction time and the status of the B2B system |
| 10 | 64 bits timestamp (param) | | | | The actual beam extraction time |
| 11 | 4 bits (param) | | | | The error information |

Appendix B

Timing Frames Transfer for the FAIR B2B Transfer System

APPENDIX B. TIMING FRAMES TRANSFER FOR THE FAIR B2B TRANSFER SYSTEM

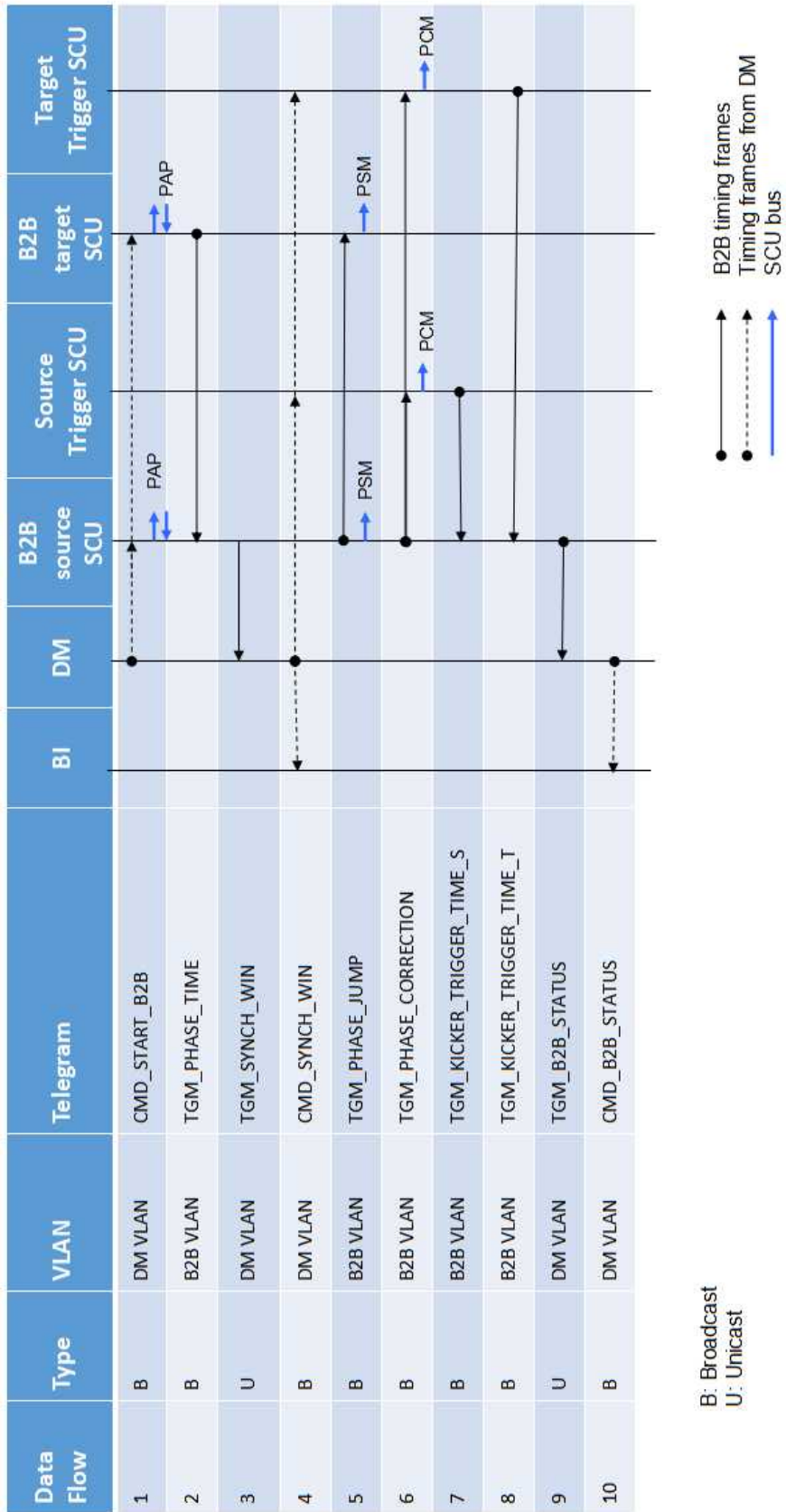


Figure B.1: Timing frames transfer for the B2B transfer

Appendix C

Parameters of FAIR B2B Transfer Use Cases

C.1 Parameters of the B2B Transfer from SIS18 to SIS100

| | | Proton | | Heavy Ion U^{28+} | |
|--|-------|--------------------------|------------|--------------------------|------------|
| | Unit | SIS18 Ext | SIS100 Inj | SIS18 Ext | SIS100 Inj |
| Design orbit | m | 216.72 | 1083.6 | 216.72 | 1083.6 |
| $C_{SIS18} : C_{SIS100}$ | | 5 | | 5 | |
| Ext kinetic energy | MeV/u | 4000 | | 200 | |
| Inj kinetic energy | MeV/u | | 4000 | | 200 |
| h | | 1 | 10(1×4) | 2 | 10(2×4) |
| f_{rf} | MHz | 1.359358 | 2.718715 | 1.572536 | 1.572536 |
| T_{rf} | μs | 0.736 | 0.368 | 0.636 | 0.636 |
| f_{rev} | MHz | 1.359358 | 0.271872 | 0.786268 | 0.157254 |
| T_{rev} | μs | 0.736 | 3.678 | 1.272 | 6.359 |
| Max $\Delta p/p$ | | ±0.008 | ±0.01 | ±0.008 | ±0.01 |
| $\Delta R/R$ | | $\pm 0.8 \times 10^{-4}$ | | $\pm 2.4 \times 10^{-4}$ | |
| $\eta = \frac{1}{\gamma^2} - \alpha_p$ | | 0.026 | | 0.647 | |
| γ_t | | 10 | | 5.8 | |
| α_p | | 0.010 | | 0.030 | |
| β | | 0.982 | 0.982 | 0.568 | 0.568 |
| γ | | 5.294 | 5.294 | 1.215 | 1.215 |
| Q_x | | 4.17 | | 4.17 | |
| Q_y | | 3.4 | | 3.4 | |
| Q'_x | | -7.5 | | -6.5 | |
| Q'_y | | -4.4 | | -4.1 | |
| | | Injection four times | | Injection four times | |

Table C.1: Parameters related to the B2B transfer from the SIS18 to the SIS100

C.2 Parameters of the B2B Transfer from SIS18 to ESR

| | | Proton/Heavy Ion | | Heavy Ion | |
|---|-------|--------------------------------------|-----------------|--------------------------------------|-----------------|
| | Unit | SIS18 Ext | ESR Inj | SIS18 Ext | ESR Inj |
| Design orbit | m | 216.72 | 108.36 | 216.72 | 108.36 |
| Inj orbit | m | | 108.36 +0.15 | | 108.36 +0.15 |
| $C_{SIS18} : C_{ESR}$ | | 1.997 | | 1.997 | |
| Ext kinetic energy | MeV/u | 550 | | 30 | |
| Inj kinetic energy | MeV/u | | 400 | | 30 |
| h | | 1 | 1 | 4 | 2 |
| f_{rf} | MHz | 0.989756 | 1.976777 | 1.373201 | 1.371302 |
| T_{rf} | μs | 1.010 | 0.506 | 0.728 | 0.879 |
| f_{rev} | MHz | 0.989756 | 1.976777 | 0.343300 | 0.685651 |
| T_{rev} | μs | 1.010 | 0.506 | 2.913 | 1.458 |
| $\Delta p/p$ compared with design orbit | | | 1% | | 1% |
| $\Delta R/R$ | | | 0.138% | | 0.138% |
| $\eta = \frac{1}{\gamma^2} - \alpha_p$ | | 0.480 | 0.310 | 0.909 | 0.759 |
| γ_t | | 10 | 2.357 | 5.8 | 2.357 |
| α_p | | 0.010 | 0.18 | 0.030 | 0.18 |
| β | | 0.715 | 0.715 | 0.248 | 0.248 |
| γ | | 1.429 | 1.429 | 1.032 | 1.032 |
| | | Accumulation beam in injection orbit | | Accumulation beam in injection orbit | |

Table C.2: Parameters related to the B2B transfer from the SIS18 to the ESR

C.3 Parameters of the B2B Transfer from SIS18 to ESR via the FRS

| | | Heavy Ion Beam | Rare Isotope Beam |
|---|-------|--------------------|-------------------|
| | Unit | SIS18 Ext | ESR Inj |
| Design orbit | m | 216.72 | 108.36 |
| Inj orbit | m | | 108.36 +0.15 |
| $C_{SIS18} : C_{ESR}$ | | 1.997 | |
| Ext kinetic energy | MeV/u | 550 | |
| Inj kinetic energy | MeV/u | | 400 |
| h | | 1 | 1 |
| f_{rf} | MHz | 1.076965 | 1.976777 |
| T_{rf} | μs | 0.929 | 0.506 |
| f_{rev} | MHz | 1.076965 | 1.976777 |
| T_{rev} | μs | 0.929 | 0.506 |
| $\Delta p/p$ compared with design orbit | | | 1% |
| $\Delta R/R$ | | | 0.138% |
| $\eta = \frac{1}{\gamma^2} - \alpha_p$ | | 0.366 | 0.310 |
| γ_t | | 5.8 | 2.357 |
| α_p | | 0.030 | 0.18 |
| β | | 0.778 | 0.715 |
| γ | | 1.590 | 1.429 |
| | | One time injection | |

Table C.3: Parameters related to the B2B transfer from the SIS18 to the ESR via the FRS

C.4 Parameters of the B2B Transfer from ESR to CRYRING

| | | Proton/Antiproton | | Heavy Ion | |
|--|-------|--------------------|----------------|-----------------------|-----------------------|
| | Unit | ESR Ext | CRYRING Inj | ESR Ext | CRYRING Inj |
| Design orbit | m | 108.36 | 54.18 | 108.36 | 54.18 |
| Ext orbit | m | 108.36 +0.15 | | 108.36 +0.15 | |
| $C_{ESR} : C_{CRYRING}$ | | 2.003 | | 2.003 | |
| Ext kinetic energy | MeV/u | 30 | | 4-10 | |
| Inj kinetic energy | MeV/u | | 30 | | 4-10 |
| h | | 1 | 1 | 1 | 1 |
| f_{rf} | MHz | 0.685651 | 1.373200 | 0.254354- 0.400885 | 0.509507- 0.802879 |
| T_{rf} | μs | 1.458 | 0.728 | 3.932- 2.494 | 1.963- 1.246 |
| f_{rev} | MHz | 0.685651 | 1.373200 | 0.254354- 0.400885 | 0.509507- 0.802879 |
| T_{rev} | μs | 1.458 | 0.728 | 3.932- 2.494 | 1.963- 1.246 |
| $\eta = \frac{1}{\gamma^2} - \alpha_p$ | | 0.759 | | 0.798-0.812 | |
| γ_t | | 2.357 | | 2.357 | |
| α_p | | 0.18 | | 0.18 | |
| β | | 0.248 | 0.248 | 0.092-0.145 | 0.092-0.145 |
| γ | | 1.032 | 1.032 | 1.004-1.011 | 1.004-1.011 |
| | | One time injection | | One time injection | |

Table C.4: Parameters related to the B2B transfer from the ESR to the CRYRING

C.5 Parameters of the B2B Transfer from CR to HESR

| | | Proton→ Antiprotron | | Heavy Ion→ RIB | |
|--|-------|------------------------------------|----------|------------------------------------|----------|
| | Unit | CR Ext | HESR Inj | CR Ext | HESR Inj |
| Design orbit | m | 221.45 | 575 | 221.45 | 575 |
| $C_{HESR} : C_{CR}$ | | 2.597 | | 2.597 | |
| Ext kinetic energy | GeV/u | 3 | | 0.74 | |
| Inj kinetic energy | GeV/u | | 3 | | 0.74 |
| h | | 1 | 1 | 1 | 1 |
| f_{rf} | MHz | 1.316775 | 0.507131 | 1.124408 | 0.433043 |
| T_{rf} | μs | 0.759 | 1.972 | 0.889 | 2.309 |
| f_{rev} | MHz | 1.316775 | 0.507131 | 1.124408 | 0.433043 |
| T_{rev} | μs | 0.759 | 1.972 | 0.889 | 2.309 |
| Max $\Delta p/p$ | | ±3% | | ±1.5% | |
| $\eta = \frac{1}{\gamma^2} - \alpha_p$ | | -0.011 | | 0.178 | |
| γ_t | | 3.85 | | 2.711 | |
| α_p | | 0.067 | | | |
| β | | 0.972 | 0.972 | 0.830 | 0.830 |
| γ | | 4.221 | 4.221 | 1.794 | 1.794 |
| | | 100 times Injection per 10 seconds | | 100 times Injection per 10 seconds | |

Table C.5: Parameters related to the B2B transfer from the CR to the HESR

C.6 Parameters of the B2B Transfer from SIS100 to CR

| | | Proton→ Antiproton | | Heavy Ion→ RIB | |
|-----------------------|-------|--------------------|----------|--------------------|----------|
| | Unit | SIS100 Ext | CR Inj | SIS100 Ext | CR Inj |
| Design orbit | m | 1083.6 | 221.45 | 1083.6 | 221.45 |
| $C_{SIS100} : C_{CR}$ | | 4.893 | | 4.893 | |
| Ext kinetic energy | GeV/u | 28.8 | | 1.5 | |
| Inj kinetic energy | GeV/u | | 3 | | 0.74 |
| h | | 5(1 bunch) | 1 | 2(1 bunch) | 1 |
| f_{rf} | MHz | 1.383509 | 1.316778 | 0.511628 | 1.124408 |
| T_{rf} | μs | 0.723 | 0.759 | 1.955 | 0.889 |
| f_{rev} | MHz | 0.276702 | 1.316778 | 0.255814 | 1.124408 |
| T_{rev} | μs | 3.614 | 0.759 | 3.909 | 0.889 |
| Max $\Delta p/p$ | | ±3% | | ±1.5% | |
| β | | 0.9995 | 0.972 | 0.924 | 0.830 |
| γ | | 31.918 | 4.221 | 2.610 | 1.794 |
| | | One time injection | | One time injection | |

Table C.6: Parameters related to the B2B transfer from the SIS100 to the CR

Appendix D

Parameters of the FAIR B2B Transfer System from Settings Management

Table D.1: Parameters for the B2B transfer provided by SM

| Parameter | Destination | Usage |
|--|--|--|
| f_{syn}^X | B2B source SCU | Start of synchronization window calculation |
| f_{syn}^{REF} | B2B source SCU | Phase advance extrapolation for PCM |
| Frequency of bucket indication signal | B2B source SCU⇒SR B2B target SCU⇒SR Trigger SCU⇒SR | Bucket label signal production |
| t_{delay} | Delay compensation for TOF, all propagation and kicker preparation | |
| Extraction kicker delay compensation | B2B source SCU | Start of synchronization window calculation |
| Injection kicker delay compensation | Trigger SCU⇒TD | Extraction kicker trigger signal production |
| Emergency kicker delay compensation | Trigger SCU⇒TD | Injection kicker trigger signal production |
| Goal time | Trigger SCU⇒TD | Emergency kicker trigger signal production |
| t_{diff_sync} | B2B source SCU | Start of synchronization window calculation or phase correction calculation for PCM |
| difference between two synchronization frequencies of two synchrotrons | | |
| Δf | B2B source SCU | Start of synchronization window calculation |
| Duration of rf frequency modulation for the phase shift method | B2B source SCU⇒PSM B2B source SCU⇒PSM | Start of synchronization window calculation and rf frequency modulation profile with certain duration T production |
| $\Delta f_{rf}, \Delta \dot{f}_{rf}$ and $\Delta \ddot{f}_{rf}$ | B2B source SCU⇒PSM | Adiabatical rf frequency modulation profile production |

Appendix E

Parameters of FAIR Kicker Magnets

Table E.1: Parameters of kicker magnets

| Kicker | Units | Preparation time | Kicker rise time | Kicker fall time |
|--|-------|------------------|------------------|----------------------|
| SIS18 extraction kicker | 9 | 5 us | 90 ns | arbitrary |
| SIS100 injection kicker | 6 | 5 us | 130 ns | $\frac{1}{4}T_{rev}$ |
| SIS100 extraction/ emergency kicker | 8 | 10 us | 750 ns | arbitrary |
| CR injection/ extraction kicker | 9 | | 320 ns | |
| ESR injection kicker | 3 | | 90 ns | |

Appendix F

Configuration for the Test Setup

The project is kept on the git repository

https://github.com/GSI-CS-CO/bel_projects/tree/lm32_B2B_merge.

In the test setup, the frame CMD_START_B2B uses the eventID of *0XDEADBEEF11111111* as an example and the frame TGM_PHASE_TIME uses the eventID of *0XDEADBEEF22222222* as an example and the frame TGM_SYNCH_WIN uses the eventID of *0XDEADBEEF33333333* as an example.

F.1 Configuration of the B2B source SCU

```
1 Login the B2B source SCU
2 # ssh root@scu_name.acc.gsi.de
3 Configure the ECA queue to storage the B2B frames CMD_B2B_START and
   TGM_PHASE_TIME
4 # saft-ecpu-ctl baseboard -c 0XDEADBEEF11111111 32 0 0
5 # saft-ecpu-ctl baseboard -c 0XDEADBEEF22222222 32 0 0
6 Configure one IO port as an input for the TTL signal of the SIS18 DS345
7 # saft-io-ctl baseboard B2 -o 0
8 Load the B2B source SCU firmware to the LM32
9 # lm32-ctl
10 # load B2B_main_src.elf
```

F.2 Configuration of the B2B target SCU

```
1 Login the B2B target SCU
2 # ssh root@scu_name.acc.gsi.de
3 Configure the ECA queue to storage the B2B frames CMD_B2B_START
4 # saft-ecpu-ctl baseboard -c 0XDEADBEEF11111111 32 0 0
5 Configure one IO port as an input for the TTL signal of the SIS100 DS345
6 # saft-io-ctl baseboard B2 -o 0
7 Load the B2B target SCU firmware to the LM32
8 # lm32-ctl
9 # load B2B_main_trg.elf
```

F.4. Configuration of the packETH

F.3 Configuration of the Trigger SCU

```

1 Login the Trigger SCU
2 # ssh root@scu_name.acc.gsi.de
3 Configure the ECA queue to storage the B2B frames TGM_SYNCH_WIN
4 # saft-ecpu-ctl baseboard -c 0XDEADBEEF33333333 32 0 0
5 Configure one IO port as an output port
6 # saft-io-ctl baseboard B2 -o 1
7 Configure ECA to produce a TTL signal at the output port, when the frame
     TGM_SYNCH_WIN is executed
8 # saft-B2B-triggerSCU baseboard 0XDEADBEEF33333333 B2
9 Load the Trigger SCU firmware to the LM32
10 # lm32-ctl
11 # load B2B.main_trigger.elf

```

F.4 Configuration of the packETH

The configuration of the packETH is shown as follows.

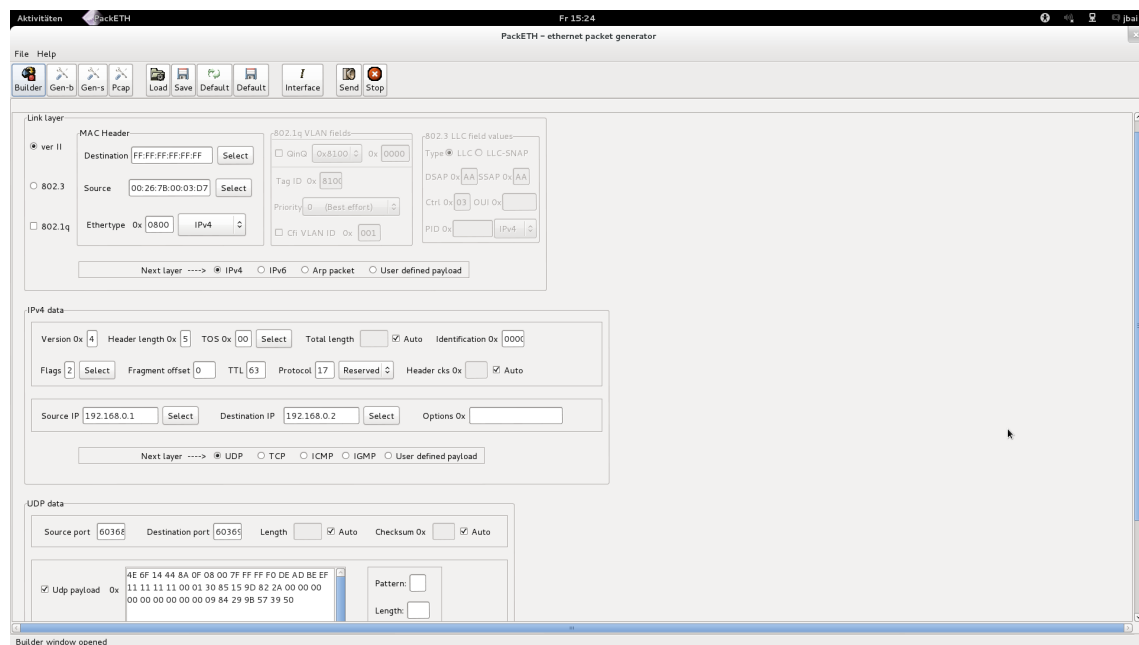


Figure F.1: The configuration of the packETH.

Bibliography

- [1] Particle Accelerator, 2017. URL https://en.wikipedia.org/wiki/Particle_accelerator.
- [2] S. P. Møller. Beam-residual Gas Interactions. Technical report, CERN, 1999. URL <http://www.chem.elte.hu-foundations/altkem/vakuumtechnika/CERN13.pdf>.
- [3] T. Ferrand, H. Klingbeil, and H. Damerau. CERN-ACC-NOTE-2015-0025, Synchronization of Synchrotrons for Bunch-to-Bucket Transfers. CERN Internal Publication, 2015. URL <http://cds.cern.ch/record/2053285>.
- [4] J-PARC, 2016. URL <https://www.kek.jp/en/Facility/ACCL/J-PARC/>.
- [5] Brookhaven National Laboratory, 2017. URL https://en.wikipedia.org/wiki/Brookhaven_national_laboratory.
- [6] Fermi National Accelerator Laboratory, 2016. URL <http://www.fnal.gov/pub/science/particle-accelerators/accelerator-complex.html>.
- [7] Institute of Modern Physics of the Chinese Academy of Sciences, 2013. URL http://english.imp.cas.cn/au/bi/201312/t20131231_115141.html.
- [8] J. Eschke. International Facility for Antiproton and Ion Research (FAIR) at GSI, Darmstadt. Journal of Physics G: Nuclear and Particle Physics, 31(6):S967, 2005. URL <http://iopscience.iop.org/article/10.1088/0954-3899/31/6/041/meta>.
- [9] FAIR - Facility for Antiproton and Ion Research, 2011. URL <https://www.gsi.de//forschungbeschleuniger/fair.htm>.
- [10] P. Spiller and G. Franchetti. The FAIR Accelerator Project at GSI. Nuclear Instruments and Methods in Physics Research Section A: Accelerators, Spectrometers, Detectors and Associated Equipment, 561(2):305–309, 2006. URL <http://www.sciencedirect.com/science/article/pii/S0168900206000507>.
- [11] M. Steck et al. Advanced Design of the FAIR Storage Ring Complex. In Proc. of PAC, Vancouver, BC, Canada, 2009. URL <https://accelconf.web.cern.ch/AccelConf/PAC2009/papers/fr1gri03.pdf>.
- [12] F. Nolden et al. The Collector Ring CR of the FAIR Project. In Proc. of EPAC, Edinburgh, Scotland, 2006. URL <http://accelconf.web.cern.ch/AccelConf/e06/PAPERS/MOPCH077.PDF>.

BIBLIOGRAPHY

- [13] R. Bär et al. Technical Design Report on the Collector Ring. GSI Internal Document, 2013. URL <https://indico.gsi.de/getFile.py/access?resId=7&materialId=slides&confId=2200>.
- [14] R. Toelle et al. HESR at FAIR: Status of technical Planning. In Proc. of PAC, Albuquerque, New Mexico, 2007. URL <http://epaper.kek.jp/p07/PAPERS/TUPAN024.PDF>.
- [15] M. Lestinsky et al. CRYRING@ ESR: present Status and future Research. Physica Scripta, 2015(T166):014075, 2015. URL <http://iopscience.iop.org/article/10.1088/0031-8949/2015/T166/014075/meta>.
- [16] M. Lestinsky et al. CRYRING@ ESR: A Study Group Report. GSI and FAIR Report, 2012.
- [17] S. Y. Lee. Accelerator Physics. WORLD SCIENTIFIC, Singapore, 3 edition, 2011. ISBN 978-981-4374-94-1 978-981-4374-95-8. URL <http://www.worldscientific.com/worldscibooks/10.1142/8335>.
- [18] W. Barletta, L. Spentzouris, and E. Harms. Lecture Note: Overview on Magnetic fields. US Particle Accelerator School. URL http://uspas.fnal.gov/materials/12MSU/xverse_dynamics.pdf.
- [19] R Garoby. CERN-PS-RF-NOTE-84-6, Timing Aspect of Bunch Transfer between Circular Machines: State of the Art in the PS Complex. CERN Internal Publication, 1984.
- [20] J. M. Grieser. Beam Phase Feedback in a heavy-ion Synchrotron with Dual-harmonic Cavity System. PhD thesis, Technical University Darmstadt, Germany, 2015. URL <http://tuprints.ulb.tu-darmstadt.de/4634/>.
- [21] K. Gross et al. Bunch-by-Bunch Longitudinal RF Feedback for Beam Stabilization at FAIR. In Proc. of IPAC, Richmond, Virginia, USA, 2015. URL <http://accelconf.web.cern.ch/AccelConf/IPAC2015/papers/mopha021.pdf>.
- [22] E. Ezura, M. Yoshii, F. Tamura, and A. Schnase. Beam-Dynamics View of RF Phase Adjustment for Synchronizing J-PARC RCS with MR or MLF. KEK Internal Document, 2008. URL <http://ccdb5fs.kek.jp/tiff/2008/0826/0826001.pdf>.
- [23] R. J. Steinhagen. Tune and Chromaticity Diagnostics. CERN Document Server, 2008. URL <https://cds.cern.ch/record/1213281/files/p317.pdf>.
- [24] B. J. Holzer. Introduction to Transverse Beam Dynamics. CERN Yellow Report, 2013. URL <http://arxiv.org/abs/1404.0923>.
- [25] I. Petzenhauser et al. Concept and Design of the Injection Kicker System for the FAIR SIS100 Synchrotron. In Proc. of IPAC, Busan, Korea, 2016.
- [26] U. Blell. Injection and Extraction Components of SIS 100/300. GSI Internal Document, 2014.

BIBLIOGRAPHY

- [27] T. Hoffmann. FESA—The front-End Software Architecture at FAIR. In Proc. of PCaPAC, Ljubljana, Slovenia, 2008. URL <http://accelconf.web.cern.ch/AccelConf/pc08/papers/wep007.pdf>.
- [28] R. Huhmann et al. The FAIR Control System—System Architecture and First Implementations. In Proc. of ICALEPCS, San Francisco, California, USA, 2013. URL <http://epaper.kek.jp/ICALEPCS2013/papers/moppc097.pdf>.
- [29] P. Moritz. BuTiS—Development of a Bunchphase Timing System. GSI Scientific Report, 2006. URL <http://citeseerx.ist.psu.edu/viewdoc/download?doi=10.1.1.162.1765&rep=rep1&type=pdf>.
- [30] B. Zipfel and P. Moritz. Recent Progress on the Technical Realization of the Bunch Phase Timing System BuTiS. In Proc. of IPAC, pages 418–420, San Sebastian, Spain, 2011. URL <http://accelconf.web.cern.ch/accelconf/ipac2011/papers/mopc145.pdf>.
- [31] D. Beck et al. The new White Rabbit based Timing System for the FAIR Facility. In Proc. of PCaPAC, Kolkata, India, 2012. URL <http://accelconf.web.cern.ch/Accelconf/pcapac2012/papers/fria01.pdf>.
- [32] D. Beck et al. The General Machine Timing System for FAIR and GSI. GSI Internal Document, 2013. URL https://www-acc.gsi.de/wiki/pub/Timing/TimingSystemDocuments/GMT_Description_v3-1.pdf.
- [33] D. Beck. Timing Messages of GMT System for FAIR, 2015. URL <https://www-acc.gsi.de/wiki/Timing/TimingSystemEvent>.
- [34] K. Kaiser. F-TN-C-008e, Detailed Documentation of the Scalable Control Unit SCU3 FG 900.112. FAIR Technical Note, 2014.
- [35] H. Klingbeil et al. New Digital Low-Level RF System for heavy-ion Synchrotrons. Physical Review Special Topics - Accelerators and Beams, 14 (10), 2011. ISSN 1098-4402. doi: 10.1103/PhysRevSTAB.14.102802. URL <http://link.aps.org/doi/10.1103/PhysRevSTAB.14.102802>.
- [36] P. Baudrenghien. Lecture Note: Low Level RF. CERN Accelerator School, 2010. URL <https://cas.web.cern.ch/cas/Denmark-2010/Lectures/Baudrenghien-1.pdf>.
- [37] M. Mandakovic. F-TC-C-02e, Conceptual Design of SIS-100 Fast Beam Abort System (MPS). FAIR Technical Concept, 2015.
- [38] H. Liebermann and D. Ondreka. FAIR and GSI Reference Cycles for SIS18. GSI Internal Document, 2013.
- [39] H. Liebermann and D. Ondreka. SIS100 Cycles. GSI Internal Document, 2013.
- [40] J. Bai, T. Ferrand, D. Beck, R. Bär, O. Kester, D. Ondreka, C. Prados, and W. Terpstra. Bunch to Bucket Transfer System for FAIR. In Proc. of ICALEPCS, Melbourne, Australia, 2015. URL <http://icalepcs.synchrotron.org.au/papers/wepgf119.pdf>.

BIBLIOGRAPHY

- [41] T. Ferrand and J. Bai. System Simulation of Bunch-to-Bucket Transfer Between Synchrotrons. GSI Scientific Report, 2014. URL <http://repository.gsi.de/record/184160/files/FG-GENERAL-28.pdf>.
- [42] T. Ferrand and J. Bai. System Design for a Deterministic Bunch-to-Bucket Transfer. In Proc. of IPAC, Richmond, Virginia, USA, 2015. URL <http://accelconf.web.cern.ch/AccelConf/IPAC2015/papers/wepma024.pdf>.
- [43] T. Ferrand. Development of the LLRF System for a Deterministic Bunch-to-Bucket Transfer for FAIR. (Unpublished doctoral thesis), Technical University Darmstadt, Germany.
- [44] M. Thieme, W. Panschow, and S. Rauch. SCU System Goes Productive. GSI Scientific Report, 2013. URL <http://repository.gsi.de/record/68061/files/FG-CS-07.pdf>.
- [45] J. Bai and T. Ferrand. F-TC-C-05, Concept of the FAIR Bunch To Bucket Transfer System. FAIR Technical Concept, 2016.
- [46] P Kainberger. PZS - SIS/ESR-Pulszentrale. GSI Internal Document, 2003. URL <https://www-acc.gsi.de/data/documentation/eq-models/pzs/gm-pzs.pdf>.
- [47] U. Krause and V. RW Schaa. Re-engineering of the GSI Control System. In Proc. of ICALEPS, San Jose, California, 2001. URL <https://arxiv.org/pdf/physics/0111060.pdf>.
- [48] J. R. Taylor. An Introduction to Error Analysis: The Study of Uncertainty in physical Measurements. Mill Valley, CA: Anonymous University Science Books, 1982.
- [49] H. Klingbeil. Detailed Specification on the LLRF DSP System for FAIR Ring RF Systems. GSI Internal Document, 2013.
- [50] P. Moritz. F-CS-RF-14e BuTiS, Common Specification on the Bunch Phase Timing System (BuTiS). FAIR Common Specification, 2012.
- [51] M. Kreider et al. Receiver Nodes of the General Machine Timing System for FAIR and GSI. GSI Internal Document, 2014.
- [52] C. Prados. (Unpublished doctoral thesis), Technical University Darmstadt, Germany.
- [53] C. Prados and J. Bai. Testing the WR Network of the FAIR General Machine Timing System. GSI Internal Document, 2016.
- [54] C. Prados and M. Lipinski. White Rabbit and Robustness, 2011. URL <http://www.ohwr.org/documents/103>.
- [55] Calculating Optical Fiber Latency, 2012. URL <http://www.m2optics.com/blog/bid/70587/Calculating-Optical-Fiber-Latency>.
- [56] U. Blell. F-DS-IE-03e, Detailed Specification of the SIS100 Injection Kicker Magnets and their Pulse Power Supplies. FAIR Detailed Specification, 2014.

BIBLIOGRAPHY

- [57] J. Roß. SIS18 Sektoren Technische Zeichnungen und Fotografien. GSI Internal Document, 2008.
- [58] W. Terpstra. Timing Receiver: Event-Condition-Action (ECA) Unit Design. GSI Internal Document, 2013.
- [59] M. Steck et al. Demonstration of Longitudinal Stacking in the ESR with Barrier Buckets and Stochastic Cooling. In Proc. of COOL, Alushta, Ukraine, 2011. URL <http://accelconf.web.cern.ch/AccelConf/COOL2011/papers/proceed.pdf#page=150>.
- [60] F. Herfurth et al. The Low Energy Storage Ring CRYRING@ ESR. In Proc. of COOL, Mürren, Switzerland, 2013. URL <https://accelconf.web.cern.ch/accelconf/COOL2013/papers/thpm1ha01.pdf>.

List of Figures

| | | |
|------|--|----|
| 1.1 | Illustration of a bunch-to-bucket transfer. | 2 |
| 1.2 | Structure of the dissertation. | 6 |
| 2.1 | Longitudinal focusing of particles by an rf voltage ($\eta > 0$). | 10 |
| 2.2 | Longitudinal motion of asynchronous particles in the longitudinal phase space plane ($\eta > 0$). | 10 |
| 2.3 | A stationary rf bucket. | 12 |
| 2.4 | A running rf bucket. | 13 |
| 2.5 | Bunch-to-Bucket injection with a phase, energy or voltage error. | 14 |
| 2.6 | A constant phase difference between two synchronization frequencies f_{syn}^l and f_{syn}^s when $\kappa = 5$, $h_{rf}^s = 1$ and $h_{rf}^l = 10$ | 17 |
| 2.7 | A periodically variable phase difference between two slightly different synchronization frequencies f_{syn}^l and f_{syn}^s when $\kappa = 2$, $\lambda = -0.003$, $h_{rf}^s = 2$ and $h_{rf}^l = 4$ | 19 |
| 2.8 | A periodically variable phase difference between two synchronization frequencies f_{syn}^l and f_{syn}^s when $m = 26$, $n = 10$, $\lambda = -0.003$, $h_{rf}^s = 1$ and $h_{rf}^l = 1$ | 20 |
| 2.9 | An example for the phase shift method with a sinusoidal rf frequency modulation. | 21 |
| 2.10 | Illustration of the frequency beating method. | 25 |
| 2.11 | Schematic diagram of a kicker magnet. | 27 |
| 2.12 | Rise time, kicker flat-top and fall time of an extraction kicker. | 28 |
| 2.13 | Rise time, kicker flat-top and fall time of an injection kicker for multiple batches injection. | 29 |
| 3.1 | Reference rf signal distribution system | 33 |
| 3.2 | Local Cavity Synchronization | 34 |
| 4.1 | Illustration of the B2B transfer from the SIS18 to the SIS100. | 37 |
| 4.2 | Frequency of the bucket indication signal equals to the revolution frequency of the target accelerator. | 40 |
| 4.3 | Frequency of the bucket indication signal equals to the synchronization frequency of the target accelerator. | 40 |
| 4.4 | Procedure for the B2B transfer within one acceleration cycle. | 42 |
| 4.5 | Phase deviation between the synchronization frequency and the synchronization reference signal. | 43 |
| 4.6 | Realization of the phase deviation measurement at one accelerator . . | 46 |
| 4.7 | Realization of the phase advance extrapolation at one accelerator . . | 47 |

LIST OF FIGURES

| | | |
|------|---|-----|
| 4.8 | Synchronization of the extrapolated phase to the timestamp in one accelerator | 48 |
| 4.9 | An example of the transfer path of the B2B timing frames in the WR network | 49 |
| 4.10 | Normalized frequency and phase modulation profile and the actual profiles | 51 |
| 4.11 | Transfer delay of the start of the synchronization window on the WR network. | 52 |
| 4.12 | Realization of the bucket label for the normal extraction and injection. . | 54 |
| 4.13 | Realization of the maximum bunch spacing label for the emergency extraction. | 55 |
| 4.14 | Illustration of the kicker delay compensation when the bucket indication signal has the frequency of f_{syn}^{trg} | 57 |
| 4.15 | Data flow of the B2B transfer system | 59 |
| 4.16 | Current realization of the bunch-to-bucket transfer between the SIS18 and the ESR with the GSI control system. | 61 |
| 5.1 | Examples of rf frequency modulation. | 66 |
| 5.2 | First derivative of three cases. | 67 |
| 5.3 | Second derivative of three cases. | 67 |
| 5.4 | Phase shift modulation of three cases. | 68 |
| 5.5 | Maximum orbit length displacement of three cases. | 69 |
| 5.6 | Relative momentum shift of three cases. | 70 |
| 5.7 | Changes in synchronous phase of three cases. | 71 |
| 5.8 | Ratio of bucket areas of a running bucket to the stationary bucket of three cases. | 71 |
| 5.9 | Adiabaticity parameter of three cases. | 72 |
| 5.10 | Illustration of the rectification for the start of the synchronization window. | 81 |
| 5.11 | Illustration of the accuracy of the start of the synchronization window. . | 82 |
| 5.12 | An overview of the Xena's Layer 2-3 test platform for the WR network. . | 83 |
| 5.13 | Relation between the FER and the fiber connections for B2B Unicast and Broadcast traffics. | 85 |
| 5.14 | Connection between WR switches and the XenaBay of the test setup. . | 86 |
| 5.15 | Maximum frame transfer latency for B2B Unicast frames. | 88 |
| 5.16 | Maximum frame transfer latency for B2B Broadcast frames. | 89 |
| 5.17 | Flowchart of the B2B source SCU. | 92 |
| 5.18 | Flowchart of the B2B target SCU. | 94 |
| 5.19 | Flowchart of the B2B Trigger SCU. | 95 |
| 5.20 | Time constraints of the B2B transfer system. | 97 |
| 5.21 | The schematic diagram of the controls and pulse electronics of the extraction kicker magnets in the SIS18 2 nd tank. | 98 |
| 5.22 | SIS18 extraction kicker. | 99 |
| 5.23 | A possible triggering delay between extraction kicker magnets in the SIS18 two tanks. | 101 |
| 5.24 | Maximum triggering delay between extraction kicker magnets in the SIS18 two tanks. | 101 |

LIST OF FIGURES

| | | |
|------|--|-----|
| 5.25 | The minimum triggering delay between extraction kicker magnets in two SIS18 tanks. | 101 |
| 5.26 | SIS100 injection kicker. | 103 |
| 5.27 | Schematic of the test setup. | 104 |
| 5.28 | Front view of the test setup. | 105 |
| 5.29 | Schematic of the final setup. | 106 |
| 5.30 | Flowchart of the firmware of the B2B source SCU for the test setup. | 108 |
| 5.31 | Flowchart of the firmware of the B2B target SCU for the test setup. | 108 |
| 5.32 | Flowchart of the firmware of the Trigger SCU for the test setup. | 109 |
| B.1 | Timing frames transfer for the B2B transfer | 156 |
| F.1 | The configuration of the packETH. | 167 |

List of Tables

| | | |
|------|---|-----|
| 5.1 | Acceptable range of the parameters accompanying with the frequency adjustment of the phase shift method for the SIS18 H^+ and U^{28+} beams | 64 |
| 5.2 | Acceptable range of the parameters accompanying with the frequency adjustment of the frequency beating method for the SIS18 H^+ and U^{28+} beams | 64 |
| 5.3 | Maximum orbit length displacement of three cases | 69 |
| 5.4 | Maximum relative momentum shift of three cases | 70 |
| 5.5 | Minimum bucket area factor of three cases | 72 |
| 5.6 | Maximum adiabaticity of three cases | 72 |
| 5.7 | Parameters accompanying with a 7 ms sinusoidal modulation for the SIS18 H^+ beam | 74 |
| 5.8 | Parameters accompanying with a 50 ms sinusoidal modulation for the SIS18 H^+ beam | 74 |
| 5.9 | Uncertainty of the phase alignment of all FAIR B2B use cases | 79 |
| 5.10 | Traffic produced by the XenaBay ports of the test setup | 87 |
| 5.11 | The maximum frame transfer latency of the B2B Broadcast frames for different number of WR switch layers | 90 |
| 5.12 | The 45 days test result of the WR network for the B2B transfer | 90 |
| 5.13 | The tolerable number of WR switch layers for the B2B related traffic | 91 |
| 5.14 | Calculated parameters related to the simultaneous trigger of the SIS18 extraction kicker magnets in a common tank | 100 |
| 5.15 | The triggering delay for the extraction kicker magnets in the two SIS18 tanks | 102 |
| 5.16 | Calculated parameters related to the simultaneous trigger of the SIS100 injection kicker magnets | 103 |
| 5.17 | The running time of the tasks of the B2B source SCU firmware | 110 |
| 6.1 | List of the FAIR B2B transfer use cases | 113 |
| 6.2 | Parameters related to the B2B transfer when the circumference ratio is an integer and the large accelerator is the target | 114 |
| 6.3 | Parameters related to the B2B transfer when the circumference ratio is an integer and the small accelerator is the target | 115 |
| 6.4 | Parameters related to the U^{28+} B2B transfer from the SIS18 to the SIS100 with the frequency beating method | 116 |
| 6.5 | Parameters related to the H^+ B2B transfer from the SIS18 to the SIS100 with the frequency beating method | 116 |
| 6.6 | Parameters related to the B2B transfer when the circumference ratio is close to an integer and the large accelerator is the target | 118 |

LIST OF TABLES

| | | |
|------|--|-----|
| 6.7 | Parameters related to the B2B transfer when the circumference ratio is close to an integer and the small accelerator is the target | 118 |
| 6.8 | Parameters related to the h=4 B2B transfer from the SIS18 to the ESR with the frequency beating method | 119 |
| 6.9 | Parameters related to the h=1 B2B transfer from the SIS18 to the ESR with the frequency beating method | 120 |
| 6.10 | Parameters related to the B2B transfer from the ESR to the CRYRING with the frequency beating method | 120 |
| 6.11 | Parameters related to the B2B transfer when the circumference ratio is far away from an integer and the large accelerator is the target . . | 121 |
| 6.12 | Parameters related to the B2B transfer when the circumference ratio is far away from an integer and the small accelerator is the target . . | 122 |
| 6.13 | Parameters related to the H^+ B2B transfer from the SIS100 to the CR with the frequency beating method | 123 |
| 6.14 | Parameters related to the RIB B2B transfer from the SIS100 to the CR with the frequency beating method | 124 |
| 6.15 | Parameters related to the B2B transfer from the CR to the HESR with the frequency beating method | 125 |
| 6.16 | Parameters related to an applied case of the B2B transfer from the SIS18 to the ESR via the FRS with the frequency beating method . . | 125 |
| 6.17 | Summary of the formulas related to the B2B transfer when the large accelerator is the target | 127 |
| 6.18 | Summary of the formulas related to the B2B transfer when the small accelerator is the target and the revolution period is longer than the period of the synchronization frequency of the target accelerator . . | 128 |
| 6.19 | Summary of the formulas related to the B2B transfer when the small accelerator is the target and the revolution period is shorter than the period of the synchronization frequency of the target accelerator . . | 129 |
| A.1 | B2B timing frames | 154 |
| C.1 | Parameters related to the B2B transfer from the SIS18 to the SIS100 | 157 |
| C.2 | Parameters related to the B2B transfer from the SIS18 to the ESR . . | 158 |
| C.3 | Parameters related to the B2B transfer from the SIS18 to the ESR via the FRS | 159 |
| C.4 | Parameters related to the B2B transfer from the ESR to the CRYRING | 160 |
| C.5 | Parameters related to the B2B transfer from the CR to the HESR . . | 161 |
| C.6 | Parameters related to the B2B transfer from the SIS100 to the CR . . | 162 |
| D.1 | Parameters for the B2B transfer provided by SM | 164 |
| E.1 | Parameters of kicker magnets | 165 |

LIST OF TABLES

Publications

- 2015 J. Bai, T. Ferrand, D. Beck, R. Bär, O. Kester, D. Ondreka, C. Prados, and W. Terpstra. Bunch to Bucket Transfer System for FAIR. In *Proc. of ICAL EPICS*, Melbourne, Australia, 2015
- T. Ferrand and J. Bai. System Design for a deterministic Bunch-to-Bucket Transfer. In *Proc. of IPAC*, Richmond, VA, USA, 2015
- 2014 J. Bai, D. Beck, R. Bär, D. Ondreka, T. Ferrand, M. Kreider, C. Prados, S. Rauch, W. Terpstra, and M. Zweig. First Idea on Bunch to Bucket Transfer for FAIR. In *Proc. of PCaPAC*, Karlsruhe, Germany, 2014
- M. Kreider, J. Bai, R. Bär, D. Beck, A. Hahn, C. Prados, S. Rauch, W. W. Terpstra, and M. Zweig. Launching the FAIR Timing System with CRYRING. In *Proc. of PCaPAC*, Karlsruhe, Germany, 2014
- T. Ferrand and J. Bai. System Simulation of Bunch-to-Bucket Transfer Between Synchrotrons. *GSI Scientific Report*, 2014
- 2013 J. Bai, L. Zeng, B. Wang, P. Li, F. Li, T. Xu, and Z. Li. Modified Read-out System of the Beam Phase Measurement System for CSNS. *Chinese physics C*, 37(10):107004, 2013
- D. Beck, J. Adamczewski-Musch, J. Bai, R. Bär, J. Frhauf, J. Hoffmann, M. Kreider, N. Kurz, C. Prados, S. Rauch, S. Voltz, and M. Zweig. Paving the Way for the General Machine Timing System. *GSI Scientific Report*, 2013
- M. Kreider, J. Bai, D. Beck, C. Prados, W. Terpstra, S. Rauch, and M. Zweig. Receiver Nodes of the General Machine Timing System for FAIR and GSI. *GSI Internal Document*, 2014
- 2012 J. Bai, S. Xiao, T. Xu, and L. Zeng. The Development of Timing Control System for RFQ. In *Proc. of LINAC*, Tel Aviv, Israel, 2012

Jiaoni Bai

Curriculum Vitae

"I am a slow walker, but I never stop walking." - Jiaoni Bai

Education

- 2013–Now **PhD of physics**, Goethe-Universität, Frankfurt am Main, Germany.
- 2010–2013 **Master of Engineering Study in Computer Technology**, Institute of High Energy Physics, Chinese Academy of Sciences, Peking, China, GPA – 8.0.
- 2006–2010 **Bachelor of Engineering Study in Medical Informatics Engineering**, Southern Medical University, Guangzhou, China, GPA – 9.0.

PhD Dissertation

- Title *Development of the timing system for the Bunch-to-Bucket transfer between the FAIR accelerators*
- Professor Prof. Dr. Oliver Kester
- Supervisors Dr. Dietrich Beck and Dr. David Ondreka
- Description
- Development of the Bunch-to-Bucket transfer system
 - C-programming of the soft CPU LatticeMico32
 - VHDL programming of Altera FPGAs
 - Measurement of the White Rabbit network performance

Master Thesis

- Title *The development of EPICS driver for customized VME hardwares*
- Supervisor Taoguang Xu
- Description
- Development of the software interface between EPICS and VME hardware
 - Development of the operator controlling and monitoring interfaces by MEDM hardware
 - VxWorks program for Motorola VME board MVME5100

Bachelor Thesis

- Title *The CCD performance test and analysis*

- Description
- Investigation of the influence factors for CCD
 - Test how these factors influence CCD

Awards

- 2012 Won “Scholarship of the head of the Institute of High Energy Physics, CAS“ for master thesis
- 2007 Won second prize of “Mathematical Contest in Modeling in Southern Medical University“

Key skills

- Intermediate Network engineering, Bash shell script and Visual Basic programming
- Advanced VHDL program for Altera FPGAs, C, accelerator technology, accelerator physics, VxWorks programming and EPICS

Computer literacy

- Basic Windows, Linux (Ubuntu/Debian), Microsoft Office and LaTeX applications
- Engineering Altera Quartus and Matlab applications
- Art design Photoshop and Corel VideoStudio application
- Web design Dreamweaver

Languages

- Mandarin Mother tongue Chinese
- English Good written and spoken
- German Goethe-Zertifikat B2